



UNIVERSITY OF CAMERINO

School of Advanced Studies

DOCTORAL COURSE IN

CHEMICAL AND PHARMACEUTICAL SCIENCES AND BIOTECHNOLOGY

CHEMICAL SCIENCES

XXXIV cycle

**DESIGN, SYNTHESIS AND CHARACTERIZATION OF
VERSATILE COPPER COMPLEXES
WITH ANTICANCER AND CATALYTIC ACTIVITY**

PhD Student

Dr. Luca Bagnarelli

Supervisors

Prof. Maura Pellei

Prof. Carlo Santini

Academic Years 2018/2019 – 2020/2021

TABLE OF CONTENT

Summary	1
1. Introduction	6
1.1 Copper	6
1.1.1. Physical, chemical and atomic properties	6
1.1.2. Applications	7
1.1.3. Oxidation states	8
1.1.3.1. Cu(I)	8
1.1.3.2. Cu(II)	8
1.1.4. Biochemistry	8
1.2. Ligands	10
1.2.1. N-donor ligands: scorpionate ligands	10
1.2.1.1. Heteroscorpionate ligands: bis(pyrazolyl)acetate ligands	13
1.2.2. P-donor ligands: phosphane coligands	13
1.2.3. C-donor ligands: N-Heterocyclic Carbenes	16
1.3. Anticancer complexes	17
1.3.1. Copper complexes with bioconjugated heteroscorpionate ligands	23
1.3.1.1. Metronidazole	23
1.3.1.2. N-methyl-D-aspartate receptor antagonist	24
1.3.1.3. Lonidamine	25
1.4. Copper-based catalysts for Kharasch-Sosnovsky reaction	26
2. Experimental part	28
2.1. Methods and materials	28
2.2. Syntheses of ligands	31
2.2.1. Syntheses of acid ligands	31
2.2.1.1. Synthesis of (Pz) ₂ CH(COOH) (L ^{1H} , 1)	31
2.2.1.2. Synthesis of (Pz ^{3,5-Me}) ₂ CH(COOH) (L ^{2H} , 2)	32
2.2.1.3. Synthesis of (Tz) ₂ CH(COOH) (L ^{3H} , 3)	33
2.2.2. Syntheses of esterified ligands	34
2.2.2.1. Synthesis of (Pz) ₂ CH(COOMe) (L ^{1Me} , 4)	34

2.2.2.2. Synthesis of $(Pz^{3,5-Me})_2CH(COOMe)$ (L^{2Me} , 5)	35
2.2.2.3. Synthesis of $(Pz)_2CH(COO^iPr)$ (L^{1iPr} , 6)	35
2.2.2.4. Synthesis of $(Pz^{3,5-Me})_2CH(COO^iPr)$ (L^{2iPr} , 7)	36
2.2.2.5. Synthesis of $(Pz)_2CH(COOHex)$ (L^{1Hex} , 8)	37
2.2.2.6. Synthesis of $(Pz^{3,5-Me})_2CH(COOHex)$ (L^{2Hex} , 9)	38
2.2.3. Syntheses of bioconjugated ligands	39
2.2.3.1. Synthesis of L^{1MN} (10)	39
2.2.3.2. Synthesis of L^{2MN} (11)	40
2.2.3.3. Synthesis of L^{1NMDA} (12)	40
2.2.3.4. Synthesis of L^{2NMDA} (13)	41
2.2.3.5. Synthesis of LONES (14)	42
2.2.3.6. Synthesis of LONAM (15)	42
2.2.3.7. Synthesis of L^{1LONES} (16)	43
2.2.3.8. Synthesis of L^{2LONES} (17)	44
2.2.3.9. Synthesis of L^{1LONAM} (18)	45
2.2.3.10. Synthesis of L^{2LONAM} (19)	46
2.2.4. Syntheses of imidazole-based ligands	46
2.2.4.1. Synthesis of $(HIm^{Bn})BH_3$ (20)	46
2.2.4.2. Synthesis of $(HIm^{Mes})BH_3$ (21)	47
2.2.4.3. Synthesis of $(HIm^{Me})BPh_3$ (22)	48
2.2.4.4. Synthesis of $(HIm^{Bn})BPh_3$ (23)	48
2.3. Syntheses of the complexes	49
2.3.1. Syntheses of the complexes bearing acid ligands	49
2.3.1.1. Synthesis of $[(PTA)_2Cu(L^{1H})]PF_6$ (24)	49
2.3.1.2. Synthesis of $[(PTA)_2Cu(L^{2H})]PF_6$ (25)	50
2.3.1.3. Synthesis of $[(PPh_3)_2Cu(L^{1H})]PF_6$ (26)	50
2.3.1.4. Synthesis of $[(PPh_3)_2Cu(L^{2H})]PF_6$ (27)	51
2.3.1.5. Synthesis of $[Cu(L^{1H})_2](ClO_4)_2$ (28)	51
2.3.1.6. Synthesis of $[(L^{2H})Cu(L^2)](ClO_4)$ (29)	52
2.3.1.7. Synthesis of $[Cu(L^{3H})_2](ClO_4)_2 \cdot MeOH$ (30)	52
2.3.2. Syntheses of the complexes bearing esterified ligands	53
2.3.2.1. Synthesis of $[(PTA)Cu(L^{1Me})]PF_6$ (31)	53
2.3.2.2. Synthesis of $[(PPh_3)Cu(L^{1Me})]PF_6$ (32)	54

2.3.2.3. Synthesis of $[\text{Cu}(\text{L}^{1\text{Me}})]\text{Cl}_2$ (33)	54
2.3.2.4. Synthesis of $[\text{Cu}(\text{L}^{1\text{Me}})]\text{Br}_2$ (34)	55
2.3.2.5. Synthesis of $[(\text{PTA})\text{Cu}(\text{L}^{2\text{Me}})]\text{PF}_6$ (35)	55
2.3.2.6. Synthesis of $[(\text{PPh}_3)\text{Cu}(\text{L}^{2\text{Me}})]\text{PF}_6$ (36)	56
2.3.2.7. Synthesis of $[\text{Cu}(\text{L}^{2\text{Me}})]\text{Cl}_2$ (37)	56
2.3.2.8. Synthesis of $[\text{Cu}(\text{L}^{2\text{Me}})]\text{Br}_2$ (38)	57
2.3.2.9. Synthesis of $[\text{Cu}(\text{L}^{1\text{Pr}})]\text{Cl}_2$ (39)	57
2.3.2.10. Synthesis of $[\text{Cu}(\text{L}^{1\text{Pr}})]\text{Br}_2$ (40)	58
2.3.2.11. Synthesis of $[\text{Cu}(\text{L}^{2\text{Pr}})]\text{Cl}_2$ (41)	58
2.3.2.12. Synthesis of $[\text{Cu}(\text{L}^{2\text{Pr}})]\text{Br}_2$ (42)	59
2.3.2.13. Synthesis of $[\text{Cu}(\text{L}^{1\text{Hex}})]\text{Cl}_2$ (43)	59
2.3.2.14. Synthesis of $\{[\text{Cu}(\text{L}^{1\text{Hex}})]\text{Br}(\mu\text{-Br})\}_2$ (44)	60
2.3.2.15. Synthesis of $[\text{Cu}(\text{L}^{2\text{Hex}})]\text{Cl}_2$ (45)	60
2.3.2.16. Synthesis of $[\text{Cu}(\text{L}^{2\text{Hex}})]\text{Br}_2$ (46)	61
2.3.3. Syntheses of the complexes bearing bioconjugated ligands	61
2.3.3.1. Synthesis of $[(\text{PTA})_2\text{Cu}(\text{L}^{1\text{MN}})]\text{PF}_6$ (47)	61
2.3.3.2. Synthesis of $[\text{Cu}(\text{L}^{1\text{MN}})_2]\text{Cl}_2$ (48)	62
2.3.3.3. Synthesis of $[(\text{PTA})_2\text{Cu}(\text{L}^{2\text{MN}})]\text{PF}_6$ (49)	63
2.3.3.4. Synthesis of $[\text{Cu}(\text{L}^{2\text{MN}})_2]\text{Cl}_2$ (50)	64
2.3.3.5. Synthesis of $[(\text{PTA})_2\text{Cu}(\text{L}^{1\text{NMDA}})]\text{PF}_6$ (51)	64
2.3.3.6. Synthesis of $[(\text{PPh}_3)_2\text{Cu}(\text{L}^{1\text{NMDA}})]\text{PF}_6$ (52)	65
2.3.3.7. Synthesis of $[(\text{PTA})_2\text{Cu}(\text{L}^{2\text{NMDA}})]\text{PF}_6$ (53)	66
2.3.3.8. Synthesis of $[(\text{PPh}_3)_2\text{Cu}(\text{L}^{2\text{NMDA}})]\text{PF}_6$ (54)	66
2.3.3.9. Synthesis of $[(\text{PTA})_2\text{Cu}(\text{L}^{1\text{LONES}})]\text{PF}_6$ (55)	67
2.3.3.10. Synthesis of $[(\text{PPh}_3)_2\text{Cu}(\text{L}^{1\text{LONES}})]\text{PF}_6$ (56)	68
2.3.3.11. Synthesis of $[\text{Cu}(\text{L}^{1\text{LONES}})]\text{Cl}_2$ (57)	69
2.3.3.12. Synthesis of $[(\text{PTA})_2\text{Cu}(\text{L}^{2\text{LONES}})]\text{PF}_6$ (58)	69
2.3.3.13. Synthesis of $[(\text{PPh}_3)_2\text{Cu}(\text{L}^{2\text{LONES}})]\text{PF}_6$ (59)	70
2.3.3.14. Synthesis of $[\text{Cu}(\text{L}^{2\text{LONES}})]\text{Cl}_2$ (60)	71
2.3.3.15. Synthesis of $[(\text{PTA})_2\text{Cu}(\text{L}^{1\text{LONAM}})]\text{PF}_6$ (61)	71
2.3.3.16. Synthesis of $[(\text{PPh}_3)_2\text{Cu}(\text{L}^{1\text{LONAM}})]\text{PF}_6$ (62)	72
2.3.3.17. Synthesis of $[\text{Cu}(\text{L}^{1\text{LONAM}})]\text{Cl}_2$ (63)	73
2.3.3.18. Synthesis of $[(\text{PTA})_2\text{Cu}(\text{L}^{2\text{LONAM}})]\text{PF}_6$ (64)	73

2.3.3.19. Synthesis of $[(PPh_3)_2Cu(L^{2LONAM})]PF_6$ (65)	74
2.3.3.20. Synthesis of $[Cu(L^{2LONAM})]Cl_2$ (66)	75
2.4. Syntheses of oxidized cycloalkenes via Kharasch-Sosnovsky reaction	76
2.4.1. General procedure for the synthesis of compounds 67-69	76
2.4.1.1. Synthesis of cyclohex-2-enyl benzoate (67)	76
2.4.1.2. Synthesis of cyclopent-2-enyl benzoate (68)	76
2.4.1.3. Synthesis of cyclooct-2-enyl benzoate (69)	77
3. Results and discussion	78
3.1. Syntheses of ligands	78
3.1.1. Syntheses of acid ligands	78
3.1.2. Syntheses of esterified ligands	79
3.1.3. Syntheses of bioconjugated ligands	82
3.1.4. Syntheses of imidazole-based ligands	86
3.2. Syntheses of the complexes	88
3.2.1. Syntheses of complexes bearing acid ligands	88
3.2.2. Syntheses of complexes bearing esterified ligands	93
3.2.3. Syntheses of complexes bearing bioconjugated ligands	105
3.3. Application of copper complexes	117
3.3.1. Cu(I) and Cu(II) complexes as anticancer agents	117
3.3.2. Cu(II) complexes as catalysts	133
4. Conclusions	139
5. References	141
Supporting information	155

SUMMARY

Although copper has a long history of medical application, copper coordination compounds have been investigated as potential anticancer agents only in the last few decades, particularly after the discovery of cisplatin, the most widely used antitumor metallodrug. Copper, as an essential cofactor in a number of enzymes and physiological processes, may be less toxic than non-essential metals, such as platinum. Up to now, a great variety of copper complexes have been tested as cytotoxic agents and found to be endowed with an antitumor activity in several *in vitro* tests and few *in vivo* experiments. Based on these assumptions, in my PhD research work copper was selected for the synthesis of potential metal-based anticancer drugs, that could be suitable alternative to platinum-based drugs that are hampered by marked side effects and chemoresistance. An important aim of this work, in the inorganic chemistry research field, was to synthesize new species able to coordinate metals useful to obtain Cu(I) and Cu(II) complexes with potential anticancer activity.

Copper complexes were synthesized employing bis(pyrazolyl)acetic acids (belonging to the family of the heteroscorpionate) as ligands. This class of ligands was selected due to their stability, flexibility and ease to be functionalized and derivatized. In fact, they were used as they are (with the carboxylic acid group) or esterified with aliphatic alcohols (branched and not) or bioconjugated with several biologically active compounds. For this purpose, the ligands were conjugated with metronidazole (an antibiotic agent investigated for hypoxia-selective cytotoxicity), NMDA-ANT (an antagonist for the *N*-methyl-D-aspartate receptor endowed with micromolar cytotoxic activity on a panel of solid tumor cell lines) and lonidamine (an antineoplastic drug) in order to obtain Cu(I) and Cu(II) complexes potentially able to exert an anticancer activity through synergistic mechanisms of action. Additionally, to stabilize copper in the +1 oxidation state (avoiding its oxidation) and to modulate the solubility profile of the related copper(I) complexes, hydrophilic or lipophilic phosphanes, such as 1,3,5-triaza-7-phosphaadamantane (PTA) and triphenylphosphine (PPh₃) respectively, were used as coligands.

My main work was the design, synthesis and characterization of the ligands and related copper complexes, both in solid state (FT-IR, elemental analysis and melting point) and in solution (¹H-, ¹¹B-, ¹³C-, ³¹P-NMR and ESI-MS) to confirm their structure, stoichiometry and purity. In parallel, X-ray diffraction studies were conducted on single crystals of ligands and complexes,^[b,e,g,s] showing in some cases new and unexpected dimeric structures.^[g] In addition, the structural characterization and the study of the local coordination environment of several

complexes were exploited by X-ray photoelectron spectroscopy (XPS) and X-ray absorption fine structure (XAFS) spectroscopy (in the near edge and in the extended regions).^[d,f,h,i,m,p,t] In all the cases, the structural investigations confirmed the hypothesized geometry of the metal center and the coordinative fashion of the ligands.

Several new complexes and the corresponding uncoordinated ligands were evaluated for their ability to promote cell death against a panel of human cancer cell lines, cisplatin resistant tumor cell lines and spheroids, evaluating also cellular uptake, mechanism of action and morphological modifications induced by the complexes once inside the tumor cells.^[a,c,h,i,j,k,n,o,q,r,t,u] In detail, for a series of selected precursors, ligands and Cu(I) and Cu(II) complexes the biological activity was evaluated by means of MTT test, cellular uptake, reactive oxygen species (ROS) production, comet assay and/or transmission electron microscope (TEM) analyses. Summarizing, even if with slight differences, it was possible to state that the complexes were, in general, more active than cisplatin (the drug used as reference compound), both in 2D and 3D cell cultures, showing their effect in the low micromolar concentration, or even lower. On the contrary, the related free ligands and precursors did not show relevant cytotoxic activity. Interestingly, the fact that the complexes proved to be significantly more active than cisplatin, even against three-dimensional spheroids of selected cancer cells, increased the relevance of the *in vitro* results. In fact, 3D spheroids of cancer cells more closely mimic the heterogeneity and complexity of *in vivo* tumors, being consequently more predictive for *in vivo* results than conventional 2D cell cultures. The most frequent mechanism of action for the tested complexes was the paraptotic one, a type of programmed cell death different from the classical apoptosis induced by drugs such as cisplatin. This alternative programmed cell death leads to the overcoming of the inherited or acquired cisplatin or multi-drug resistance. Regarding the ligands esterified with aliphatic alcohols and the related copper complexes the biological studies are still in progress but, according to the preliminary data, these complexes seem to be very promising.

Another field of interest of my research work was the investigation of the catalytic activity of new copper(II) compounds in the Kharasch-Sosnovsky reaction,^[d,g,n] that is a useful reaction for the synthesis of protected allylic alcohols, via radical oxidation of olefins leaving the double bond in its original position. In particular, the catalytic activity of the copper(II) complexes, containing the isopropyl or hexyl ester chain, was evaluated in the Kharasch-Sosnovsky reaction. The original reaction conditions were optimized changing several parameters and very high yields were obtained employing the compounds containing bromide as counterion. The

major limitations of this reaction, such as long reaction times, employ of benzene as solvent and high waste of olefins, were overcome replacing the original cheap but no-so-effective CuBr with the new synthesized Cu(II) complexes. In order to validate the generality of the method, different olefin substrates were tested (obtaining excellent yields) and other promising Cu(II) complexes are under evaluation as catalysts.

References:

- [a] M. Pellei, V. Gandin, C. Cimarelli, W. Quaglia, N. Mosca, **L. Bagnarelli**, C. Marzano, C. Santini; "Syntheses and biological studies of nitroimidazole conjugated heteroscorpionate ligands and related Cu(I) and Cu(II) complexes"; *Journal of Inorganic Biochemistry* (IF: 4.155); 187, 33, **2018**. DOI: 10.1016/j.jinorgbio.2018.07.008
- [b] M. Pellei, V. Gandin, L. Marchiò, C. Marzano, **L. Bagnarelli**, C. Santini; "Syntheses and biological studies of Cu(II) complexes bearing bis(pyrazol-1-yl)- and bis(triazol-1-yl)-acetato heteroscorpionate ligands"; *Molecules* (IF: 4.412); 24, 1761, **2019**. DOI: 10.3390/molecules24091761
- [c] M. Pellei, **L. Bagnarelli**, L. Luciani, F. Del Bello, G. Giorgioni, A. Piergentili, W. Quaglia, M. De Franco, V. Gandin, C. Marzano, C. Santini; "Synthesis and cytotoxic activity evaluation of new Cu(I) complexes of bis(pyrazol-1-yl) acetate ligands functionalized with an NMDA receptor antagonist"; *International Journal of Molecular Sciences* (IF: 5.924); 21, 2616, **2020**. DOI: 10.3390/ijms21072616
- [d] S. Gabrielli, M. Pellei, I. Venditti, I. Fratoddi, C. Battocchio, G. Iucci, I. Schiesaro, C. Meneghini, A. Palmieri, E. Marcantoni, **L. Bagnarelli**, R. Vallesi, C. Santini; "Development of new and efficient copper(II) complexes of hexyl bis(pyrazolyl)acetate ligands as catalysts for allylic oxidation"; *Dalton Transactions* (IF: 4.390); 49, 15622, **2020**. DOI: 10.1039/D0DT02952A
- [e] M. Pellei, R. Vallesi, **L. Bagnarelli**, H. V. Rasika Dias, C. Santini; "Syntheses and reactivity of new zwitterionic imidazolium trihydridoborate and triphenylborate species"; *Molecules* (IF: 4.412); 25, 3148, **2020**. DOI: 10.3390/molecules25143184
- [f] Schiesaro, I. Venditti, M. Pellei, C. Santini, **L. Bagnarelli**, G. Iucci, C. Battocchio, C. Meneghini; "Metal coordination core in copper(II) complexes investigated by XAFS"; *Synchrotron Radiation Science and Applications*; 220, 169, **2021**. DOI: 10.1007/978-3-030-72005-6_13
- [g] **L. Bagnarelli**, A. Dolmella, C. Santini, R. Vallesi, R. Giacomantonio, S. Gabrielli, M. Pellei; "A new dimeric copper(II) complex of hexyl bis(pyrazolyl)acetate ligand as an efficient catalyst for allylic oxidations"; *Molecules* (IF: 4.412); 26, 6271, **2021**. DOI: 10.3390/molecules26206271
- [h] F. Del Bello, M. Pellei, **L. Bagnarelli**, C. Santini, G. Giorgioni, A. Piergentili, W. Quaglia, C. Battocchio, G. Iucci, I. Schiesaro, C. Meneghini, I. Venditti, N. Ramanan, M. De Franco, P. Sgarbossa, C. Marzano, V. Gandin; "Cu(I) and Cu(II) complexes based on Ionidamine-conjugated ligands designed to promote synergistic antitumor effects"; *Inorganic Chemistry* (IF: 5.165); 61, 4919, **2022**.

- [i] C. Santini, **L. Bagnarelli**, L. Luciani, F. Scorcelletti, F. Del Bello, W. Quaglia, C. Marzano, V. Gandin, M. Pellei; "Synthesis, reactivity and biological studies of bioconjugated bis(pyrazolyl)acetate copper complexes"; *BioMet19 - XVIII Workshop PharmacoBiometallics*; Book of abstracts, page 47; **2019**.
- [j] **L. Bagnarelli**, C. Santini, M. Porchia, F. Tisato, C. Marzano, V. Gandin, M. Pellei; "Synthesis, reactivity and cytotoxic properties of water soluble coinage metal N-Heterocyclic Carbene complexes"; *BioMet19 - XVIII Workshop PharmacoBiometallics*; Book of abstracts, page 33; **2019**.
- [k] **L. Bagnarelli**, C. Santini, R. Vallesi, C. Marzano, V. Gandin, M. Pellei; "Hydrosoluble coinage metal N-Heterocyclic Carbene complexes: synthesis and anticancer studies"; *ISOC 2019 - 12th International School of Organometallic Chemistry*; Book of abstracts (ISBN 9788867680412), P2, page 28; **2019**.
- [l] C. Battocchio, I. Schiesaro, C. Meneghini, M. Pellei, C. Santini, **L. Bagnarelli**, G. Iucci, I. Venditti; "Study of the molecular and electronic structure of copper coordination compounds conjugated to gold nanoparticles as innovative anticancer drugs"; *47th Congresso Nazionale della Divisione di Chimica Inorganica*; Book of abstracts (ISBN 9788880803522), P3, page 108; **2019**.
- [m] I. Schiesaro, I. Venditti, M. Pellei, C. Santini, **L. Bagnarelli**, G. Iucci, C. Battocchio, C. Meneghini; "Copper coordination compounds conjugated to gold nanoparticles as innovative anticancer drugs: structural investigation carried out by synchrotron radiation-induced techniques"; *SILS 2019 (Annual Meeting of the Italian Synchrotron Radiation Society)*; Book of abstracts, YI 06, page 73; **2019**.
- [n] **L. Bagnarelli**, C. Santini, S. Gabrielli, V. Gandin, C. Marzano, F. Del Bello, P. Maura; "Syntheses, biological and catalytic studies of copper complexes bearing bis(azol-1-yl)-acetato heteroscorpionate ligands"; *XXXVII TUMA 2019 - Convegno delle Sezioni Toscana Umbria Marche Abruzzo della Società Chimica Italiana*; Book of abstracts, P2, page 37; **2019**.
- [o] C. Santini, M. Pellei, **L. Bagnarelli**, L. Luciani, F. del Bello, C. Marzano, V. Gandin; "Chemistry and antitumor investigations of new Cu(I) complexes of bis(pyrazol-1-yl)acetate ligands functionalized with an NMDA receptor antagonist"; *BioMet2020 - XIX Workshop PharmacoBiometallics*; Book of abstracts, page 46; **2020**.
- [p] C. Battocchio, I. Schiesaro, I. Venditti, M. Pellei, C. Santini, **L. Bagnarelli**, G. Iucci, C. Meneghini; "Copper coordination compounds conjugated to gold nanoparticles as innovative anticancer drugs: structural investigation carried out by synchrotron radiation-induced techniques"; *BioMet2020 - XIX Workshop PharmacoBiometallics*; Book of abstracts, page 34; **2020**.
- [q] **L. Bagnarelli**, C. Santini, F. del Bello, W. Quaglia, M. Pellei; "New Cu(I) complexes of bis(pyrazol-1-yl)acetate ligands functionalized with an NMDA receptor antagonist with cytotoxic activity"; *ISC 2020 - International School of Chemistry: Chemistry for everyday life web edition*; Book of abstracts (ISBN 9788867680467), P3, page 75; **2020**.
- [r] **L. Bagnarelli**, M. Pellei, C. Santini, F. Del Bello, W. Quaglia, G. Giorgioni, C. Marzano, V. Gandin; "Novel antitumor Cu(I) and Cu(II) complexes based on bioconjugate ligands rationally designed to act through synergistic mechanisms"; *BioMet2021 - XX Workshop PharmacoBiometallics*; Book of abstracts, page 8; **2021**.
- [s] **L. Bagnarelli**, R. Vallesi, M. Pellei, H. V. Rasika Dias, C. Santini; "Design, synthesis and reactivity of new zwitterionic imidazolium-based species"; *ISOC 2021 - 13th International School of Organometallic Chemistry*; Book of abstracts (ISBN 9788867680528), abstract 5, page 22; **2021**.

-
- [t] **L. Bagnarelli**, M. Pellei, C. Santini, F. Del Bello, W. Quaglia, G. Giorgioni, M. De Franco, C. Marzano, C. Battocchio, G. Iucci, I. Schiesaro, I. Venditti, V. Gandin; "New anticancer copper complexes containing ligands conjugated with biologically active molecules"; *SCI2021 - XXVII Congresso Nazionale della Società Chimica Italiana*; Book of abstracts (ISBN 9788894952247), INO PO006; **2021**.
- [u] **L. Bagnarelli**, M. Pellei, C. Santini, M. Caviglia, M. De Franco, C. Marzano, V. Gandin; "Copper complexes bearing heteroscorpionate ligands conjugated with bioactive compounds as potential anticancer agents"; *BioMet2022 - XXI Workshop Pharmacobiometallics*; Book of abstracts, page 6; **2022**.

1. Introduction

1.1. Copper

Copper is the chemical element with symbol Cu and atomic number 29. The most representative data about copper are reported in **Table 1.1**.

Name	Copper
Symbol	Cu
Atomic number	29
Atomic weight	63.546 Da
Group; Period	11; 4
Category; Block	Transition metal; d
Electronic configuration	[Ar]3d ¹⁰ 4s ¹
Main oxidation states	+1 ([Ar]3d ¹⁰), +2 ([Ar]3d ⁹)
Electronegativity (Pauling)	1.90
Ionization energies	1 st : 745.5, 2 nd : 1957.9, 3 rd : 3555 KJ/mol
Atomic radius (empirical)	128 pm
Covalent radius	132±4 pm
Van der Waals radius	140 pm
Phase (at STP)	Solid
Density (at rt)	8.96 g/cm ³
Melting point	1048.62 °C - 1357.77 K
Boiling point	2562 °C - 2835 K
Thermal conductivity	401 W/(m·K)
Electrical resistivity (at 20 °C)	16.78 nΩ·m
Magnetic susceptibility	-5.46·10 ⁻⁶ cm ³ /mol
Crystal structure	FCC (Face-Centered Cubic)
Mohs hardness	3.0
CAS number	7440-50-8

Table 1.1. - Most important data about copper.

1.1.1. Physical, chemical and atomic properties

In the group of copper it's possible to find silver and gold and, for this reason, the 11th group of the periodic table is also called "the group of the coinage metals". All the coinage metals are excellent conductors of electricity and, in particular, copper is second only to silver among pure metals at room temperature as conductor.^[1]

Copper doesn't react with water (unlike alkali metals and alkaline earth metals), but slowly reacts with atmospheric oxygen. This kind of oxidation is called "passivation": a thin layer of oxidized copper protects the surface of copper objects, preventing further oxidation (unlike what happens to iron which gets rust because of the air moisture). As occurs with other metals,

if copper enters in contact with another metal, galvanic corrosion takes place. This phenomenon is at the base of the voltaic pile (that employs alternated discs of copper and zinc).

There are two naturally existing isotopes of copper (^{63}Cu and ^{65}Cu), 27 synthetic isotopes (^{61}Cu , ^{64}Cu and ^{67}Cu are the most important ones) and 7 metastable isotopes (**Table 1.2.**).

Isotope	N. of neutrons	Abundance	Half-life	Decay mode(s)	Decay product
^{61}Cu	32	Synthetic	3.33 h	β^+	^{61}Ni
^{63}Cu	34	69.15 %	Stable		
^{64}Cu	35	Synthetic	12.70 h	β^+ (61 %)	^{64}Ni
				β^- (39 %)	^{64}Zn
^{65}Cu	36	30.85 %	Stable		
^{67}Cu	38	Synthetic	61.83 h	β^-	^{67}Zn

Table 1.2. - Most important copper isotopes.

After the decay, all the resulting isotopes showed in **Table 1.2.** are stable. The synthetic and metastable nuclides are radioactive: those with atomic mass below 63 tend to undergo to β^+ decay, the isotopes with atomic mass above 65 tend to undergo to β^- decay and ^{64}Cu decays both in β^+ and in β^- modes.^[2] Copper offers a quite large number of radioisotopes, that are potentially suitable for the use in nuclear medicine: ^{60}Cu , ^{61}Cu , ^{62}Cu and ^{64}Cu for diagnostic purposes and ^{64}Cu and ^{67}Cu for radiotherapy. In particular, ^{64}Cu (with an half-life of 12.70 hours) is ideal in positron emission tomography (PET) imaging^[3] and the ^{62}Cu complex with pyruvaldehyde bis(N^4 -methylthiosemicarbazone) (^{62}Cu -PTSM) has been studied as brain radioactive tracer (also in this case for PET imaging).^[4]

1.1.2. Applications

Copper is a malleable, ductile and soft metal that shows very high electrical and thermal conductivity: for these reasons it is used as conductor of heat and electricity (in copper wires, for example). This metal is also employed in rain gutters, in architecture and as constituent of alloys among the most used, such as bronze (copper-tin) and brass (copper-zinc). Copper is also used as pigment (thanks to the blue or green color of its compounds in the +2 oxidation state) and some of its compounds are employed as antimicrobial, wood preservatives or fungicides (such as in the Bordeaux mixture, that is an aqueous mixture of copper(II) sulfate and calcium hydroxide).

1.1.3. Oxidation states

The most common and representative oxidation states for copper are +1 and +2. It forms salts and complexes in the form of Cu(I) (cuprous ion) and Cu(II) (cupric ion). Derivatives of copper in +3 oxidation state have been supposed as intermediates, mainly in biological environments, when it is involved in catalytic cycles in the presence of metalloproteins and/or metalloenzymes, but rarely isolated or observed. Nevertheless, organometallic compounds of Cu(III) have been found as intermediates,^[5] for example in the Kharasch-Sosnovsky reaction.^[6]

1.1.3.1. Cu(I)

Copper in its +1 oxidation state assumes configuration d^{10} and it forms diamagnetic and white complexes. Cuprous ion is not extremely stable tending to be oxidized and, for this reason, according to the Hard Soft Acid Base (HSAB) theory by Pearson,^[7] it needs for "soft" or "borderline" ligands that own phosphorus or nitrogen as donor atoms. Therefore, the stability of Cu(I) complexes depends on the nature of the ligands. Thanks to the several coordination numbers (CN) that these complexes can have, different geometries are possible and the most common is the tetrahedral one (CN = 4).^[8]

1.1.3.2. Cu(II)

Copper in its +2 oxidation state assumes configuration d^9 and it forms paramagnetic complexes of different colours according to their coordination numbers and geometries, such as green, blue, orange, brown and violet. Cupric ion is stable, since it has already reached its maximum oxidation state, and for this reason, according to the HSAB theory by Pearson, it prefers "borderline" or "hard" ligands that own nitrogen or oxygen as donor atoms. Thanks to the several CN that these complexes can have, different geometries are possible and the main ones are: square planar (CN = 4), compressed tetrahedral (CN = 4), distorted trigonal bipyramidal (CN = 5), distorted square pyramidal (CN = 5), octahedral (CN = 6), elongated tetragonal octahedral (CN = 6).^[9]

1.1.4. Biochemistry

The biological role of copper began with the appearance of oxygen in Earth's atmosphere^[10] and now it plays several important functions. Copper is an essential metal and it is present in animals and plants in traces, but it is not essential for all the microorganisms. The human body

contains an amount of copper from 1.4 to 2.1 mg per kg and the absorption, concentration and excretion of this metal are efficiently regulated by means of enterohepatic circulation. If necessary, the body is able to excrete the excess of copper, in order to avoid poisoning, realizing a strict control (homeostasis) about the presence of this essential, but potentially dangerous, metal.^[11]

Copper is absorbed in the intestine and then transported to the liver, bound to the albumin. In a second phase, copper is distributed to the other tissues by means of the ceruloplasmin (**Figures 1.1. and 1.2.**), which is responsible for the transportation of most of this metal in the blood.^[12-14]



Figure 1.1. - Ceruloplasmin.

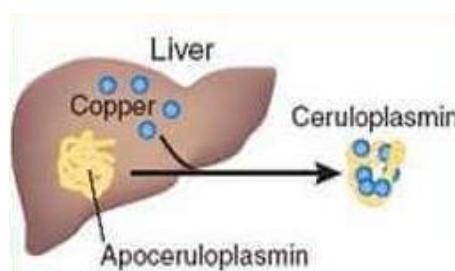


Figure 1.2. - Schematic representation of ceruloplasmin formation.

Copper is an essential metal in the aerobic respiration of all eukaryotes. In mitochondria, it is found in the cytochrome c oxidase (complex IV) (**Figures 1.3. and 1.4.**), a membrane enzyme which is the last one involved in the oxidative phosphorylation, the oxidative pathway in which cells use enzymes to oxidize the nutrients and reduce O_2 to H_2O , with the aim to produce adenosine triphosphate (ATP).

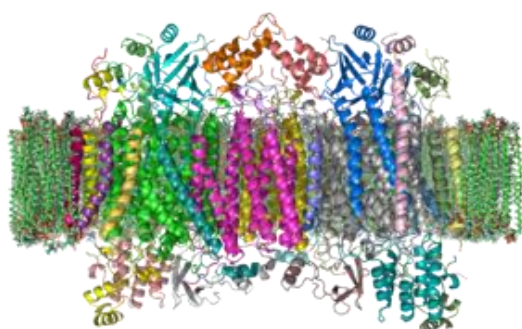


Figure 1.3.
Bovine cytochrome c oxidase in membrane.

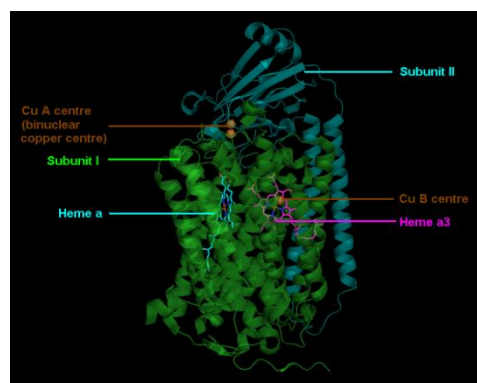


Figure 1.4.
Cytochrome c oxidase: subunits I and II.

Copper is also found in the superoxide dismutase (SOD) (**Figure 1.5.**), an enzyme with an efficient antioxidant activity that catalyzes the decomposition of the reactive oxygen species (ROS), in particular the disproportionation of the dangerous radical superoxide (by-product naturally formed by some physiological reactions) converting it to O_2 and H_2O_2 .

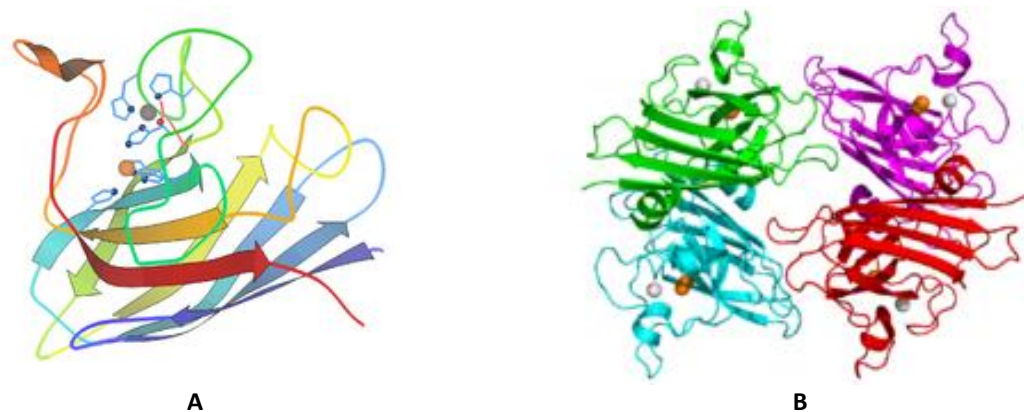


Figure 1.5.
A) Human SOD 1; B) Human SOD 3. [Orange spheres = Copper atoms]

Finally, another important copper-based protein is the hemocyanin: it is the carrier protein for the oxygen in most mollusks and some arthropods, responsible for the blue color of the blood of the above-mentioned animals.

In these last years the chemistry and the biochemistry of copper have been widely investigated also because of the role of this transition metal in medicine, in the pathology treatment (such as in Menkes and Wilson diseases) and in the chelation therapy to fight cancers^[15] and neurodegenerative disorders due to the copper accumulation (such as Alzheimer and Parkinson). Menkes syndrome consists in the deficiency of copper in the body caused by mutations in genes responsible to encode copper transporters, while Wilson disease consists in an excess of copper, also in this case due to mutations in particular genes.

1.2. Ligands

1.2.1. N-donor ligands: scorpionate ligands

The first and the most important scorpionate ligand was the hydrotris(pyrazolyl)borate $[HB(Pz)_3]^-$ and its first appearance in publications was in 1966.^[16,17] It was synthesized by the DuPont chemist Swiatoslaw Trofimenko by reacting three equivalents of pyrazole with one equivalent of potassium borohydride. The product of the reaction was the potassium salt $K[HB(Pz)_3]$ with the production of three equivalents of molecular hydrogen.^[18] The nitrogens

that are not bound to the boron atom are basic and, therefore, they can act as Lewis base binding three adjacent coordination sites of a metal center (**Figure 1.6.** and **Figure 1.7.**).

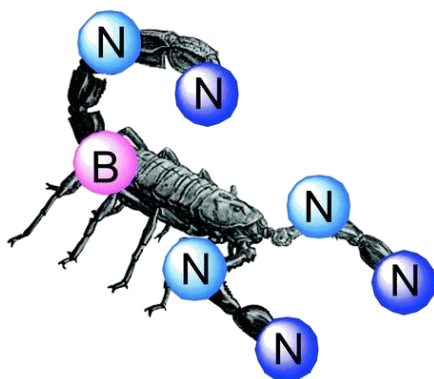


Figure 1.6.

Schematic representation of hydrotris(pyrazolyl)borates overlapped on a scorpion image.

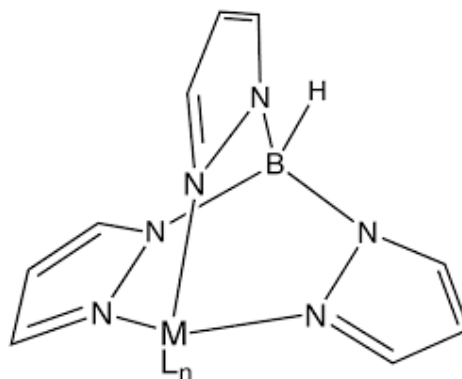


Figure 1.7.

Coordination mode of $[\text{HB}(\text{Pz})_3]^-$.

The Trofimenko's ligand $[\text{HB}(\text{Pz})_3]^-$ was the precursor of other hydrotris(pyrazolyl)borates with different substituents in the pyrazolyl rings: also these derivatives belong to the family of the scorpionate ligands.^[19,20]

The term "scorpionate ligand" refers to a tridentate ligand that binds a metal center in a *fac* manner (**Figure 1.8.**).

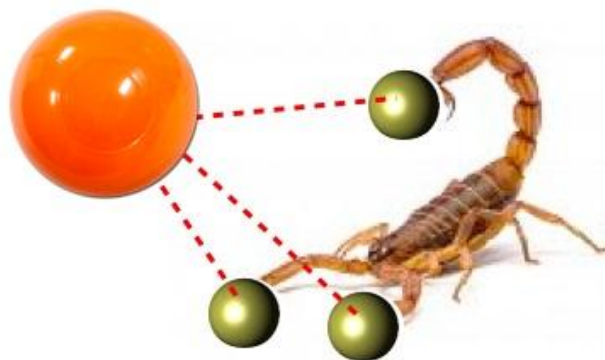


Figure 1.8. - Way to bind a metal center of a general scorpionate ligand.

As shown in **Figure 1.8.**, it is possible to see that the term "scorpionate" comes from the fact that this class of ligands can bind a metal with three donor atoms. The first two act like the pincers of a scorpion and the third one reaches the metal above the plane described by the other two donor atoms and the metallic center. Definitely, it is possible to imagine the coordination manner like a scorpion that blocks its prey (the metal center) with its pincers (first two donor atoms) before to sting it by means of its stinger (third donor atom).

Poly(pyrazolyl)borates (with or without substituted pyrazoles) are not immediately formed: the reaction begins with the coordination of two pyrazoles to give a bis(pyrazolyl)borate and, increasing the temperature, subsequently a third and, potentially, a fourth coordination occurs, giving a tris(pyrazolyl)borate and a tetrakis(pyrazolyl)borate, respectively (**Figure 1.9.**).

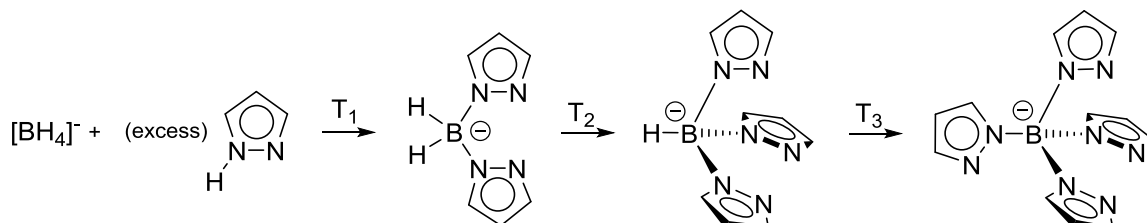


Figure 1.9. - Formation of poly(pyrazolyl)borates ($T_1 < T_2 < T_3$).

The interest about hydrotris(pyrazolyl)borates (in particular the bulky ones) has risen because they have proven to be excellent catalysts and models of enzymes active sites; in fact, the bulky ligands provide a good shielding of the bound metal against oxidations, while strong σ bonds between nitrogens and the metal stabilize the metal center.

Trofimenko's pioneering work reported three pyrazolyl groups bound to a boron atom and the ligands obtained were later called "homoscorpionate ligands". Starting from his work, a lot of novel scorpionate ligands were synthesized, where groups of different nature could be attached to boron. If at least one of the groups was different from the others, these novel types of ligands were called "heteroscorpionate ligands" (**Figure 1.10.**).

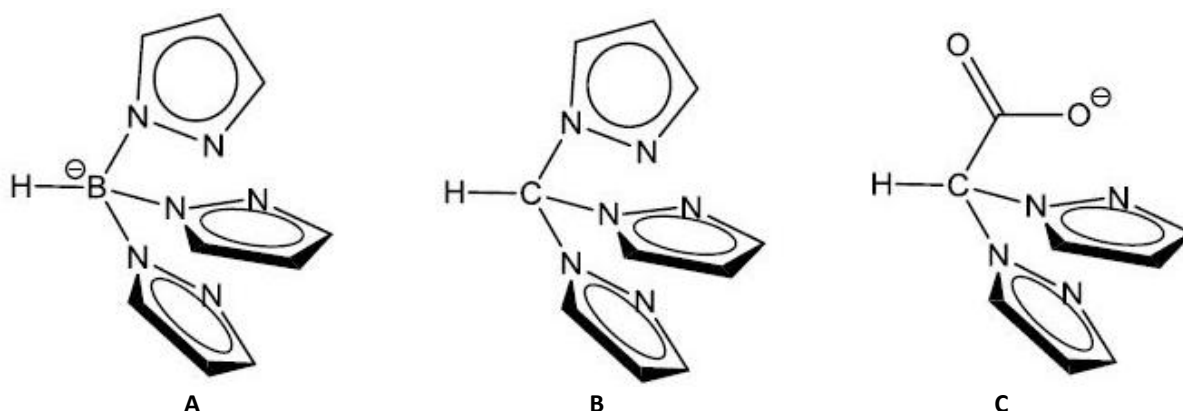


Figure 1.10. - Structure of poly(pyrazolyl): **A**) -borates; **B**) -alkanes; **C**) -acetates.

Many other chemists continue to explore this research field experimenting the use of alternative donor atoms/groups such as sulfur or oxygen in place of nitrogen^[21] or imidazole, triazole, pyrrole or indole in place of pyrazole. Other attempts were also made to change the geometry of the coordination groups in order to force a particular geometry of the resulting complex or to alter the type of encapsulation of the metal center. The pyrazolyl rings can be

variously substituted in 3-, 4- and/or 5-position,^[22,23] as well as other azoles that can be functionalized in their own characteristic sites, and can be employed as starting materials. Thus, it is easy to imagine that a huge number of different scorpionate ligands can be synthesized.

1.2.1.1. Heteroscorpionate ligands: bis(pyrazolyl)acetate ligands

Even though many scorpionate ligands have a central boron atom, it is possible to synthesize ligands that have other central atoms.

Otero and co-workers first synthesized, in 1999, a bis(pyrazol-1-yl)acetate ligand by means of a multistep synthesis that involved *n*-butyllithium (*n*-BuLi) and, for this reason, it presented quite difficult reaction conditions. They also studied the coordination ability of bis(3,5-dimethylpyrazol-1-yl)acetate ligands towards groups IV and V of the transition metals.^[24]

Then, Burzlaff and co-workers designed a faster and simpler synthesis starting from commercially available dibromo- or dichloro-acetic acid and two equivalents of 3,5-dimethylpyrazole (or simple pyrazole), with a large excess of potassium hydroxide and potassium carbonate, employing tetra-*n*-butylammonium bromide as phase-transfer catalyst.^[25,26]

It's interesting to know the dissimilarity between the borate ligands and the acetate ones, since they exhibit several significant differences. Poly(pyrazolyl)borate ligands are symmetrical with respect to the nitrogen donors and are unable to mimic many metalloprotein active sites which lack similar monofunctional and highly organized donor atoms. Bis(pyrazolyl)acetates are ligands closely related to both neutral tris(pyrazolyl)methanes and anionic tris(pyrazolyl)borates, where one of the pyrazolyl groups is replaced by a carboxylate moiety. This change introduces a small degree of steric hindrance and a considerable coordinative flexibility. Finally, bis(pyrazolyl)acetates can be easily deprotonated, behaving in the anionic form as κ^3 -N,N,O tripodal donors, similarly to tris(pyrazolyl)borates; alternatively they can coordinate in the neutral form like the tris(pyrazolyl)alkanes.

1.2.2. P-donor ligands: phosphane coligands

Phosphanes could be primary, secondary or tertiary depending on their alkylation degree or, in the simplest case (PH₃), without substituents. Phosphanes are Lewis bases, thanks to the presence of a lone pair, and this characteristic is maintained until the third substitution, such as trialkylphosphanes (PR₃) or triarylphosphanes (PAR₃).

The steric hindrance of tertiary phosphanes is commonly evaluated using Tolman cone angle. This parameter is a measure of the space occupied by the phosphanes in the coordination sphere of a complex. The solid angle is formed by the metal center at the vertex and the outer edge of the phosphane atoms on the perimeter of the cone.

Phosphanes are P-donor compounds and they can be used as coligands in metal complexes, because phosphorus is a good σ -donor and π -acceptor. This is due to the presence of empty $3d$ orbitals that can overlap with occupied d orbitals of a metal center. Phosphanes have a property that is called synergistic effect: the more is the degree of σ -donation and the less is the π -acceptance by the phosphorus and vice versa.^[27]

The electronic and steric effects of the phosphorus substituents influence the coordination properties of the phosphane coligands. In addition, the availability of electrons in the d orbitals of the metal center influences the strength of the P-M bond. Thanks to these characteristics, phosphanes are very useful in organometallic chemistry, homogeneous catalysis and medicinal chemistry.

Phosphane complexes of the 11th group metals, especially those with gold(I) ion, have been proposed as anticancer drugs alternative to cisplatin. One of the first metal-phosphane complexes investigated that showed *in vivo* anticancer activity was Auranofin, which is a thioglucose derivate of triethylphosphane gold(I).

The study was then extended to analogues Cu(I) complexes such as $[\text{Cu}(\text{dppe})_2]\text{Cl}$ and $[\text{Cu}(\text{dppey})_2]\text{Cl}$ (where $\text{dppe} = 1,2\text{-bis}(\text{diphenylphosphino})\text{ethane}$ and $\text{dppey} = 1,2\text{-bis}(\text{diphenylphosphino})\text{ethylene}$). Copper-based complexes were investigated on the assumption that the essential metals may be less toxic for the healthy cells with respect to the cancer ones.

Over the years, complexes with hydrophilic phosphines (1,3,5-triaza-7-phosphaadamantane = PTA or tris(hydroxymethyl)phosphane = thp, **Figure 1.11.**) of the general formula $[\text{M}(\text{P})_4]^+$ were developed.^[28] In these compounds PTA and thp are used as neutral P-donor ligands with the advantages of low steric demand (small cone angle) allowing a strong bond to the metal center.^[29] Hydrophilic tertiary phosphanes were employed to obtain stable, water-soluble $[\text{Cu}(\text{P})_4]^+$ species that proved to be easy to handle during the *in vitro* tests and showed promising antiproliferative effects. Among them, the $[\text{Cu}(\text{thp})_4]\text{PF}_6$ complex (**Figure 1.12.**) showed an excellent *in vitro* antitumor activity against a wide range of solid tumors, including platinum-based drugs refractory/resistant tumors.^[28]

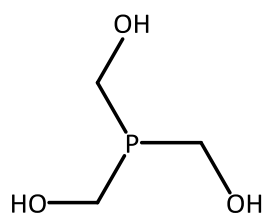


Figure 1.11. - Structure of thp.

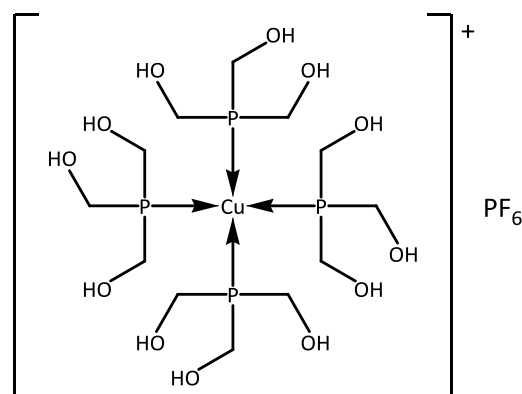


Figure 1.12. - Structure of $[\text{Cu}(\text{thp})_4]\text{PF}_6$.

Moreover, $[\text{Cu}(\text{thp})_4]\text{PF}_6$ was much less cytotoxic against non-tumor cells than Pt(II) drugs with selectivity index (SI = quotient of the average IC_{50} toward non-malignant cells divided by the average IC_{50} for the malignant cells) values about 35- and 10-fold higher than those calculated for cisplatin and oxaliplatin, respectively, used as reference compounds.^[30] Hydrophilic $[\text{Cu}(\text{P})_4]^+$ species, besides having a broader spectrum of activity and a lower toxicity, are able to overcome inherited and/or acquired resistance to cisplatin. These features are consistent with the hypothesis that copper complexes possess mechanism(s) of action different from those showed by platinum-based drugs.^[31]

In order to stabilize copper in the +1 oxidation state (avoiding its oxidation) and to modulate the solubility profile of the copper(I) complexes, phosphanes are required. Among the most important and used phosphanes, PTA (**Figure 1.13.**) and triphenylphosphine (PPh_3) (**Figure 1.14.**) play a leading role, where the first is a hydrophilic phosphine ($\text{LogP} = -0.67$), while the second is a lipophilic one ($\text{LogP} = 4.82$).

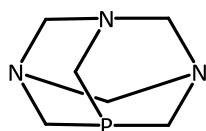


Figure 1.13. - Structure of PTA.

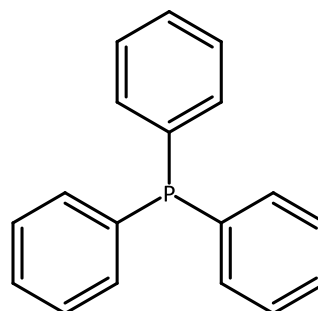


Figure 1.14. - Structure of PPh_3 .

1.2.3. C-donor ligands: N-Heterocyclic Carbenes

N-Heterocyclic Carbenes (NHCs) have attracted attention in the past two decades and their chemistry has been studied and understood. The main advantages are their applicability and versatility (Figure 1.15.).

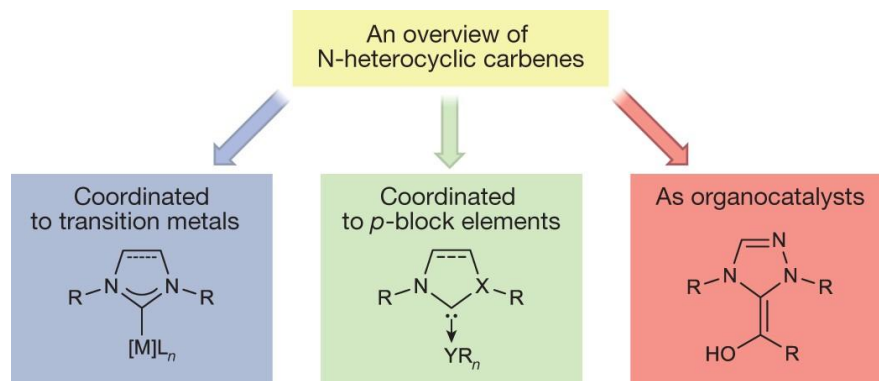


Figure 1.15. - Examples of the NHCs reactivity.

Their first applications were introduced almost in the beginning of the 20th century by the work of Tschugajeff's research group.^[32] Only three decades ago, NHCs were characterised as a class of compounds by, firstly, Arduengo's work and, secondly, by the huge research efforts in their activity as promising ligands for the homogeneous catalysis.^[33,34]

Most NHCs are based on five-membered heterocycles, such as imidazole and imidazoline derivatives. Nowadays, a correct and standard representation about them is not fully recognized and, thus, different versions are found in literature: however, the most accurate one displays the charges.^[35]

According to Molecular Orbitals theory (MO theory), NHCs are σ -basic and π^* -acids ligands: they have a lone electron pair in a high energy σ orbital, which gives them a greater σ -donor character (higher basicity) with respect to phosphanes;^[36,37] the presence of an empty low-energetic π^* orbital is fundamental for this property because it gives to NHCs the electron-acceptor character. This is important because they can accept the electrons from the filled d orbitals of the metals in $d \rightarrow \pi^*$ back donation process.^[38] In the presence of an electron-deficient metal, this class of compounds can also show $\pi \rightarrow d$ donation.^[39-41] The electronic properties of the N-heterocyclic carbenes can be tailored by different means: changing N-substituent groups or varying the substituents on C atoms of the NHC skeleton.

The steric effect on NHCs is one of the critical aspects to consider: however, differently from phosphanes, they present a local C₂ symmetry axis. As a consequence, the Tolman cone angle cannot be employed for NHC ligands.^[42] An useful value was introduced to solve the problem: it

is called "percent buried volume" (%V_{Bur}) and it describes the fraction of the volume of the first coordination sphere around the metal occupied by a certain ligand.^[43]

NHCs based on imidazole-2-ylidene and imidazoline-2-ylidene were synthesized and reported in literature.^[44] These NHCs derivatives are characterized by the presence of only organic substituents on the nitrogen atoms. The substitution of one of these groups by boranes leads to NHCs borate anions (NHC-BR₃⁻) which are anionic analogues of the neutral imidazole-2-ylidenes (**Figures 1.16.** and **1.17.**).

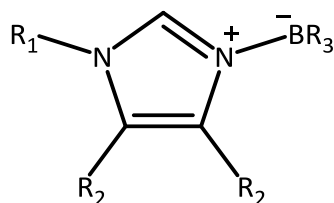


Figure 1.16.
General structure of NHC-BR₃.
(R = H, alkyl or aryl group.)

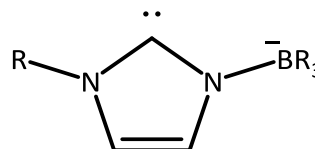


Figure 1.17.
General structure of deprotonated NHC-BR₃.
(R = H, alkyl or aryl group.)

The formation of isomers is the main result derived from the various efforts of deprotonation reactions of different imidazoles and benzimidazoles because of the ring closure caused by rapid intramolecular nucleophilic aromatic substitution.^[45] Additionally, Contreas's work describes the imidazoboles synthesis by H₂ elimination from (N-alkylimidazolium)borate species with iodine at high temperature.^[46]

A special attention is given to functionalized imidazole-based NHCs due to their versatility in tuning properties and environment at coordinated metal. Fehlhammer's work primarily described the synthesis of tris(3-methylimidazolin-2-ylidene-1-yl)borate with the topology of Trofimenko's scorpionates, where BH groups connect the carbene units.^[47] In the last decade, Santini and Pelli's research group developed new several complexes of coinage metals NHCs from different precursors, like [HB(RImH)₃]Br₂ (R = benzyl, mesityl or t-butyl), [H₂N(HTz^{Bn})₂]Br, H₂C(HIm^R)₂ and H₂C(HTz^R)₂ (HIm = imidazole, HTz: 1,2,4-triazole, R = (CH₂)₂COO⁻ or (CH₂)₃SO₂⁻).^[48-50]

1.3. Anticancer complexes

Medicinal inorganic chemistry offers additional opportunities for the design of drugs not accessible to organic compounds.^[51] The wide range of coordination numbers and geometries, several available oxidation states, kinetic and thermodynamic properties and intrinsic

characteristics of the metal cation offer to the medicinal inorganic chemists a large variety of possibilities during the process of the drug discovery.^[52]

The huge success of *cis*-diamminedichloroplatinum(II) (CDDP or, more commonly and simply, cisplatin), the first approved metal-based drug for the treatment of several types of tumors, placed the coordination chemistry of the transition metals in the frontline in the fight against cancer.^[53] Although highly effective to treat a big number of solid cancers, the cure with cisplatin causes heavy side effects (neurotoxicity, nephrotoxicity and ototoxicity, just to name a few)^[54] and inherited or acquired resistance phenomena, only partially solved by the use of new platinum-based drugs.^[55] These problems have stimulated an extensive research and the development of alternative strategies based on other transition metals with improved pharmacological properties.^[56] Once reached the cell, cisplatin binds the DNA and the impossibility for the cell to fix the damages leads to the programmed cell death, by means of the apoptosis pathway.

In this field, copper complexes have shown encouraging perspectives and they have been investigated on the assumption that a metal that the body is able to manage could be less toxic for the healthy cells with respect to the cancer ones. However, copper could also be toxic due to its redox activity and the affinity for binding sites that should be occupied by other essential metals. The altered metabolism of copper in the cancer cells and the different response between normal and tumor cells are the basis for the development of copper complexes endowed with selected antineoplastic characteristics.^[52] Interest in the field of copper complexes as anticancer drugs has rapidly grown in recent years, as illustrated by the increasing number of publications in **Figure 1.18**.^[57,58]

It is important to highlight that, for the success of the metal-based anticancer drugs, the chemical structure of the complex and the type of ligand donor atoms are crucial in order to modulate the hard/soft character of the metal, the lipophilic/hydrophilic balance of the resulting complexes and their solubility in the physiological medium as well as their ability to permeate the lipid bilayer of the cell membrane. Other important aspects that should be considered in the design of copper compounds include their stability toward transchelation reactions with physiological molecules (free amino acids, peculiar peptide sequences or whole proteins). These processes may sometimes preclude the expected tumor targeting or, on the contrary, might sometimes facilitate the cellular internalization of the metal!^[59,60]

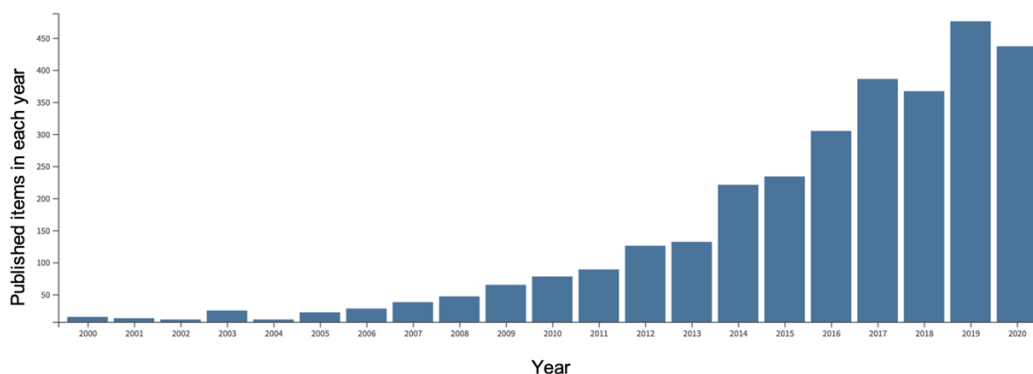


Figure 1.18. - Number of articles in Web of Science on the topic "copper and anticancer" from 2000 to 2020.

In order to fight cancers, two general strategies can be followed: subtract to the carcinoma the substances essential for its growth, development and metastasis (indirect approach) or assume agents able to kill cancerous cells (direct approach).

Since copper is an essential element for human body, neither the healthy cells nor the diseased ones can survive without this metal. In addition, in several *ex vivo* cancer tissues (such as breast, prostate, lung and brain) the copper concentration was found to exceed that of the normal cells, up to 1.7 times more (especially in the breast tumor), even if the exact molecular mechanisms that leads to this abnormal level are not completely clear.^[61]

One of the explanations of the high content of copper in carcinomas is the fact that this metal plays a central role as cofactor in the angiogenesis, which is the set of complex processes that lead to the formation of new blood vessels from the existing ones.^[62] For this reason, according to the point of view of the above mentioned indirect approach, a good strategy to block the tumor growth and its invasion may be the chelation of copper, although only the high demanding cancer would be attacked or attenuated in this way.^[63] With this aim, small molecules with high copper binding ability were synthesized^[64] and, among them, trientine (trien), D-penicillamine (D-pen) and tetrathiomolybdate (TM) are worthy of mention. They actually act as chelating ligands toward copper atoms and *in vivo* studies employing mice have demonstrated a significant inhibition of the tumor growth associated with the suppression of angiogenesis;^[65] in particular TM was also selected for clinical trials in humans.^[66] Even if copper chelators were recognized as potential therapeutic agents for the treatment of some types of cancer, their clinically approved use has generally been restricted only to patients with heavy metal poisoning or diseases with severe metal accumulation (for example Wilson disease).

On the other hand, according to the point of view of the direct approach, in a reverse and alternative anticancer strategy, tumor cells can represent a suitable and selective target for

copper-based anticancer compounds. In particular, because of the increased need of the diseased cells for this metal, they can be more exposed to the antitumor effect of chemical entities containing copper (**Figure 1.19.**).

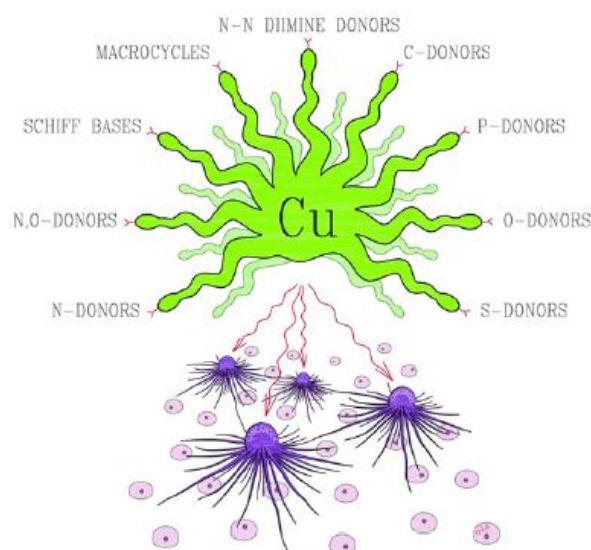


Figure 1.19.

Main classes of ligands that can coordinate copper in order to obtain compounds with anticancer activity.

Copper forms a rich variety of complexes in its +1 and +2 oxidation states, but the coordination chemistry of copper is dominated by Cu(II) derivatives with little, but important, examples of Cu(I) compounds. An important characteristic of the Cu(I) or Cu(II) complexes is their less structural predictability than other first-row transition metal complexes.

The redox potential of the physiologically accessible Cu(I)/Cu(II) couple changes a lot according to the ligand environment due to donor atoms, geometry, electronic and steric effects of the substituents.^[67] In addition, the possibility to release coordinating groups ongoing, for example, from octahedral Cu(II) to tetrahedral Cu(I) species, are chemical factors that demonstrate the complexity of the Cu(I)/Cu(II) system in physiological media.^[68]

Copper species showed to possess a broader spectrum of activity and a lower toxicity than platinum drugs. These features are consistent with the hypothesis that copper complexes possess mechanism(s) of action different from platinum compounds that covalently bind the DNA. However, little information is available regard the molecular basis for the mode of action of these compounds. Most the investigations is focused on the ability of these complexes, or fragments of them, to interact with DNA. However, other cellular constituents, such as topoisomerases or the proteasome multiprotein complex are emerging as new possible targets.

Copper was found to possess high DNA binding affinity since 1969,^[69] analogously to what was widely illustrated for cisplatin,^[70] bounding a guanine residue. This bond is dependent on

copper complex size, electron affinity and geometry of the formed adduct, inducing an irreversible modification of the DNA conformational structure. Several copper derivatives were found capable to interact with DNA double helix in a noncovalently way, rather than forming covalent adducts. The noncovalent DNA interactions include intercalative, electrostatic and/or groove bindings of metal complexes. In most cases, the metal acts as an inorganic modifier of the organic backbone.

Topoisomerases (Topos) are essential nuclear enzymes that play fundamental functions in DNA replication and transcription and their inhibitors are central components in many therapeutic regimens. Topo I and Topo II were identified as clinically important targets for cancer chemotherapy because, blocking these enzymes, the cell cycle is stopped.^[71] There is still increasing interest focusing on the development of new kinds of drugs targeting human topoisomerases and the development of metal complexes as Topo I/II inhibitors. However, unlike that involving DNA, interaction of copper compounds with Topos is a relatively new field of research.

The proteasome is a large multiprotein complex that selectively modulates and degrades intracellular proteins and it is located in both the nucleus and the cytoplasm. The eukaryotic proteasome contains one core structure and two regulatory caps. The core is hollow and provides an enclosed cavity in which proteins are degraded. Each end of the core is associated with a regulatory subunit that contains multiple ATPase active sites and ubiquitin binding sites. In order to be recognized and processed by the proteasome, a protein needs to be linked to ubiquitin.^[72] After polyubiquitinated proteins have been recognized, they are transferred into the core that contains multiple peptidases, including the chymotrypsin-like (cleavage after hydrophobic residues), trypsin-like (cleavage after basic residues) and caspase-like (cleavage after acidic residues) activities.^[73] The proteasome is part of a major mechanism by which cells decompose unfolded proteins and regulate the concentration and the stability of particular proteins (among them, p53 is worthy to be highlighted because this protein is one of those responsible for preventing genome mutation and, therefore, tumor formation). The ubiquitin proteasome-dependent degradation system is essential for many cellular functions, including processes for carcinogenesis such as apoptosis, angiogenesis, proliferation and metastasis formation.^[74] It has been shown that cancer cells are more sensitive to proteasome inhibition than normal cells. Thus, targeting the ubiquitin-proteasome pathway has emerged as a good anticancer strategy,^[75] and the development of copper compounds that can act as proteasome inhibitors (i. e. as novel anticancer agents) is under intensive investigation. In particular,

proteasome was identified as the main molecular target for a series of copper(I) complexes with hydrophilic phosphine ligands (**Figure 1.20.**)^[76]

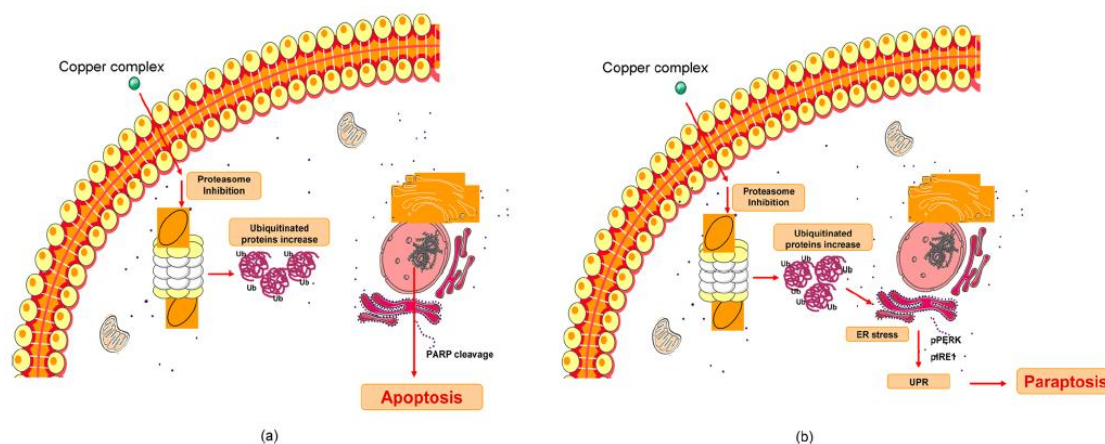


Figure 1.20. - Schematic diagrams of cellular pathways involved in proteasome inhibition induced by copper compounds: **(a)** apoptosis triggered by DTC copper(II) complexes; **(b)** paraptosis caused by phosphine copper(I) and thioxotriazole copper(II) complexes.

Although many different *in vitro* assays, both cell-based and molecular-target driven, have been used to identify lead compounds, the most common step following *in vitro* assays is efficacy assessments in animal tumor models. Actually, there are series of reports in the scientific literature describing *in vitro* cytotoxic activity investigations as no predictive assays of *in vivo* antitumor efficacy.^[77] Animal models have several advantages with respect to *in vitro* cell cultures, for example tumors develop vasculature and interaction with the stroma, therefore they allow a more realistic evaluation of toxicity and provide pharmacokinetic data of the agent. The typical development plan for an anticancer agent requires studies on preclinical models in which fundamental measures of antitumor effectiveness (such as the increase in the lifetime and/or tumor growth delay in tumor bearing mice) must be monitored, according to the standard protocols of the experimental evaluation of antitumor drugs. Despite huge interest in the development of copper-based compounds and the studies that have demonstrated that they are poorly toxic and highly active as antitumor drugs, there is still a paucity of studies regarding the *in vivo* antitumor activity of copper complexes, although several classes of Cu(I) and Cu(II) complexes showed to be very promising cytotoxic agents and for very few of them a remarkable *in vivo* activity has been demonstrated so far.

1.3.1. Copper complexes with bioconjugated heteroscorpionate ligands

An anticancer strategy based on copper complexes as chemotherapeutics can be pursued via design and synthesis of ligands to conjugate with selected bioactive molecules, able to coordinate Cu(I) or Cu(II).

A huge number of potential copper-based anticancer drugs can be prepared employing heteroscorpionate acetate ligands. In fact, the acetate group in this type of ligands can remain as it is (protonated or not) or it can undergo to several reactions or different functionalizations. When reactions take place with biologically active compounds, the obtained modified ligands are called "bioconjugated". These types of reactions are performed with the aim to synthesize complexes hopefully acting through synergistic mechanisms of action, due to the presence of copper and of a biomolecule (that can be accumulated inside the tumor cells or can interact with the overexpressed receptors in the cancer tissues) in the same chemical entity. Among the numerous classes of molecules with biological activity, for the bioconjugation can be chosen antibiotics (such as metronidazole), receptor antagonists (such as NMDA receptor antagonist) or antineoplastic agents (such as lonidamine).

1.3.1.1. Metronidazole

Nitroimidazoles are a class of hypoxia tracers that have been extensively investigated for hypoxia-selective cytotoxicity and hypoxic cell radiosensitisation *in vitro* and *in vivo*.^[78] The results showed that nitroimidazoles can be trapped in cells with low pO₂ values^[79] and the 2-nitroimidazole compounds, such as the [¹⁸F]fluoromisonidazole (¹⁸FMISO), were used for PET imaging of stroke, myocardium ischemia and tumor hypoxia.^[80] 2-Nitroimidazole cyclam derivatives radiolabelled with ^{99m}Tc, ⁶⁴Cu and ⁶⁷Cu were also investigated as potential PET/SPECT agents for tumor hypoxia.^[81] 4-Nitroimidazole-based thioflavin-T derivatives were synthesized, radiolabeled with iodine-131 and showed *in vitro* binding to viable hypoxic or aerobic tumor cells.^[82] Recently, bis(thiosemicarbazonato)copper(II)-nitroimidazole conjugates were successfully synthesized in their cold and ⁶⁴Cu radiolabelled forms.^[83] Nitroimidazole conjugates of bis(thiosemicarbazonato)copper(II) showed additive or synergistic selectivity for tumor hypoxia compared to their individual components. The 5-nitro derivatives of imidazole, in particular metronidazole (**Figure 1.21.**), have made their way to clinics and are accepted as

drugs against protozoa, parasite, bacterial infections, anaerobic bacteria and also for the radiosensitization of hypoxic tumors.

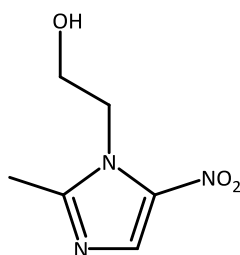


Figure 1.21. - Structure of metronidazole.

The efficiency of these molecules depends on the generation of the nitro radical anion^[84] by reduction, that makes 5-nitroimidazoles ready for entering into cells by passive diffusion, creating a favorable concentration gradient. Once inside the cell, the nitro radical anion interacts with DNA and disrupts the double helical structure and strands leading to cell death.^[85] Since 5-nitroimidazole derivatives are associated with some serious toxic side effects that require attention,^[86] efforts were done to modify their structure in a way that toxic side effects are controlled, but maintaining their efficacy in the modified form.^[87]

1.3.1.2. *N*-methyl-D-aspartate receptor antagonist

N-methyl-D-aspartate (NMDA) receptors (**Figure 1.22.**) are mainly present in neurons and play an important role in the development of central nervous system (CNS) for the generation of rhythms for breathing and locomotion and for the regulation of processes underlying learning, memory and neuron maturation.^[88,89] NMDA receptors belong to the family of ionotropic glutamate receptors and are cation channels with high calcium permeability, which are assembled by tetrameric combination of seven subunits (**Figure 1.23.**)^[90]



Figure 1.22.
Representation of the human NMDA receptor
(each subunit has a different color).

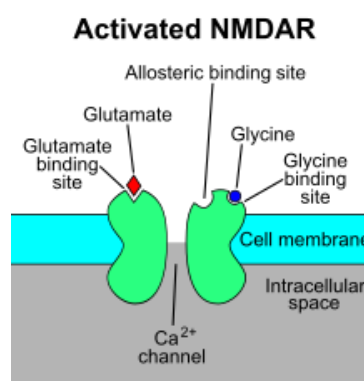


Figure 1.23.
Schematic representation of an
activated NMDA receptor (NMDAR).

Consequently, altered NMDA receptor expression and/or function (**Figure 1.24.**) is implicated in several neurological diseases and this misregulation can be due to the presence of an NMDA receptor antagonist (NMDA-ANT). NMDA receptors were also characterized for their surface expression and role in different types of cancer models.^[91] In particular, a subunit of the NMDA receptor is highly expressed in small-cell lung cancer, as well as in cancerous colon or prostate cancer cell lines, while its expression is very low or absent in normal prostate tissue and in benign prostate hyperplasia. Different combinations or single subunits of NMDA receptors were observed in colon, oral, lung, prostate and thyroid cancer cell lines, as well as in laryngeal, gastric, esophageal and hepatocellular carcinomas.^[92]

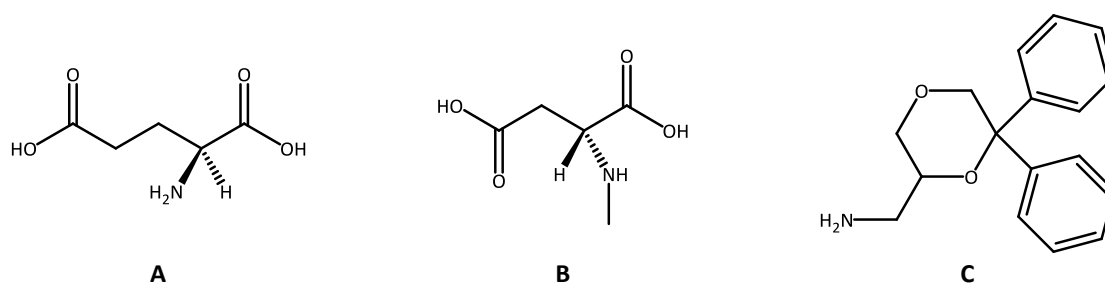


Figure 1.24. - Structure of: **A)** L-glutamic acid, the major physiological agonist of the main site of the NMDA receptor; **B)** NMDA, one of the endogenous agonists of the main site of the NMDA receptor; **C)** NMDA-ANT, an antagonist of the NMDA receptor.

1.3.1.3. Lonidamine

Lonidamine (LND) (**Figures 1.25.** and **1.26.**) is an antineoplastic drug able to sensitize tumors to radio-, chemo- and photodynamic-therapy.

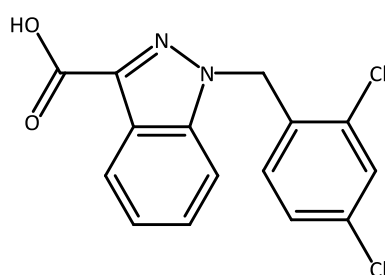


Figure 1.25. - Structure of Lonidamine.



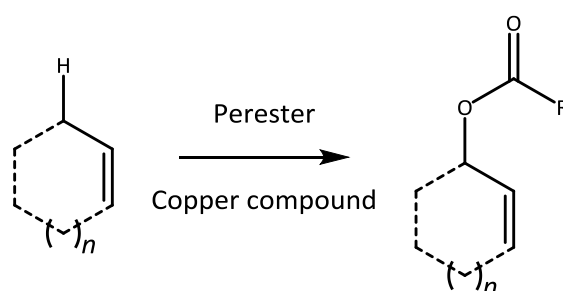
Figure 1.26. - Lonidamine.

Although its mechanism of action is not completely clear yet, its treatment was reported to affect the metabolic pathways of cancer cells, by inhibiting mitochondrial respiration and glycolysis.^[93-95] It has also been suggested that LND induces intracellular tumor acidification by inhibiting the efflux of L-lactic acid from cells mediated by monocarboxylate transporters and the mitochondrial uptake of pyruvate mediated by the mitochondrial pyruvate carrier.^[96]

Moreover, this drug induces a mitochondrial transmembrane potential disruption through a direct effect on the mitochondrial permeability transition pore.^[97] Although the antitumor activity of LND as a single agent is limited, this drug has a great potential in increasing the efficacy of traditional chemotherapeutic agents, including cisplatin and other platinum-based drugs.^[98] Platinum complexes conjugated with LND or its derivatives showed interesting antitumor activity profiles *in vitro*, with improved cytotoxic effects compared to cisplatin and other reference drugs.^[99]

1.4. Copper-based catalysts for Kharasch-Sosnovsky reaction

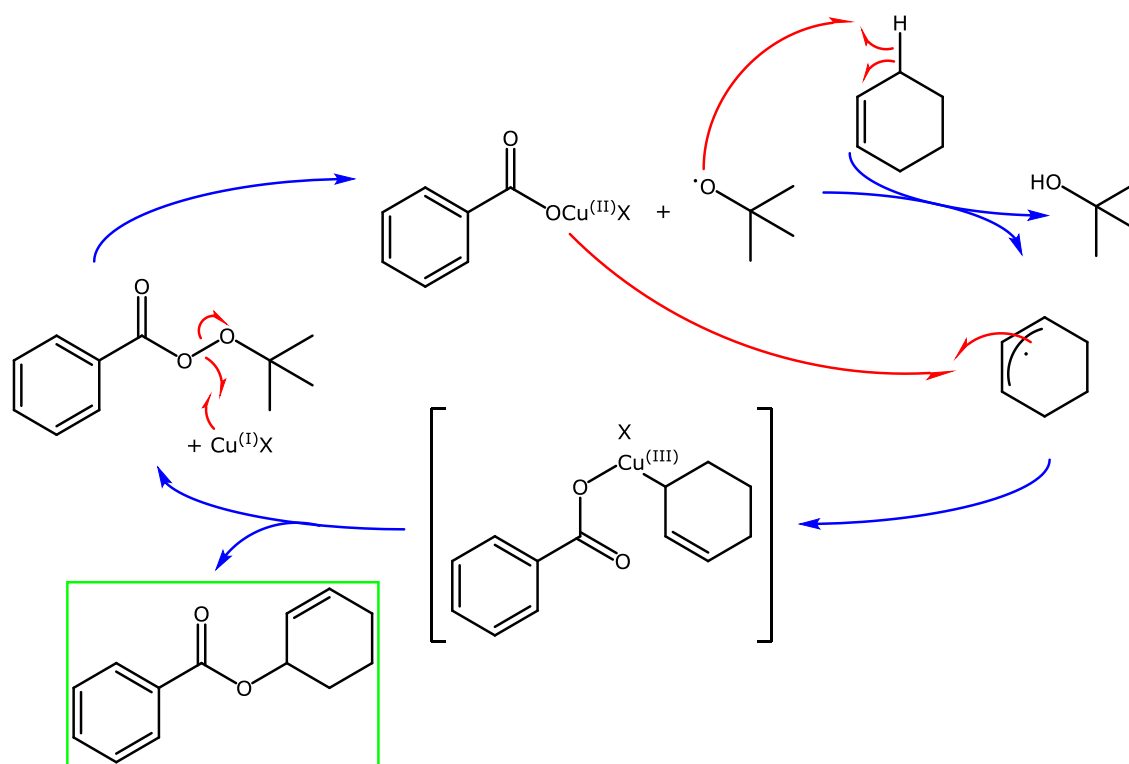
In the last decades, the research about innovative and catalytic metal complexes for the synthesis of functionalized intermediates has grown a lot. Among the most studied reaction there is the allylic oxidation of alkenes.^[100,101] This type of reactions allows the synthesis of highly functionalized products, such as carboxylic acids, alcohols, aldehydes, ketones and epoxides, which are useful and important starting materials for industrial applications.^[102] One of the most applied synthetic method for this aim is the Kharasch-Sosnovsky reaction, which consists in a radical oxidation of an alkene to an allylic protected alcohol, using a copper compound as catalyst and a perester as oxidant agent, leaving the double bond in its original position. Its name comes from the Ukrainian chemist Morris S. Kharasch and the Russian chemist George Sosnovsky: they are the first scientists that studied this particular reaction in 1958 (**Scheme 1.1.**).^[103-105]



Scheme 1.1. - General Kharasch-Sosnovsky reaction.

The main disadvantage of Kharasch-Sosnovsky reaction is the lack of a general approach due to issues like overoxidation, long reaction time, poor compatibility with other functional groups, superstoichiometric amounts of olefins. Several compounds of Se, Cr, Pd, Rh and Cu were also employed as catalysts in this reaction.^[106] Copper sources can be of different origin, from Cu(I) (CuBr, CuCl, Cu₂O) or Cu(II) salts (CuO, Cu(OAc)₂) to more substituted copper complexes. The

precise mechanism of the reaction is quite complex because no direct relationship between copper salt and ligand has been discovered (**Scheme 1.2.**)^[107]



Scheme 1.2. - Supposed mechanism of the catalytic cycle of the Kharasch-Sosnovsky reaction.

Copper(II) salts, due to their stability and handling safety, are suitable catalysts for the Kharasch-Sosnovsky reaction. However, performing the reaction with Cu(I) complexes higher and more reproducible yields can be obtained but, in turn, Cu(II) needs the presence of an external reducing agent, usually phenylhydrazine (PhNHNH_2).^[108] The increase in interest and application of copper-catalysed organic reactions has increased recently because copper is an earth-abundant metal and, as a consequence, the main advantages of its use are the cost effectiveness and sustainability.^[109] According to the literature, studies on the catalytic activity of Cu(II) complexes with bis(pyrazoyl)acetates are unknown, despite the huge research work based on poly(azoyl)acetates (mainly focused on the anticancer activity, rather than the catalytic one).

2. Experimental part

2.1. Methods and materials

All the reagents and solvents were purchased from chemical suppliers and used without further purifications.

Melting points (MP) were obtained by an SMP3 Stuart Scientific Instrument (Bibby Sterilin Ltd., London, UK).

Elemental analyses (EA) (C, H, N, S) were performed by a Fisons Instruments EA-1108 CHNS-O Elemental Analyzer (Thermo Fisher Scientific Inc., Waltham, MA, USA).

Fourier-transform infrared (FT-IR) spectra of the powder samples (with the unique exception of the oily compound **8**) were recorded from 4000 to 200 cm^{-1} by a PerkinElmer Frontier Instrument (PerkinElmer Inc., Waltham, MA, USA), equipped with attenuated total reflection (ATR) unit using universal diamond top-plate as sample holder. Abbreviations used in the analyses of the FT-IR spectra: m = medium, mbr = medium broad, s = strong, sbr = strong broad, sh = shoulder, vb = very broad, vs = very strong, vw = very weak, w = weak, wbr = weak broad.

Nuclear magnetic resonance (NMR) spectra for the nuclei ^1H , ^{13}C , ^{31}P and ^{11}B were recorded by an Oxford AS400 Varian Spectrometer (Agilent Technologies Inc., Santa Clara, CA, USA) (400.4 MHz for ^1H , 100.1 MHz for ^{13}C , 162.1 MHz for ^{31}P and 128.4 MHz for ^{11}B) or by a Bruker 500 Ascend Spectrometer (Bruker BioSpin Corporation, Billerica, MA, USA) (500.1 MHz for ^1H , 125 MHz for ^{13}C , 202.4 MHz for ^{31}P and 160.5 MHz for ^{11}B). The chemical shifts (δ) were reported in ppm. Abbreviations used in the analyses of the NMR spectra: br = broad, d = doublet, dbr = doublet broad, hept = heptet, m = multiplet, q = quartet, qbr = quartet broad, s = singlet, sbr = singlet broad, t = triplet, tbr = triplet broad.

Electrospray ionization mass spectra (ESI-MS) were recorded in positive- (ESI-MS(+)) or negative-ion (ESI-MS(-)) mode by a Waters Micromass ZQ Spectrometer equipped with a single quadrupole (Waters Corporation, Milford, MA, USA), using water, methanol or acetonitrile as mobile phase. The compounds were added to water, methanol or acetonitrile to give solutions of approximately 0.1 mM, which were injected (1 μL) into the spectrometer fitted with an autosampler. The pump delivered the solutions to the mass spectrometer source at a flow rate of 200 $\mu\text{L}/\text{min}$ and nitrogen was employed both as drying and nebulizing gas. Capillary voltage was typically 2500 V. The temperature of the source was 100 $^\circ\text{C}$, while the temperature of the desolvation was 400 $^\circ\text{C}$. In the analyses of ESI-MS spectra, the confirmation of the main peaks

was supported by comparison of the observed and predicted isotopic distribution patterns, the latter calculated using the IsoPro 3.1 computer software (T-Tech Inc., Norcross, GA, USA).

Gas chromatography-mass spectra (GC-MS) analyses were obtained on an Agilent GC(6850N)/MS(5973N) (Stevens Creek Blvd, Santa Clara, CA, USA), using the electronic impact (EI) technique (70 eV), a GC/MSD software and an HP-5MS column (30 m, Id 0.25 μm , film thickness 0.25 μm).

Synchrotron radiation-induced X-ray photoelectron spectroscopy (SR-XPS) measurements were performed at the materials science beamline (MSB) at the Elettra synchrotron radiation source (Trieste, Italy). MSB is placed at the left end of the bending magnet 6.1 and it is equipped with a plane grating monochromator that provides light in the energy range of 21-1000 eV. The base pressure in the UHV end-station is of $2 \cdot 10^{-10}$ mbar; the end-station is equipped with: SPECS PHOIBOS 150 hemispherical electron analyser, low-energy electron diffraction optics, a dual-anode Mg/Al X-ray source, an ion gun and a sample manipulator with a K-type thermocouple attached to the rear side of the sample. For this experiment, photoelectrons emitted by C1s, N1s, Cl2p, Cu2p, O1s core levels at normal emission geometry were detected. A photon energy of 650 eV impinging at 60° was selected for all signals, with the aim to maximise especially N1s signal intensity; Cu2p spectra were also collected using the Al K- α anode source (1487.0 eV) to maximize its photoemission signal. Charging correction of binding energies (BEs) was always performed using the aromatic C1s as a reference (BE 284.70 eV). To fit core-level spectra, a Shirley background was subtracted and then Gaussian peak functions were used as signal components. The BE resolution was 0.6 eV for the measured core levels.

Near edge X-ray absorption fine structure (NEXAFS) spectroscopy experiments were performed at the Elettra storage ring at the bending magnet for emission absorption and reflectivity (BEAR) beamline, installed at the left exit of the 8.1 bending magnet exit. The apparatus is based on a bending magnet as a source, a beamline optics delivering photons from 5 eV up to about 1600 eV with selectable degree of ellipticity. The carbon and nitrogen K-edge spectra were collected at grazing (20°), magic (54.7°) and normal (90°) incidence angles of the linearly polarized photon beam with respect to the sample surface. The photon energy and resolution were calibrated and experimentally tested at the K absorption edges of Ar, N₂ and Ne. The normalization procedure consists of three steps: (1) the energy calibration, in which the I_0 reference current (drain current) of the sample is shifted on the I_0 reference current (drain current) of the Au clean sample recorded; (2) the signal is obtained by the double ratio

$(I_{\text{sample}}/I_{0_{\text{sample}}})/(I_{\text{Au}}/I_{0_{\text{Au}}})$ after the interpolation of each signal to the Au reference. The double ratio allows to correct for variations of the incident X-ray intensity with time as a function of photon energy due to instabilities of the electron beam in the storage ring or to changes of the X-ray optics in the beamline; (3) finally the signal is reduced to the standard form through a pre-edge and post-edge fit: a linear pre-edge background is subtracted from the data and a linear post-edge fit is applied to the post-edge region to evaluate the jump and obtain the normalized signal.

The X-ray absorption fine structure (XAFS) experiments were performed at the XAFS beamline of the Elettra synchrotron at the Cu K-edge ($E_{\text{Cu}} = 8980$ eV) in transmission geometry at room temperature (complexes **9**, **43**, **45**, **46**, **63** and **66**) and at the B18 beamline of the Diamond Light Source (UK) (complex **65**). The Cu-complexes **9**, **43**, **45**, **46**, **63** and **66** were dried, mixed with light elements inert PVP matrix (in which the weight ratio between the PVP matrix and the Cu complex sample was approximately 5:1) and pressed in highly homogeneous, easy-to-handle pellets suitable for high quality XAS spectra. Complex **65** was measured in the fluorescence geometry using a 36 element Ge detector. The sample was homogeneously mixed with boron nitride, pressed into a pellet and measured at 77 K using a liquid nitrogen cryostat. The X-ray absorption spectroscopy (XAS) spectra were carried out in the near edge (XANES) and in the extended (EXAFS) regions. The raw data were treated following the standard procedures for pre-edge background subtraction and edge jump normalization to obtain the normalized absorption coefficients $\mu(E)$. The structural signals $\chi(k)$ in the extended region (EXAFS) were calculated as $\chi(k) = (\mu - \mu_0)/\mu_0$, where μ_0 is the bare atom post-edge absorption background calculated using polynomial splines through the post-edge absorption signal, $k = \sqrt{\frac{2m_e}{\hbar^2}(E - E_{\text{Cu}})}$ is the photoelectron wavevector. The XANES and EXAFS regions of the spectra may get access to complementary information about the average electronic structure, local coordination chemistry and local atomic structure around the absorbers: the XANES analysis provides information about the electronic structure and the local coordination geometry around the average Cu absorber in the sample. It was carried out by comparing the experimental spectra of the complexes with the features of Cu compounds from reference samples and literature. Further details were obtained from *ab initio* simulation of XANES spectra using FEFF 8.2 program with the Hedin-Lundqvist model for the exchange-correlation potential calculated in self consistent mode. This allowed to individuate how geometrical modification of the local atomic structure around the Cu absorber induce changes in the XANES

spectral features. The more quantitative EXAFS data analysis allows to understand details about the local structure around the absorber and it was performed with the FitEXA program assuming a Gaussian distribution of neighbor shells through the standard EXAFS formula. A non-linear least square data refinement procedure was used to minimize the k^2 weighted sum of square differences between the experimental EXAFS data χ and the model χ^{th} function. The $\chi^{th} = \sum_i \chi_i^{th}$ is modeled as the sum of partial contributions (shells) χ_i^{th} defined by three structural parameters, which are the average coordination distance R_i , the mean square relative displacement σ_i^2 and the multiplicity number N_i : $\chi_i^{th} = \frac{A_i}{kR_i^2} \sin(2kR_i - \varphi_i) e^{-2\frac{R_i}{\lambda}} e^{-2k^2\sigma_i^2}$. The amplitude A_i , the phase shift φ_i and the mean free path λ functions were calculated using FEFF 8.2 program for atomic clusters based on the expected geometry of the Cu-complexes.

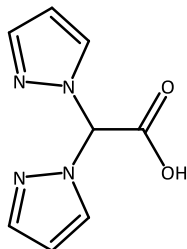
2.2. Syntheses of ligands

2.2.1. Syntheses of acid ligands

2.2.1.1. Synthesis of (Pz)₂CH(COOH) (L^{1H}, 1)

In a round-bottom flask, dichloroacetic acid (Cl₂CHCOOH; 128.942 g/mol, 24.375 mmol, 3.143 g) was dissolved in tetrahydrofuran (THF; 250 mL). Then, potassium hydroxide (KOH; 56.106 g/mol, 97.500 mmol, 5.470 g), potassium carbonate (K₂CO₃; 138.206 g/mol, 97.500 mmol, 13.475 g), pyrazole (Pz; 68.077 g/mol, 48.750 mmol, 3.319 g) and tetra-*n*-butylammonium bromide (TBAB; 322.368 g/mol, 1.500 mmol, 0.484 g) were added, giving an opalescent mixture with a white suspension. TBAB was added as phase-transfer catalyst. The reaction was carried out under magnetic stirring at reflux for 24 hours and the reaction color changed from white to yellow to slightly pink. At the end, the solvent was dried at reduced pressure and the obtained brown-orange residue was solubilized in water (H₂O; about 50 mL). The brown solution was acidified to neutral pH (about 7-7.5) by addition of hydrochloric acid (HCl; 6 M, about 20 mL) and it was extracted with diethyl ether (Et₂O; 3 x 50 mL). The yellowish aqueous phase was further acidified to acid pH (about 2) by addition of HCl (6 M, about 20 mL) and it was vigorously stirred at room temperature for 10-15 minutes, observing the formation of a white precipitate. The obtained precipitate was recovered by filtration, poured into a separatory funnel and dissolved in THF (50 mL). Et₂O (150 mL) was also added into the separatory funnel, in order to improve the separation between organic and aqueous phase.

Extractions with H₂O (3 x 25 mL) were performed, to purify the product from potassium chloride (KCl). The organic phase was collected into a flask and anhydrous sodium sulfate (Na₂SO₄) was added to remove moisture. The mixture was filtered and the organic phase was dried at reduced pressure to give the white solid ligand (Pz)₂CH(COOH) (L^{1H}, **1**) in 82% yield.

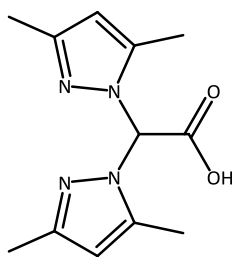


Molar mass (MM): 192.175 g/mol. **Solubility:** methanol (MeOH), ethanol (EtOH), THF, acetonitrile (MeCN), dimethyl sulfoxide (DMSO), acetone (Me₂CO). **MP:** 164-167 °C. **¹H-NMR** ((CD₃)₂CO, 293 K): δ 6.35 (t, 2H, 4-CH), 7.46 (s, 1H, CHCO), 7.57 (d, 2H, 5-CH), 7.99 (d, 2H, 3-CH), 12.01 (br, 1H, COOH). **¹³C{¹H}-NMR** ((CD₃)₂CO, 293 K): δ 74.13 (CHCO), 106.43 (4-C_{Pz}), 130.50 (5-C_{Pz}), 140.10 (3-C_{Pz}), 165.21 (CO). **FT-IR** (cm⁻¹): 3177w, 3149w, 3131w, 3108w, 2977w (C-H); 2457wbr (O-H); 1824wbr; 1722m (ν_{asym} C=O); 1518m (C=C/C=N); 1446w, 1435w, 1403m, 1392s, 1352m, 1318w, 1291m, 1260vs, 1232s, 1223s, 1186m, 1171s, 1092s, 1059s, 1049s, 986m, 966mbr, 918m, 887w, 863m, 850m, 821s, 763vs, 752vs, 715vs. **ESI-MS(+)** (major positive ions, MeCN), *m/z* (%): 231 (100) [L^{1H} + K]⁺. **ESI-MS(-)** (major negative ions, MeCN), *m/z* (%): 147 (25) [(Pz)₂CH]⁻, 191 (100) [L¹]⁻. **EA** (%) calculated for C₈H₈N₄O₂: N 29.15, C 50.00, H 4.20; found: N 29.31, C 50.25, H 4.23.

2.2.1.2. Synthesis of (Pz^{3,5-Me})₂CH(COOH) (L^{2H}, **2**)

In a round-bottom flask, Cl₂CHCOOH (128.942 g/mol, 24.375 mmol, 3.143 g) was dissolved in THF (250 mL). Then, KOH (56.106 g/mol, 97.500 mmol, 5.470 g), K₂CO₃ (138.206 g/mol, 97.500 mmol, 13.475 g), 3,5-dimethylpyrazole (Pz^{3,5-Me}; 96.130 g/mol, 48.750 mmol, 4.686 g) and TBAB (322.368 g/mol, 1.500 mmol, 0.484 g) were added, giving an opalescent mixture with a white suspension. TBAB was added as phase-transfer catalyst. The reaction was carried out under magnetic stirring at reflux for 24 hours and the reaction color changed from white to yellow. At the end, the solvent was dried at reduced pressure and the obtained yellowish residue was solubilized in H₂O (about 50 mL). The orange-yellow solution was acidified to neutral pH (about 7-7.5) by addition of HCl (6 M, about 20 mL) and it was extracted with Et₂O (3 x 50 mL). The yellowish aqueous phase was further acidified to acid pH (about 2) by addition of HCl (6 M, about 20 mL) and it was vigorously stirred at room temperature for 10-15 minutes, observing the formation of a white precipitate. The obtained precipitate was recovered by filtration, poured into a separatory funnel and dissolved in THF (50 mL). Et₂O (150 mL) was also added into the separatory funnel, in order to improve the separation between organic and aqueous phase. Extractions with H₂O (3 x 25 mL) were performed, to purify the product from KCl. The

organic phase was collected into a flask and anhydrous Na_2SO_4 was added to remove moisture. The mixture was filtered and the organic phase was dried at reduced pressure to give the white solid ligand $(\text{Pz}^{3,5\text{-Me}})_2\text{CH}(\text{COOH})$ ($\text{L}^{2\text{H}}$, **2**) in 78% yield.



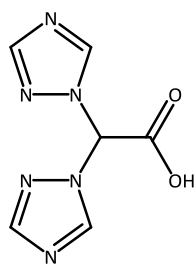
MM: 248.281 g/mol. **Solubility:** MeOH, EtOH, THF, CH_2Cl_2 , CHCl_3 , MeCN, DMSO, Me_2CO . **MP:** 174-177 °C. **$^1\text{H-NMR}$** (CDCl_3 , 293 K): δ 2.21 (s, 6H, 3- or 5- CH_3), 2.27 (s, 6H, 3- or 5- CH_3), 5.92 (s, 2H, 4- CH), 6.92 (s, 1H, CHCO), 9.32 (br, 1H, COOH). **$^{13}\text{C}\{^1\text{H}\}\text{-NMR}$** (CDCl_3 , 293 K): δ 11.22 (5- CCH_3), 13.03 (3- CCH_3), 70.78 (CHCO), 107.91 (4- C_{Pz}), 142.59 (5- C_{Pz}), 148.71 (3- C_{Pz}), 164.92 (CO). **FT-IR** (cm^{-1}): 2967w, 2926w, 2856wbr (C-H); 2446wbr (O-H); 1739m ($\nu_{\text{asym}} \text{C=O}$); 1562m (C=C/C=N); 1443w, 1415m, 1378m, 1367m, 1345m, 1319m, 1266m, 1229s, 1161m, 1148m, 1116m, 1041m, 1030sh, 975m, 946m, 890m, 828m, 814m, 808m, 788m, 766m, 725m, 706vs. **ESI-MS(+)** (major positive ions, MeCN), m/z (%): 249 (30) [$\text{L}^{2\text{H}} + \text{H}$] $^+$, 271 (100) [$\text{L}^{2\text{H}} + \text{Na}$] $^+$. **ESI-MS(-)** (major negative ions, MeCN), m/z (%): 203 (70) [$(\text{Pz}^{3,5\text{-Me}})_2\text{CH}$] $^-$, 247 (100) [$\text{L}^{2\text{H}}$] $^-$. **EA** (%) calculated for $\text{C}_{12}\text{H}_{16}\text{N}_4\text{O}_2$: N 22.57, C 58.05, H 6.50; found: N 22.56, C 58.00, H 6.46.

2.2.1.3. Synthesis of $(\text{Tz})_2\text{CH}(\text{COOH})$ ($\text{L}^{3\text{H}}$, **3**)

In a round-bottom flask, Cl_2CHCOOH (128.942 g/mol, 36.200 mmol, 4.668 g) was dissolved in THF (300 mL). Then, KOH (56.106 g/mol, 107.000 mmol, 6.003 g), K_2CO_3 (138.206 g/mol, 72.400 mmol, 10.006 g), 1,2,4-triazole (Tz; 69.067 g/mol, 72.400 mmol, 5.000 g) and TBAB (322.368 g/mol, 2.171 mmol, 0.700 g) were added. TBAB was added as phase-transfer catalyst. The reaction was carried out under magnetic stirring at reflux for 24 hours. At the end, the solvent was dried at reduced pressure, the obtained yellowish residue was solubilized in H_2O (about 50 mL) and stirred at room temperature for 15 minutes. The solution was acidified to acid pH (about 2) by addition of HCl (6 M, about 30 mL), the acid solution was washed with CHCl_3 (3 x 50 mL) and then the aqueous layer was dried at reduced pressure. Me_2CO (100 mL) was poured into the round-bottom flask and the obtained mixture was stirred at reflux for 1 hour. The mixture was filtered and the mother liquors were dried at reduced pressure. Finally, EtOH (50 mL) was poured into the round-bottom flask, the obtained mixture was stirred few minutes and filtered. The precipitate was washed with cold EtOH and dried at reduced pressure. The whitish solid ligand $(\text{Tz})_2\text{CH}(\text{COOH})$ ($\text{L}^{3\text{H}}$, **3**) was obtained in 53% yield.

MM: 194.154 g/mol. **Solubility:** H_2O , MeOH, DMSO, Me_2CO . **MP:** 177-179 °C. **$^1\text{H-NMR}$** (D_2O , 293 K): δ 7.53 (s, 1H, CHCO), 8.16 (s, 2H, 3- or 5- CH), 8.97 (s, 2H, 3- or 5- CH). **$^{13}\text{C}\{^1\text{H}\}\text{-NMR}$** (D_2O , 293 K): δ 72.11 (CHCO), 145.35 (3- or 5- C_{Tz}), 150.18 (3- or 5- C_{Tz}), 165.50 (CO). **FT-IR** (cm^{-1}):

3137w, 3118w, 2992w (C-H); 2404wbr (O-H); 1701mbr (ν_{asym} C=O); 1544m, 1501m (C=C/C=N);

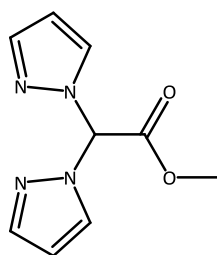


1419m, 1359m, 1276s, 1219m, 1184s, 1159s, 1125s, 1080sh, 1005vs, 947m, 877s, 862s, 826vs, 741vs. **ESI-MS(+)** (major positive ions, H₂O), m/z (%): 195 (100) [L^{3H} + H]⁺. **ESI-MS(-)** (major negative ions, H₂O), m/z (%): 149 (100) [(Tz)₂CH]⁻, 193 (40) [L³]⁻. **EA** (%) calculated for C₆H₆N₆O₂: N 43.29, C 37.12, H 3.12; found: N 41.76, C 37.09, H 3.09.

2.2.2. Syntheses of esterified ligands

2.2.2.1. Synthesis of (Pz)₂CH(COOMe) (L^{1Me}, **4**)

In a round-bottom flask, ligand L^{1H} (**1**; 192.175 g/mol, 5.000 mmol, 0.961 g) was solubilized in MeOH (50 mL), giving a colorless solution, and stirred for 30 minutes slightly warming to promote the complete solubilization. Then, concentrated sulfuric acid (H₂SO₄; 98% V/V, 1 mL) was added. The reaction was carried out under magnetic stirring, at reflux, for 24 hours. At the end, the solvent was dried at reduced pressure. The yellow oily residue was treated with a saturated solution of sodium bicarbonate (NaHCO₃; about 50 mL) until a basic pH (about 8) was reached, with subsequent formation of CO₂ and of a white to yellowish precipitate. At this point, the mixture was collected in a separatory funnel and the extractions were performed with CH₂Cl₂ (3 x 50 mL), in order to isolate the product from the aqueous solution. The organic phase was collected into a flask and anhydrous Na₂SO₄ was added to remove moisture. The mixture was filtered and CH₂Cl₂ was dried at reduced pressure, to give the whitish solid ligand (Pz)₂CH(COOMe) (L^{1Me}, **4**) in 67% yield.



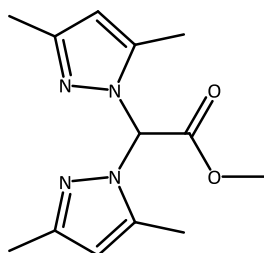
MM: 206.201 g/mol. **Solubility**: MeOH, EtOH, Et₂O, THF, CH₂Cl₂, CHCl₃, ethyl acetate (EtOAc), MeCN, DMSO, Me₂CO. **MP**: 90-93 °C. **¹H-NMR** (CD₃CN, 293 K): δ 3.81 (s, 3H, OCH₃), 6.36 (t, 2H, 4-CH), 7.30 (s, 1H, CHCO), 7.58 (d, 2H, 5-CH), 7.84 (d, 2H, 3-CH). **¹H-NMR** (CDCl₃, 293 K): δ 3.87 (s, 3H, OCH₃), 6.35 (t, 2H, 4-CH), 7.15 (s, 1H, CHCO), 7.61 (d, 2H, 5-CH), 7.75 (d, 2H, 3-CH). **¹³C{¹H}-NMR** (CD₃CN, 293 K): δ 53.33 (OCH₃), 74.19 (CHCO), 106.97 (4-C_{Pz}), 130.48 (5-C_{Pz}), 140.59 (3-C_{Pz}), 165.27 (CO). **¹³C{¹H}-NMR** ((CD₃)₂CO, 293 K): δ 53.10 (OCH₃), 74.37 (CHCO), 106.84 (4-C_{Pz}), 130.65 (5-C_{Pz}), 140.47 (3-C_{Pz}), 165.39 (CO). **FT-IR** (cm⁻¹): 3149w, 3123m, 2991w, 2956w, 2854w

(C-H); 1753vs (ν_{asym} C=O); 1622wbr, 1519m (C=C/C=N); 1445s, 1434s, 1388vs, 1372m, 1354m, 1329m, 1287s, 1265s, 1226s, 1211s, 1196s, 1183s, 1169s, 1087vs, 1052m, 1043s, 999s, 967sh, 958s, 922m, 914m, 892m, 850m, 810s, 762sh, 755vs. **ESI-MS(+)** (major positive ions, MeCN),

m/z (%): 139 (20) [(Pz)CH(COOMe)]⁺, 207 (5) [L^{1Me} + H]⁺, 229 (100) [L^{1Me} + Na]⁺. **EA** (%) calculated for C₉H₁₀N₄O₂: N 27.17, C 52.42, H 4.89; found: N 26.79, C 52.47, H 4.89.

2.2.2.2. Synthesis of (Pz^{3,5-Me})₂CH(COOMe) (L^{2Me}, 5)

This compound was prepared following the procedure described for L^{1Me} (**4**), starting from L^{2H} (**2**; 248.281 g/mol, 5.000 mmol, 1.241 g), to give the whitish solid ligand (Pz^{3,5-Me})₂CH(COOMe) (L^{2Me}, **5**) in 74% yield.



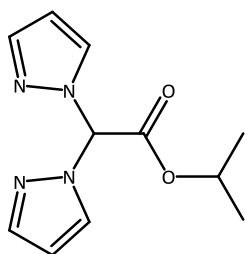
MM: 262.308 g/mol. **Solubility**: MeOH, CH₂Cl₂, CHCl₃, MeCN, DMSO, Me₂CO. **MP**: 105-110 °C. ¹H-NMR (CD₃CN, 293 K): δ 2.13 (s, 6H, 3- or 5-CH₃), 2.19 (s, 6H, 3- or 5-CH₃), 3.83 (s, 3H, OCH₃), 5.90 (s, 2H, 4-CH), 7.02 (s, 1H, CHCO). ¹H-NMR (CDCl₃, 293 K): δ 2.15 (s, 6H, 3- or 5-CH₃), 2.22 (s, 6H, 3- or 5-CH₃), 3.91 (s, 3H, OCH₃), 5.88 (s, 2H, 4-CH), 7.01 (s, 1H, CHCO).

¹³C{¹H}-NMR (CD₃CN, 293 K): δ 10.24 (3- or 5-CCH₃), 12.53 (3- or 5-CCH₃), 52.97 (OCH₃), 71.76 (CHCO), 106.86 (4-C_{Pz}), 141.16 (5-C_{Pz}), 148.29 (3-C_{Pz}), 165.64 (CO). ¹³C{¹H}-NMR (CDCl₃, 293 K): δ 11.28 (3- or 5-CCH₃), 13.20 (3- or 5-CCH₃), 53.65 (OCH₃), 72.26 (CHCO), 107.84 (4-C_{Pz}), 142.49 (5-C_{Pz}), 148.43 (3-C_{Pz}), 164.75 (CO). **FT-IR** (cm⁻¹): 3134w, 3104wbr, 3004sh, 2991wbr, 2955w, 2926w, 2855wbr (C-H); 1760s (ν_{asym} C=O); 1563m (C=C/C=N); 1455mbr, 1440m, 1416m, 1384m, 1377m, 1351m, 1334sh, 1323m, 1263s, 1231sbr, 1191sh, 1158m, 1138w, 1118w, 1036m, 1026m, 1002s, 974m, 954sh, 920w, 890m, 822m, 803m, 796s, 775s, 746m, 715m. **ESI-MS(+)** (major positive ions, MeCN), m/z (%): 263 (15) [L^{2Me} + H]⁺, 285 (100) [L^{2Me} + Na]⁺, 301 (15) [L^{2Me} + K]⁺. **EA** (%) calculated for C₁₃H₁₈N₄O₂: N 21.36, C 59.53, H 6.92; found: N 21.32, C 59.96, H 7.02.

2.2.2.3. Synthesis of (Pz)₂CH(COOⁱPr) (L^{1Pr}, 6)

In a round-bottom flask, ligand L^{1H} (**1**; 192.175 g/mol, 5.000 mmol, 0.961 g) and 4-dimethylaminopyridine (DMAP; 122.168 g/mol, 0.500 mmol, 0.061 g) were added to a solution of dry THF (30 mL) and 2-propanol (ⁱPrOH; 60.095 g/mol, 5.500 mmol, 0.331 g). The obtained mixture was cooled to 0 °C and left under magnetic stirring for 30 minutes. Subsequently, a solution of *N*-(3-dimethylaminopropyl)-*N'*-ethylcarbodiimide hydrochloride (EDCI·HCl; 191.702 g/mol, 6.000 mmol, 1.150 g) in dry THF (30 mL) was added drop by drop. The resulting mixture was left under magnetic stirring, at room temperature, for 24 hours. After that, THF was dried at reduced pressure, H₂O (30 mL) and CHCl₃ (30 mL) were poured into the round-bottom flask and the organic phase was further washed with H₂O (2 x 30 mL). The organic phase was

collected into a flask, anhydrous Na_2SO_4 was added to remove moisture, the obtained mixture was filtered and the organic phase was dried at reduced pressure. The crude residue was purified by chromatographic column (packed with SiO_2 ; elution with *n*-hexane:EtOAc 90:10, then 80:20 and finally 70:30). The final product was recovered and dried under reduced pressure. The white solid ligand $(\text{Pz})_2\text{CH}(\text{COO}^i\text{Pr})$ ($\text{L}^{1\text{iPr}}$, **6**) was obtained in 55% yield.

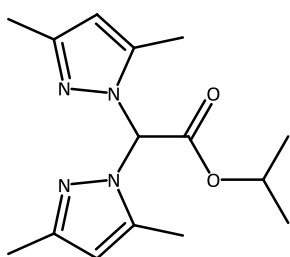


MM: 234.254 g/mol. **Solubility:** *n*-hexane, CHCl_3 , EtOAc, MeCN. **MP:** 96-99 °C. **$^1\text{H-NMR}$** (CD_3CN , 293 K): δ 1.23 (d, 6H, $\text{CH}(\text{CH}_3)_2$), 5.14 (hept, 1H, $\text{CH}(\text{CH}_3)_2$), 6.36 (t, 2H, 4-CH), 7.24 (s, 1H, CHCO), 7.57 (d, 2H, 5-CH), 7.83 (d, 2H, 3-CH). **$^{13}\text{C}\{^1\text{H}\}\text{-NMR}$** (CD_3CN , 293 K): δ 20.95 ($\text{CH}(\text{CH}_3)_2$), 71.44 ($\text{CH}(\text{CH}_3)_2$), 74.60 (CHCO), 107.13 (4- C_{Pz}), 130.71 (5- C_{Pz}), 140.74 (3- C_{Pz}),

164.45 (CO). **FT-IR** (cm^{-1}): 3121w, 3092m, 3017w, 2980w, 2928m, 2854w (C-H); 1747vs (ν_{asym} C=O); 1658w, 1629w, 1514m (C=C/C=N); 1455m, 1441m, 1393s, 1378s, 1319m, 1295vs, 1277m, 1247m, 1221vs, 1201vs, 1182s, 1146m, 1093vs, 1056m, 1044s, 983m, 968m, 949s, 940s, 919m, 905s, 893m, 854vs, 798vs, 785vs, 765vs. **ESI-MS(+)** (major positive ions, MeCN), m/z (%): 257 (100) [$\text{L}^{1\text{iPr}} + \text{Na}$] $^+$. **EA** (%) calculated for $\text{C}_{11}\text{H}_{14}\text{N}_4\text{O}_2$: N 23.92, C 56.40, H 6.02; found: N 23.40, C 57.32, H 6.34.

2.2.2.4. Synthesis of $(\text{Pz}^{3,5\text{-Me}})_2\text{CH}(\text{COO}^i\text{Pr})$ ($\text{L}^{2\text{iPr}}$, **7**)

This compound was prepared following the procedure described for $\text{L}^{1\text{iPr}}$ (**6**), starting from $\text{L}^{2\text{H}}$ (**2**; 248.281 g/mol, 5.000 mmol, 1.241 g), to give the white solid ligand $(\text{Pz}^{3,5\text{-Me}})_2\text{CH}(\text{COO}^i\text{Pr})$ ($\text{L}^{2\text{iPr}}$, **7**) in 67% yield. Crystals of ligand **7**, suitable for Single Crystal X-Ray Diffraction (SC-XRD), were obtained by slow evaporation of an EtOAc solution of **7**.

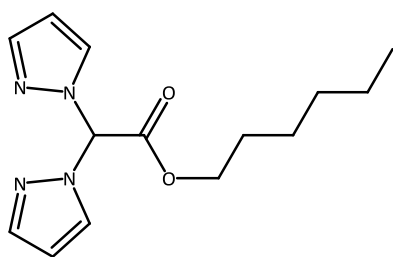


MM: 290.361 g/mol. **Solubility:** MeOH, Et_2O , THF, *n*-hexane, CHCl_3 , EtOAc, MeCN, Me_2CO . **MP:** 119-123 °C. **$^1\text{H-NMR}$** (CDCl_3 , 293 K): δ 1.28 (d, 6H, $\text{CH}(\text{CH}_3)_2$), 2.09 (s, 6H, 3- or 5- CH_3), 2.18 (s, 6H, 3- or 5- CH_3), 5.22 (hept, 1H, $\text{CH}(\text{CH}_3)_2$), 5.83 (s, 2H, 4-CH), 6.86 (s, 1H, CHCO). **$^{13}\text{C}\{^1\text{H}\}\text{-NMR}$** (CDCl_3 , 293 K): δ 10.95 (3- or 5- CCH_3), 13.45 (3- or 5- CCH_3), 21.55 ($\text{CH}(\text{CH}_3)_2$), 70.71 ($\text{CH}(\text{CH}_3)_2$), 73.44 (CHCO), 107.36 (4- C_{Pz}), 141.19 (5- C_{Pz}), 148.21 (3- C_{Pz}), 164.27 (CO). **FT-IR** (cm^{-1}): 2983m, 2923m, 2853w (C-H); 1748vs (ν_{asym} C=O); 1625w, 1564s (C=C/C=N); 1464m, 1454m, 1418m, 1400m, 1374s, 1348s, 1327s, 1272s, 1228vs, 1184m, 1168m, 1144m, 1103vs, 1035m, 993m, 971s, 909m, 896m, 856s, 815sh, 797s, 750s, 717m. **ESI-MS(+)** (major positive ions, MeCN), m/z (%): 195 (20) [$(\text{Pz}^{3,5\text{-Me}})_2\text{CH}(\text{COO}^i\text{Pr})$] $^+$, 291 (95) [$\text{L}^{2\text{iPr}} + \text{H}$] $^+$, 313 (100)

$[L^{2iPr} + Na]^+$, 329 (15) $[L^{2iPr} + K]^+$, 603 (40) $[2L^{2iPr} + Na]^+$. EA (%) calculated for $C_{15}H_{22}N_4O_2$: N 19.30, C 62.05, H 7.64; found: N 19.16, C 62.25, H 7.67.

2.2.2.5. Synthesis of $(Pz)_2CH(COOHex)$ (L^{1Hex} , **8**)

In a round-bottom flask, ligand L^{1H} (**1**; 192.175 g/mol, 4.000 mmol, 0.769 g) was added to a solution of dry THF (30 mL) and 1-hexanol (HexOH; 102.175 g/mol, 4.000 mmol, 0.409 g). The obtained mixture was cooled to 0 °C and left under magnetic stirring for 30 minutes. Subsequently, a solution of *N,N'*-dicyclohexylcarbodiimide (DCC; 206.333 g/mol, 8.000 mmol, 1.651 g) in dry THF (70 mL) was added drop by drop. The resulting mixture was left under magnetic stirring, at room temperature, for 24 hours. After that, THF was dried at reduced pressure, EtOAc was poured into the round-bottom flask and the obtained mixture was filtered. The mother liquors were washed with a dilute aqueous solution of citric acid (pH \approx 4, 2 x 50 mL) and, subsequently, with a saturated aqueous solution of $NaHCO_3$ (2 x 50 mL). The organic phase was collected into a flask, anhydrous Na_2SO_4 was added to remove moisture, the obtained mixture was filtered and the organic phase was dried at reduced pressure. The crude residue was purified by chromatographic column (packed with SiO_2 ; elution with cyclohexane:EtOAc 90:10 and then with cyclohexane:EtOAc 80:20). The final product was recovered and dried under reduced pressure. The pale yellow oily ligand $(Pz)_2CH(COOHex)$ (L^{1Hex} , **8**) was obtained in 80% yield.

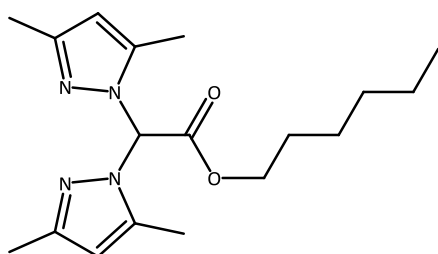


MM: 276.334 g/mol. **Solubility:** MeOH, EtOH, Et_2O , THF, CH_2Cl_2 , $CHCl_3$, MeCN, EtOAc, DMSO, Me_2CO . **1H -NMR** ($CDCl_3$, 293 K): δ 0.88 (t, 3H, $O(CH_2)_5CH_3$), 1.25-1.31 (m, 6H, $O(CH_2)_2(CH_2)_3CH_3$), 1.61-1.68 (m, 2H, $OCH_2CH_2(CH_2)_3CH_3$), 4.29 (t, 2H, $OCH_2(CH_2)_4CH_3$), 6.36 (t, 2H, 4-CH), 7.09 (s, 1H, CHCO), 7.61 (d, 2H, 5-CH), 7.77 (d, 2H, 3-CH). **1H -NMR** (CD_3CN , 293 K): δ 0.89 (t, 3H, $O(CH_2)_5CH_3$), 1.24-1.31 (m, 6H, $O(CH_2)_2(CH_2)_3CH_3$), 1.55-1.60 (m, 2H, $OCH_2CH_2(CH_2)_3CH_3$), 4.23 (t, 2H, $OCH_2(CH_2)_4CH_3$), 6.36 (t, 2H, 4-CH), 7.28 (s, 1H, CHCO), 7.57 (d, 2H, 5-CH), 7.84 (d, 2H, 3-CH). **1H -NMR** ($DMSO-d_6$, 293 K): δ 0.81 (t, 3H, $O(CH_2)_5CH_3$), 1.13-1.19 (m, 6H, $O(CH_2)_2(CH_2)_3CH_3$), 1.47 (mbr, 2H, $OCH_2CH_2(CH_2)_3CH_3$), 4.14 (t, 2H, $OCH_2(CH_2)_4CH_3$), 6.33 (t, 2H, 4-CH), 7.56 (d, 2H, 5-CH), 7.71 (s, 1H, CHCO), 7.94 (d, 2H, 3-CH). **$^{13}C\{^1H\}$ -NMR** ($CDCl_3$, 293 K): δ 13.91 ($O(CH_2)_5CH_3$); 22.43, 25.21, 28.21, 31.19 ($OCH_2(CH_2)_4CH_3$); 67.23 ($OCH_2(CH_2)_4CH_3$); 74.63 (CHCO); 107.28 (4- C_{Pz}); 130.12 (5- C_{Pz}); 140.90 (3- C_{Pz}); 164.40 (CO). **FT-IR** (cm^{-1}): 3322vw, 3139w, 3109w, 2956m, 2923s, 2871m, 2851m (C-H); 1754vs ($\nu_{asym} C=O$); 1626w, 1574w, 1517m (C=C/C=N); 1465m, 1451m, 1436m,

1393vs, 1385vs, 1354m, 1329m, 1292vs, 1253vs, 1223vs, 1213vs, 1187m, 1161vs, 1088vs, 1053vs, 1022m, 993m, 972s, 957vs, 938sh, 912s, 905vs, 892m, 858m, 845m, 827m, 806vs, 777vs, 762vs, 725s. **ESI-MS(+)** (major positive ions, MeCN), m/z (%): 209 (10) $[(Pz)CH(COOHex)]^+$, 277 (15) $[L^{1Hex} + H]^+$, 299 (100) $[L^{1Hex} + Na]^+$, 315 (5) $[L^{1Hex} + K]^+$. **ESI-MS(-)** (major negative ions, MeCN), m/z (%): 147 (100) $[(Pz)_2CH]^-$. **EA** (%) calculated for $C_{14}H_{20}N_4O_2$: N 20.28, C 60.85, H 7.30; found: N 19.85, C 61.38, H 7.43.

2.2.2.6. Synthesis of $(Pz^{3,5-Me})_2CH(COOHex)$ (L^{2Hex} , **9**)

In a round-bottom flask, ligand L^{2H} (**2**; 248.281 g/mol, 3.000 mmol, 0.745 g) and cerium trichloride heptahydrate ($CeCl_3 \cdot 7H_2O$; 372.571 g/mol, 0.600 mmol, 0.224 g) were added to dry THF (15 mL), obtaining a mixture which was cooled to 0 °C and left under magnetic stirring for 30 minutes. Subsequently, a mixture of DCC (206.333 g/mol, 6.000 mmol, 1.238 g) and DMAP (122.168 g/mol, 1.000 mmol, 0.122 g) in dry THF (15 mL) was added drop by drop. HexOH (102.175 g/mol, 3.000 mmol, 0.307 g) was then added and the mixture was left under magnetic stirring, at room temperature, for 24 hours. After that, THF was dried at reduced pressure, EtOAc (60 mL) was poured into the round-bottom flask and the crude product was extracted from the residue, obtaining a mixture which was filtered. The obtained mother liquors were washed with a dilute aqueous solution of citric acid (pH \approx 4, 2 x 40 mL) and with a saturated aqueous solution of $NaHCO_3$ (2 x 40 mL). The organic phase was collected into a flask, anhydrous Na_2SO_4 was added to remove moisture, the obtained mixture was filtered and the organic phase was dried at reduced pressure. The crude residue was purified by chromatographic column (packed with SiO_2 ; elution with *n*-hexane:EtOAc 90:10 and then with *n*-hexane:EtOAc 80:20). The final product was recovered and dried under reduced pressure. The white solid ligand $(Pz^{3,5-Me})_2CH(COOHex)$ (L^{2Hex} , **9**) was obtained in 75% yield.



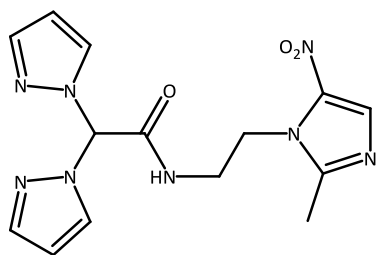
MM: 332.448 g/mol. **Solubility**: MeOH, EtOH, Et_2O , THF, *n*-hexane, CH_2Cl_2 , $CHCl_3$, EtOAc, MeCN, DMSO, Me_2CO . **MP**: 43-45 °C. **1H -NMR** ($CDCl_3$, 293 K): δ 0.90 (t, 3H, $O(CH_2)_5CH_3$), 1.32 (sbr, 6H, $O(CH_2)_2(CH_2)_3CH_3$), 1.65-1.71 (m, 2H, $OCH_2CH_2(CH_2)_3CH_3$), 2.16 (s, 6H, 3- CH_3), 2.22 (s, 6H, 5- CH_3), 4.31 (t, 2H, $OCH_2(CH_2)_4CH_3$), 5.88 (s, 2H, 4- CH), 7.02 (s, 1H, $CHCO$). **$^{13}C\{^1H\}$ -NMR** ($CDCl_3$, 293 K): δ 11.36, 13.17, 13.97 ($O(CH_2)_5CH_3$, 3- CCH_3 and 5- CCH_3); 22.51, 25.36, 28.27, 31.29 ($OCH_2(CH_2)_4CH_3$); 67.20 ($OCH_2(CH_2)_4CH_3$); 72.35 ($CHCO$); 107.73 (4- C_{Pz}); 142.59, 148.25 (3- C_{Pz} and 5- C_{Pz}); 164.31 (CO). **FT-IR** (cm^{-1}): 3100vw, 2935m, 2871m (C-H); 1755s (ν_{asym} C=O); 564m

(C=C/C=N); 1454m, 1440m, 1416m, 1402m, 1380m, 1349m, 1334s, 1327m, 1297w, 1266s, 1227s, 1211s, 1157m, 1123m, 1075m, 1035m, 1010m, 978s, 937m, 911m, 897m, 823m, 804s, 789s, 754s, 723m. **ESI-MS(+)** (major positive ions, MeCN), m/z (%): 333 (90) [$L^{2Hex} + H$] $^+$, 355 (100) [$L^{2Hex} + Na$] $^+$. **EA** (%) calculated for $C_{18}H_{28}N_4O_2$: N 16.85, C 65.03, H 8.49; found: N 16.46, C 65.21, H 8.49.

2.2.3. Syntheses of bioconjugated ligands

2.2.3.1. Synthesis of *N*-(2-(2-methyl-5-nitro-1*H*-imidazol-1-yl)ethyl)-2,2-bis(1*H*-pyrazol-1-yl)acetamide (L^{1MN} , **10**)

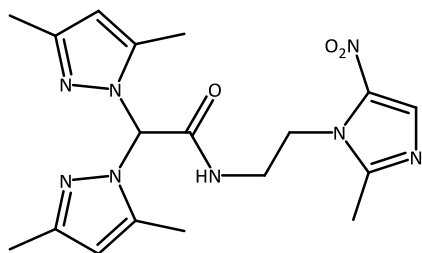
To a solution of L^{1H} (**1**; 192.175 g/mol, 0.500 mmol, 0.096 g) in $CH_2Cl_2:N,N$ -dimethylformamide (DMF) (5:1, 9 mL), triethylamine (NEt_3 ; 101.193 g/mol, 2.000 mmol, 0.202 g), 1-(2-aminoethyl)-2-methyl-5-nitroimidazole dihydrochloride monohydrate (261.103 g/mol, 1.000 mmol, 0.261 g), 1-hydroxybenzotriazole hydrate ($HOBt \cdot xH_2O$; 153.141 g/mol anhydrous, 1.000 mmol, 0.153 g) and $EDCI \cdot HCl$ (191.702 g/mol, 1.000 mmol, 0.192 g) were added at 0 °C. The mixture was allowed to reach room temperature and stir for 48 hours. $CHCl_3$ (30 mL) was added, the organic layer was washed with H_2O and dried at reduced pressure. The residue was re-crystallized from $CH_2Cl_2:Et_2O$ (1:2), to obtain the ligand *N*-(2-(2-methyl-5-nitro-1*H*-imidazol-1-yl)ethyl)-2,2-di(1*H*-pyrazol-1-yl)acetamide (L^{1MN} , **10**) as a white solid in 80% yield.



MM: 344.335 g/mol. **Solubility**: MeOH, EtOH, CH_2Cl_2 , $CHCl_3$, MeCN, Me_2CO . **MP**: 139-141 °C. **1H -NMR** ($CDCl_3$, 293 K): δ 2.42 (s, 3H, CH_3), 3.72 (q, 2H, $HNCH_2$), 4.48 (t, 2H, CH_2N), 6.33 (sbr, 2H, 4-CH), 6.91 (s, 1H, $CHCO$), 7.60 (d, 2H, 5-CH), 7.69 (br, 2H, 5-CH), 7.92 (s, 1H, CH_{MN}). **$^{13}C\{^1H\}$ -NMR** ($CDCl_3$, 293 K): δ 14.24 (CH_3), 39.70 ($HNCH_2$), 44.85 (CH_2N), 75.59 ($CHCO$), 107.56 (4- C_{Pz}), 130.47 (5- C_{Pz}), 133.50 (CH_{MN}), 138.00 (CNO_2), 141.81 (3- C_{Pz}), 151.23 (CCH_3), 165.04 (CO). **FT-IR** (cm^{-1}): 3265m (N-H); 3155w, 3128m, 3108w, 3085m, 2965w (C-H); 1686s ($\nu_{asym} C=O$); 1548m, 1523s ($\nu_{asym} NO_2$, C=C/C=N); 1457s, 1431s; 1390sh, 1368s ($\nu_{sym} NO_2$); 1294s, 1260s, 1234m, 1184s, 1152s, 1090s, 1050m, 1031m, 964s, 912m, 884m, 844m, 825m, 795s, 754sh, 744s, 727s, 704s. **ESI-MS(+)** (major positive ions, MeOH), m/z (%): 345 (100) [$L^{1MN} + H$] $^+$, 367 (90) [$L^{1MN} + Na$] $^+$, 711 (30) [$2L^{1MN} + Na$] $^+$. **ESI-MS(-)** (major negative ions, MeOH), m/z (%): 126 (100) [$2\text{-methyl-5-nitroimidazole-H}$] $^-$, 343 (20) [$L^{1MN} - H$] $^-$. **EA** (%) calculated for $C_{14}H_{16}N_8O_3$: N 32.54, C 48.83, H 4.68; found: N 32.17, C 48.56, H 4.74.

2.2.3.2. Synthesis of 2,2-bis(3,5-dimethyl-1H-pyrazol-1-yl)-N-(2-(2-methyl-5-nitro-1H-imidazol-1-yl)ethyl)acetamide (L^{2MN} , **11**)

This compound was prepared following the procedure described for **10** but employing the ligand L^{2H} (**2**; 248.281 g/mol, 0.500 mmol, 0.124 g). The white ligand 2,2-bis(3,5-dimethyl-1H-pyrazol-1-yl)-N-(2-(2-methyl-5-nitro-1H-imidazol-1-yl)ethyl)acetamide (L^{2MN} , **11**) was obtained in 79% yield. Crystals of the ligand **11**, suitable for SC-XRD, were obtained by slow evaporation of a CH_2Cl_2 :Et₂O (1:3) solution of **11**.

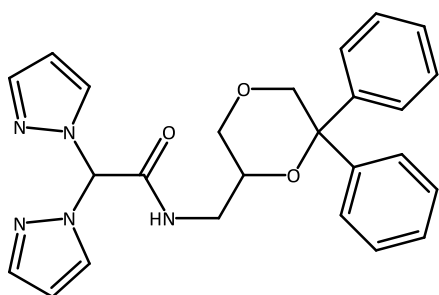


MM: 400.443 g/mol. **Solubility:** MeOH, EtOH, CH_2Cl_2 , $CHCl_3$, MeCN, Me_2CO . **MP:** 163-165 °C. 1H NMR ($CDCl_3$, 293 K): δ 2.19 (s, 6H, 3- or 5- CH_3), 2.30 (s, 6H, 3- or 5- CH_3), 2.46 (s, 3H, CH_3), 3.75 (sbr, 2H, $HNCH_2$), 4.50 (t, 2H, CH_2N), 5.85 (s, 2H, 4- CH), 6.54 (s, 1H, $CHCO$), 7.93 (s, 1H, CH_{MN}), 8.26 (mbr, 1H, NH). $^{13}C\{^1H\}$ -NMR ($CDCl_3$, 293 K): δ 11.42 (CH_3), 13.96 (CH_3), 14.39 (CH_3), 39.58 ($HNCH_2$), 45.04 (CH_2N), 69.97 ($CHCO$), 107.48 (4- C_{Pz}), 133.44 (CH_{MN}), 138.20 (CNO_2), 140.83 (CCH_3), 150.27 (CCH_3), 151.32 (CCH_3), 165.94 (CO). **FT-IR** (cm^{-1}): 3288br (N-H); 3125w, 3055sh, 2927m (C-H); 1667s ($\nu_{asym} C=O$); 1561m, 1527m, 1464s, 1424s, 1384s, 1362s, 1302m, 1259s, 1186s, 1149m, 1093m, 1063w, 1032m, 973m, 926w, 887w, 865w, 824m, 784m, 742s, 706sh. **ESI-MS(+)** (major positive ions, MeOH), m/z (%): 401 (50) [$L^{2MN} + H$]⁺, 423 (100) [$L^{2MN} + Na$]⁺, 824 (60) [$2L^{2MN} + Na$]⁺. **ESI-MS(-)** (major negative ions, MeOH), m/z (%): 399 (80) [$L^{2MN} - H$]⁻, 436 (100) [$L^{2MN} + Cl$]⁻. **EA** (%) calculated for $C_{18}H_{24}N_8O_3$: N 27.98, C 53.99, H 6.04; found: N 27.78, C 54.07, H 6.02.

2.2.3.3. Synthesis of N-((6,6-diphenyl-1,4-dioxan-2-yl)methyl)-2,2-bis(1H-pyrazol-1-yl)acetamide (L^{1NMDA} , **12**)

Carbonyldiimidazole (CDI; 162.152 g/mol, 1.860 mmol, 0.302 g) was added to a solution of L^{1H} (**1**; 192.175 g/mol, 1.860 mmol, 0.357 g) in THF. The reaction mixture was stirred at reflux for 2 hours, then it was cooled to 0 °C. Subsequently, (6,6-diphenyl-1,4-dioxan-2-yl)methanamine (269.344 g/mol, 1.860 mmol, 0.501 g) was added and the solution was stirred at room temperature for 3 hours. After that, the reaction was dried at reduced pressure, the oily residue was dissolved in $CHCl_3$ and washed with a saturated solution of $NaHCO_3$ and with a solution of HCl (2 M). The organic phase was collected into a flask and anhydrous Na_2SO_4 was added to remove moisture. The mixture was filtered and the organic phase was dried at reduced pressure. The crude residue was purified by chromatographic column (packed with

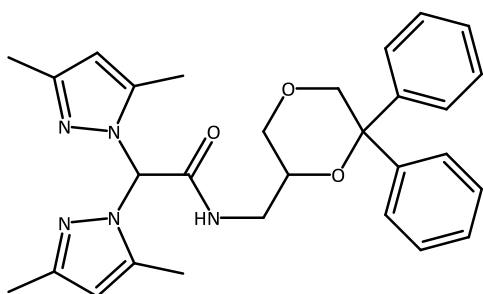
SiO₂; elution with cyclohexane:EtOAc 50:50). The final product was recovered and dried at reduced pressure. The ligand *N*-((6,6-diphenyl-1,4-dioxan-2-yl)methyl)-2,2-bis(1*H*-pyrazol-1-yl)acetamide (L^{1NMDA}, **12**) was obtained in 47% yield.



MM: 443.507 g/mol. **Solubility:** MeCN, CHCl₃, DMSO. **MP:** 172-173 °C. **¹H-NMR** (CDCl₃, 293 K): δ 3.37-3.76 (m, 6H, dioxan and HNCH₂), 4.58 (d, 1H, dioxan), 6.35 (t, 2H, 4-CH), 7.10 (s, 1H, CHCO), 7.18-7.39 (m, 14H, 3-CH, 5-CH and ArH), 7.83 (sbr, 1H, NH). **FT-IR** (cm⁻¹): 3287br (N-H); 3121w, 3103w, 3052w, 3026w, 2978w, 2935w, 2915w, 2860w (C-H); 1682s (ν_{asym} C=O); 1560m (C=C/C=N); 1516w, 1495m, 1451m, 1432m, 1388m, 1350w, 1312m, 1293m, 1271m, 1244m, 1211w, 1188w, 1163w, 1122s, 1088s, 1065s, 1050s, 1026m, 1000m, 991s, 958m, 916s, 886w, 858m, 844m, 809s, 766s, 750s, 729s, 705s. **ESI-MS(+)** (major positive ions, MeCN), *m/z* (%): 444 (100) [L^{1NMDA} + H]⁺. **ESI-MS(-)** (major negative ions, MeCN), *m/z* (%): 442 (100) [L^{1NMDA} - H]⁻. **EA** (%) calculated for C₂₅H₂₅N₅O₃: N 15.79, C 67.70, H 5.68; found: N 15.50, C 67.38, H 5.75.

2.2.3.4. Synthesis of 2,2-bis(3,5-dimethyl-1*H*-pyrazol-1-yl)-*N*-((6,6-diphenyl-1,4-dioxan-2-yl)methyl)acetamide (L^{2NMDA}, **13**)

This compound was prepared following the procedure described for **12**, but employing the ligand L^{2H} (**2**; 248.281 g/mol, 1.860 mmol, 0.462 g) and purifying the crude residue by chromatographic column (packed with SiO₂; elution with cyclohexane:EtOAc 70:30). The white ligand 2,2-bis(3,5-dimethyl-1*H*-pyrazol-1-yl)-*N*-((6,6-diphenyl-1,4-dioxan-2-yl)methyl)acetamide (L^{2NMDA}, **13**) was obtained in 54% yield.

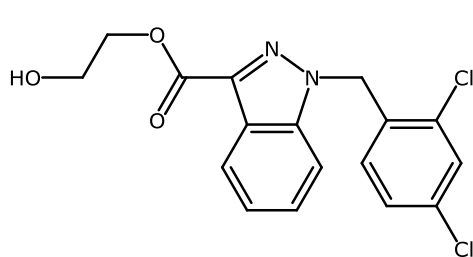


MM: 499.615 g/mol. **Solubility:** MeOH, CHCl₃, MeCN, DMSO. **MP:** 171-172 °C. **¹H-NMR** (CDCl₃, 293 K): δ 2.10 (s, 3H, 3- or 5-CH₃), 2.13 (s, 3H, 3- or 5-CH₃), 2.38 (s, 3H, 3- or 5-CH₃), 2.39 (s, 3H, 3- or 5-CH₃), 3.30-3.79 (m, 6H, dioxan and HNCH₂), 4.61 (d, 1H, dioxan), 5.84 (s, 1H, 4-CH), 5.85 (s, 1H, 4-CH), 6.77 (s, 1H, CHCO), 7.18-7.39 (m, 10H, ArH), 8.10 (sbr, 1H, NH). **FT-IR** (cm⁻¹): 3423w (N-H); 3090w, 3062w, 2985w, 2961w, 2926w, 2907w, 2869w (C-H); 1702s (ν_{asym} C=O); 1568m (C=C/C=N); 1520s, 1465m, 1446s, 1415m, 1372m, 1364m, 1335w, 1316m, 1295m, 1260m, 1240m, 1221w, 1128m, 1102s, 1064s, 1028m, 998m, 985m, 940m, 919m, 874m, 835m, 814m, 799m, 773s, 757s, 739s, 722m, 707s. **ESI-MS(+)**

(major positive ions, MeOH), m/z (%): 522 (20) [$L^{2NMDA} + Na$] $^+$, 1022 (100) [$2L^{2NMDA} + Na$] $^+$. **ESI-MS(-)** (major negative ions, MeOH), m/z (%): 498 (100) [$L^{2NMDA} - H$] $^-$. **EA (%)** calculated for $C_{29}H_{33}N_5O_3$: N 14.02, C 69.72, H 6.66; found: N 13.81, C 69.93, H 6.85.

2.2.3.5. Synthesis of 2-hydroxyethyl 1-(2,4-dichlorobenzyl)-1H-indazole-3-carboxylate (LONES, 14)

Concentrated H_2SO_4 (98% V/V, 2 mL) was added to a solution of Lonidamine (LND; 321.157 g/mol, 1.557 mmol, 0.500 g) in ethylene glycol (35 mL) and the reaction was stirred at 85 °C for 1 hour. After cooling to room temperature, the reaction was poured into the ice and the aqueous phase (50 mL) was extracted with CH_2Cl_2 (3 x 30 mL). The organic phase was collected into a flask, anhydrous Na_2SO_4 was added to remove moisture, the obtained mixture was filtered and the organic phase was dried at reduced pressure. The crude residue was purified by chromatographic column (packed with SiO_2 ; elution with cyclohexane:EtOAc 60:40). The final product was recovered and dried under reduced pressure. The white solid product 2-hydroxyethyl 1-(2,4-dichlorobenzyl)-1H-indazole-3-carboxylate (LONES, 14) was obtained in 65% yield.



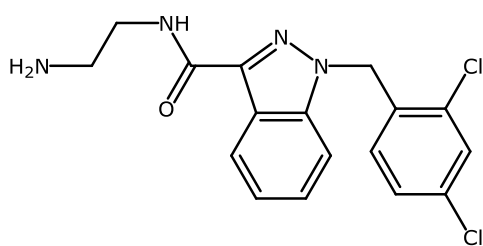
MM: 365.210 g/mol. **MP:** 121-122 °C. **1H -NMR** ($CDCl_3$, 293 K): δ 4.07 (m, 2H, $HOCH_2$), 4.65 (m, 2H, CH_2O), 5.81 (s, 2H, NCH_2Ph), 6.72 (d, 1H, ArH), 7.10-7.49 (m, 6H, ArH and OH), 8.28 (d, 1H, ArH). **FT-IR** (cm^{-1}): 3480mbr (O-H); 3084wbr, 2949wbr (C-H); 1713s (ν_{asym} C=O); 1585m;

1560sh (C=C/C=N); 1479m, 1472s, 1446m, 1436s, 1421m, 1311s, 1275m, 1249s, 1225s, 1167s, 1157s, 1129s, 1096m, 1084s, 1044m, 1025m, 1009m, 990m, 977m, 944m, 898m, 855m, 839m, 807m, 789m, 776m, 747s, 737s. **ESI-MS(+)** (major positive ions, MeOH), m/z (%): 365 (20) [$LONES + H$] $^+$, 387 (100) [$LONES + Na$] $^+$, 753 (60) [$2LONES + Na$] $^+$. **ESI-MS(-)** (major negative ions, MeOH), m/z (%): 363 (100) [$LONES - H$] $^-$.

2.2.3.6. Synthesis of N-(2-aminoethyl)-1-(2,4-dichlorobenzyl)-1H-indazole-3-carboxamide (LONAM, 15)

1,1'-carbonyldiimidazole (CDI; 162.152 g/mol, 3.740 mmol, 0.606 g) was added to a solution of LND (321.157 g/mol, 3.114 mmol, 1.000 g) in dry THF (20 mL) and the mixture was stirred at room temperature for 1 hour. Then, ethylenediamine (60.100 g/mol, 15.600 mmol, 0.938 g)

was added and the reaction was left under magnetic stirring, at room temperature, for 18 hours. After that, THF was dried at reduced pressure obtaining an oily residue, which was solubilized in CHCl_3 (30 mL) and washed with H_2O (2 x 20 mL). The organic phase was collected into a flask, anhydrous Na_2SO_4 was added to remove moisture, the obtained mixture was filtered and the organic phase was dried at reduced pressure. The crude residue was purified by chromatographic column (packed with SiO_2 ; elution with $\text{EtOAc}:\text{MeOH}$ 90:10). The final product was recovered and dried under reduced pressure. The white solid ligand *N*-(2-aminoethyl)-1-(2,4-dichlorobenzyl)-1*H*-indazole-3-carboxamide (LONAM, **15**) was obtained in 65% yield.



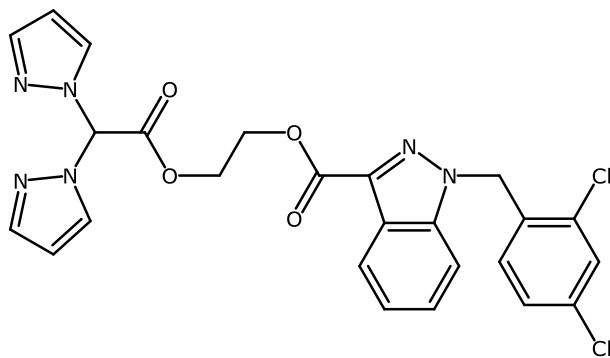
MM: 363.242 g/mol. **MP:** 71-72 °C. **$^1\text{H-NMR}$** (CDCl_3 , 293 K): δ 3.01-3.58 (m, 4H, $\text{H}_2\text{N}(\text{CH}_2)_2\text{NH}$), 4.87 (br, 2H, NH_2), 5.64 (s, 2H, NCH_2Ph), 6.63 (d, 1H, *ArH*), 7.02-7.48 (m, 6H, *ArH* and *NH*), 8.46 (d, 1H, *ArH*). **FT-IR** (cm^{-1}): 3282br (N-H); 3060w, 3030w, 2937wbr (C-H); 1657sh, 1642s (ν_{asym}

C=O); 1620sh, 1588m; 1575m, 1538s (C=C/C=N); 1491s, 1473s, 1436s, 1406m, 1386m, 1372m, 1357m, 1310sbr, 1282m, 1233s, 1175s, 1155m, 1132m, 1097s, 1048s, 1005m, 968mbr, 942m, 859m, 836s, 788s, 772s, 742s. **ESI-MS(+)** (major positive ions, MeOH), m/z (%): 363 (100) [$\text{LONAM} + \text{H}$] $^+$, 385 (20) [$\text{LONAM} + \text{Na}$] $^+$, 727 (40) [$2\text{LONAM} + \text{H}$] $^+$. **ESI-MS(-)** (major negative ions, MeOH), m/z (%): 361 (100) [$\text{LONAM} - \text{H}$] $^-$.

2.2.3.7. Synthesis of 2-(2,2-bis(1*H*-pyrazol-1-yl)acetoxy)ethyl 1-(2,4-dichlorobenzyl)-1*H*-indazole-3-carboxylate ($\text{L}^{1\text{LONES}}$, **16**)

A mixture of $\text{L}^{1\text{H}}$ (**1**; 192.175 g/mol, 1.560 mmol, 0.300 g), LONES (**14**; 365.210 g/mol, 1.710 mmol, 0.625 g) and DMAP (122.168 g/mol, 0.157 mmol, 0.019 g) in THF (20 mL) was cooled to 0 °C. EDCI·HCl (191.702 g/mol, 1.880 mmol, 0.360 g) was added and the reaction was stirred at room temperature for 16 hours. After that, the reaction was quenched with H_2O (30 mL) and the aqueous phase was extracted with EtOAc (2 x 30 mL). Subsequently, the organic phase was washed with a saturated aqueous solution of sodium chloride (brine; 2 x 20 mL) and collected into a flask, where anhydrous Na_2SO_4 was added to remove moisture. The obtained mixture was filtered and the organic phase was dried at reduced pressure. The crude residue was purified by chromatographic column (packed with SiO_2 ; elution with cyclohexane: EtOAc 70:30). The final product was recovered and dried under reduced pressure. The white solid product 2-(2,2-bis(1*H*-pyrazol-1-yl)acetoxy)ethyl 1-(2,4-dichlorobenzyl)-1*H*-indazole-3-carboxylate ($\text{L}^{1\text{LONES}}$, **16**) was obtained in 72% yield.

MM: 539.373 g/mol. **Solubility:** MeOH, CH₂Cl₂, CHCl₃, MeCN, DMSO. **MP:** 95-96 °C. **¹H-NMR**

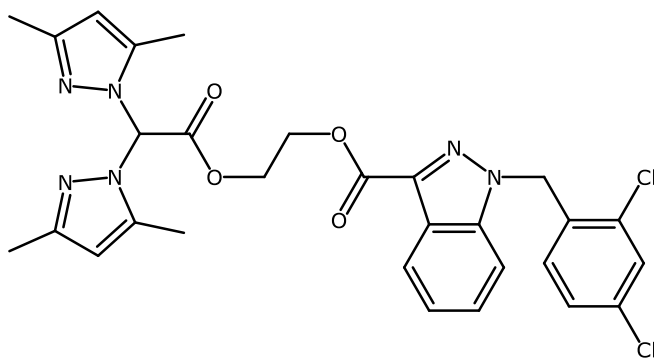


(DMSO-*d*₆, 293 K): δ 4.52-4.61 (m, 4H, O(CH₂)₂O), 5.89 (s, 2H, NCH₂Ph), 6.26 (t, 2H, 4-CH), 6.96 (d, 1H, ArH), 7.37-8.01 (m, 11H, 3-CH, 5-CH, ArH and CHCO). **¹H-NMR** (CDCl₃, 293 K): δ 4.72 (m, 4H, O(CH₂)₂O), 5.81 (s, 2H, NCH₂Ph), 6.30 (t, 2H, 4-CH), 6.73 (d, 1H, ArH), 7.11-7.81 (m, 10H, 3-CH, 5-CH, ArH and CHCO),

8.15 (d, 1H, ArH). **FT-IR** (cm⁻¹): 3121wbr, 2958wbr (C-H); 1762m, 1716mbr (*v*_{asym} C=O); 1616w; 1590w, 1564w, 1518w (C=C/C=N); 1476m, 1434m, 1387s, 1317m, 1291m, 1259m, 1221s, 1191m, 1156s, 1123s, 1088s, 1046s, 1008m, 967m, 948m, 916m, 884m, 835m, 817m, 801m, 788m, 748s. **ESI-MS(+)** (major positive ions, MeOH), *m/z* (%): 539 (20) [L^{1LONES} + H]⁺, 561 (100) [L^{1LONES} + Na]⁺. **EA** (%) calculated for C₂₅H₂₀Cl₂N₆O₄: N 15.58, C 55.67, H 3.74; found: N 15.20, C 55.33, H 3.94.

2.2.3.8. Synthesis of 2-(2,2-bis(3,5-dimethyl-1H-pyrazol-1-yl)acetoxy)ethyl 1-(2,4-dichlorobenzyl)-1H-indazole-3-carboxylate (L^{2LONES}, 17)

This compound was prepared starting from L^{2H} (2) and LONES (14) following the procedure described for L^{1LONES} (16): the white solid product 2-(2,2-bis(3,5-dimethyl-1H-pyrazol-1-yl)acetoxy)ethyl 1-(2,4-dichlorobenzyl)-1H-indazole-3-carboxylate (L^{2LONES}, 17) was obtained in 75% yield.



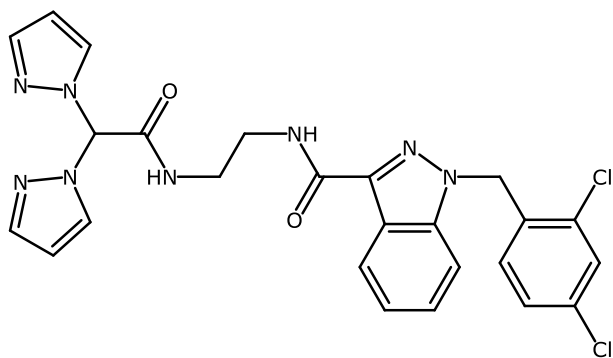
MM: 595.481 g/mol. **Solubility:** MeOH, CH₂Cl₂, CHCl₃, MeCN, DMSO. **MP:** 139-140 °C. **¹H-NMR** (DMSO-*d*₆, 293 K): δ 1.96 (s, 6H, 3- or 5-CH₃), 2.09 (s, 6H, 3- or 5-CH₃), 4.55-4.63 (m, 4H, O(CH₂)₂O), 5.79 (s, 2H, NCH₂Ph), 5.88 (s, 2H, 4-CH), 6.97 (d, 1H, ArH), 7.33-8.05 (m, 7H, ArH and CHCO). **¹H-NMR**

(CDCl₃, 293 K): δ 2.11 (s, 6H, 3- or 5-CH₃), 2.14 (s, 6H, 3- or 5-CH₃), 4.74 (m, 4H, O(CH₂)₂O), 5.81 (s, 2H, NCH₂Ph), 5.83 (s, 2H, 4-CH), 6.73 (d, 1H, ArH), 7.06-8.16 (m, 7H, ArH and CHCO). **FT-IR** (cm⁻¹): 3063wbr, 2958w, 2928w (C-H); 1763s, 1726sbr (*v*_{asym} C=O); 1616w; 1590m, 1562s (C=C/C=N); 1476s, 1416s, 1378s, 1316s, 1265s, 1218vs, 1202vs, 1156vs, 1123vs, 1102vs, 1048s, 1035vs, 1008s, 970s, 947m, 892m, 862m, 835s, 787vs, 748vs. **ESI-MS(+)** (major positive ions,

MeOH), m/z (%): 595 (20) [$L^{2LONES} + H$]⁺, 617 (100) [$L^{2LONES} + Na$]⁺, 633 (20) [$L^{2LONES} + K$]⁺, 1213 (10) [$2L^{2LONES} + Na$]⁺. **EA** (%) calculated for $C_{29}H_{28}Cl_2N_6O_4$: N 14.11, C 58.49, H 4.74; found: N 13.88, C 58.71, H 4.45.

2.2.3.9. Synthesis of *N*-(2-(2,2-bis(1*H*-pyrazol-1-yl)acetamido)ethyl)-1-(2,4-dichlorobenzyl)-1*H*-indazole-3-carboxamide (L^{1LONAM} , **18**)

A mixture of L^{1H} (**1**; 192.175 g/mol, 0.810 mmol, 0.156 g), LONAM (**15**; 363.242 g/mol; 0.900 mmol, 0.327 g), EDCI·HCl (191.702 g/mol, 1.200 mmol, 0.230 g), HOBT·xH₂O (153.141 g/mol anhydrous, 1.045 mmol, 0.160 g) and NEt₃ (101.193 g/mol, 1.060 mmol, 0.107 g) in DMF (10 mL) was stirred at room temperature for 16 hours. After that, the reaction was quenched with H₂O (30 mL) and the aqueous phase was extracted with EtOAc (2 x 20 mL). Subsequently, the organic phase was washed with brine (3 x 20 mL) and with a saturated aqueous solution of NaHCO₃ (3 x 20 mL). The organic phase was collected into a flask, anhydrous Na₂SO₄ was added to remove moisture, the obtained mixture was filtered and the organic phase was dried at reduced pressure. The crude residue was purified by chromatographic column (packed with SiO₂; elution with cyclohexane:EtOAc 30:70). The final product was recovered and dried under reduced pressure. The white solid ligand *N*-(2-(2,2-bis(1*H*-pyrazol-1-yl)acetamido)ethyl)-1-(2,4-dichlorobenzyl)-1*H*-indazole-3-carboxamide (L^{1LONAM} , **18**) was obtained in 68% yield.



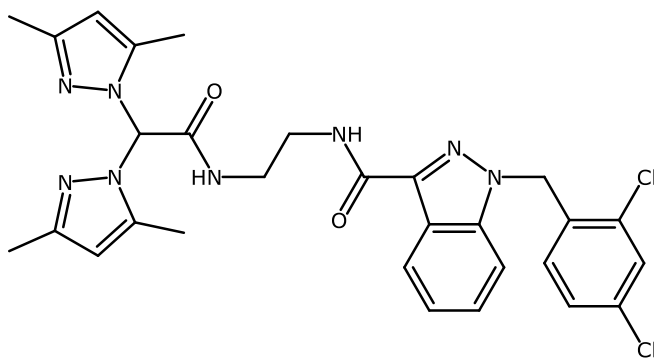
MM: 537.405 g/mol. **Solubility**: MeOH, CH₂Cl₂, CHCl₃, MeCN, DMSO. **MP**: 179-181 °C. **¹H-NMR** (DMSO-*d*₆, 293 K): δ 3.30-3.47 (m, 4H, HN(CH₂)₂NH), 5.83 (s, 2H, NCH₂Ph), 6.27 (t, 2H, 4-CH), 6.78 (d, 1H, ArH), 7.25-8.64 (m, 13H, 3-CH, 5-CH, ArH, CHCO and NH). **¹H-NMR** (CDCl₃, 293 K): δ 3.65-3.75 (m, 4H, HN(CH₂)₂NH), 5.67

(s, 2H, NCH₂Ph), 6.26 (t, 2H, 4-CH), 6.68 (d, 1H, ArH), 7.00-7.72 (m, 12H, 3-CH, 5-CH, ArH, CHCO and NH), 8.38 (d, 1H, ArH). **FT-IR** (cm⁻¹): 3275mbr, 3223m (N-H); 3075m, 2951m (C-H); 1673vs, 1641vs (ν_{asym} C=O); 1587m, 1539vs, 1515s (C=C/C=N); 1493s, 1473s, 1449s, 1433m, 1389vs, 1371s, 1313s, 1285s, 1249s, 1230vs, 1195s, 1177vs, 1154s, 1131m, 1112m, 1099s, 1092s, 1084s, 1064m, 1049vs, 1005m, 985w, 969m, 946m, 935m, 915m, 896w, 883w, 864s, 837vs, 812vs, 788s, 751vs. **ESI-MS(+)** (major positive ions, MeOH), m/z (%): 559 (100) [$L^{1LONAM} + Na$]⁺, 1097 (30) [$2L^{1LONAM} + Na$]⁺. **ESI-MS(-)** (major negative ions, MeOH), m/z (%): 557 (100) [$L^{1LONAM} -$

HJ⁻. EA (%) calculated for C₂₅H₂₂Cl₂N₈O₂: N 20.85, C 55.87, H 4.13; found: N 20.59, C 55.53, H 3.97.

2.2.3.10. Synthesis of *N*-(2-(2,2-bis(3,5-dimethyl-1*H*-pyrazol-1-yl)acetamido)ethyl)-1-(2,4-dichlorobenzyl)-1*H*-indazole-3-carboxamide (L^{2LONAM}, **19**)

This compound was prepared starting from L^{2H} (**2**) and LONAM (**15**) following the procedure described for L^{1LONAM} (**18**): the white solid product *N*-(2-(2,2-bis(3,5-dimethyl-1*H*-pyrazol-1-yl)acetamido)ethyl)-1-(2,4-dichlorobenzyl)-1*H*-indazole-3-carboxamide (L^{2LONAM}, **19**) was obtained in 75% yield.



MM: 593.513 g/mol. **Solubility:** MeOH, CH₂Cl₂, CHCl₃, DMSO. **MP:** 170-172 °C. **¹H-NMR** (DMSO-*d*₆, 293 K): δ 2.02 (s, 6H, 3- or 5-CH₃), 2.08 (s, 6H, 3- or 5-CH₃), 3.37-3.47 (m, 4H, HN(CH₂)₂NH), 5.81 (s, 2H, NCH₂Ph), 5.83 (s, 2H, 4-CH), 6.74 (d, 1H, ArH), 6.91-8.38 (m, 9H, ArH, CHCO and NH). **¹H-NMR**

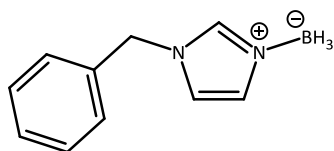
(CDCl₃, 293 K): δ 2.09 (s, 6H, 3- or 5-CH₃), 2.30 (s, 6H, 3- or 5-CH₃), 3.62-3.76 (m, 4H, HN(CH₂)₂NH), 5.66 (s, 2H, NCH₂Ph), 5.80 (s, 2H, 4-CH), 6.67 (d, 1H, ArH), 6.97-8.36 (m, 8H, ArH, CHCO and NH). **FT-IR** (cm⁻¹): 3288br (N-H); 3070wbr, 2947wbr (C-H); 1669s, 1644s (ν_{asym} C=O); 1590m, 1562sh, 1536s (C=C/C=N); 1491m, 1473s, 1456m, 1439s, 1415m, 1374s, 1363m, 1338m, 1312s, 1272s, 1246s, 1228s, 1198m, 1178s, 1154m, 1111m, 1099m, 1081m, 1050m, 1033m, 1028m, 1002m, 974m, 948m, 885m, 861m, 834s, 807s, 794m, 780s, 751vs, 740s, 709s. **ESI-MS(+)** (major positive ions, MeOH), *m/z* (%): 593 (100) [L^{2LONAM} + H]⁺, 615 (50) [L^{2LONAM} + Na]⁺. **ESI-MS(-)** (major negative ions, MeOH), *m/z* (%): 591 (100) [L^{2LONAM} - H]⁻. EA (%) calculated for C₂₉H₃₀Cl₂N₈O₂: N 18.88, C 58.69, H 5.10; found: N 19.14, C 58.43, H 4.97.

2.2.4. Syntheses of imidazole-based ligands

2.2.4.1. Synthesis of (HIm^{Bn})BH₃ (**20**)

1-Benzylimidazole (HIm^{Bn}; 158.204 g/mol, 11.631 mmol, 1.840 g) was dissolved in dry THF (50 mL) under N₂ atmosphere and BH₃·THF complex (1 M, 12.0 mL) was added drop by drop. The reaction mixture was stirred at room temperature for 24 hours. After that, the reaction was

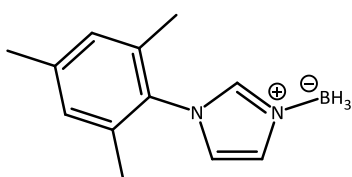
dried at reduced pressure to give a colourless oil, that was re-crystallized by $\text{CHCl}_3\text{:Et}_2\text{O:n}$ -hexane (1:3:3) solution. The mixture was filtered and the precipitate was washed with Et_2O and dried at reduced pressure to give the white ligand $(\text{HIm}^{\text{Bn}})\text{BH}_3$ (**20**) in 80% yield. Crystals of the ligand **20**, suitable for SC-XRD, were obtained by slow evaporation of a CHCl_3 solution of **20**.



MM: 172.038 g/mol. **Solubility:** MeOH, THF, CH_2Cl_2 , CHCl_3 , DMSO, Me_2CO . **MP:** 92-94 °C. $^1\text{H-NMR}$ (CDCl_3 , 293 K): δ 2.20 (br, 3H, BH_3), 5.13 (s, 2H, PhCH_2N), 6.91 (s, 1H, 4-CH or 5-CH), 7.14 (s, 1H, 4-CH or 5-CH), 7.23-7.44 (m, 5H, ArH), 7.79 (s, 1H, 2-CH). $^1\text{H-NMR}$ (CD_3OD , 293 K): δ 2.20 (qbr, 3H, BH_3), 5.24 (s, 2H, PhCH_2N), 7.03 (s, 1H, 4-CH or 5-CH), 7.19 (s, 1H, 4-CH or 5-CH), 7.26-7.43 (m, 5H, ArH), 8.13 (s, 1H, 2-CH). $^{13}\text{C}\{^1\text{H}\}\text{-NMR}$ (CDCl_3 , 293 K): δ 52.35 (PhCH_2N); 119.94, 127.98, 128.21, 129.33, 129.47, 133.46 (CH); 136.33 (2-CH). $^{11}\text{B}\{^1\text{H}\}\text{-NMR}$ (CDCl_3 , 293 K): δ -19.38 (s, BH_3). $^{11}\text{B-NMR}$ (CDCl_3 , 293 K): δ -19.38 (q, $J_{(\text{B-H})} = 96$ Hz, BH_3). **FT-IR** (cm^{-1}): 3159w, 3135m, 3061w, 3038w (C-H); 2352m, 2297m, 2255m (B-H); 1540m, 1533m (C=C/C=N). **ESI-MS(+)** (major positive ions, MeOH), m/z (%): 159 (40) [$\text{HIm}^{\text{Bn}} + \text{H}$] $^+$, 181 (40) [$\text{HIm}^{\text{Bn}} + \text{Na}$] $^+$, 195 (90) [($\text{HIm}^{\text{Bn}}\text{BH}_3 + \text{Na}$)] $^+$, 329 (100) [($\text{HIm}^{\text{Bn}}\text{BH}_2$)] $^+$. **EA** (%) calculated for $\text{C}_{10}\text{H}_{13}\text{BN}_2$: N 16.28, C 69.82, H 7.62; found: N 15.91, C 69.52, H 7.30.

2.2.4.2. Synthesis of $(\text{HIm}^{\text{Mes}})\text{BH}_3$ (**21**)

This compound was prepared following the procedure described for **20** but employing 1-mesitylimidazole (HIm^{Mes} ; 186.258 g/mol, 11.631 mmol, 2.166 g). The brown ligand $(\text{HIm}^{\text{Mes}})\text{BH}_3$ (**21**) was obtained in 68% yield. Crystals of the ligand **21**, suitable for SC-XRD, were obtained by slow evaporation of a $\text{CHCl}_3\text{:Et}_2\text{O}$ solution of **21**.

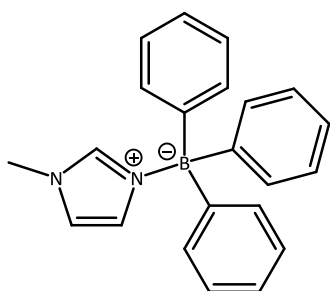


MM: 200.092 g/mol. **Solubility:** MeOH, THF, CH_2Cl_2 , CHCl_3 , DMSO, Me_2CO . **MP:** 109-111 °C. $^1\text{H-NMR}$ (CDCl_3 , 293 K): δ 2.03 (s, 6H, $o\text{-CH}_3$), 2.30 (br, 3H, BH_3), 2.37 (s, 3H, $p\text{-CH}_3$), 6.90 (s, 1H, 4-CH or 5-CH), 7.02 (s, 2H, $m\text{-CH}$), 7.31 (s, 1H, 4-CH or 5-CH), 7.75 (s, 1H, 2-CH). $^1\text{H-NMR}$ (CD_3OD , 293 K): δ 2.04 (s, 6H, $o\text{-CH}_3$), 2.10 (br, 3H, BH_3), 2.35 (s, 3H, $p\text{-CH}_3$), 7.08 (s, 2H, $m\text{-CH}$), 7.23 (s, 1H, 4-CH or 5-CH), 7.25 (s, 1H, 4-CH or 5-CH), 8.14 (s, 1H, 2-CH). $^{13}\text{C}\{^1\text{H}\}\text{-NMR}$ (CDCl_3 , 293 K): δ 17.33, 21.06 ($o\text{-}$ and $p\text{-CH}_3$); 121.25, 128.12, 129.49, 131.71, 134.86, 136.85 (CH); 140.34 (2-CH). $^{11}\text{B-NMR}$ (CDCl_3 , 293 K): δ -19.21 (dbr, BH_3). **FT-IR** (cm^{-1}): 3177w, 3155w, 3132w, 3061w, 3028w (C-H); 2374m, 2338m, 2323m, 2300m, 2259m (B-H); 1526s (C=C/C=N). **ESI-MS(+)** (major positive ions, MeOH), m/z (%): 187 (15) [$\text{HIm}^{\text{Mes}} + \text{H}$] $^+$, 223 (55)

$[(\text{HIm}^{\text{Mes}})\text{BH}_3 + \text{Na}]^+$, 385 (100) $[(\text{HIm}^{\text{Mes}})_2\text{BH}_2]^+$. **EA** (%) calculated for $\text{C}_{12}\text{H}_{17}\text{BN}_2$: N 14.00, C 72.03, H 8.56; found: N 13.60, C 71.81, H 8.25.

2.2.4.3. Synthesis of $(\text{HIm}^{\text{Me}})\text{BPh}_3$ (**22**)

A large excess of 1-methylimidazole (HIm^{Me} ; 82.106 g/mol, 7.344 mmol, 0.603 g) was solubilized in MeCN (60 mL). Then, ammonium tetraphenylborate (NH_4BPh_4 ; 337.273 g/mol, 5.248 mmol, 1.770 g) was added to the solution. A white precipitate was formed, but the solution became limpid after 1 hour. The reaction was carried out under magnetic stirring at reflux for 70 hours. After that, the reaction was dried at reduced pressure, obtaining a white residue. Et_2O was poured into the round-bottom flask to solubilize the starting materials that did not react. The obtained mixture was filtered, the mother liquors were dried at reduced pressure and CHCl_3 was poured into the round-bottom flask to precipitate the excess of NH_4BPh_4 . The mixture was filtered and the mother liquors were dried at reduced pressure to give the white ligand $(\text{HIm}^{\text{Me}})\text{BPh}_3$ (**22**) in 76% yield.



MM: 324.234 g/mol. **Solubility**: THF, CH_2Cl_2 , CHCl_3 , MeCN, DMSO, Me_2CO . **MP**: 209-212 °C. **$^1\text{H-NMR}$** ($\text{DMSO-}d_6$, 293 K): δ 3.79 (s, 3H, CH_3), 6.90 (d, 1H, 4-CH or 5-CH), 7.03-7.15 (m, 15H, ArH), 7.44 (d, 1H, 4-CH or 5-CH), 8.09 (s, 1H, 2-CH). **$^{13}\text{C}\{^1\text{H}\}\text{-NMR}$** ($\text{DMSO-}d_6$, 293 K): δ 35.13 (CH_3); 122.34, 124.85, 126.42, 127.02, 134.49, 138.58 (ArC). **$^{11}\text{B-NMR}$** ($(\text{CD}_3)_2\text{CO}$, 293 K): δ -6.52 (s, BPh_3). **FT-IR** (cm^{-1}):

3158w, 3133m, 3085w, 3064m, 3054mbr, 3010mbr (C-H); 1546m, 1531m, 1483mbr (C=C/C=N).

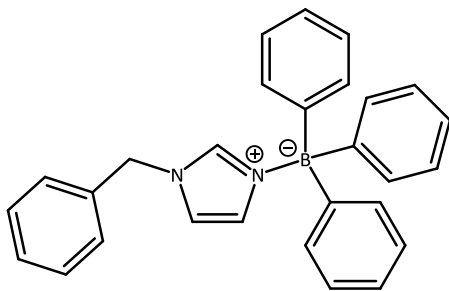
ESI-MS(+) (major positive ions, MeCN), m/z (%): 83 (100) $[\text{HIm}^{\text{Me}} + \text{H}]^+$, 247 (25) $[(\text{HIm}^{\text{Me}})\text{BPh}_2]^+$.

EA (%) calculated for $\text{C}_{22}\text{H}_{21}\text{BN}_2$: N 8.64, C 81.50, H 6.53; found: N 8.38, C 81.14, H 6.56.

2.2.4.4. Synthesis of $(\text{HIm}^{\text{Bn}})\text{BPh}_3$ (**23**)

A large excess of HIm^{Bn} (158.204 g/mol, 4.000 mmol, 0.633 g) was solubilized in MeCN (60 mL). Then, NH_4BPh_4 (337.273 g/mol, 2.850 mmol, 0.961 g) was added to the solution. A white precipitate was formed, but the solution became limpid after 1 hour. The reaction was carried out under magnetic stirring at reflux for 70 hours. After that, the reaction was dried at reduced pressure, obtaining a white residue. EtOH was poured into the round-bottom flask to solubilize the starting materials that did not react. The obtained mixture was filtered, the mother liquors were dried at reduced pressure to give the white ligand $(\text{HIm}^{\text{Bn}})\text{BPh}_3$ (**23**) in 50% yield.

MM: 400.332 g/mol. **Solubility:** THF, CH₂Cl₂, CHCl₃, MeCN, DMSO, Me₂CO. **MP:** 175-178 °C. **¹H-NMR**



NMR (DMSO-*d*₆, 293 K): δ 5.39 (s, 2H, PhCH₂N), 6.91 (s, 1H, 4-CH or 5-CH), 7.04-7.43 (m, 20H, ArH), 7.49 (s, 1H, 4-CH or 5-CH), 8.37 (s, 1H, 2-CH). **¹³C{¹H}-NMR** (DMSO-*d*₆, 293 K): δ 51.24 (PhCH₂N); 121.25, 124.90, 127.23, 128.21, 129.33, 129.47, 133.46 (ArC), 136.33 (2-CH). **¹¹B-NMR** (CDCl₃, 293 K): δ -6.37 (s, BPh₃). **FT-IR** (cm⁻¹): 3163m, 3140m, 3125m,

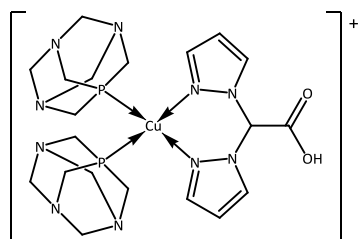
3064mbr, 3023m (C-H); 1531mbr, 1506m, 1489mbr (C=C/C=N). **ESI-MS(+)** (major positive ions, MeCN), *m/z* (%): 91 (80) [C₇H₇]⁺, 159 (100) [HIm^{Bn} + H]⁺, 242 (50) [BPh₃ + H]⁺, 481 (45) [(Im^{Bn})₂BPh₂]⁺. **EA** (%) calculated for C₂₈H₂₅BN₂: N 7.00, C 84.01, H 6.29; found: N 7.06, C 83.72, H 6.03.

2.3. Syntheses of the complexes

2.3.1. Syntheses of the complexes bearing acid ligands

2.3.1.1. Synthesis of [(PTA)₂Cu(L^{1H})]PF₆ (**24**)

The metal precursor tetrakis(acetonitrile)copper(I) hexafluorophosphate ([Cu(MeCN)₄]PF₆; 372.722 g/mol, 0.750 mmol, 0.280 g) was added to a solution of 1,3,5-triaza-7-phosphaadamantane (PTA; 157.157 g/mol, 1.500 mmol, 0.236 g) in MeCN (50 mL) and the mixture was stirred at room temperature for 3 hours. Then, a solution of L^{1H} (**1**, 192.175 g/mol, 0.750 mmol, 0.144 g) in MeOH was added and the mixture was stirred at room temperature for 24 hours. The reaction was filtered and dried at reduced pressure to give the complex [(PTA)₂Cu(L^{1H})]PF₆ (**24**) in 63% yield.



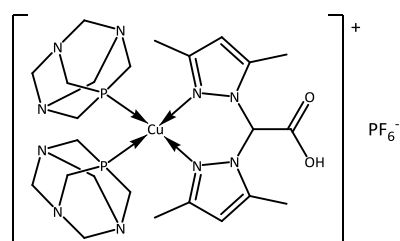
MM: 715.002 g/mol. **Solubility:** H₂O, MeCN, DMSO. **MP:** 109-112 °C. **¹H-NMR** (DMSO-*d*₆, 293 K): δ 4.11 (br, 12H, NCH₂P), 4.53-4.67 (m, 12H, NCH₂N), 6.42 (sbr, 2H, 4-CH), 7.29 (s, 1H, CHCO), 7.67 (sbr, 2H, 5-CH), 8.04 (sbr, 2H, 3-CH). **¹H-NMR** (D₂O, 293 K): δ 4.05 (br, 12H, NCH₂P), 4.58-4.70 (m, 12H, NCH₂N),

6.48 (sbr, 2H, 4-CH), 7.15 (sbr, 1H, CHCO), 7.62 (sbr, 2H, 5-CH), 7.94 (sbr, 2H, 3-CH). **³¹P{¹H}-NMR** (D₂O, 293 K): δ -87.01 (br), -145.02 (hept, J_{(P-F)}} = 709 Hz, PF₆). **FT-IR** (cm⁻¹): 3372br (O-H); 3124br, 2945br (C-H); 1645s (ν_{asym} C=O); 1515w (C=C/C=N); 1450w, 1405m, 1359w, 1292s, 1242m, 1207sh, 1119sh, 1100m, 1060w, 1016m, 972m, 950m, 893w, 831s, 748s. **ESI-MS(+)** (major positive ions, MeCN), *m/z* (%): 412 (100) [(PTA)Cu(L^{1H})]⁺. **ESI-MS(-)** (major negative ions,

MeCN), m/z (%): 145 (100) $[\text{PF}_6]^-$, 191 (10) $[\text{L}^1]^-$. **EA** (%) calculated for $\text{C}_{20}\text{H}_{32}\text{CuF}_6\text{N}_{10}\text{O}_2\text{P}_3$: N 19.59, C 33.60, H 4.51; found: N 18.75, C 33.27, H 4.38.

2.3.1.2. Synthesis of $[(\text{PTA})_2\text{Cu}(\text{L}^{2\text{H}})]\text{PF}_6$ (**25**)

This compound was prepared following the procedure described for **24** but employing the ligand $\text{L}^{2\text{H}}$ (**2**; 248.281 g/mol, 0.750 mmol, 0.186 g) and washing the solid in the filter with fresh MeCN before drying it at reduced pressure. The white complex $[(\text{PTA})_2\text{Cu}(\text{L}^{2\text{H}})]\text{PF}_6$ (**25**) was obtained in 52% yield.



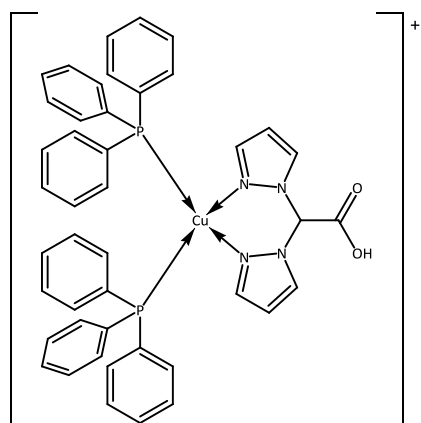
MM: 771.110 g/mol. **Solubility**: H_2O , MeCN, DMSO. **MP**: 190-193 °C. **$^1\text{H-NMR}$** (DMSO- d_6 , 293 K): δ 2.19 (s, 6H, 3- or 5- CH_3), 2.37 (s, 6H, 3- or 5- CH_3), 4.13 (sbr, 12H, NCH_2P), 4.53-4.82 (m, 12H, NCH_2N), 6.07 (s, 2H, 4- CH), 6.44 (sbr, 1H, CHCO). **$^1\text{H-NMR}$** (D_2O , 293 K): δ 2.21 (s, 6H, 3- or 5- CH_3), 2.40 (s, 6H, 3- or 5- CH_3), 4.12 (sbr, 12H, NCH_2P), 4.63-4.70 (m, 12H, NCH_2N), 6.12 (s, 2H, 4- CH), 6.60 (br, 1H, CHCO). **$^{31}\text{P}\{^1\text{H}\}$ -NMR** (D_2O , 293 K): δ -85.87 (br), -144.03 (hept, $J_{(\text{P-F})} = 709$ Hz, PF_6). **$^{31}\text{P}\{^1\text{H}\}$ -NMR** (CD_3CN , 293 K): δ -90.70 (br), -144.53 (hept, $J_{(\text{P-F})} = 706$ Hz, PF_6). **FT-IR** (cm^{-1}): 3384br (O-H); 2924br (C-H); 1640s (ν_{asym} C=O); 1560m (C=C/C=N); 1449w, 1418w, 1393w, 1351w, 1294s, 1242m, 1120w, 1103m, 1043w, 1014m, 971m, 948m, 830s, 741m. **ESI-MS(+)** (major positive ions, MeCN), m/z (%): 468 (100) $[(\text{PTA})\text{Cu}(\text{L}^{2\text{H}})]^+$. **ESI-MS(-)** (major negative ions, MeCN), m/z (%): 145 (100) $[\text{PF}_6]^-$. **EA** (%) calculated for $\text{C}_{24}\text{H}_{40}\text{CuF}_6\text{N}_{10}\text{O}_2\text{P}_3$: N 18.16, C 37.38, H 5.23; found: N 17.01, C 36.32, H 4.88.

2.3.1.3. Synthesis of $[(\text{PPh}_3)_2\text{Cu}(\text{L}^{1\text{H}})]\text{PF}_6$ (**26**)

This compound was prepared following the procedure described for **24** but employing the coligand triphenylphosphine (PPh_3 ; 262.292 g/mol, 2.000 mmol, 0.525 g), adding the ligand $\text{L}^{1\text{H}}$ (**1**) as a powder and not as a solution and washing the solid in the filter with fresh Et_2O (50 mL) before drying it at reduced pressure. The white complex $[(\text{PPh}_3)_2\text{Cu}(\text{L}^{1\text{H}})]\text{PF}_6$ (**26**) was obtained in 51% yield.

MM: 925.272 g/mol. **Solubility**: MeOH, CHCl_3 , MeCN, DMSO. **MP**: 98-101 °C. **$^1\text{H-NMR}$** (DMSO- d_6 , 293 K): δ 6.36 (sbr, 2H, 4- CH), 7.26-7.61 (m, 33H, CHCO , 5- CH and ArH), 8.06 (sbr, 2H, 3- CH). **$^{13}\text{C}\{^1\text{H}\}$ -NMR** (DMSO- d_6 , 293 K): δ 74.0 (CHCO); 107.2 (4- C_{Pz}); 129.5, 130.8, 132.1, 132.2, 132.7, 133.3, 133.6, 133.9, 134.0 (3- C_{Pz} , 5- C_{Pz} and ArC); 141.9 (ArC); 166.2 (CO). **$^{31}\text{P}\{^1\text{H}\}$ -NMR** (DMSO- d_6 , 293 K): δ -3.77 (sbr), -143.10 (hept, $J_{(\text{P-F})} = 713$ Hz, PF_6). **FT-IR** (cm^{-1}): 3635br (O-H); 3138w,

3056w 3004w, 2987w (C-H); 1752m (ν_{asym} C=O); 1616w, 1586w (C=C/C=N); 1523w, 1481m,

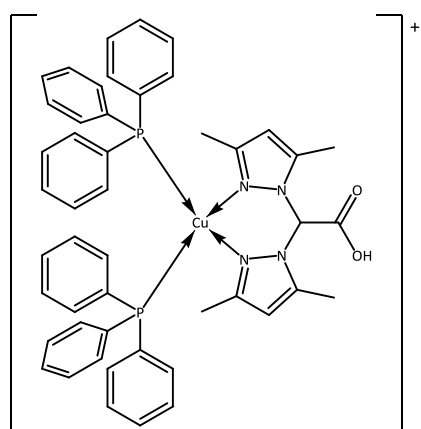


PF_6^-

1455w, 1435m, 1403m, 1298m, 1226w, 1207w, 1187w, 1160w, 1096m, 1058w, 1027w, 999w, 986w, 916w, 833s, 741s. **ESI-MS(+)** (major positive ions, MeOH), m/z (%): 587 (100) $[(\text{PPh}_3)_2\text{Cu}]^+$, 517 (60) $[(\text{PPh}_3)\text{Cu}(\text{L}^{1\text{H}})]^+$. **ESI-MS(-)** (major negative ions, MeOH), m/z (%): 145 (100) $[\text{PF}_6]^-$. **EA** (%) calculated for $\text{C}_{44}\text{H}_{38}\text{CuF}_6\text{N}_4\text{O}_2\text{P}_3$: N 6.06, C 57.12, H 4.14; found: N 5.58, C 56.29, H 4.14.

2.3.1.4. Synthesis of $[(\text{PPh}_3)_2\text{Cu}(\text{L}^{2\text{H}})]\text{PF}_6$ (**27**)

This compound was prepared following the procedure described for **24** but employing the coligand PPh_3 (262.292 g/mol, 2.000 mmol, 0.525 g) and the ligand $\text{L}^{2\text{H}}$ (**2**; 248.281 g/mol, 1.000 mmol, 0.248 g), the latter added to the reaction as a powder and not as a solution, and washing the solid in the filter with fresh Et_2O (50 mL) before drying it at reduced pressure. The white complex $[(\text{PPh}_3)_2\text{Cu}(\text{L}^{2\text{H}})]\text{PF}_6$ (**27**) was obtained in 58% yield.



PF_6^-

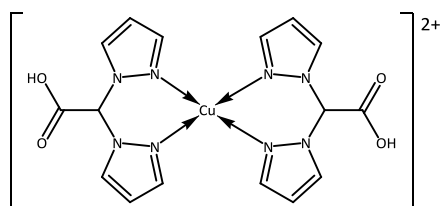
MM: 981.380 g/mol. **Solubility**: MeOH, CHCl_3 , MeCN, DMSO, Me_2CO . **MP**: 116-118 °C. **$^1\text{H-NMR}$** (CDCl_3 , 293 K): δ 2.01 (s, 6H, 3- or 5- CH_3), 2.47 (s, 6H, 3- or 5- CH_3), 6.14 (s, 2H, 4- CH), 6.81 (br, 1H, CHCO), 7.26-7.68 (m, 30H, ArH). **$^{31}\text{P}\{^1\text{H}\}\text{-NMR}$** (CDCl_3 , 293 K): δ -2.85 (sbr), -143.31 (hept, $J_{\text{(P-F)}} = 713$ Hz, PF_6). **FT-IR** (cm^{-1}): 3144w, 3053w, 2990w, 2930w (C-H); 1740m (ν_{asym} C=O); 1586w, 1563m (C=C/C=N); 1482m, 1469sh, 1436w, 1394w, 1314w,

1298sh, 1260w, 1233w, 1181w, 1097m, 1062w, 1047w, 1028w, 999w, 898w, 878w, 832s, 762sh, 744m, 720w. **ESI-MS(+)** (major positive ions, MeOH), m/z (%): 573 (100) $[(\text{PPh}_3)\text{Cu}(\text{L}^{2\text{H}})]^+$. **ESI-MS(-)** (major negative ions, MeOH), m/z (%): 145 (100) $[\text{PF}_6]^-$. **EA** (%) calculated for $\text{C}_{48}\text{H}_{46}\text{CuF}_6\text{N}_4\text{O}_2\text{P}_3$: N 5.71, C 58.75, H 4.72; found: N 5.64, C 57.58, H 5.03.

2.3.1.5. Synthesis of $[\text{Cu}(\text{L}^{1\text{H}})_2](\text{ClO}_4)_2$ (**28**)

A solution of copper(II) perchlorate hexahydrate ($\text{Cu}(\text{ClO}_4)_2 \cdot 6\text{H}_2\text{O}$; 370.529 g/mol, 0.500 mmol, 0.185 g) in EtOH (25 mL) was added to a solution of $\text{L}^{1\text{H}}$ (**1**; 192.175 g/mol, 1.000 mmol, 0.192 g) in EtOH (25 mL). The reaction mixture was stirred at room temperature for 24 hours.

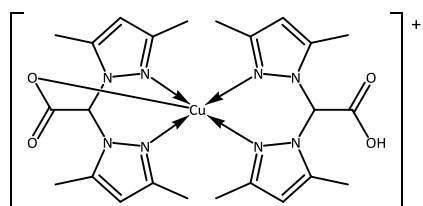
After that, the reaction was filtered and the precipitate dried at reduced pressure. The blue complex $[\text{Cu}(\text{L}^{1\text{H}})_2](\text{ClO}_4)_2$ (**28**) was obtained in 58% yield.



MM: 646.795 g/mol. **Solubility:** H₂O, MeOH, MeCN, DMSO. **MP:** 206-210 °C dec. **FT-IR** (cm⁻¹): 3557wbr (O-H); 3133w, 3117w, 3016w (C-H); 1736br (ν_{asym} C=O); 1515m (C=C/C=N); 1451m, 1409s, 1372m, 1348w, 1284w, 1218br; 1085s, 1067s (ClO₄); 996m, 928m, 906br, 861m, 847m, 790m, 765s, 712sbr. **ESI-MS(+)** (major positive ions, MeCN), m/z (%): 446 (100) $[\text{Cu}(\text{L}^1)_2 + \text{H}]^+$. **ESI-MS(-)** (major negative ions, MeCN), m/z (%): 99 (100) $[\text{ClO}_4]^-$. **EA** (%) calculated for C₁₆H₁₆Cl₂CuN₈O₁₂: N 17.32, C 29.71, H 2.49; found: N 16.96, C 30.14, H 2.15.

2.3.1.6. Synthesis of $[(\text{L}^{2\text{H}})\text{Cu}(\text{L}^2)](\text{ClO}_4)$ (**29**)

This compound was prepared following the procedure described for **28** but employing the ligand L^{2H} (**2**; 248.281 g/mol, 0.800 mmol, 0.199 g). The blue complex $[(\text{L}^{2\text{H}})\text{Cu}(\text{L}^2)](\text{ClO}_4)$ (**29**) was obtained in 62% yield. Crystals of the complex **29**, suitable for SC-XRD, were obtained by slow evaporation of an MeCN solution of **29**.



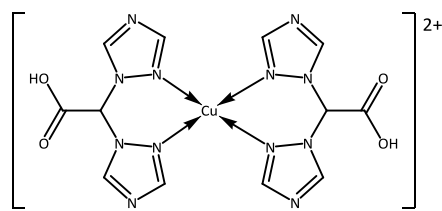
MM: 658.557 g/mol. **Solubility:** MeOH, MeCN, DMSO. **MP:** 211-215 °C dec. **FT-IR** (cm⁻¹): 3459vbr (O-H); 3139w, 2972w (C-H); 1705br, 1667sh (ν_{asym} C=O); 1560m (C=C/C=N); 1464m, 1419m, 1390m, 1377m, 1312m, 1246m, 1222br; 1081s, 1050sh (ClO₄); 987m, 939m, 909m, 883m, 815m, 804m, 774m, 743m, 712m. **ESI-MS(+)** (major positive ions, MeCN), m/z (%): 558 (100) $[(\text{L}^{2\text{H}})\text{Cu}(\text{L}^2)]^+$, 869 (30) $[\text{Cu}_2(\text{L}^2)_3]^+$, 1117 (10) $[\text{Cu}_2(\text{L}^2)_4 + \text{H}]^+$. **ESI-MS(-)** (major negative ions, MeCN), m/z (%): 99 (100) $[\text{ClO}_4]^-$. **EA** (%) calculated for C₂₄H₃₂ClCuN₈O₈: N 17.02, C 43.77, H 4.74; found: N 16.75, C 43.80, H 4.77.

2.3.1.7. Synthesis of $[\text{Cu}(\text{L}^{3\text{H}})_2](\text{ClO}_4)_2 \cdot \text{MeOH}$ (**30**)

This compound was prepared following the procedure described for **28** but employing the ligand L^{3H} (**3**; 194.154 g/mol, 1.000 mmol, 0.194 g) and using MeOH (70 mL) as solvent. The pale blue complex $[\text{Cu}(\text{L}^{3\text{H}})_2](\text{ClO}_4)_2 \cdot \text{MeOH}$ (**30**) was obtained in 51% yield.

MM: 682.789 g/mol. **Solubility:** DMSO. **MP:** 195-199 °C dec. **FT-IR** (cm⁻¹): 3446br (O-H); 3134m, 2977w (C-H); 1664br (ν_{asym} C=O); 1528m (C=C/C=N); 1456w, 1365m, 1283m, 1208m; 1125s, 1083sbr (ClO₄); 1021m, 995m, 931w, 889m, 832m, 760s. **ESI-MS(+)** (major positive ions,

DMSO/MeCN), m/z (%): 290 (30) $[(L^3)Cu(MeOH)]^+$. **ESI-MS(-)** (major negative ions,

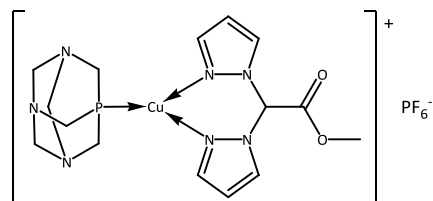


DMSO/MeCN), m/z (%): 99 (100) $[ClO_4]^-$, 149 (10) $[(Tz)_2CH]^-$, 193 (10) $[L^3]^-$, 221 (100) $[Na(ClO_4)_2]^-$, 360 (60) $[Cu(ClO_4)_3]^-$. **EA** (%) calculated for $C_{13}H_{16}Cl_2CuN_{12}O_{13}$: N 24.62, C 22.87, H 2.36; found: N 24.14, C 22.49, H 2.55.

2.3.2. Syntheses of the complexes bearing esterified ligands

2.3.2.1. Synthesis of $[(PTA)Cu(L^{1Me})]PF_6$ (**31**)

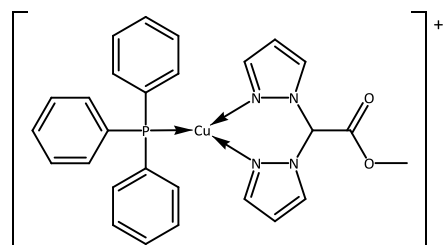
$[Cu(MeCN)_4]PF_6$ (372.722 g/mol, 0.533 mmol, 0.199 g) was solubilized in MeCN (30 mL) and stirred at room temperature for 15 minutes. Subsequently, the phosphane PTA (157.157 g/mol, 0.533 mmol, 0.084 g) was added and, after further 3 hours of stirring at room temperature, the ligand L^{1Me} (**4**; 206.201 g/mol, 0.533 mmol, 0.110 g) was added as well. The reaction was carried out under magnetic stirring at room temperature for 24 hours. At the end, the mixture was filtered and the mother liquors (limpid and colorless) were dried at reduced pressure, to give the whitish complex $[(PTA)Cu(L^{1Me})]PF_6$ (**31**) in 81% yield.



MM: 571.872 g/mol. **Solubility**: H_2O , MeOH, MeCN, DMSO, Me_2CO . **MP**: 180-185 °C. **1H -NMR** (CD_3CN , 293 K): δ 3.78 (s, 3H, OCH_3), 4.09 (s, 6H, NCH_2P), 4.48-4.57 (m, 6H, NCH_2N), 6.44 (t, 2H, 4-CH), 7.32 (s, 1H, $CHCO$), 7.66 (d, 2H, 5-CH), 7.92 (d, 2H, 3-CH). **$^{13}C\{^1H\}$ -NMR** (CD_3CN , 293 K): δ 49.89, 53.65, 72.49, 73.07, 106.97, 132.11, 141.86, 164.73. **$^{31}P\{^1H\}$ -NMR** (CD_3CN , 293 K): δ -93.52 (sbr), -143.51 (hept, $J_{(P-F)} = 708$ Hz, PF_6). **$^{31}P\{^1H\}$ -NMR** (CD_3CN , 243 K): δ -95.28 (sbr), -144.75 (hept, $J_{(P-F)} = 707$ Hz, PF_6). **FT-IR** (cm^{-1}): 3135wbr, 2954wbr (C-H); 1759m ($\nu_{asym} C=O$); 1654wbr; 1519w (C=C/C=N); 1451wbr, 1416sh, 1403m, 1395wbr, 1353wbr, 1295mbr, 1238mbr, 1206w, 1179w, 1099m, 1057w, 1039w, 1017m, 970m, 950m, 918w, 895wbr; 831vs (PF_6); 817sh, 758s, 741sh, 655m, 610m; 555vs (PF_6); 445m, 396m. **ESI-MS(+)** (major positive ions, MeCN), m/z (%): 158 (65) $[PTA + H]^+$, 269 (100) $[Cu(L^{1Me})]^+$, 426 (20) $[(PTA)Cu(L^{1Me})]^+$, 475 (10) $[Cu(L^{1Me})_2]^+$. **ESI-MS(-)** (major negative ions, MeCN), m/z (%): 145 (100) $[PF_6]^-$. **EA** (%) calculated for $C_{15}H_{22}CuF_6N_7O_2P_2$: N 17.15, C 31.50, H 3.88; found: N 16.86, C 31.56, H 3.68.

2.3.2.2. Synthesis of $[(PPh_3)Cu(L^{1Me})]PF_6$ (**32**)

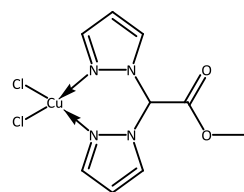
This compound was prepared following the procedure described for **31** but employing the coligand PPh_3 (262.292 g/mol, 0.600 mmol, 0.157 g). The whitish complex $[(PPh_3)Cu(L^{1Me})]PF_6$ (**32**) was obtained in 74% yield.



MM: 677.007 g/mol. **Solubility:** MeOH, $CHCl_3$, MeCN, DMSO, Me_2CO . **MP:** 60-65 °C. **1H -NMR** (CD_3CN , 293 K): δ 3.65 (s, 3H, OCH_3), 6.42 (t, 2H, 4-CH), 7.34-7.53 (m, 16H, $CHCO$ and ArH), 7.59 (d, 2H, 5-CH), 7.93 (d, 2H, 3-CH). **$^{13}C\{^1H\}$ -NMR** (CD_3CN , 293 K): δ 53.51, 73.26, 106.99, 128.92, 130.36, 132.00, 132.40, 132.66, 133.42, 141.75, 164.80. **$^{31}P\{^1H\}$ -NMR** (CD_3CN , 293 K): δ -1.48 (sbr), -144.62 (hept, $J_{(P-F)} = 707$ Hz, PF_6). **FT-IR** (cm^{-1}): 3137wbr, 3055wbr, 3006wbr, 2959w, 2918w, 2850w (C-H); 1760m (ν_{asym} C=O); 1523wbr, 1481m (C=C/C=N); 1454m, 1436m, 1403m, 1376w, 1356w, 1307sh, 1295mbr, 1227m, 1207w, 1180w, 1161w, 1097s, 1058m, 1027w, 998m, 982sh, 974m, 921w, 872sh; 830vs (PF_6); 760sh, 744vs, 693s, 610m; 556s (PF_6); 531s, 504s, 430m, 334m, 280m, 252m, 218m. **ESI-MS(+)** (major positive ions, MeCN), m/z (%): 269 (15) $[Cu(L^{1Me})]^+$, 531 (100) $[(PPh_3)Cu(L^{1Me})]^+$, 587 (65) $[(PPh_3)_2Cu]^+$. **ESI-MS(-)** (major negative ions, MeCN), m/z (%): 145 (100) $[PF_6]^-$. **EA** (%) calculated for $C_{27}H_{25}CuF_6N_4O_2P_2$: N 8.28, C 47.90, H 3.72; found: N 7.96, C 48.45, H 3.77.

2.3.2.3. Synthesis of $[Cu(L^{1Me})]Cl_2$ (**33**)

The metal precursor copper(II) chloride dihydrate ($CuCl_2 \cdot 2H_2O$; 170.476 g/mol, 1.000 mmol, 0.170 g) was solubilized in MeOH (50 mL) and stirred at room temperature for 15 minutes, obtaining a light green solution. Subsequently, the ligand L^{1Me} (**4**; 206.201 g/mol, 1.000 mmol, 0.206 g) was added. The reaction was carried out under magnetic stirring at room temperature for 24 hours. At the end, the mixture was filtered and the precipitate was dried at reduced pressure, to give the light green complex $[Cu(L^{1Me})]Cl_2$ (**33**) in 75% yield.

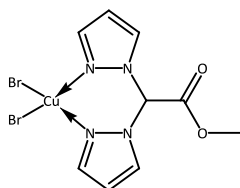


MM: 340.651 g/mol. **Solubility:** H_2O , MeOH, DMSO. **MP:** 208-212 °C. **FT-IR** (cm^{-1}): 3139w, 3117w, 2990wbr, 2959wbr (C-H); 1748vs (ν_{asym} C=O); 1518w, 1510w (C=C/C=N); 1454m, 1431m, 1415m, 1403s, 1355w, 1293sh, 1285vs, 1255m, 1230s, 1198m, 1176m, 1148w, 1105m, 1093m, 1072s, 1059s, 1003m, 989m, 973s, 924w, 911w, 869w, 854m, 805m, 771vs, 654m, 607s, 597s, 400m, 352m, 342m, 305s; 278vs (Cu-Cl); 223m. **ESI-MS(+)** (major positive ions, MeOH), m/z (%): 206 (50) $[L^{1Me} + H]^+$, 229 (100) $[L^{1Me} + Na]^+$, 269 (55) $[Cu(L^{1Me} - H)]^+$, 475 (20) $[(L^{1Me})Cu(L^{1Me} - H)]^+$. **ESI-**

MS(-) (major negative ions, MeOH), m/z (%): 170 (100) $[\text{CuCl}_3]^-$. **EA** (%) calculated for $\text{C}_9\text{H}_{10}\text{Cl}_2\text{CuN}_4\text{O}_2$: N 16.45, C 31.73, H 2.96; found: N 16.63, C 31.79, H 2.66.

2.3.2.4. Synthesis of $[\text{Cu}(\text{L}^{1\text{Me}})]\text{Br}_2$ (**34**)

This compound was prepared following the procedure described for **33** but employing the metal precursor copper(II) bromide (CuBr_2 ; 223.354 g/mol, 1.000 mmol, 0.223 g). The reddish-brown complex $[\text{Cu}(\text{L}^{1\text{Me}})]\text{Br}_2$ (**34**) was obtained in 60% yield.

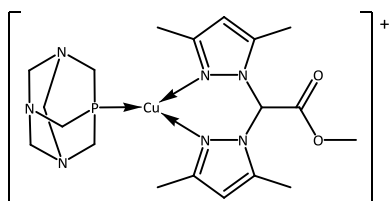


MM: 429.559 g/mol. **Solubility:** H_2O , MeOH, DMSO. **MP:** 192-195 °C. **FT-IR** (cm^{-1}): 3147w, 3133w, 3119m, 2979wbr, 2956wbr (C-H); 1748s (ν_{asym} C=O); 1515wbr (C=C/C=N); 1454m, 1430m, 1412m, 1400s, 1354w, 1296sh, 1283s, 1254m, 1226s, 1197m, 1175m, 1148wbr, 1105m, 1091m, 1071m, 1058s,

1003m, 987m, 972sbr, 922wbr, 907m, 862w, 852m, 806m, 765vs, 651m, 605s, 595s, 398m, 341m, 306m; 235vs (Cu-Br); 202m. **ESI-MS(+)** (major positive ions, MeOH), m/z (%): 229 (100) $[\text{L}^{1\text{Me}} + \text{Na}]^+$, 269 (60) $[\text{Cu}(\text{L}^{1\text{Me}} - \text{H})]^+$, 350 (85) $[(\text{L}^{1\text{Me}})\text{CuBr}]^+$. **ESI-MS(-)** (major negative ions, MeOH), m/z (%): 304 (100) $[\text{CuBr}_3]^-$. **EA** (%) calculated for $\text{C}_9\text{H}_{10}\text{Br}_2\text{CuN}_4\text{O}_2$: N 13.04, C 25.16, H 2.35; found: N 12.59, C 25.35, H 2.27.

2.3.2.5. Synthesis of $[(\text{PTA})\text{Cu}(\text{L}^{2\text{Me}})]\text{PF}_6$ (**35**)

This compound was prepared following the procedure described for **31** but employing the ligand $\text{L}^{2\text{Me}}$ (**5**; 262.308 g/mol, 0.600 mmol, 0.157 g). The white complex $[(\text{PTA})\text{Cu}(\text{L}^{2\text{Me}})]\text{PF}_6$ (**35**) was obtained in 86% yield.

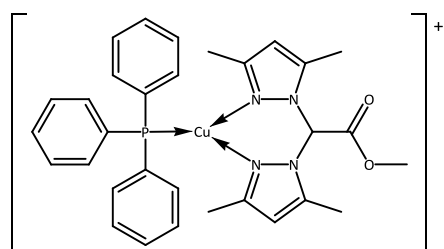


MM: 627.980 g/mol. **Solubility:** MeOH, MeCN, DMSO, Me_2CO . **MP:** 189-193 °C. **$^1\text{H-NMR}$** (CD_3CN , 293 K): δ 2.27 (sbr, 6H, 3- or 5- CH_3), 2.41 (sbr, 6H, 3- or 5- CH_3), 3.76 (s, 3H, OCH_3), 4.10 (s, 6H, NCH_2P), 4.48-4.58 (m, 6H, NCH_2N), 6.11 (sbr, 2H, 4- CH), 6.81 (s, 1H, CHCO). **$^{13}\text{C}\{^1\text{H}\}$ -NMR** (CD_3CN , 293 K): δ 10.22, 13.25, 50.48, 53.81, 65.96, 72.59, 106.50, 143.43, 151.25, 164.75. **$^{31}\text{P}\{^1\text{H}\}$ -NMR** (CD_3CN , 293 K): δ -95.72 (sbr), -144.78 (hept, $J_{\text{P-F}} = 711$ Hz, PF_6). **FT-IR** (cm^{-1}): 3147vw, 2954sh, 2924wbr (C-H); 1759m (ν_{asym} C=O); 1640wbr; 1562w (C=C/C=N); 1446sh, 1420m, 1392w, 1317m, 1285w, 1270w, 1242m, 1230m, 1155sh, 1126w, 1102w, 1037w, 1016m, 972m, 950m, 895w, 868sh; 833vs (PF_6); 742m, 712m, 556s (PF_6); 453m, 397m, 297m, 249m, 223m. **ESI-MS(+)** (major positive ions, MeCN), m/z (%): 158 (5) $[\text{PTA} + \text{H}]^+$, 263 (15) $[\text{L}^{2\text{Me}} + \text{H}]^+$, 285 (30) $[\text{L}^{2\text{Me}} + \text{Na}]^+$, 325 (20) $[\text{Cu}(\text{L}^{2\text{Me}})]^+$, 424 (15) $[(\text{PTA})\text{Cu}\{(\text{Pz}^{3,5-\text{Me}})_2\text{CH}_2\}]^+$, 482 (100) $[(\text{PTA})\text{Cu}(\text{L}^{2\text{Me}})]^+$, 529 (40) $[(\text{L}^{2\text{Me}})\text{Cu}\{(\text{Pz}^{3,5-\text{Me}})_2\text{CH}_2\}]^+$, 587

(50) $[\text{Cu}(\text{L}^{2\text{Me}})_2]^+$. **ESI-MS(-)** (major negative ions, MeCN), m/z (%): 145 (100) $[\text{PF}_6]^-$. **EA** (%) calculated for $\text{C}_{19}\text{H}_{30}\text{CuF}_6\text{N}_7\text{O}_2\text{P}_2$: N 15.61, C 36.34, H 4.82; found: N 14.95, C 37.06, H 4.96.

2.3.2.6. Synthesis of $[(\text{PPh}_3)\text{Cu}(\text{L}^{2\text{Me}})]\text{PF}_6$ (**36**)

$[\text{Cu}(\text{MeCN})_4]\text{PF}_6$ (372.722 g/mol, 0.600 mmol, 0.224 g), PPh_3 (262.292 g/mol, 0.600 mmol, 0.157 g) and $\text{L}^{2\text{Me}}$ (**5**; 262.308 g/mol, 0.600 mmol, 0.157 g) were solubilized in MeCN (30 mL). The reaction was carried out under magnetic stirring at room temperature for 24 hours. At the end, the solution was dried at reduced pressure, few milliliters of MeCN were poured into the round-bottom flask and, after that, Et_2O (about 30 mL) was added. The mixture was filtered and the precipitate was dried at reduced pressure, to give the whitish complex $[(\text{PPh}_3)\text{Cu}(\text{L}^{2\text{Me}})]\text{PF}_6$ (**36**) in 86% yield.

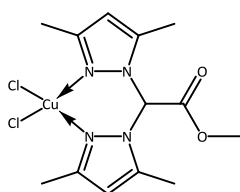


MM: 733.104 g/mol. **Solubility**: MeOH, CHCl_3 , MeCN, DMSO, Me_2CO . **MP**: 199-204 °C. **$^1\text{H-NMR}$** (CD_3CN , 293 K): δ 2.17 (s, 6H, 3- or 5- CH_3), 2.47 (s, 6H, 3- or 5- CH_3), 3.05 (sbr, 3H, OCH_3), 6.19 (sbr, 2H, 4- CH), 6.91 (s, 1H, CHCO), 7.41-7.51 (m, 15H, ArH). **$^{13}\text{C}\{^1\text{H}\}$ -NMR** (CD_3CN , 293 K): δ 10.55, 13.64, 53.73, 106.99, 129.07, 130.50, 132.24, 133.43, 143.84, 151.70, 164.96. **$^{31}\text{P}\{^1\text{H}\}$ -NMR** (CD_3CN , 293 K): δ -2.08 (sbr), -144.63 (hept, $J_{(\text{P-F})} = 706$ Hz, PF_6). **FT-IR** (cm^{-1}): 3145vw, 3057vw, 2994vw, 2957vw, 2923vw (C-H); 1768m ($\nu_{\text{asym C=O}}$); 1564w (C=C/C=N); 1481w, 1465w, 1436m, 1420w, 1394wbr, 1375w, 1317m, 1300w, 1277w, 1263w, 1224wbr, 1184w, 1161w, 1127w, 1113w, 1096w, 1072w, 1040w, 1028sh, 999w, 877sh; 836vs (PF_6); 780m, 747m, 698s, 636w, 585w; 557s (PF_6); 527s, 512m, 491m, 444w, 363w, 298w, 279m, 251m, 229w, 213m. **ESI-MS(+)** (major positive ions, MeCN), m/z (%): 285 (15) $[\text{L}^{2\text{Me}} + \text{Na}]^+$, 325 (15) $[\text{Cu}(\text{L}^{2\text{Me}})]^+$, 529 (20) $[(\text{PPh}_3)\text{Cu}\{(\text{Pz}^{3,5-\text{Me}})_2\text{CH}_2\}]^+$, 587 (100) $[(\text{PPh}_3)\text{Cu}(\text{L}^{2\text{Me}})]^+$. **ESI-MS(-)** (major negative ions, MeCN), m/z (%): 145 (100) $[\text{PF}_6]^-$. **EA** (%) calculated for $\text{C}_{31}\text{H}_{33}\text{CuF}_6\text{N}_4\text{O}_2\text{P}_2$: N 7.64, C 50.79, H 4.54; found: N 7.98, C 50.59, H 4.50.

2.3.2.7. Synthesis of $[\text{Cu}(\text{L}^{2\text{Me}})]\text{Cl}_2$ (**37**)

The metal precursor $\text{CuCl}_2 \cdot 2\text{H}_2\text{O}$ (170.476 g/mol, 0.305 mmol, 0.052 g) was solubilized in MeOH (20 mL) and stirred at room temperature for 15 minutes, obtaining a light green solution. Subsequently, the ligand $\text{L}^{2\text{Me}}$ (**5**; 262.308 g/mol, 0.305 mmol, 0.080 g) was added. The reaction was carried out under magnetic stirring at room temperature for 24 hours. At the end, the limpid light green solution was dried at reduced pressure, few milliliters of MeOH were

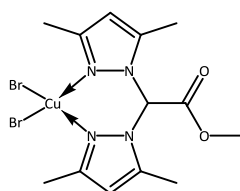
poured into the round-bottom flask and, after that, Et₂O (about 30 mL) was added. The mixture was filtered and the precipitate was dried at reduced pressure, to give the orange complex [Cu(L^{2Me})]Cl₂ (**37**) in 64% yield.



MM: 396.760 g/mol. **Solubility:** H₂O, MeOH, DMSO. **MP:** 179-182 °C. **FT-IR** (cm⁻¹): 3143w, 3105wbr, 2972w, 2955w (C-H); 1761m (ν_{asym} C=O); 1645wbr; 1561m (C=C/C=N); 1489sh, 1460m, 1440m, 1423m, 1388mbr, 1316m, 1282m, 1260m, 1223m, 1169w, 1134w, 1125w, 1047m, 997sh, 985m, 912w, 902m, 870w, 846m, 821m, 784m, 760wbr, 722m, 709m, 662w, 636m, 582w, 488w, 365m, 326s; 279vs (Cu-Cl); 228m, 208m. **ESI-MS(+)** (major positive ions, MeOH), *m/z* (%): 203 (10) [(Pz^{3,5-Me})₂CH]⁺, 266 (25) [Cu{(Pz^{3,5-Me})₂CH}]⁺, 325 (10) [Cu(L^{2Me} - H)]⁺, 420 (30) [(L^{2Me})CuCl₂ + Na]⁺, 572 (100) [(L^{2Me})Cu(L²)]⁺, 586 (10) [(L^{2Me})Cu(L^{2Me} - H)]⁺. **ESI-MS(-)** (major negative ions, MeOH), *m/z* (%): 170 (100) [CuCl₃]⁻. **EA** (%) calculated for C₁₃H₁₈Cl₂CuN₄O₂: N 14.12, C 39.35, H 4.57; found: N 13.78, C 39.44, H 4.58.

2.3.2.8. Synthesis of [Cu(L^{2Me})]Br₂ (**38**)

This compound was prepared following the procedure described for **33** but employing the metal precursor CuBr₂ (223.354 g/mol, 0.500 mmol, 0.112 g) and the ligand L^{2Me} (**5**; 262.308 g/mol, 0.500 mmol, 0.131 g). The greenish-brown complex [Cu(L^{2Me})]Br₂ (**38**) was obtained in 51% yield.

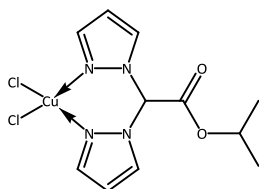


MM: 485.662 g/mol. **Solubility:** H₂O, MeOH, DMSO. **MP:** 176-180 °C. **FT-IR** (cm⁻¹): 3150wbr, 2951wbr, 2922wbr (C-H); 1757m (ν_{asym} C=O); 1562mbr (C=C/C=N); 1486wbr, 1462mbr, 1434m, 1417m, 1372mbr, 1318m, 1299m, 1273m, 1242m, 1194wbr, 1156wbr, 1140w, 1114w, 1059w, 1047m, 1034m, 985mbr, 914m, 903m, 864m, 814s, 783m, 721m, 704m, 634m, 579m, 487m, 363m, 305m, 275m, 253s; 229vs (Cu-Br). **ESI-MS(+)** (major positive ions, MeOH), *m/z* (%): 167 (30) [(Pz^{3,5-Me})CH(COOMe)]⁺, 263 (50) [(L^{2Me} + H)]⁺, 285 (100) [(L^{2Me} + Na)]⁺, 558 (10) [(L^{2H})Cu(L²)]⁺, 572 (50) [(L^{2Me})Cu(L²)]⁺, 587 (80) [(L^{2Me})Cu(L^{2Me} - H)]⁺. **ESI-MS(-)** (major negative ions, MeOH), *m/z* (%): 304 (100) [CuBr₃]⁻. **EA** (%) calculated for C₁₃H₁₈Br₂CuN₄O₂: N 11.54, C 32.15, H 3.74; found: N 11.39, C 32.16, H 3.77.

2.3.2.9. Synthesis of [Cu(L^{1iPr})]Cl₂ (**39**)

The metal precursor CuCl₂·2H₂O (170.476 g/mol, 0.500 mmol, 0.085 g) was solubilized in MeCN (30 mL) and stirred for 15 minutes, obtaining a light green solution. Subsequently, the

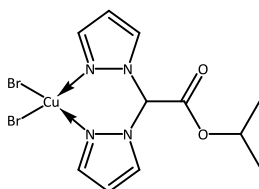
ligand L^{1iPr} (**6**; 234.254 g/mol, 0.500 mmol, 0.117 g) was added and the reaction was carried out under magnetic stirring at room temperature for 24 hours. The mixture was filtered and the precipitate was dried at reduced pressure, to give the light green complex [Cu(L^{1iPr})]Cl₂ (**39**) in 95% yield.



MM: 368.705 g/mol. **Solubility:** MeCN (slightly soluble), DMSO. **MP:** 191-193 °C. **FT-IR** (cm⁻¹): 3139w, 3123w, 3109w, 2986w (C-H); 1736vs (ν_{asym} C=O); 1516w (C=C/C=N); 1454m, 1404s, 1377m, 1357w, 1345w, 1284vs, 1255s, 1231s, 1198s, 1148m, 1094s, 1070s, 1059vs, 990m, 954m, 923m, 901m, 867m, 840s, 789m, 774vs, 764vs. **ESI-MS(+)** (major positive ions, MeCN), *m/z* (%): 257 (25) [L^{1iPr} + Na]⁺, 297 (100) [Cu(L^{1iPr} - H)]⁺, 531 (20) [(L^{1iPr})Cu(L^{1iPr} - H)]⁺. **EA** (%) calculated for C₁₁H₁₄Cl₂CuN₄O₂: N 15.20, C 35.83, H 3.83; found: N 15.41, C 35.95, H 3.78.

2.3.2.10. Synthesis of [Cu(L^{1iPr})]Br₂ (**40**)

The ligand L^{1iPr} (**6**; 234.254 g/mol, 0.299 mmol, 0.070 g) and the metal precursor CuBr₂ (223.354 g/mol, 0.299 mmol, 0.067 g) were solubilized in MeCN (5 mL). The red-violet solution was left under magnetic stirring at room temperature for 24 hours. A red-brown precipitate was obtained, it was recovered by filtration and dried at reduced pressure obtaining the red-brown complex [Cu(L^{1iPr})]Br₂ (**40**) in 81% yield.

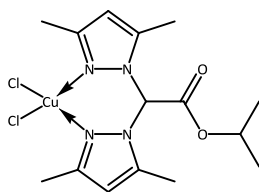


MM: 457.608 g/mol. **Solubility:** H₂O, MeOH, MeCN, DMSO. **MP:** 156-159 °C. **FT-IR** (cm⁻¹): 3137m, 3118w, 3104m, 3000w, 2978m, 2936w (C-H); 1735vs (ν_{asym} C=O); 1515m, 1453m (C=C/C=N); 1403s, 1388m, 1374m, 1357w, 1344m, 1291sh, 1283vs, 1255s, 1231s, 1198m, 1179m, 1149m, 1101s, 1094s, 1069s, 1058vs, 989m, 954m, 943m, 922m, 911m, 901m, 865m, 841s, 789s, 775vs, 764vs. **ESI-MS(+)** (major positive ions, MeCN), *m/z* (%): 257 (30) [L^{1iPr} + Na]⁺, 297 (100) [Cu(L^{1iPr} - H)]⁺, 531 (20) [(L^{1iPr})Cu(L^{1iPr} - H)]⁺. **EA** (%) calculated for C₁₁H₁₄Br₂CuN₄O₂: N 12.24, C 28.87, H 3.08; found: N 12.07, C 29.16, H 3.05.

2.3.2.11. Synthesis of [Cu(L^{2iPr})]Cl₂ (**41**)

The ligand L^{2iPr} (**7**; 290.361 g/mol, 0.400 mmol, 0.116 g) and the metal precursor CuCl₂·2H₂O (170.476 g/mol, 0.400 mmol, 0.068 g) were solubilized in MeCN (20 mL). The solution was left under magnetic stirring at room temperature for 24 hours and then it was dried at reduced pressure. Few milliliters of MeCN were poured into the round-bottom flask and, after that, Et₂O

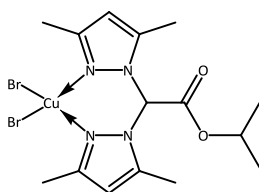
was added. The mixture was filtered and the precipitate was dried at reduced pressure, to give the orange complex $[\text{Cu}(\text{L}^{2\text{IPr}})]\text{Cl}_2$ (**41**) in 93% yield.



MM: 424.813 g/mol. **Solubility:** H_2O , MeOH, CHCl_3 , MeCN, DMSO. **MP:** 177-181 °C. **FT-IR** (cm^{-1}): 3149w, 3127w, 3092w, 2984w, 2961w, 2928w, 2853w (C-H); 1748s (ν_{asym} C=O); 1628w, 1561m (C=C/C=N); 1465m, 1447sh, 1419m, 1388sh, 1377m, 1317m, 1300m, 1270m, 1231s, 1185w, 1149w, 1100s, 1050m, 992w, 953m, 905m, 883m, 823s, 797w, 771w, 721m, 703w. **ESI-MS(+)** (major positive ions, MeCN), m/z (%): 313 (60) $[\text{L}^{2\text{IPr}} + \text{Na}]^+$, 329 (20) $[\text{L}^{2\text{IPr}} + \text{K}]^+$, 353 (100) $[\text{Cu}(\text{L}^{2\text{IPr}} - \text{H})]^+$, 643 (70) $[(\text{L}^{2\text{IPr}})\text{Cu}(\text{L}^{2\text{IPr}} - \text{H})]^+$. **EA** (%) calculated for $\text{C}_{15}\text{H}_{22}\text{Cl}_2\text{CuN}_4\text{O}_2$: N 13.19, C 42.41, H 5.22; found: N 13.66, C 42.95, H 5.29.

2.3.2.12. Synthesis of $[\text{Cu}(\text{L}^{2\text{IPr}})]\text{Br}_2$ (**42**)

This compound was prepared following the procedure described for **40** but employing the ligand $\text{L}^{2\text{IPr}}$ (**7**; 290.361 g/mol, 0.400 mmol, 0.116 g). The red-brown complex $[\text{Cu}(\text{L}^{2\text{IPr}})]\text{Br}_2$ (**42**) was obtained in 85% yield.



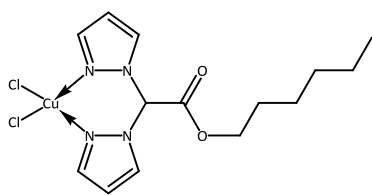
MM: 513.715 g/mol. **Solubility:** H_2O , MeOH, CHCl_3 , MeCN (slightly soluble), DMSO. **MP:** 176-179 °C. **FT-IR** (cm^{-1}): 3128w, 3090w, 2987w, 2973w, 2933w (C-H); 1747s (ν_{asym} C=O); 1561m (C=C/C=N); 1463m, 1419m, 1380s, 1374s, 1348w, 1313m, 1297m, 1268s, 1232s, 1185m, 1148m, 1102s, 1049m, 998m, 955m, 940m, 904m, 883m, 820s, 777w, 723m, 707m. **ESI-MS(+)** (major positive ions, MeCN), m/z (%): 291 (15) $[\text{L}^{2\text{IPr}} + \text{H}]^+$, 313 (35) $[\text{L}^{2\text{IPr}} + \text{Na}]^+$, 353 (70) $[\text{Cu}(\text{L}^{2\text{IPr}} - \text{H})]^+$, 434 (10) $[(\text{L}^{2\text{IPr}})\text{CuBr}]^+$. **ESI-MS(-)** (major negative ions, MeCN), m/z (%): 304 (100) $[\text{CuBr}_3]^-$. **EA** (%) calculated for $\text{C}_{15}\text{H}_{22}\text{Br}_2\text{CuN}_4\text{O}_2$: N 10.91, C 35.07, H 4.32; found: N 10.54, C 35.41, H 4.28.

2.3.2.13. Synthesis of $[\text{Cu}(\text{L}^{1\text{Hex}})]\text{Cl}_2$ (**43**)

The ligand $\text{L}^{1\text{Hex}}$ (**8**; 276.334 g/mol, 1.086 mmol, 0.300 g) and the metal precursor $\text{CuCl}_2 \cdot 2\text{H}_2\text{O}$ (170.476 g/mol, 1.086 mmol, 0.185 g) were solubilized in MeCN (50 mL). The reaction was left under magnetic stirring at room temperature for 6 hours. After that, the mixture was filtered and the precipitate was dried at reduced pressure. The light green complex $[\text{Cu}(\text{L}^{1\text{Hex}})]\text{Cl}_2$ (**43**) was obtained in 51% yield.

MM: 410.786 g/mol. **Solubility:** MeOH, EtOH, MeCN, DMSO, Me_2CO . **MP:** 175-181 °C. **FT-IR** (cm^{-1}): 3142w, 3122w, 3101m, 2993w, 2930m, 2867m (C-H); 1742vs (ν_{asym} C=O); 1517w, 1455m

(C=C/C=N); 1403m, 1356w, 1287vs, 1256m, 1229m, 1196m, 1103m, 1093w, 1069m, 1059s,

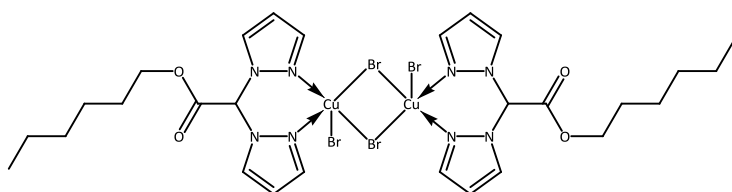


990m, 978w, 953w, 924w, 914m, 880w, 865w, 823w, 803w, 763vs, 726w. **ESI-MS(+)** (major positive ions, MeCN), m/z (%): 277 (20) $[L^{1Hex} + H]^+$, 339 (50) $[Cu(L^{1Hex} - H)]^+$, 374 (60) $[(L^{1Hex})CuCl]^+$, 615 (100) $[(L^{1Hex})Cu(L^{1Hex} - H)]^+$, 650 (40)

$[(L^{1Hex})_2CuCl]^+$. **ESI-MS(-)** (major negative ions, MeCN), m/z (%): 170 (100) $[CuCl_3]^-$. **EA** (%) calculated for $C_{14}H_{20}Cl_2CuN_4O_2$: N 13.64, C 41.93, H 4.91; found: N 12.81, C 42.90, H 5.01.

2.3.2.14. Synthesis of $\{[Cu(L^{1Hex})]Br(\mu-Br)\}_2$ (**44**)

This compound was prepared following the procedure described for **43** but employing the metal precursor $CuBr_2$ (223.354 g/mol, 0.750 mmol, 0.168 g). The brown-violet complex $\{[Cu(L^{1Hex})]Br(\mu-Br)\}_2$ (**44**) was obtained in 96% yield. Crystals of the complex **44**, suitable for SC-XRD, were obtained by slow evaporation of a Me_2CO solution of **44**.



MM: 999.388 g/mol. **Solubility**:

MeOH, $CHCl_3$, MeCN, DMSO, Me_2CO .

MP: 163-166 °C. **FT-IR** (cm^{-1}): 3146w,

3134w, 3122w, 3101m, 2983w,

2952m, 2929m, 2908sh, 2865m (C-H); 1740vs ($\nu_{asym} C=O$); 1525sh, 1515m, 1463sh, 1455m

(C=C/C=N); 1402s, 1373w, 1356w, 1345w, 1286vs, 1255s, 1227vs, 1195s, 1179m, 1102m,

1094m, 1068m, 1058vs, 1019w, 989m, 976m, 951m, 922m, 911m, 878w, 864m, 823m, 803m,

762vs, 723m. **ESI-MS(+)** (major positive ions, MeCN), m/z (%): 145 (100) $[CuBr]^+$, 299 (10) $[L^{1Hex}$

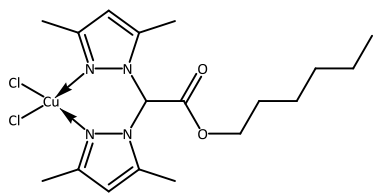
$+ Na]^+$, 339 (20) $[Cu(L^{1Hex} - H)]^+$, 615 (25) $[(L^{1Hex})Cu(L^{1Hex} - H)]^+$. **EA** (%) calculated for

$C_{14}H_{20}Br_2CuN_4O_2$: N 11.21, C 33.65, H 4.03; found: N 10.48, C 33.98, H 3.98.

2.3.2.15. Synthesis of $[Cu(L^{2Hex})]Cl_2$ (**45**)

The ligand L^{2Hex} (**9**; 332.448 g/mol, 1.000 mmol, 0.332 g) was solubilized in MeCN (50 mL) and stirred at room temperature for 15 minutes. Subsequently, the metal precursor $CuCl_2 \cdot 2H_2O$ (170.476 g/mol, 1.000 mmol, 0.170 g) was added, obtaining a green solution. The reaction was carried out under magnetic stirring at room temperature for 24 hours. After that, the reaction was dried at reduced pressure obtaining a green oil, Et_2O (30 mL) was poured into the round-bottom flask and the mixture was left under magnetic stirring at room temperature for 15 minutes. The mixture was filtered and the precipitate was dried at reduced pressure, to give the dark yellow complex $[Cu(L^{2Hex})]Cl_2$ (**45**) in 91% yield.

MM: 466.894 g/mol. **Solubility:** MeOH, EtOH, CHCl₃, MeCN, DMSO, Me₂CO. **MP:** 156-166 °C.

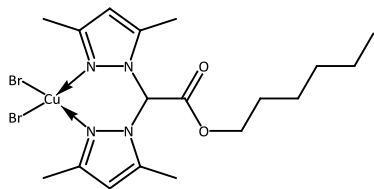


FT-IR (cm⁻¹): 3137w, 3100w, 2958m, 2933m, 2860w (C-H); 1761s (v_{asym} C=O); 1559m (C=C/C=N); 1463s, 1418m, 1382s, 1316s, 1299m, 1282m, 1264s, 1230s, 1216m, 1166w, 1139w, 1118w, 1049m, 988m, 905m, 868m, 842m, 807m, 784m, 718m, 708m.

ESI-MS(+) (major positive ions, MeCN), *m/z* (%): 333 (70) [L^{2Hex} + H]⁺, 395 (10) [Cu(L^{2Hex} - H)]⁺, 430 (75) [(L^{2Hex})CuCl]⁺, 642 (60) [(L^{2Hex})Cu(L²)]⁺, 727 (100) [(L^{2Hex})Cu(L^{2Hex} - H)]⁺, 762 (20) [(L^{2Hex})₂CuCl]⁺. **ESI-MS(-)** (major negative ions, MeCN), *m/z* (%): 170 (100) [CuCl₃]⁻. **EA** (%) calculated for C₁₈H₂₈Cl₂CuN₄O₂: N 12.00, C 46.30, H 6.04; found: N 11.65, C 45.96, H 5.76.

2.3.2.16. Synthesis of [Cu(L^{2Hex})]Br₂ (46)

The ligand L^{2Hex} (**9**; 332.448 g/mol, 1.000 mmol, 0.332 g) was solubilized in MeCN (50 mL) and stirred at room temperature for 15 minutes. Subsequently, the metal precursor CuBr₂ (223.354 g/mol, 1.000 mmol, 0.223 g) was added, obtaining a green solution. The reaction was carried out under magnetic stirring at room temperature for 24 hours. After that, the mixture was filtered and the precipitate was dried at reduced pressure. The brown complex [Cu(L^{2Hex})]Br₂ (**46**) was obtained in 90% yield.



MM: 555.802 g/mol. **Solubility:** MeOH, EtOH, CHCl₃, MeCN, DMSO, Me₂CO. **MP:** 132-135 °C. **FT-IR** (cm⁻¹): 3136w, 3102w, 2957m, 2928m, 2859wbr (C-H); 1756vs (v_{asym} C=O); 1563s (C=C/C=N), 1465s, 1421m, 1385s, 1377sh, 1315s, 1298m, 1271s,

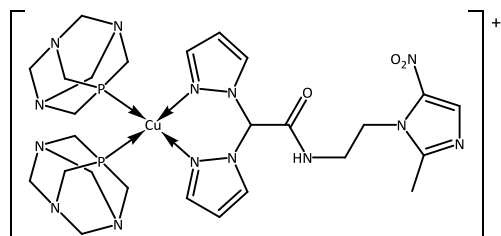
1230s, 1163w, 1134w, 1119m, 1050m, 990m, 953m, 910m, 877m, 826m, 790m, 724m, 707m. **ESI-MS(+)** (major positive ions, MeCN), *m/z* (%): 395 (20) [Cu(L^{2Hex} - H)]⁺, 476 (70) [(L^{2Hex})CuBr]⁺, 727 (100) [(L^{2Hex})Cu(L^{2Hex} - H)]⁺, 808 (25) [(L^{2Hex})₂CuBr]⁺. **ESI-MS(-)** (major negative ions, MeCN), *m/z* (%): 304 (100) [CuBr₃]⁻, 636 (5) [(L^{2Hex})CuBr₂ + Br]⁻. **EA** (%) calculated for C₁₈H₂₈Br₂CuN₄O₂: N 10.08, C 38.90, H 5.08; found: N 9.84, C 39.19, H 5.09.

2.3.3. Syntheses of the complexes bearing bioconjugated ligands

2.3.3.1. Synthesis of [(PTA)₂Cu(L^{1MN})]PF₆ (47)

The coligand PTA (157.157 g/mol, 2.000 mmol, 0.314 g) was solubilized in MeCN (25 mL), then a solution of the metal precursor [Cu(MeCN)₄]PF₆ (372.722 g/mol, 1.000 mmol, 0.373 g) in MeCN (25 mL) was added and the mixture was stirred at room temperature for 3 hours.

Subsequently, the ligand L^{1MN} (**10**; 344.335 g/mol, 1.000 mmol, 0.344 g) was added and the reaction was carried out under magnetic stirring at room temperature for 15 hours. After that, the yellow solution was dried at reduced pressure, to give the yellow complex $[(PTA)_2Cu(L^{1MN})]PF_6$ (**47**) in 79% yield.



MM: 867.159 g/mol. **Solubility**: H₂O, MeOH, MeCN, DMSO. **MP**: 167-169 °C. **¹H-NMR** (D₂O, 293 K): δ 2.23 (s, 3H, CH₃), 3.46 (br, 2H, HNCH₂), 4.29 (br, 2H, CH₂N), 4.39-4.65 (m, 24H, NCH₂P and NCH₂N), 6.41 (sbr, 2H, 4-CH), 7.25 (s, 1H, CHCO), 7.62 (sbr, 2H, 5-

CH), 7.81 (br, 3H, 3-CH and CH_{MN}). **¹H-NMR** (DMSO, 293 K): δ 2.32 (s, 3H, CH₃), 3.21 (br, 2H, HNCH₂), 4.24 (br, 2H, CH₂N), 4.40-4.64 (m, 24H, NCH₂P and NCH₂N), 6.49 (sbr, 2H, 4-CH), 7.56 (s, 1H, CHCO), 7.79 (sbr, 2H, 5-CH), 7.96 (br, 1H, CH_{MN}), 8.00 (br, 2H, 3-CH). **¹³C{¹H}-NMR** (DMSO, 293 K): δ 14.12 (CH₃), 39.10 (HNCH₂), 45.18 (CH₂N), 51.73 (NCH₂P), 72.38 (NCH₂N), 107.20 (4-C_{Pz}), 129.56 (5-C_{Pz}), 133.12 (CH_{MN}), 138.00 (CNO₂), 142.74 (3-C_{Pz}), 151.23 (CCH₃), 164.21 (CO). **³¹P{¹H}-NMR** (CD₃OD, 293 K): δ -90.59 (sbr), -143.39 (hept, J_{(P-F)}} = 709 Hz, PF₆). **³¹P{¹H}-NMR** (CD₃OD, 218 K): δ -92.90 (s), 143.52 (hept, J_{(P-F)}} = 709 Hz, PF₆). **³¹P{¹H}-NMR** (D₂O, 293 K): δ -87.29 (br), -143.93 (hept, J_{(P-F)}} = 710 Hz, PF₆). **FT-IR** (cm⁻¹): 3453br (N-H); 2927w, 2905sh (C-H); 1695m (ν_{asym} C=O); 1524br (ν_{asym} NO₂, C=C/C=N); 1471m, 1449m, 1415m, 1389m, 1365m (ν_{sym} NO₂); 1293m, 1263m, 1242s, 1188m, 1101s, 1014s, 969s, 947s, 893w, 830s, 765m, 740s. **ESI-MS(+)** (major positive ions, MeOH), *m/z* (%): 158 (50) [PTA + H]⁺, 345 (20) [L^{1MN} + H]⁺, 367 (100) [L^{1MN} + Na]⁺, 722 (10) [(PTA)₂Cu(L^{1MN})]⁺. **ESI-MS(-)** (major negative ions, MeOH), *m/z* (%): 126 (10) [2-methyl-5-nitroimidazole - H]⁻, 145 (95) [PF₆]⁻, 313 (100) [2PTA - H]⁻, 343 (40) [L^{1MN} - H]⁻. **EA** (%) calculated for C₂₆H₄₀CuF₆N₁₄O₃P₃: N 22.61, C 36.01, H 4.65; found: N 21.91, C 35.58, H 4.75.

2.3.3.2. Synthesis of [Cu(L^{1MN})₂]Cl₂ (**48**)

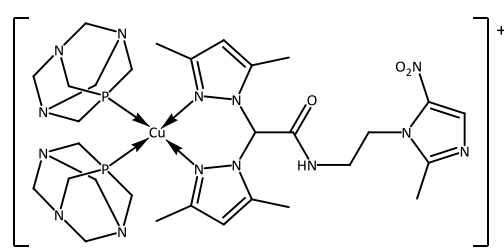
The ligand L^{1MN} (**10**; 344.335 g/mol, 1.000 mmol, 0.344 g) was solubilized in MeOH (25 mL), then a solution of the metal precursor CuCl₂·2H₂O (170.476 g/mol, 0.500 mmol, 0.085 g) in MeOH (25 mL) was added. The reaction was carried out under magnetic stirring at room temperature for 15 hours. After that, the mixture was filtered and the precipitate was dried at reduced pressure. The blue complex [Cu(L^{1MN})₂]Cl₂ (**48**) was obtained in 53% yield.

MM: 823.117 g/mol. **Solubility**: H₂O, MeOH (slightly soluble), DMSO. **MP**: 140-142 °C. **FT-IR** (cm⁻¹): 3276m (N-H); 3115m, 3080sh, 2960w, 2749mbr (C-H); 1668s (ν_{asym} C=O); 1564m, 1523s

($\nu_{\text{asym}} \text{NO}_2$, C=C/C=N); 1457m, 1424m, 1406m; 1360m ($\nu_{\text{sym}} \text{NO}_2$); 1325m, 1282m, 1259s, 1239w, 1146m, 1098m, 1184s, 1066s, 994m, 972m, 913m, 894m, 824s, 755s, 742s. **ESI-MS(+)** (major positive ions, MeOH), m/z (%): 345 (70) [$\text{L}^{1\text{MN}} + \text{H}$]⁺, 367 (100) [$\text{L}^{1\text{MN}} + \text{Na}$]⁺, 406 (30) [$\text{Cu}(\text{L}^{1\text{MN}} - \text{H})$]⁺. **ESI-MS(-)** (major negative ions, MeOH), m/z (%): 343 (100) [$\text{L}^{1\text{MN}} - \text{H}$]⁻, 379 (60) [$\text{L}^{1\text{MN}} + \text{Cl}$]⁻. **EA** (%) calculated for $\text{C}_{28}\text{H}_{32}\text{Cl}_2\text{CuN}_{16}\text{O}_6$: N 27.23, C 40.86, H 3.92; found: N 26.97, C 40.51, H 3.83.

2.3.3.3. Synthesis of [(PTA)₂Cu(L^{2MN})]PF₆ (49)

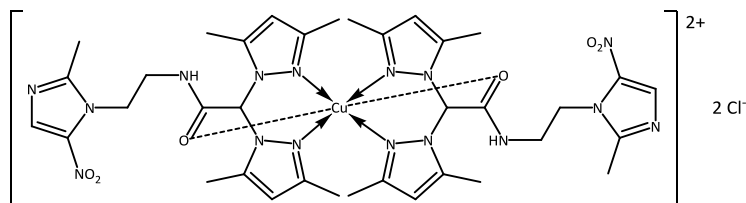
This compound was prepared following the procedure described for **47** but employing the ligand $\text{L}^{2\text{MN}}$ (**11**; 400.443 g/mol, 1.000 mmol, 0.400 g). The yellow complex [(PTA)₂Cu(L^{2MN})]PF₆ (**49**) was obtained in 70% yield.



MM: 923.267 g/mol. **Solubility**: H₂O, MeOH, MeCN, DMSO. **MP**: 183-185 °C. **¹H-NMR** (D₂O, 293 K): δ 2.06 (s, 6H, 3- or 5-CH₃), 2.22 (s, 6H, 3- or 5-CH₃), 2.25 (s, 3H, CH₃), 3.56 (br, 2H, HNCH₂), 4.33 (br, 2H, CH₂N), 4.40-4.65 (m, 24H, NCH₂P and NCH₂N), 6.02 (s, 2H, 4-CH), 6.50 (s, 1H, CHCO), 7.82 (s, 1H, CH_{MN}). **¹³C{¹H}-NMR** (D₂O, 293 K): δ 10.17 (CH₃), 12.58 (CH₃), 13.32 (CH₃), 38.73 (HNCH₂), 45.00 (CH₂N), 49.84 (NCH₂P), 70.78 (NCH₂N), 107.46 (4-C_{Pz}), 132.90 (CH_{MN}), 138.79 (CNO₂), 142.76 (CCH₃), 151.32 (CCH₃), 152.33 (CCH₃), 167.00 (CO). **³¹P{¹H}-NMR** (CD₃OD, 293 K): δ -89.05 (sbr), -143.44 (hept, $J_{\text{(P-F)}} = 708$ Hz, PF₆). **³¹P{¹H}-NMR** (CD₃OD, 218 K): δ -88.21 (s), -143.24 (hept, $J_{\text{(P-F)}} = 712$ Hz, PF₆). **³¹P{¹H}-NMR** (D₂O, 293 K): δ -81.00 (br), -143.90 (hept, $J_{\text{(P-F)}} = 710$ Hz, PF₆). **FT-IR** (cm⁻¹): 3398br (N-H); 3261w, 2924mbr (C-H); 1673s ($\nu_{\text{asym}} \text{C=O}$); 1561m, 1532m ($\nu_{\text{asym}} \text{NO}_2$, C=C/C=N); 1466m, 1448m, 1418m, 1386sh; 1363m ($\nu_{\text{sym}} \text{NO}_2$); 1316w, 1290m, 1261sh, 1242s, 1187s, 1150w, 1101m, 1044m, 1014s, 970s, 947s, 893w, 875w, 830s, 740s. **ESI-MS(+)** (major positive ions, MeOH), m/z (%): 158 (40) [PTA + H]⁺, 401 (100) [$\text{L}^{2\text{MN}} + \text{H}$]⁺, 423 (95) [$\text{L}^{2\text{MN}} + \text{Na}$]⁺, 463 (30) [$\text{Cu}(\text{L}^{2\text{MN}})$]⁺, 620 (70) [(PTA)Cu(L^{2MN})]⁺. **ESI-MS(-)** (major negative ions, MeOH), m/z (%): 145 (100) [PF₆]⁻, 313 (80) [2PTA - H]⁻, 399 (55) [$\text{L}^{2\text{MN}} - \text{H}$]⁻. **EA** (%) calculated for $\text{C}_{30}\text{H}_{48}\text{CuF}_6\text{N}_{14}\text{O}_3\text{P}_3$: N 21.24, C 39.03, H 5.24; found: N 21.05, C 38.77, H 5.55.

2.3.3.4. Synthesis of $[\text{Cu}(\text{L}^{2\text{MN}})_2]\text{Cl}_2$ (**50**)

This compound was prepared following the procedure described for **48** but employing the ligand $\text{L}^{2\text{MN}}$ (**11**; 400.443 g/mol, 1.000 mmol, 0.400 g). The pale blue complex $[\text{Cu}(\text{L}^{2\text{MN}})_2]\text{Cl}_2$ (**50**) was obtained in 76% yield.

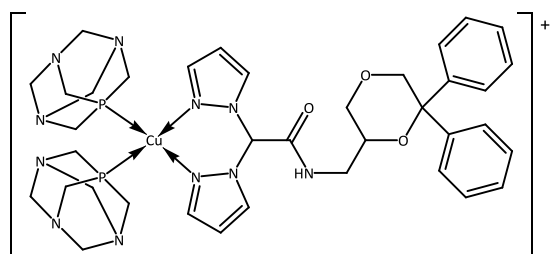


MM: 935.333 g/mol. **Solubility:** H_2O , MeOH (slightly soluble), CH_2Cl_2 , CHCl_3 . **MP:** 219-221 °C dec. **FT-IR** (cm^{-1}): 3409br (N-H); 3161w, 3082w,

2962w (C-H); 1665s ($\nu_{\text{asym}} \text{C}=\text{O}$); 1578m, 1560m, 1524m ($\nu_{\text{asym}} \text{NO}_2$, C=C/C=N); 1460s, 1423s, 1387m; 1361s ($\nu_{\text{sym}} \text{NO}_2$); 1312m, 1292w, 1257s, 1248s, 1183s, 1157m, 1106w, 1050m, 985w, 907m, 878w, 822s, 763m, 741m, 708m. **ESI-MS(+)** (major positive ions, MeOH), m/z (%): 401 (70) $[\text{L}^{2\text{MN}} + \text{H}]^+$, 432 (100) $[\text{Cu}(\text{L}^{2\text{MN}})_2]^{2+}$, 863 (20) $[(\text{L}^{2\text{MN}})\text{Cu}(\text{L}^{2\text{MN}} - \text{H})]^+$. **ESI-MS(-)** (major negative ions, MeOH), m/z (%): 399 (40) $[\text{L}^{2\text{MN}} - \text{H}]^-$, 436 (100) $[\text{L}^{2\text{MN}} + \text{Cl}]^-$. **EA** (%) calculated for $\text{C}_{36}\text{H}_{48}\text{Cl}_2\text{CuN}_{16}\text{O}_6$: N 23.96, C 46.23, H 5.17; found: N 23.64, C 45.89, H 4.98.

2.3.3.5. Synthesis of $[(\text{PTA})_2\text{Cu}(\text{L}^{1\text{NMDA}})]\text{PF}_6$ (**51**)

The phosphane PTA (157.157 g/mol, 0.600 mmol, 0.094 g) was solubilized in MeCN (50 mL), then the metal precursor $[\text{Cu}(\text{MeCN})_4]\text{PF}_6$ (372.722 g/mol, 0.300 mmol, 0.112 g) was added and the mixture was stirred at room temperature for 3 hours. Subsequently, a suspension of the ligand $\text{L}^{1\text{NMDA}}$ (**12**; 443.507 g/mol, 0.300 mmol, 0.133 g) in MeOH was added and the reaction was carried out under magnetic stirring at room temperature for 24 hours. After that, the mixture was filtered and the mother liquors were dried at reduced pressure to give the complex $[(\text{PTA})_2\text{Cu}(\text{L}^{1\text{NMDA}})]\text{PF}_6$ (**51**) in 62% yield.



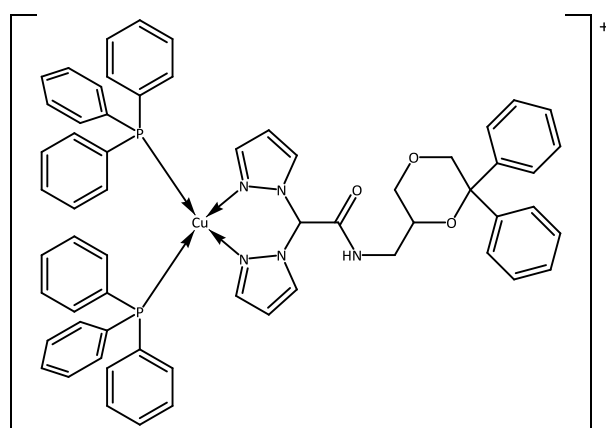
MM: 966.331 g/mol. **Solubility:** MeCN, CHCl_3 , DMSO. **MP:** 107-110 °C. **$^1\text{H-NMR}$** (CDCl_3 , 293 K): δ 3.32-3.67 (m, 6H, dioxane and HNCH_2), 4.04 (sbr, 12H, NCH_2P), 4.38-4.81 (m, 13H, dioxane and NCH_2N), 6.43 (m, 2H, 4-CH), 7.10-8.04 (m,

15H, CHCO , 3-CH, 5-CH and ArH), 8.53 (sbr, 1H, NH). **$^1\text{H-NMR}$** ($\text{DMSO-}d_6$, 293 K): δ 3.33-3.80 (m, 6H, dioxane and HNCH_2), 4.06 (sbr, 12H, NCH_2P), 4.41-4.82 (m, 13H, dioxane and NCH_2N), 6.45 (m, 2H, 4-CH), 7.22-8.05 (m, 15H, CHCO , 3-CH, 5-CH and ArH), 8.56 (sbr, 1H, NH). **$^{13}\text{C}\{^1\text{H}\}\text{-NMR}$** ($\text{DMSO-}d_6$, 293 K): δ 50.4, 51.8 (NCH_2P); 64.0 (CHCO); 68.5, 68.7, 71.5, 72.4, 78.8 (dioxane, NCH_2N and CH_2N); 107.1 (4- C_{P_2}); 125.6, 127.4, 128.1, 128.4, 128.9 (3- C_{P_2} , 5- C_{P_2} and Arc); 142.2,

144.4 (ArC); 164.0 (CO). $^{31}\text{P}\{^1\text{H}\}$ -NMR (CD_3CN , 293 K): δ -91.63 (br), -143.52 (hept, $J_{\text{P-F}} = 706$ Hz, PF_6). **FT-IR** (cm^{-1}): 3421w (N-H); 2925br (C-H); 1738sh, 1696br (ν_{asym} C=O); 1520br (C=C/C=N); 1449w, 1403w, 1366w, 1292m, 1242m, 1127w, 1100m, 1061w, 1044w, 1015s, 970s, 948s, 917w, 893w, 831s, 757s, 742s, 729m, 700s. **ESI-MS(+)** (major positive ions, MeCN), m/z (%): 506 (100) $[\text{Cu}(\text{L}^{1\text{NMDA}})]^+$, 663 (70) $[(\text{PTA})\text{Cu}(\text{L}^{1\text{NMDA}})]^+$. **ESI-MS(-)** (major negative ions, MeCN), m/z (%): 145 (100) $[\text{PF}_6]^-$. **EA** (%) calculated for $\text{C}_{37}\text{H}_{49}\text{CuF}_6\text{N}_{11}\text{O}_3\text{P}_3$: N 15.94, C 45.99, H 5.11; found: N 15.07, C 44.97, H 4.81.

2.3.3.6. Synthesis of $[(\text{PPh}_3)_2\text{Cu}(\text{L}^{1\text{NMDA}})]\text{PF}_6$ (**52**)

The phosphane PPh_3 (262.292 g/mol, 1.000 mmol, 0.262 g) was solubilized in MeCN (50 mL), then the metal precursor $[\text{Cu}(\text{MeCN})_4]\text{PF}_6$ (372.722 g/mol, 0.500 mmol, 0.186 g) was added and the mixture was stirred at room temperature for 3 hours. Subsequently, the ligand $\text{L}^{1\text{NMDA}}$ (**12**; 443.507 g/mol, 0.500 mmol, 0.222 g) was added and the reaction was carried out under magnetic stirring at room temperature for 24 hours. The mixture was filtered and the mother liquors dried at reduced pressure, few milliliters of MeCN were poured into the round-bottom flask to dissolve the solid residue and a *n*-hexane:Et₂O (2:1) mixture was added. The mixture was filtered and the precipitate was dried at reduced pressure, to give the complex $[(\text{PPh}_3)_2\text{Cu}(\text{L}^{1\text{NMDA}})]\text{PF}_6$ (**52**) in 88% yield.



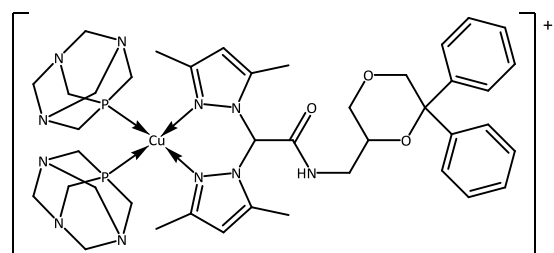
MM: 1176.601 g/mol. **Solubility**: MeOH, CHCl_3 , MeCN, DMSO. **MP**: 117-120 °C. ^1H -NMR (CDCl_3 , 293 K): δ 3.33-3.68 (m, 6H, dioxane and HNCH_2), 4.57 (d, 1H, dioxane), 6.35 (m, 2H, 4-CH), 7.20-7.68 (m, 45H, CHCO, 3-CH, 5-CH and ArH), 8.17 (sbr, 1H, NH). $^{31}\text{P}\{^1\text{H}\}$ -NMR (CDCl_3 , 293 K): δ 0.25 (sbr), -143.75 (hept, $J_{\text{P-F}} = 714$ Hz, PF_6). **FT-**

IR (cm^{-1}): 3639w, 3404w (N-H); 3291w, 3122w, 3055w, 2972w, 2936w, 2860w (C-H); 2273w, 2098w, 1978w, 1905w, 1823w; 1757w, 1681s (ν_{asym} C=O); 1561m, 1519w (C=C/C=N); 1495w, 1481m, 1451m, 1435s, 1402m, 1388m, 1373m, 1350w, 1312m, 1291m, 1271m, 1244m, 1228m, 1210w, 1184w, 1162w, 1138sh, 1122s, 1096s, 1065m, 1052m, 1026m, 999m, 991m, 959w, 926m, 916m, 834s, 774s, 743s. **ESI-MS(+)** (major positive ions, MeOH), m/z (%): 587 (100) $[(\text{PPh}_3)_2\text{Cu}]^+$, 768 (20) $[(\text{PPh}_3)\text{Cu}(\text{L}^{1\text{NMDA}})]^+$, 506 (10) $[\text{Cu}(\text{L}^{1\text{NMDA}})]^+$, 325 (5) $[(\text{PPh}_3)\text{Cu}]^+$. **ESI-MS(-)**

(major negative ions, MeOH), m/z (%): 145 (100) [PF₆]⁻. **EA** (%) calculated for C₆₁H₅₅CuF₆N₅O₃P₃: N 5.95, C 62.27, H 4.71; found: N 6.49, C 61.92, H 4.75.

2.3.3.7. Synthesis of [(PTA)₂Cu(L^{2NMDA})]PF₆ (**53**)

This compound was prepared following the procedure described for **51** but employing the ligand L^{2NMDA} (**13**; 499.615 g/mol, 0.300 mmol, 0.150 g). The complex [(PTA)₂Cu(L^{2NMDA})]PF₆ (**53**) was obtained in 59% yield.



MM: 1022.439 g/mol. **Solubility**: MeCN, DMSO.

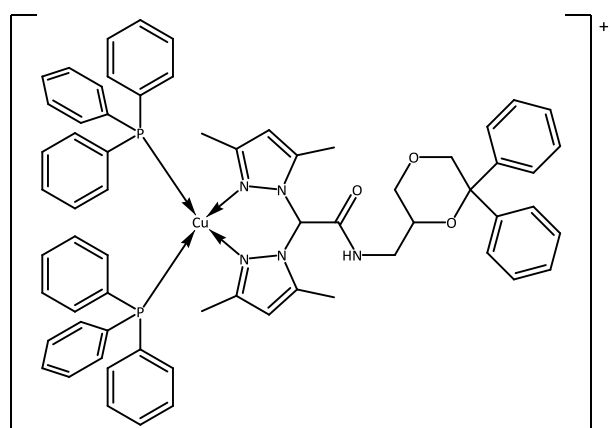
MP: 118-121 °C. ¹H-NMR (CDCl₃, 293 K): δ 2.06-2.17 (m, 12H, 3- and 5-CH₃) 3.24-3.63 (m, 6H, dioxane and HNCH₂), 4.02 (sbr, 12H, NCH₂P), 4.20-4.62 (m, 13H, dioxane and NCH₂N), 6.19 (s,

1H, 4-CH), 6.21 (s, 1H, 4-CH), 6.98 (s, 1H, CHCO), 7.22-7.46 (m, 10H, ArH), 9.01 (sbr, 1H, NH). ¹H-NMR (DMSO-*d*₆, 293 K): δ 2.03-2.26 (m, 12H, 3- and 5-CH₃), 3.32-3.78 (m, 6H, dioxane and HNCH₂), 4.04 (sbr, 12H, NCH₂P), 4.23-4.65 (m, 12H, NCH₂N), 4.81 (d, 1H, dioxane), 6.19 (s, 1H, 4-CH), 6.23 (s, 1H, 4-CH), 7.08 (sbr, 1H, CHCO), 7.23-7.49 (m, 10H, ArH), 9.25 (sbr, 1H, NH). ¹³C{¹H}-NMR (DMSO-*d*₆, 293 K): δ 14.2, 14.4 (3- and 5-CH₃); 50.7, 51.9 (NCH₂P); 64.0 (CHCO); 68.7, 71.5, 72.4, 78.8 (dioxane, NCH₂N and CH₂N); 107.1 (4-C_{Pz}); 125.6, 127.5, 128.0, 128.4, 128.9 (ArC); 142.2, 142.8, 144.3, 150.6 (3-C, 5-C and ArC); 164.2 (CO). ³¹P{¹H}-NMR (CD₃CN, 293 K): δ -89.0 (br), -143.52 (hept, J_{(P-F)}} = 706 Hz, PF₆). **FT-IR** (cm⁻¹): 3420w (N-H); 2921br (C-H); 1699br (ν_{asym} C=O); 1563w (C=C/C=N); 1519br, 1449m, 1416m, 1315w, 1293m, 1242s, 1127w, 1102m, 1062w, 1045w, 1014s, 959s, 947s, 893w, 873w, 830s, 800s, 741s, 731s, 700s. **ESI-MS(+)** (major positive ions, MeCN), m/z (%): 719 (100) [(PTA)Cu(L^{2NMDA})]⁺. **ESI-MS(-)** (major negative ions, MeCN), m/z (%): 145 (100) [PF₆]⁻. **EA** (%) calculated for C₄₁H₅₇CuF₆N₁₁O₃P₃: N 15.07, C 48.16, H 5.62; found: N 14.32, C 47.46, H 5.55.

2.3.3.8. Synthesis of [(PPh₃)₂Cu(L^{2NMDA})]PF₆ (**54**)

The phosphane PPh₃ (262.292 g/mol, 0.600 mmol, 0.157 g) was solubilized in MeCN (50 mL), then the metal precursor [Cu(MeCN)₄]PF₆ (372.722 g/mol, 0.300 mmol, 0.112 g) was added and the mixture was stirred at room temperature for 3 hours. Subsequently, the ligand L^{2NMDA} (**13**; 499.615 g/mol, 0.300 mmol, 0.150 g) was added and the reaction was carried out under magnetic stirring at room temperature for 24 hours. After that, the mixture was filtered and the

mother liquors were dried at reduced pressure to give the complex $[(PPh_3)_2Cu(L^{2NMDA})]PF_6$ (**54**) in 70% yield.

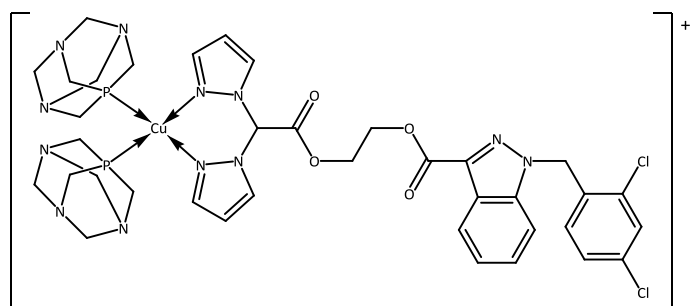


MM: 1232.709 g/mol. **Solubility:** MeOH, EtOH, Et₂O, THF, CH₂Cl₂, CHCl₃, EtOAc, MeCN, DMSO, Me₂CO. **MP:** 75-78 °C. **¹H-NMR** (CDCl₃, 293 K): δ 2.20 (s, 6H, 3- or 5-CH₃), 2.60 (s, 6H, 3- or 5-CH₃), 3.36-3.75 (m, 6H, dioxane and HNCH₂), 4.61 (d, 1H, dioxane), 6.01 (sbr, 1H, 4-CH), 6.06 (sbr, 1H, 4-CH), 6.80 (s, 1H, CHCO), 7.25-7.70 (m,

41H, ArH and NH). **³¹P{¹H}-NMR** (CDCl₃, 293 K): δ -3.85 (sbr), -143.99 (hept, $J_{(P-F)} = 714$ Hz, PF₆). **FT-IR** (cm⁻¹): 3394w (N-H); 3054w, 2918w, 2853w (C-H); 1674m (ν_{asym} C=O); 1562m (C=C/C=N); 1478m, 1449sh, 1435m, 1419sh, 1310w, 1270w, 1242w, 1224w, 1182w, 1158w, 1123sh, 1095m, 1060w, 1041w, 1026w, 996w, 983w, 937w, 916w, 835s, 743s. **ESI-MS(+)** (major positive ions, MeCN), *m/z* (%): 587 (100) [(PPh₃)₂Cu]⁺, 824 (40) [(PPh₃)₂Cu(L^{2NMDA})]⁺. **ESI-MS(-)** (major negative ions, MeCN), *m/z* (%): 145 (100) [PF₆]⁻. **EA** (%) calculated for C₆₅H₆₃CuF₆N₅O₃P₃: N 5.68, C 63.33, H 5.15; found: N 5.42, C 62.78, H 4.93.

2.3.3.9. Synthesis of $[(PTA)_2Cu(L^{1LONES})]PF_6$ (**55**)

The phosphane PTA (157.157 g/mol, 0.742 mmol, 0.117 g) was solubilized in MeCN (80 mL), then the metal precursor [Cu(MeCN)₄]PF₆ (372.722 g/mol, 0.371 mmol, 0.138 g) was added and the mixture was stirred at room temperature for 3 hours. Subsequently, the ligand L^{1LONES} (**16**; 539.373 g/mol, 0.371 mmol, 0.200 g) was added and the reaction was carried out under magnetic stirring at room temperature for 24 hours. The mixture was filtered and the precipitate was dried at reduced pressure to give the crystalline white complex $[(PTA)_2Cu(L^{1LONES})]PF_6$ (**55**) in 73% yield.



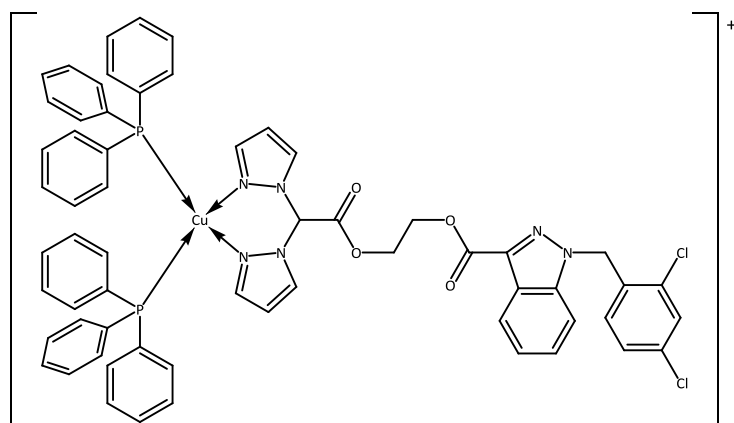
MM: 1062.197 g/mol. **Solubility:** MeCN (slightly soluble), DMSO. **MP:** 147-150 °C. **¹H-NMR** (DMSO-*d*₆, 293 K): δ 4.07 (sbr, 12H, NCH₂P), 4.41-4.65 (m, 16H, NCH₂N and O(CH₂)₂O), 5.89 (s, 2H, NCH₂Ph), 6.35 (sbr, 2H, 4-CH),

6.98 (d, 1H, ArH), 7.39-8.02 (m, 11H, CHCO, 3-CH, 5-CH and ArH). **¹³C{¹H}-NMR** (DMSO-*d*₆, 293

K): δ 49.7 (NCH₂Ph); 50.2, 50.9 (NCH₂P); 64.2, 66.0 (O(CH₂)₂O); 71.4 (NCH₂N); 106.2 (4-C_{Pz}); 110.4, 121.3, 123.1, 123.2, 127.0, 127.5, 128.8, 130.6, 130.7, 132.8, 140.6, 141.5 (CHCO, 3-C_{Pz}, 5-C_{Pz} and ArC); 160.8, 163.8 (CO). ³¹P{¹H}-NMR (DMSO-*d*₆, 293 K): δ -95.02 (br), -144.18 (hept, $J_{(P-F)} = 711$ Hz, PF₆). ³¹P{¹H}-NMR (CD₃CN, 293 K): δ -90.42 (br), -143.49 (hept, $J_{(P-F)} = 706$ Hz, PF₆). **FT-IR** (cm⁻¹): 3128wbr, 2937wbr (C-H); 1761m, 1718m (ν_{asym} C=O); 1616w; 1590w, 1564w, 1519w (C=C/C=N); 1477m, 1446m, 1418m, 1403m, 1390m, 1289m, 1242m, 1218m, 1161m, 1126m, 1098m, 1049m, 1015m, 971s, 948m, 917w, 893w, 876w, 833vs, 817m, 789m, 752s, 742s. **ESI-MS(+)** (major positive ions, MeCN), m/z (%): 158 (20) [PTA + H]⁺, 603 (100) [Cu(L^{1LONES})]⁺. **ESI-MS(-)** (major negative ions, MeCN), m/z (%): 145 (100) [PF₆]⁻. **EA** (%) calculated for C₃₇H₄₄Cl₂CuF₆N₁₂O₄P₃: N 15.82, C 41.84, H 4.18; found: N 15.47, C 41.67, H 4.12.

2.3.3.10. Synthesis of [(PPh₃)₂Cu(L^{1LONES})]PF₆ (56)

This compound was prepared following the procedure described for **55** but employing the phosphane PPh₃ (262.292 g/mol, 0.742 mmol, 0.195 g). The crystalline white complex [(PPh₃)₂Cu(L^{1LONES})]PF₆ (**56**) was obtained in 74% yield.



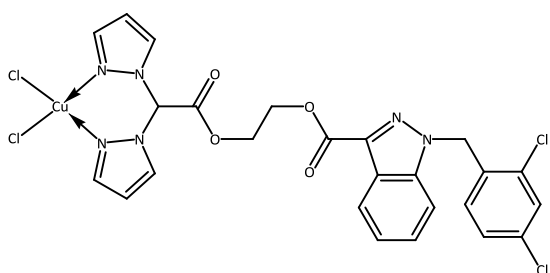
MM: 1272.467 g/mol. **Solubility:** MeOH, CHCl₃, MeCN (slightly soluble), DMSO. **MP:** 105-109 °C. ¹H-NMR (DMSO-*d*₆, 293 K): δ 4.47 (sbr, 4H, O(CH₂)₂O), 5.88 (s, 2H, NCH₂Ph), 6.28 (sbr, 2H, 4-CH), 6.98 (d, 1H, ArH), 7.26-7.99 (m, 41H, CHCO, 3-CH, 5-CH and ArH).

¹³C{¹H}-NMR (DMSO-*d*₆, 293 K): δ 52.7 (NCH₂Ph); 64.7, 67.2 (O(CH₂)₂O); 106.1 (4-C_{Pz}); 110.6, 122.4, 122.6, 123.0, 128.6, 128.8, 129.1, 129.3, 129.4, 130.0, 131.7, 132.5, 132.6, 132.8, 133.0, 133.4, 133.8, 138.8, 142.4 (CHCO, 3-C_{Pz}, 5-C_{Pz} and ArC); 161.6, 163.9 (CO). ³¹P{¹H}-NMR (DMSO-*d*₆, 293 K): δ -3.33 (br), -148.80 (hept, $J_{(P-F)} = 713$ Hz, PF₆). ³¹P{¹H}-NMR (CD₃CN, 293 K): δ 0.15 (br), -143.51 (hept, $J_{(P-F)} = 705$ Hz, PF₆). **FT-IR** (cm⁻¹): 3133wbr, 3056wbr (C-H); 1765m, 1716mbr (ν_{asym} C=O); 1616w; 1588m, 1564w, 1523w (C=C/C=N); 1479m, 1455m, 1435m, 1403m, 1353m, 1299m, 1286m, 1216m, 1161s, 1125m, 1095s, 1055m, 1027m, 1008m, 999m, 986m, 955m, 919w, 834vs, 788m, 742vs. **ESI-MS(+)** (major positive ions, MeCN), m/z (%): 587 (100) [(PPh₃)₂Cu]⁺, 603 (40) [Cu(L^{1LONES})]⁺. **ESI-MS(-)** (major negative ions, MeCN), m/z (%): 145 (100)

[PF₆]⁻. **EA** (%) calculated for C₆₁H₅₀Cl₂CuF₆N₆O₄P₃: N 6.60, C 57.58, H 3.96; found: N 6.39, C 57.27, H 3.98.

2.3.3.11. Synthesis of [Cu(L^{1LONES})]Cl₂ (**57**)

The ligand L^{1LONES} (**16**; 539.373 g/mol, 0.371 mmol, 0.200 g) was solubilized in MeCN (80 mL), then the metal precursor CuCl₂·2H₂O (170.476 g/mol, 0.371 mmol, 0.063 g) was added and the reaction was carried out under magnetic stirring at room temperature for 24 hours. After that, the mixture was filtered and the precipitate was washed with fresh MeCN and dried at reduced pressure to give the green complex [Cu(L^{1LONES})]Cl₂ (**57**) in 87% yield.

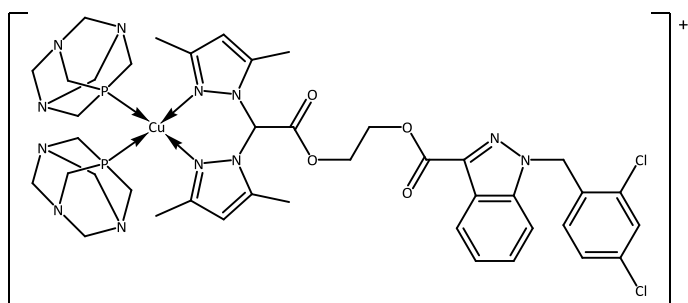


MM: 673.819 g/mol. **Solubility**: MeOH, CHCl₃, MeCN (slightly soluble), DMSO. **MP**: 193-195 °C. **FT-IR** (cm⁻¹): 3129w, 3112wbr, 2996w (C-H); 1748s, 1710s (ν_{asym} C=O); 1591w, 1567w (C=C/C=N); 1500w, 1478m, 1452m, 1429m, 1403s, 1361w,

1301m, 1284m, 1254m, 1230m, 1220s, 1195m, 1168vs, 1129s, 1090s, 1060s, 1040m, 1008m, 994m, 953m, 920w, 891m, 852m, 818m, 800m, 781s, 764s, 751s. **ESI-MS(+)** (major positive ions, MeCN), *m/z* (%): 602 (100) [Cu(L^{1LONES} - H)]⁺. **ESI-MS(-)** (major negative ions, MeCN), *m/z* (%): 170 (100) [CuCl₃]⁻. **EA** (%) calculated for C₂₅H₂₀Cl₄CuN₆O₄: N 12.47, C 44.56, H 2.99; found: N 12.71, C 44.80, H 3.11.

2.3.3.12. Synthesis of [(PTA)₂Cu(L^{2LONES})]PF₆ (**58**)

This compound was prepared following the procedure described for **55** but employing the ligand L^{2LONES} (**17**; 595.481 g/mol, 0.336 mmol, 0.200 g). At the end of the reaction, the mixture was filtered and the mother liquors were dried at reduced pressure. The white complex [(PTA)₂Cu(L^{2LONES})]PF₆ (**58**) was obtained in 94% yield.



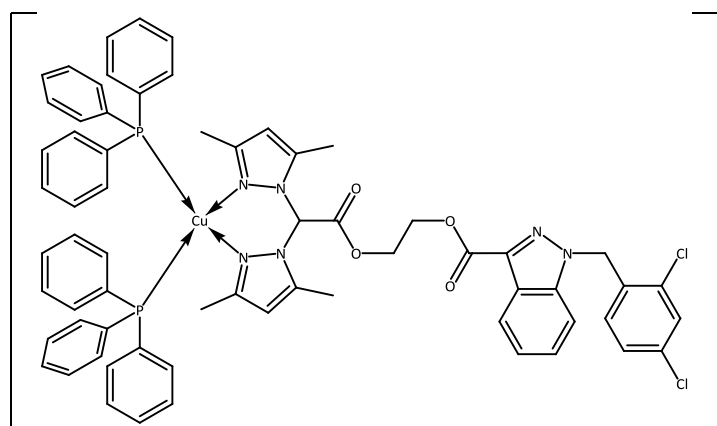
MM: 1118.305 g/mol. **Solubility**: MeCN, DMSO, Me₂CO. **MP**: 187-191 °C. **¹H-NMR** (DMSO-*d*₆, 293 K): δ 2.05 (s, 6H, 3- or 5-CH₃), 2.36 (s, 6H, 3- or 5-CH₃), 4.04 (s, 12H, NCH₂P), 4.40-4.73 (m, 16H, NCH₂N and O(CH₂)₂O),

5.79-5.96 (m, 4H, NCH₂Ph and 4-CH), 6.90-8.03 (m, 8H, CHCO and ArH). **¹³C{¹H}-NMR** (DMSO-*d*₆, 293 K): δ 11.0 (3- or 5-CH₃); 14.3 (3- or 5-CH₃); 50.3 (NCH₂Ph); 50.5, 51.8 (NCH₂P); 72.4 (NCH₂N);

65.1, 66.7 (O(CH₂)₂O); 106.2 (4-C_{Pz}); 111.3, 122.0, 123.2, 123.9, 127.9, 128.2, 129.6, 131.6, 133.5, 135.0, 141.4, 144.3, 148.2, 151.4 (CHCO, 3-C_{Pz}, 5-C_{Pz} and ArC); 161.9, 163.4 (CO). ³¹P{¹H}-NMR (DMSO-*d*₆, 293 K): δ -92.78 (sbr), -144.19 (hept, J_(P-F) = 711 Hz, PF₆). ³¹P{¹H}-NMR (CD₃CN, 293 K): δ -94.0 (br), -143.52 (hept, J_(P-F) = 706 Hz, PF₆). FT-IR (cm⁻¹): 3080br, 2985sh, 2950sh, 2925wbr, 2893sh (C-H); 1763m, 1719mbr (ν_{asym} C=O); 1647wbr, 1616wbr; 1590w, 1563m (C=C/C=N); 1475m, 1449m, 1418m, 1389m, 1316m, 1297mbr, 1268mbr, 1242m, 1218mbr, 1163mbr, 1123m, 1104m, 1043mbr, 1014s, 969sbr, 948s, 895m, 874sh, 834vs, 803sh, 744s, 718m. ESI-MS(+) (major positive ions, MeCN), *m/z* (%): 659 (100) [Cu(L^{2LONES})]⁺. ESI-MS(-) (major negative ions, MeCN), *m/z* (%): 145 (100) [PF₆]⁻. EA (%) calculated for C₄₁H₅₂Cl₂CuF₆N₁₂O₄P₃: N 15.03, C 44.03, H 4.69; found: N 14.78, C 43.77, H 4.80.

2.3.3.13. Synthesis of [(PPh₃)₂Cu(L^{2LONES})]PF₆ (59)

This compound was prepared following the procedure described for **55** but employing the phosphane PPh₃ (262.292 g/mol, 0.672 mmol, 0.176 g) and the ligand L^{2LONES} (**17**; 595.481 g/mol, 0.336 mmol, 0.200 g). At the end of the reaction, the mixture was filtered, the mother liquors were dried at reduced pressure and the obtained residue was washed with hot Et₂O (3 x 30 mL). The white complex [(PPh₃)₂Cu(L^{2LONES})]PF₆ (**59**) was obtained in 51% yield.



MM: 1328.575 g/mol. **Solubility:**

MeOH, CHCl₃, MeCN (slightly soluble), DMSO. **MP:** 118-122 °C.

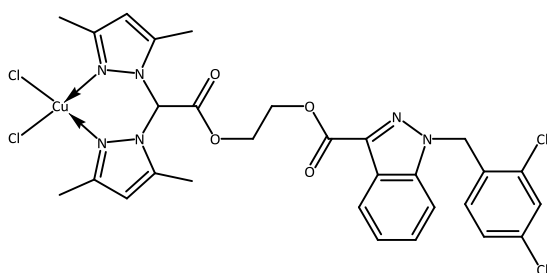
¹H-NMR (DMSO-*d*₆, 293 K): δ 1.92 (s, 6H, 3- or 5-CH₃), 2.41 (s, 6H, 3- or 5-CH₃), 3.70, 4.27 (sbr, 4H, O(CH₂)₂O), 5.88 (s, 2H, NCH₂Ph), 6.02 (s, 2H, 4-CH), 7.07 (d, 1H,

ArH), 7.28-7.71 (m, 35H, CHCO and ArH), 7.93 (d, 1H, ArH), 8.05 (d, 1H, ArH). ¹³C{¹H}-NMR (DMSO-*d*₆, 293 K): δ 11.1 (3- or 5-CH₃); 14.4 (3- or 5-CH₃); 50.7 (NCH₂Ph); 64.8, 66.3 (O(CH₂)₂O); 107.2 (4-C_{Pz}); 111.3, 122.0, 123.3, 123.9, 128.0, 128.4, 130.0, 131.6, 133.6, 135.2, 141.7, 141.8, 144.2, 151.3 (CHCO, 3-C_{Pz}, 5-C_{Pz} and ArC); 161.8, 164.4 (CO). ³¹P{¹H}-NMR (DMSO-*d*₆, 293 K): δ -1.97 (sbr), -144.20 (hept, J_(P-F) = 710 Hz, PF₆). FT-IR (cm⁻¹): 3055wbr, 2959wbr, 2924wbr (C-H); 1763m, 1718mbr (ν_{asym} C=O); 1635w, 1616w; 1588w, 1563m (C=C/C=N); 1478m, 1435m, 1422sh, 1389m, 1315m, 1265mbr, 1217mbr, 1163m, 1123m, 1095m, 1049m, 1029m, 1008w, 998m, 961w, 896w, 875m, 837vs, 789m, 743s. ESI-MS(+) (major positive ions, MeCN), *m/z* (%):

587 (100) $[(PPh_3)_2Cu]^+$, 659 (80) $[Cu(L^{2LONES})]^+$, 921 (10) $[(PPh_3)Cu(L^{2LONES})]^+$. **ESI-MS(-)** (major negative ions, MeCN), m/z (%): 145 (100) $[PF_6]^-$. **EA** (%) calculated for $C_{65}H_{58}Cl_2CuF_6N_6O_4P_3$: N 6.33, C 58.76, H 4.40; found: N 6.06, C 58.42, H 4.23.

2.3.3.14. Synthesis of $[Cu(L^{2LONES})]Cl_2$ (**60**)

The ligand L^{2LONES} (**17**; 595.481 g/mol, 0.336 mmol, 0.200 g) was solubilized in MeCN (80 mL), the metal precursor $CuCl_2 \cdot 2H_2O$ (170.476 g/mol, 0.336 mmol, 0.057 g) was added and the reaction was carried out under magnetic stirring at room temperature for 24 hours. After that, the solution was dried at reduced pressure, few milliliters of MeCN were poured into the round-bottom flask and Et_2O (about 30 mL) was added. The mixture was filtered and the precipitate was dried at reduced pressure. The dark green complex $[Cu(L^{2LONES})]Cl_2$ (**60**) was obtained in 60% yield.



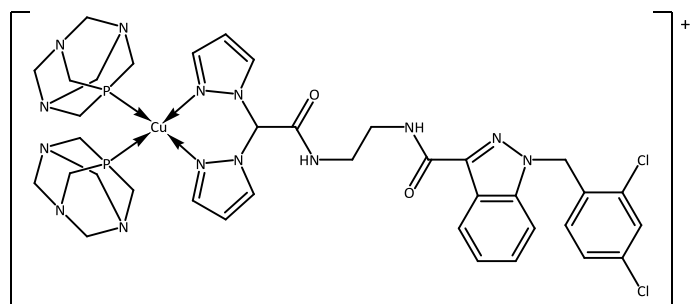
MM: 729.927 g/mol. **Solubility**: MeOH, CH_2Cl_2 , $CHCl_3$, MeCN, DMSO. **MP**: 148-150 °C. **FT-IR** (cm^{-1}): 3137mbr, 2960mbr, 2926mbr, 2856mbr (C-H); 1765m, 1716mbr ($\nu_{asym} C=O$); 1590m, 1563m (C=C/C=N); 1472m, 1442m, 1419m, 1386m, 1316m, 1273m, 1217s, 1162s, 1124s, 1105s, 1047s, 1007m, 954mbr, 899m, 858m, 835m, 788s, 752s, 721m, 708m. **ESI-MS(+)** (major positive ions, MeCN), m/z (%): 658 (100) $[Cu(L^{2LONES} - H)]^+$. **ESI-MS(-)** (major negative ions, MeCN), m/z (%): 170 (100) $[CuCl_3]^-$. **EA** (%) calculated for $C_{29}H_{28}Cl_4CuN_6O_4$: N 11.51, C 47.72, H 3.87; found: N 11.23, C 47.48, H 3.94.

2.3.3.15. Synthesis of $[(PTA)_2Cu(L^{1LONAM})]PF_6$ (**61**)

This compound was prepared following the procedure described for **55** but employing the ligand L^{1LONAM} (**18**; 537.405 g/mol, 0.372 mmol, 0.200 g). At the end of the reaction, the mixture was filtered and the precipitate was washed with Et_2O (2 x 20 mL) and, subsequently, with *n*-hexane (2 x 20 mL). Finally it was dried at reduced pressure obtaining the crystalline white complex $[(PTA)_2Cu(L^{1LONAM})]PF_6$ (**61**) in 57% yield.

MM: 1060.229 g/mol. **Solubility**: $CHCl_3$, MeCN (slightly soluble), DMSO, Me_2CO . **MP**: 163-167 °C. **1H -NMR** (DMSO- d_6 , 293 K): δ 3.39 (sbr, 4H, $HN(CH_2)_2NH$), 4.07 (sbr, 12H, NCH_2P), 4.40-4.64 (m, 12H, NCH_2N), 5.83 (s, 2H, NCH_2Ph), 6.42 (br, 2H, 4-CH), 6.78 (d, 1H, ArH), 7.32-8.01 (m, 10H, CHCO, 3-CH, 5-CH and ArH), 8.22 (d, 1H, ArH), 8.40 (tbr, 1H, NH), 8.46 (sbr, 1H, NH). **$^{13}C\{^1H\}$ -NMR** (DMSO- d_6 , 293 K): δ 38.2 ($HN(CH_2)_2NH$); 50.0 (NCH_2Ph); 50.3, 51.8 (NCH_2P); 72.3 (NCH_2N);

105.5; 107.1 (4- C_{P_2}); 110.8, 122.5, 122.7, 123.2, 127.7, 128.3, 129.5, 130.6, 132.4, 133.3, 133.7,

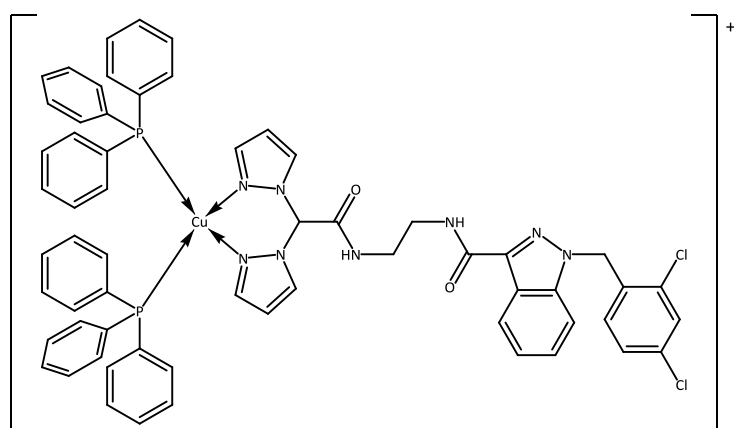


133.9, 138.5, 141.6 (CHCO, 3-CH, 5-CH and ArC); 162.5, 164.1 (CO). $^{31}\text{P}\{^1\text{H}\}$ -NMR (DMSO- d_6 , 293 K): δ -93.70 (sbr), -144.19 (hept, $J_{(P-F)} = 711$ Hz, PF_6^-). $^{31}\text{P}\{^1\text{H}\}$ -NMR (CD_3CN , 293 K): δ -91.0 (br), -143.51 (hept, $J_{(P-F)} = 706$ Hz, PF_6^-).

$^{31}\text{P}\{^1\text{H}\}$ -NMR (CDCl_3 , 293 K): δ -92.02 (sbr), -143.80 (hept, $J_{(P-F)} = 714$ Hz, PF_6^-). FT-IR (cm^{-1}): 3281wbr (N-H); 3127wbr, 2936wbr (C-H); 1691mbr, 1652mbr ($\nu_{\text{asym}} \text{C=O}$); 1589w, 1537mbr (C=C/C=N); 1493m, 1474m, 1446m, 1417sh, 1403m, 1372mbr, 1291m, 1242m, 1177m, 1136w, 1099m, 1048m, 1015s, 970s, 949s, 917w, 894w, 833vs, 742sbr. ESI-MS(+) (major positive ions, MeCN), m/z (%): 158 (10) [PTA + H] $^+$, 220 (5) [(PTA)Cu] $^+$, 377 (30) [(PTA) $_2$ Cu] $^+$, 601 (100) [Cu(L $^{1\text{LONAM}}$)] $^+$, 758 (10) [(PTA)Cu(L $^{1\text{LONAM}}$)] $^+$. ESI-MS(-) (major negative ions, MeCN), m/z (%): 145 (100) [PF_6^-]. EA (%) calculated for $\text{C}_{37}\text{H}_{46}\text{Cl}_2\text{CuF}_6\text{N}_{14}\text{O}_2\text{P}_3$: N 18.50, C 41.92, H 4.37; found: N 18.18, C 41.66, H 4.58.

2.3.3.16. Synthesis of $[(\text{PPh}_3)_2\text{Cu}(\text{L}^{1\text{LONAM}})]\text{PF}_6$ (**62**)

This compound was prepared following the procedure described for **55** but employing the phosphane PPh_3 (262.292 g/mol, 0.744 mmol, 0.195 g) and the ligand $\text{L}^{1\text{LONAM}}$ (**18**; 537.405 g/mol, 0.372 mmol, 0.200 g). At the end of the reaction, the mixture was filtered and the precipitate was washed with Et_2O (3 x 20 mL) and dried at reduced pressure. The white complex $[(\text{PPh}_3)_2\text{Cu}(\text{L}^{1\text{LONAM}})]\text{PF}_6$ (**62**) was obtained in 65% yield.



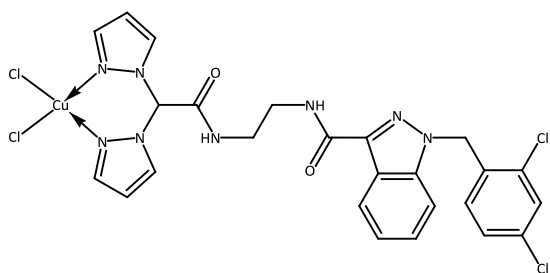
MM: 1270.499 g/mol. Solubility: MeOH, CHCl_3 , MeCN (slightly soluble), DMSO, Me_2CO . MP: 186-189 °C. ^1H -NMR (DMSO- d_6 , 293 K): δ 3.37-3.41 (m, 4H, $\text{HN}(\text{CH}_2)_2\text{NH}$), 5.82 (s, 2H, NCH_2Ph), 6.36 (sbr, 2H, 4-CH), 6.79 (d, 1H, ArH), 7.31-7.97 (m, 40H, CHCO, 3-CH, 5-CH and ArH), 8.22 (d, 1H, ArH), 8.35 (tbr, 1H, NH), 8.65 (tbr, 1H, NH).

$^{13}\text{C}\{^1\text{H}\}$ -NMR (DMSO- d_6 , 293 K): δ 38.1 ($\text{HN}(\text{CH}_2)_2\text{NH}$); 50.0 (NCH_2Ph); 107.1 (4- C_{P_2}); 110.8, 122.5, 122.7, 123.2, 127.7, 128.3, 129.2, 129.4, 129.5, 130.8, 132.0, 132.5, 132.7, 132.9, 133.4, 133.8, 133.9, 138.5, 141.6, 141.9 (CHCO,

3- C_{Pz} , 5- C_{Pz} and ArC); 162.5, 164.0 (CO). $^{31}P\{^1H\}$ -NMR (DMSO- d_6 , 293 K): δ 0.35 (sbr), -144.00 (hept, $J_{(P-F)} = 714$ Hz, PF_6). $^{31}P\{^1H\}$ -NMR (CD_3CN , 293 K): δ 0.26 (sbr), -143.53 (hept, $J_{(P-F)} = 707$ Hz, PF_6). **FT-IR** (cm^{-1}): 3399wbr, 3288wbr (N-H); 3128wbr, 3055wbr (C-H); 1702sh, 1674mbr (ν_{asym} C=O); 1626m, 1615m; 1588m, 1540mbr (C=C/C=N); 1479m, 1435s, 1403m, 1373m, 1361m, 1289mbr, 1245mbr, 1231mbr, 1181mbr, 1119m, 1095m, 1056m, 1027m, 999m, 981mbr, 919wbr, 834vs, 741vs. **ESI-MS(+)** (major positive ions, MeCN), m/z (%): 587 (100) $[(PPh_3)_2Cu]^+$, 601 (10) $[Cu(L^{1LONAM})]^+$, 863 (20) $[(PPh_3)Cu(L^{1LONAM})]^+$. **ESI-MS(-)** (major negative ions, MeCN), m/z (%): 145 (100) $[PF_6]^-$. **EA** (%) calculated for $C_{61}H_{52}Cl_2CuF_6N_8O_2P_3$: N 8.82, C 57.67, H 4.13; found: N 8.50, C 57.38, H 4.06.

2.3.3.17. Synthesis of $[Cu(L^{1LONAM})]Cl_2$ (**63**)

This compound was prepared following the procedure described for **57** but employing the ligand L^{1LONAM} (**18**; 537.405 g/mol, 0.372 mmol, 0.200 g) and MeOH as solvent. The light blue complex $[Cu(L^{1LONAM})]Cl_2$ (**63**) was obtained in 68% yield.



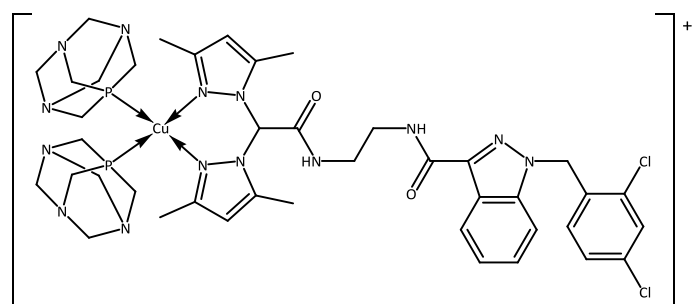
MM: 671.851 g/mol. **Solubility**: MeCN, DMSO. **MP**: 216-219 °C dec. **FT-IR** (cm^{-1}): 3494wbr, 3407m, 3290mbr (N-H); 3152w, 3121m, 3091m, 3065w, 2977w, 2943w, 2832w (C-H); 1672vs, 1659sh (ν_{asym} C=O); 1565sbr, 1539s (C=C/C=N); 1491s, 1471s,

1450m, 1428m, 1406s, 1384s, 1361m, 1330s, 1313s, 1282vs, 1244s, 1230s, 1205m, 1197m, 1172s, 1150m, 1130m, 1095s, 1063vs, 1046m, 1026m, 1007s, 990s, 956m, 942m, 924m, 892m, 861s, 841s, 833vs, 787vs, 765vs, 748vs, 729s. **ESI-MS(+)** (major positive ions, MeCN), m/z (%): 537 (80) $[L^{1LONAM} + H]^+$, 559 (100) $[L^{1LONAM} + Na]^+$, 600 (55) $[Cu(L^{1LONAM} - H)]^+$, 1097 (40) $[2L^{1LONAM} + Na]^+$, 1137 (20) $[Cu(L^{1LONAM})_2]^+$. **ESI-MS(-)** (major negative ions, MeCN), m/z (%): 170 (10) $[CuCl_3]^-$, 573 (100) $[L^{1LONAM} + Cl]^-$. **EA** (%) calculated for $C_{25}H_{22}Cl_4CuN_8O_2$: N 16.68, C 44.69, H 3.30; found: N 16.34, C 45.02, H 3.52.

2.3.3.18. Synthesis of $[(PTA)_2Cu(L^{2LONAM})]PF_6$ (**64**)

This compound was prepared following the procedure described for **55** but employing the ligand L^{2LONAM} (**19**; 593.513 g/mol, 0.337 mmol, 0.200 g). At the end of the reaction, the mixture was filtered and the mother liquors were dried at reduced pressure. The white complex $[(PTA)_2Cu(L^{2LONAM})]PF_6$ (**64**) was obtained in 52% yield.

MM: 1116.337 g/mol. **Solubility:** MeOH, MeCN, DMSO. **MP:** 227-230 °C. **¹H-NMR** (DMSO-*d*₆,



293 K): δ 2.19 (s, 6H, 3- or 5- CH_3), 2.37 (s, 6H, 3- or 5- CH_3), 3.36-3.48 (m, 4H, $HN(CH_2)_2NH$), 4.04-4.66 (m, 24H, NCH_2P and NCH_2N), 5.82 (s, 2H, NCH_2Ph), 6.10 (sbr, 2H, 4- CH), 6.76 (d, 1H, ArH), 6.92 (s, 1H, $CHCO$), 7.33-

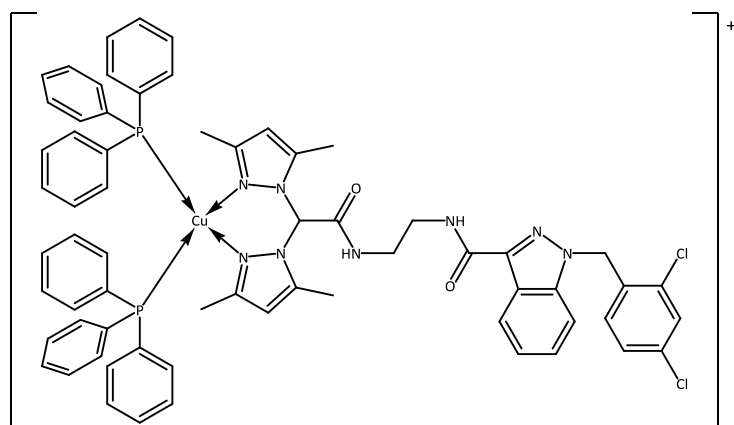
7.79 (m, 5H, ArH), 8.22 (d, 1H, ArH), 8.43 (br, 1H, NH), 9.07 (br, 1H, NH). **¹³C{¹H}-NMR** (DMSO-*d*₆, 293 K): δ 11.1 (3- or 5- CH_3); 14.4 (3- or 5- CH_3); 38.3 ($HN(CH_2)_2NH$); 50.0 (NCH_2Ph); 50.5, 51.9 (NCH_2P); 72.4 (NCH_2N); 107.0 (4- C_{Pz}); 110.8, 122.5, 122.7, 123.2, 127.7, 128.3, 129.6, 130.6, 133.3, 133.7, 133.9, 138.5, 141.6, 142.3 ($CHCO$, 3- C_{Pz} , 5- C_{Pz} and ArC); 162.6, 164.2 (CO). **³¹P{¹H}-NMR** (DMSO-*d*₆, 293 K): δ -92.29 (s), -144.02 (hept, $J_{(P-F)} = 714$ Hz, PF_6). **FT-IR** (cm^{-1}): 3389wbr, 3252wbr (N-H); 2923wbr, 2887wbr (C-H); 1692m, 1658mbr ($\nu_{asym} C=O$); 1590w, 1562m, 1533mbr (C=C/C=N); 1493m, 1472m, 1449m, 1416m, 1388m, 1373m, 1314m, 1295mbr, 1267m, 1242m, 1230sh, 1176m, 1158sh, 1135w, 1104m, 1042mbr, 1013s, 968sbr, 948s, 894m, 874m, 833vs, 806sh, 776sh, 744s, 729s. **ESI-MS(+)** (major positive ions, MeCN), m/z (%): 657 (100) $[Cu(L^{2LONAM})]^+$, 814 (25) $[(PTA)Cu(L^{2LONAM})]^+$. **ESI-MS(-)** (major negative ions, MeCN), m/z (%): 145 (100) $[PF_6]^-$. **EA** (%) calculated for $C_{41}H_{54}Cl_2CuF_6N_{14}O_2P_3$: N 17.57, C 44.11, H 4.88; found: N 17.21, C 43.80, H 4.61.

2.3.3.19. Synthesis of $[(PPh_3)_2Cu(L^{2LONAM})]PF_6$ (**65**)

This compound was prepared following the procedure described for **55** but employing the phosphane PPh_3 (262.292 g/mol, 0.674 mmol, 0.177 g) and the ligand L^{2LONAM} (**19**; 593.513 g/mol, 0.337 mmol, 0.200 g). At the end of the reaction, the mixture was filtered, the solution was dried at reduced pressure, $CHCl_3$ (10 mL) was poured into the round-bottom flask, the obtained mixture was filtered and the mother liquors were dried at reduced pressure. The white complex $[(PPh_3)_2Cu(L^{2LONAM})]PF_6$ (**65**) was obtained in 54% yield.

MM: 1326.607 g/mol. **Solubility:** EtOH, $CHCl_3$, MeCN, DMSO. **MP:** 100-105 °C. **¹H-NMR** (DMSO-*d*₆, 293 K): δ 1.82 (sbr, 6H, 3- or 5- CH_3), 2.43 (s, 6H, 3- or 5- CH_3), 3.37-3.41 (m, 4H, $HN(CH_2)_2NH$), 5.80 (s, 2H, NCH_2Ph), 6.08 (s, 2H, 4- CH), 6.79 (d, 1H, ArH), 7.07 (s, 1H, $CHCO$), 7.26-7.52 (m, 33H, ArH), 7.73 (d, 1H, ArH), 7.79 (d, 1H, ArH), 8.20 (d, 1H, ArH), 8.38 (t, 1H, NH), 9.35 (tbr, 1H, NH). **¹³C{¹H}-NMR** (DMSO-*d*₆, 293 K): 11.0 (3- or 5- CH_3); 13.8 (3- or 5- CH_3); 37.6 ($HN(CH_2)_2NH$); 50.0 (NCH_2Ph); 107.2 (4- C_{Pz}); 110.8, 122.5, 122.8, 123.2, 127.7, 128.2, 129.4, 129.6, 129.8, 130.8,

131.9, 132.0, 132.5, 133.4, 133.7, 133.8, 138.5, 141.6, 143.0, 150.5 (CHCO, 3-C_{Pz}, 5-C_{Pz} and ArC);

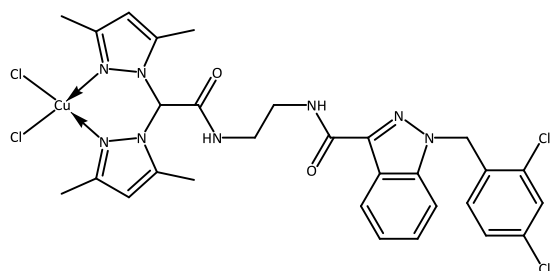


162.6, 164.5 (CO). ³¹P{¹H}-NMR (DMSO-*d*₆, 293 K): δ 4.99 (s), -144.20 (hept, *J*_(P-F) = 711 Hz, PF₆). ³¹P{¹H}-NMR (CD₃CN, 293 K): δ -1.06 (sbr), -143.53 (hept, *J*_(P-F) = 705 Hz, PF₆). FT-IR (cm⁻¹): 3401wbr, 3284wbr (N-H); 3056wbr, 2926wbr, 2869wbr (C-

H); 1694sh, 1672mbr (*v*_{asym} C=O); 1587m, 1562m, 1535m (C=C/C=N); 1492m, 1476m, 1435s, 1388m, 1311m, 1271m, 1230m, 1177m, 1158m, 1096m, 1071m, 1048m, 1028m, 998m, 918w, 835vs, 742vs. **ESI-MS(+)** (major positive ions, MeCN), *m/z* (%): 587 (100) [(PPh₃)₂Cu]⁺, 657 (15) [Cu(L^{2LONAM})]⁺, 919 (45) [(PPh₃)Cu(L^{2LONAM})]⁺. **ESI-MS(-)** (major negative ions, MeCN), *m/z* (%): 145 (100) [PF₆]⁻. **EA** (%) calculated for C₆₅H₆₀Cl₂CuF₆N₈O₂P₃: N 8.45, C 58.85, H 4.56; found: N 8.12, C 58.51, H 4.27.

2.3.3.20. Synthesis of [Cu(L^{2LONAM})]Cl₂ (66)

This compound was prepared following the procedure described for **57** but employing the ligand L^{2LONAM} (**19**; 593.513 g/mol, 0.337 mmol, 0.200 g) and MeOH as solvent. The light blue complex [Cu(L^{2LONAM})]Cl₂ (**66**) was obtained in 83% yield.



MM: 727.959 g/mol. **Solubility**: CH₂Cl₂, CHCl₃, MeCN, DMSO. **MP**: 248-250 °C. FT-IR (cm⁻¹): 3426wbr (N-H); 3169wbr, 2904mbr, 2799mbr (C-H); 1669s, 1620sh (*v*_{asym} C=O); 1576m, 1559s (C=C/C=N); 1528s, 1493m, 1467m, 1448m, 1428m,

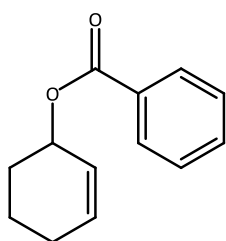
1415m, 1397m, 1384m, 1375m, 1349m, 1314m, 1268w, 1248m, 1220m, 1194m, 1177m, 1157m, 1133m, 1116m, 1103m, 1064m, 1042m, 1005m, 987m, 949w, 913m, 875m, 861m, 837s, 807m, 787s, 754s, 744s, 708m. **ESI-MS(+)** (major positive ions, MeCN), *m/z* (%): 1248 (100) [(L^{2LONAM})Cu(L^{2LONAM} - H)]⁺. **ESI-MS(-)** (major negative ions, MeCN), *m/z* (%): 170 (100) [CuCl₃]⁻. **EA** (%) calculated for C₂₉H₃₀Cl₄CuN₈O₂: N 15.39, C 47.85, H 4.15; found: N 15.09, C 48.02, H 4.43.

2.4. Syntheses of oxidized cycloalkenes via Kharasch-Sosnovsky reaction

2.4.1. General procedure for the synthesis of compounds 67-69

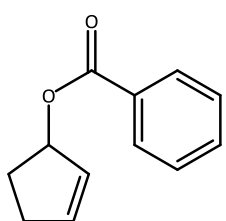
The reactions were performed in a sealed vial in which complex, *tert*-butylperoxybenzoate (Luperox) and finally the alkene were introduced and the reaction was stirred at 60 °C (for further data and details see section 3.3.2.). The work-up consisted in a pre-pad chromatographic column (packed with SiO₂; elution with 150 mL of *n*-hexane:EtOAc 70:30). The purification of the crude residue was performed by chromatographic column (packed with SiO₂, elution with *n*-hexane:EtOAc 98:2) to give the pure products.

2.4.1.1. Synthesis of cyclohex-2-enyl benzoate (67)



Yield 90%. Colorless oil. ¹H-NMR (CDCl₃, 293 K): δ 1.66-1.75 (m, 1H, CH₂CH₂CH₂(CH=CH)), 1.81-2.21 (m, 5H, (CHCO)(CH₂)₃), 5.48-5.54 (m, 1H, CH₂CH=CH), 5.81-5.87 (m, 1H, CH=CH(CHCO)), 5.97-6.02 (m, 1H, CHCO), 7.42 (t, J = 7.7 Hz, 2H, C₆H₅), 7.57 (t, J = 7.6 Hz, 1H, C₆H₅), 8.08 (d, J = 7.9 Hz, 2H, C₆H₅). ¹³C-NMR (CDCl₃, 293 K): δ 19.0, 25.0, 28.4, 68.6, 125.8, 128.3, 129.6, 130.8, 132.8, 132.9, 166.2. FT-IR (cm⁻¹): 3064w, 3033w, 2934m, 2868w, 2835w (C-H); 1710vs (ν_{asym} C=O); 1602m, 1585m, 1491w, 1451s, 1396m, 1336m, 1314s, 1266vs, 1176s, 1163s, 1143m, 1109vs, 1100sh, 1069vs, 1057vs, 1051vs, 1026vs, 1008vs, 1001vs, 915vs, 853m, 837m, 806m, 708vs. GC-MS (70eV), *m/z* (%): 202 ([M]⁺, 11), 157 (4), 120 (3), 105 (100), 97 (13), 81 (30), 77 (38), 51 (13), 41 (8). EA (%) calculated for C₁₃H₁₄O₂: C 77.20, H 6.98; found: C 77.96, H 7.14.

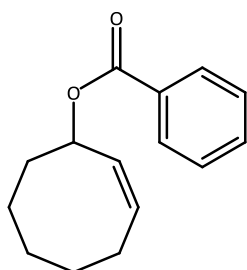
2.4.1.2. Synthesis of cyclopent-2-enyl benzoate (68)



Yield 75%. Pale yellow oil. ¹H-NMR (CDCl₃, 293 K): δ 1.96-2.03 (m, 1H, (CH=CH)CH₂), 2.38-2.47 (m, 2H, CH₂(CHCO) and (CH=CH)CH₂), 2.55-2.66 (m, 1H, CH₂(CHCO)), 5.96-5.99 (m, 2H, CH₂CH=CH), 6.17-6.19 (m, 1H, CHCO), 7.45 (t, J = 7.5 Hz, 2H, C₆H₅), 7.56 (t, J = 7.5 Hz, 1H, C₆H₅), 8.05-8.07 (m, 2H, C₆H₅). ¹³C-NMR (CDCl₃, 293 K): δ 29.9, 31.2, 81.1, 128.3, 129.4, 129.6, 130.7, 132.7, 137.7, 166.6. FT-IR (cm⁻¹): 3062w, 2973w, 2939w, 2855w (C-H); 1709vs (ν_{asym} C=O); 1602m, 1585m, 1491w, 1451s, 1366m, 1338vs, 1314s, 1267vs, 1176s, 1161m, 1110vs, 1100vs, 1069vs, 1026vs,

1001s, 946vs, 937vs, 917s, 884vs, 850m, 806m, 788m, 708vs. **GC-MS** (70 eV), m/z (%): 188 ($[M]^+$, 26), 170 (7), 143 (10), 122 (5), 105 (100), 84 (55), 77 (56), 67 (97), 51 (26), 41 (18), 39 (20), 29 (5). **EA** (%) calculated for $C_{12}H_{12}O_2$: C 76.57, H 6.43; found: C 76.09, H 6.05.

2.4.1.3. Synthesis of cyclooct-2-enyl benzoate (69)



Yield 57%. Colorless oil. $^1\text{H-NMR}$ (CDCl_3 , 293 K): δ 1.44-1.52 (m, 1H, $(\text{CH}=\text{CH})\text{CH}_2$), 1.59-1.79 (m, 6H, $(\text{CH}_2)_3\text{CH}_2(\text{CHCO})$), 2.05-2.11 (m, 1H, $(\text{CH}=\text{CH})\text{CH}_2$), 2.16-2.22 (m, 1H, $\text{CH}_2(\text{CHCO})$), 2.33-2.41 (m, 1H, $\text{CH}_2(\text{CHCO})$), 5.63-5.68 (m, 1H, $\text{CH}_2(\text{CH}=\text{CH})$), 5.72-5.77 (m, 1H, $\text{CH}=\text{CH}(\text{CHCO})$), 5.91-5.95 (m, 1H, CHCO), 7.46 (t, $J = 7.7$ Hz, 2H, C_6H_5), 7.57 (t, $J = 7.4$ Hz, 1H, C_6H_5), 8.07-8.09 (m, 2H, C_6H_5). $^{13}\text{C-NMR}$ (CDCl_3 , 293 K): δ 23.4, 25.9, 26.4, 28.8, 36.1, 73.0, 128.3, 129.6, 129.9, 130.7, 130.8, 132.7, 166.0. **FT-IR** (cm^{-1}): 3063vw, 3023w, 2927m, 2856m (C-H); 1714vs ($\nu_{\text{asym}} \text{C}=\text{O}$); 1602w, 1585w, 1491w, 1451s, 1362w, 1314s, 1270vs, 1195m, 1176m, 1150m, 1110vs, 1069vs, 1025vs, 1003sh, 947vs, 893m, 868w, 851w, 835w, 805w, 781m, 754vs, 708vs. **GC-MS** (70 eV), m/z (%): 230 ($[M]^+$, 3), 202 (10), 149 (1), 123 (6), 105 (100), 93 (10), 77 (44), 67 (9), 51 (10), 41 (8). **EA** (%) calculated for $C_{15}H_{18}O_2$: C 78.23, H 7.88; found: C 78.83, H 7.81.

3. Results and discussion

3.1. Syntheses of ligands

Several ligands were synthesized (**Figure 3.1**) to obtain novel copper(I) and copper(II) complexes with the aim to investigate their anticancer and catalytic activity.

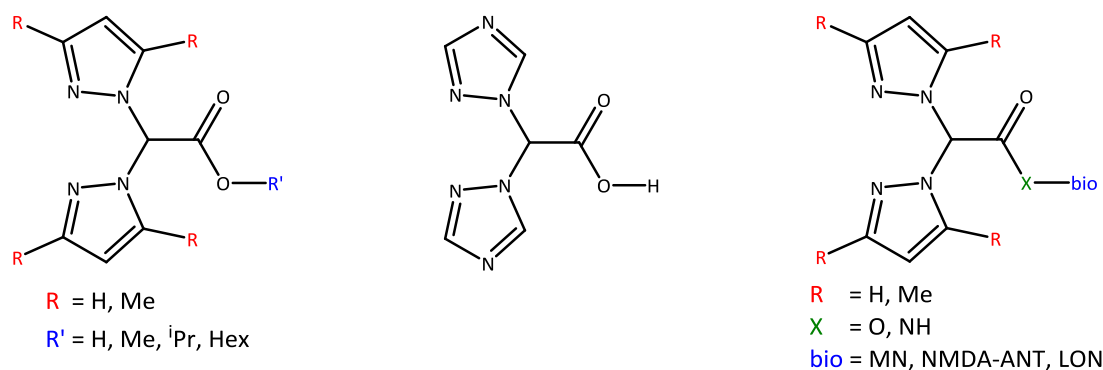
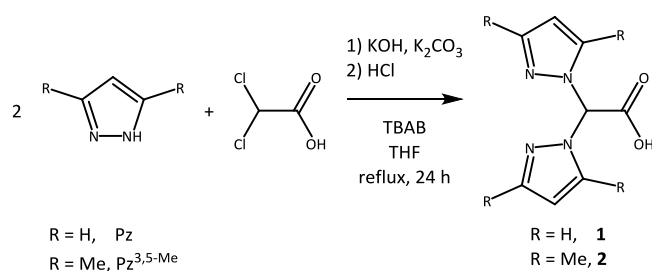


Figure 3.1. - General structures of employed ligands (MN = metronidazole, NMDA-ANT = *N*-methyl-D-aspartate receptor antagonist, LON = lonidamine).

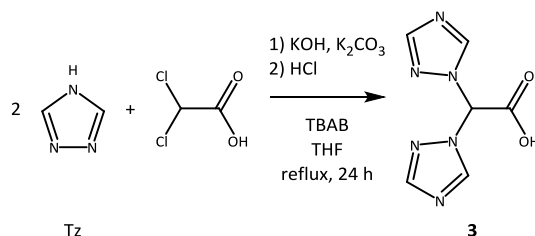
3.1.1. Syntheses of acid ligands

Bis(pyrazolyl)acetic acids L^{1H} (**1**) and L^{2H} (**2**) were synthesized using the corresponding starting materials pyrazole (Pz) or 3,5-dimethylpyrazole (Pz^{3,5-Me}) and dichloroacetic acid (Cl₂CHCOOH) in the presence of a large excess of bases (in order to deprotonate the pyrazoles and to have a strong basic environment) and a small amount of TBAB (as phase-transfer catalyst), according to the procedure reported in **Scheme 3.1**. The FT-IR spectra showed all the expected bands for the ligands: in particular weak absorptions due to the C-H stretching were observed in the range 2856-3177 cm⁻¹. The asymmetric stretching of the C=O groups is detected as a medium peak at 1722 and 1739 cm⁻¹, respectively, in the typical range of the carboxylic acids. The ¹H- and ¹³C-NMR spectra of **1** and **2**, recorded in (CD₃)₂CO and CDCl₃ solution respectively, showed all the expected signals for the ligands and only one set of resonances for the pyrazoles, indicating that the rings are equivalent. The ESI-MS study was performed solubilizing ligands **1** and **2** in MeCN. The ESI-MS(+) spectra showed the molecular adducts at *m/z* 231 and 271, attributable to the [L^{1H} + K]⁺ and [L^{2H} + Na]⁺ species, respectively, and the ESI-MS(+) spectrum of **2** showed also the molecular peak at *m/z* 249 assignable to the [L^{2H} + H]⁺ species. On the contrary, the ESI-MS(-) spectra showed the peak of the deprotonated compounds at *m/z* 191 and 247, respectively.



Scheme 3.1. - Synthesis of ligands **1** and **2**.

Bis(triazolyl)acetic acid L^{3H} (**3**) was synthesized using 1,2,4-triazole (Tz) and Cl₂CHCOOH in the presence of a large excess of bases and a small amount of TBAB according to the procedure reported in **Scheme 3.2**. The FT-IR spectrum showed all the expected bands for the ligand: weak absorptions due to the C-H stretching were observed in the range 2992-3137 cm⁻¹, while the asymmetric stretching of the C=O group is detected as a medium peak at 1701 cm⁻¹, in the typical range of the carboxylic acids. The ¹H- and ¹³C-NMR spectra of **3**, recorded in D₂O solution, showed all the expected signals for the ligand and only one set of resonances for the triazoles, indicating that the rings are equivalent. The ESI-MS study was performed solubilizing ligand **3** in H₂O. The ESI-MS(+) and ESI-MS(-) spectra showed the molecular peak at *m/z* 195 and 193, attributable to the [L^{3H} + H]⁺ and [L³]⁻ species, respectively.

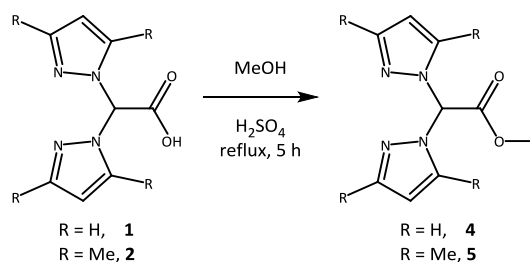


Scheme 3.2. - Synthesis of ligand **3**.

3.1.2. Syntheses of esterified ligands

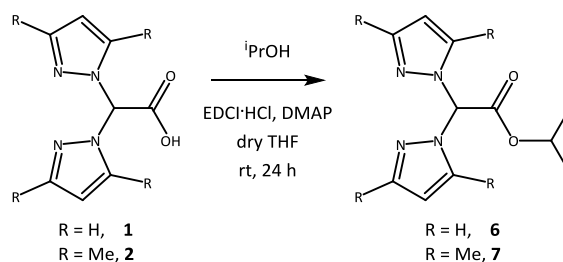
Bis(pyrazolyl)acetate methyl ester ligands L^{1Me} (**4**) and L^{2Me} (**5**) were synthesized using the precursors L^{1H} (**1**) and L^{2H} (**2**), respectively, and MeOH (both as reagent and as solvent) as starting materials, performing a classical Fisher esterification in the presence of a small quantity of acid acting as catalyst, according to the procedure reported in **Scheme 3.3**. The FT-IR spectra showed all the expected bands for the ligands: in particular weak absorptions due to the C-H stretching were observed in the range 2854-3149 cm⁻¹. The asymmetric stretching of the C=O groups is detected as strong peaks at 1753 and 1760 cm⁻¹, respectively for **4** and **5**, in the typical range of the ester groups. The ¹H- and ¹³C-NMR spectra of **4** and **5**, recorded both in CDCl₃ and CD₃CN solution, showed all the expected signals for the ligands and only one set of

resonances for the pyrazoles, indicating that the rings are equivalent. In the $^1\text{H-NMR}$ spectra in CDCl_3 , the presence of the singlet signal of the methyl group integrating three hydrogens, at 3.87 and 3.91 ppm, respectively for **4** and **5**, indicates that the reaction was successful. The ESI-MS study was performed solubilizing ligands **4** and **5** in MeCN. The ESI-MS(+) spectra showed main peaks at m/z 229 and 285, attributable to the $[\text{L}^{1\text{Me}} + \text{Na}]^+$ and $[\text{L}^{2\text{Me}} + \text{Na}]^+$ molecular adducts, respectively.



Scheme 3.3. - Synthesis of ligands **4** and **5**.

Bis(pyrazolyl)acetate isopropyl ester ligands $\text{L}^{1\text{iPr}}$ (**6**) and $\text{L}^{2\text{iPr}}$ (**7**) were synthesized using the precursors $\text{L}^{1\text{H}}$ (**1**) and $\text{L}^{2\text{H}}$ (**2**), respectively, and $^i\text{PrOH}$ as starting materials, according to the procedure reported in **Scheme 3.4**. The FT-IR spectra showed all the expected bands for the ligands: weak and medium absorptions due to the C-H stretching were observed in the range $2853\text{-}3121\text{ cm}^{-1}$, while the asymmetric stretching of the C=O groups is detected as very strong peaks at 1747 and 1748 cm^{-1} , respectively for **6** and **7**, in the typical range of the ester groups. The $^1\text{H-}$ and $^{13}\text{C-NMR}$ spectra of **6** and **7**, recorded in CD_3CN and CDCl_3 solution respectively, showed all the expected signals for the ligands and only one set of resonances for the pyrazoles, indicating that the rings are equivalent. In the $^1\text{H-NMR}$ spectra, the presence of the heptet signal integrating one hydrogen of the isopropyl group, centered at 5.14 and 5.22 ppm, respectively for **6** and **7**, indicates that the reaction was successful. The ESI-MS study was performed solubilizing ligands **6** and **7** in MeCN. The ESI-MS(+) spectra showed main peaks at m/z 257 and 313, attributable to the $[\text{L}^{1\text{iPr}} + \text{Na}]^+$ and $[\text{L}^{2\text{iPr}} + \text{Na}]^+$ molecular adducts, for **6** and **7** respectively, and the ESI-MS(+) spectrum of **7** showed also the molecular peak at m/z 291 assignable to the $[\text{L}^{2\text{iPr}} + \text{H}]^+$ species.



Scheme 3.4. - Synthesis of ligands **6** and **7**.

Crystals of ligand L^{2iPr} (**7**) were obtained by slow evaporation of an EtOAc solution of **7**. The crystalline structure of the ligand was resolved and a preliminary representation of **7** is given in **Figure 3.2**, confirming the hypothesized stoichiometry. The N-N (N(1)-N(2) = 1.364(2) Å, N(3)-N(4) = 1.361(2) Å) and C-N bond distances in the bis-pyrazolyl residues and C-C bonds in the isopropyl chain appear in line with known data. The N(1)-C(1) and N(1)-C(3) distances are 1.449(1) and 1.445(2) Å, respectively, and so not appreciably different. The N(1)-C(1)-N(3) angle of 113.3(1)° is slightly bigger than the N(1)-C(1)-C(2) and N(3)-C(1)-C(2) angles of 111.4(1)° and 110.4(1)°, respectively.

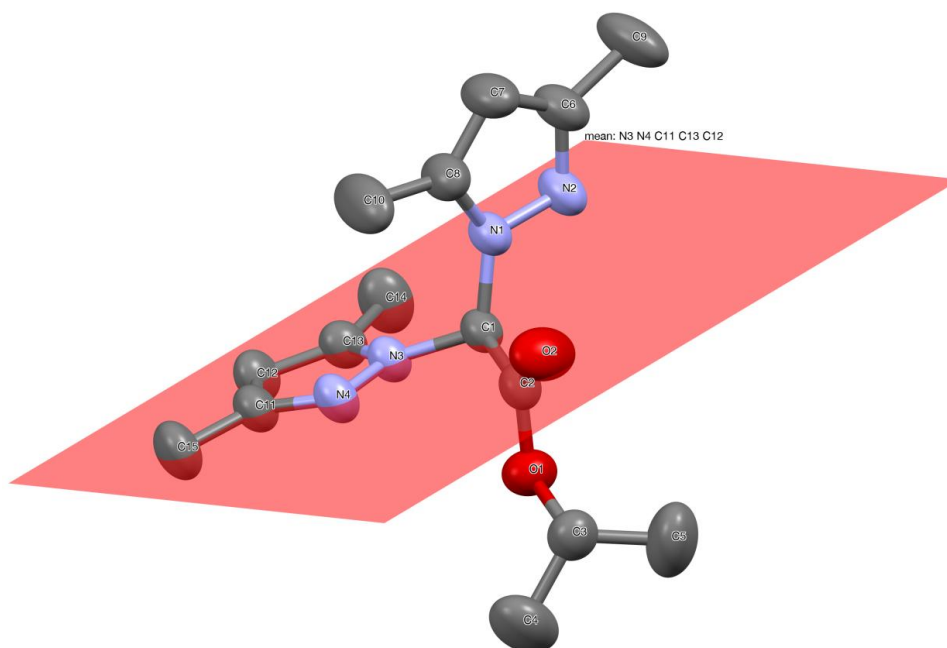
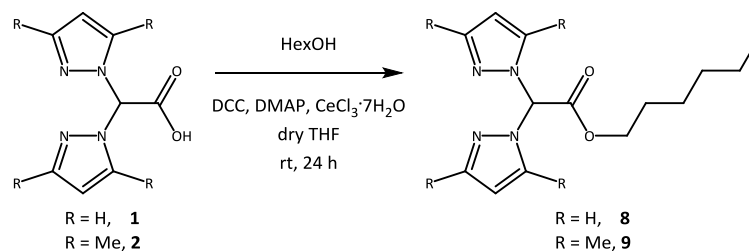


Figure 3.2. - ORTEP view of **7** with thermal ellipsoids drawn at the 30% probability level. Disordered molecular fragments and hydrogen atoms have been removed for clarity.

Bis(pyrazolyl)acetate hexyl ester ligands L^{1Hex} (**8**) and L^{2Hex} (**9**) were synthesized using precursors L^{1H} (**1**) and L^{2H} (**2**), respectively, and HexOH as starting materials, according to the procedure reported in **Scheme 3.5**. The FT-IR spectra showed all the expected bands for the ligands: weak and medium absorptions due to the C-H stretching in the range 2851-3322 cm^{-1} and strong peaks due to the asymmetric stretching of the C=O groups at 1754 and 1755 cm^{-1} , respectively, in the typical range of the ester groups. The 1H - and ^{13}C -NMR spectra of **8** and **9**, recorded in $CDCl_3$ solution, showed all the expected signals for the ligands and only one set of resonances for the pyrazoles, indicating that the rings are equivalent. The ESI-MS study was performed solubilizing ligands **8** and **9** in MeCN. The ESI-MS(+) spectra showed the molecular adducts as main peaks at m/z 299 and 355, attributable to the species $[L^{1Hex} + Na]^+$ and $[L^{2Hex} +$

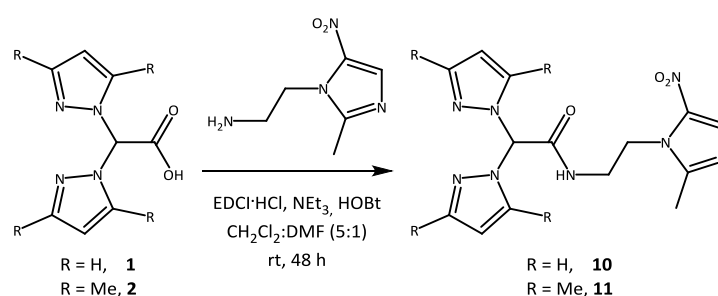
$\text{Na}]^+$, respectively, and the ESI-MS(+) spectrum of **9** showed also the molecular peak at m/z 333 assignable to the $[\text{L}^{2\text{Hex}} + \text{H}]^+$ species.



Scheme 3.5. - Synthesis of ligands **8** and **9**.

3.1.3. Syntheses of bioconjugated ligands

Ligands $\text{L}^{1\text{MN}}$ (**10**) and $\text{L}^{2\text{MN}}$ (**11**) were synthesized using precursors $\text{L}^{1\text{H}}$ (**1**) and $\text{L}^{2\text{H}}$ (**2**), respectively, and the preformed side chain 1-(2-aminoethyl)-2-methyl-5-nitroimidazole dihydrochloride monohydrate as starting materials, according to the procedure reported in **Scheme 3.6**. From this reaction, three tautomers are possible: amide-like, iminol-like and enamino-like,^[110] however $^1\text{H-NMR}$, $^{13}\text{C-NMR}$ and FT-IR data indicate that only one tautomer (the amide-like) is present. The FT-IR spectra showed all the expected bands for the ligands: absorptions due to the N-H stretching were observed in the range $3265\text{--}3288\text{ cm}^{-1}$, while weak and medium absorptions due to the C-H stretching were observed in the range $2927\text{--}3155\text{ cm}^{-1}$. The asymmetric stretching of the C=O groups is detected as strong peaks at 1686 and 1667 cm^{-1} , for **10** and **11** respectively, in the typical range of the amide groups. The $^1\text{H-}$ and $^{13}\text{C-NMR}$ spectra of **10** and **11**, recorded in CDCl_3 solution, showed all the expected signals for the ligands and only one set of resonances for the pyrazoles, indicating that the rings are equivalent. The ESI-MS study was performed solubilizing ligands **10** and **11** in MeOH. The ESI-MS(+) spectra showed the molecular peaks at m/z 345 and 401, attributable to the $[\text{L}^{1\text{MN}} + \text{H}]^+$ and $[\text{L}^{2\text{MN}} + \text{H}]^+$ species, and the molecular adducts at m/z 367 and 423, attributable to the $[\text{L}^{1\text{MN}} + \text{Na}]^+$ and $[\text{L}^{2\text{MN}} + \text{Na}]^+$ species, respectively. On the contrary, the ESI-MS(-) spectra showed the peaks of the deprotonated compounds at m/z 343 and 399, respectively.



Scheme 3.6. - Synthesis of ligands **10** and **11**.

Crystals of ligand L^{2MN} (**11**) were obtained by slow evaporation of a $CH_2Cl_2:Et_2O$ (1:3) solution of **11**. The crystalline structure of the ligand was resolved and the representation of **11** is given in **Figure 3.3**.

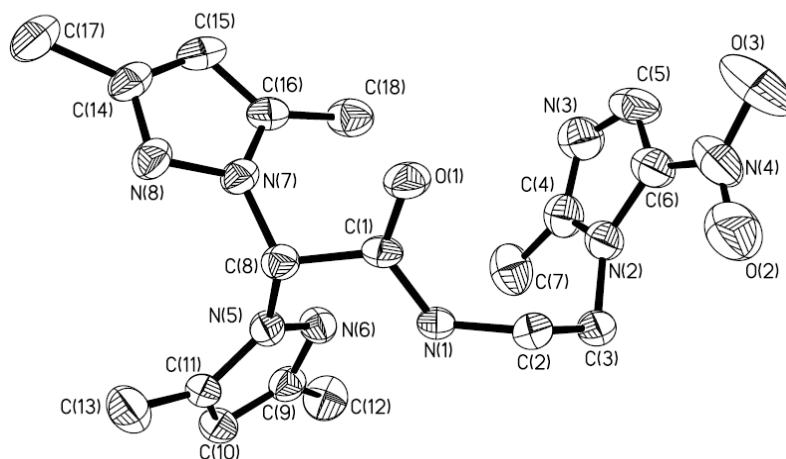
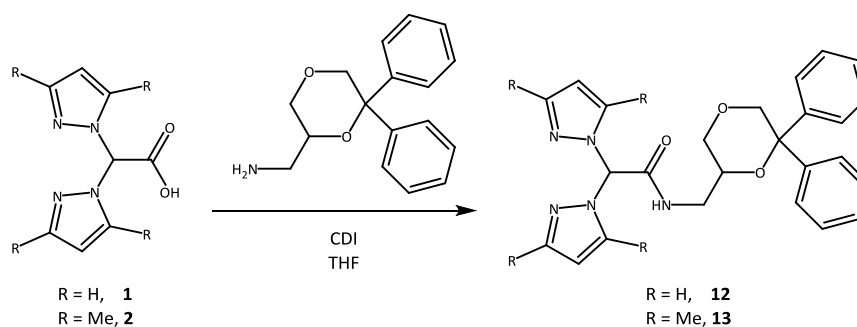


Figure 3.3. - ORTEP view of **11** showing the numbering scheme. Thermal ellipsoids are drawn at the 40% probability level. Hydrogen atoms have been omitted for clarity.

The crystal structure was compared to similar structures available from the Cambridge Crystallographic Data Centre (CCDC),^[111] revealing that the bond lengths and angles do not show exceptional differences from similar structures. The pyrazole and imidazole rings are planar within 0.01 Å and also the C8-C1-O1-N1 (the "amide" plane) atoms are planar within 0.03 Å. The mean planes encompassing the five-membered rings and the amide plane define with each other dihedral angles ranging from 56.6° to 84.4°. In the absence of a coordinated metal core, the ligand assumes an overall arrangement that is determined by the number and efficiency of intra- and inter-molecular nonbonding contacts. The ligand has a folded shape, with the two pyrazole rings oriented in a way to have N6 facing H18C and N8 facing H13C, at a mean distance of about 2.8 Å. At the same time, the imidazole ring is bent towards the O1 atom so that the centroid of the imidazole is about 4.0 Å far from O1. An examination of crystal packing reveals two very loose hydrogen bonds, in which the donor atom is always the HN1 hydrogen and the acceptors are either the pyrazole N6 of the same molecule (intramolecular bonding) or the O1 atom of an adjacent molecule. The donor-hydrogen-donor angles are far from the ideal 180° (117 and 138°, respectively) and so are the distances between the nucleophiles involved in the interactions (N1/N6 2.95 Å; N1/O1 3.01 Å); the intermolecular hydrogen bond involving O1 runs along the crystallographic *c* axis.

Ligands L^{1NMDA} (**12**) and L^{2NMDA} (**13**) were synthesized using precursors L^{1H} (**1**) and L^{2H} (**2**), respectively, and the preformed side chain (6,6-diphenyl-1,4-dioxan-2-yl)methanamine as

starting materials, according to the procedure reported in **Scheme 3.7**. The FT-IR spectra showed all the expected bands for the ligands: absorptions due to the N-H stretching were observed in the range 3287-3423 cm^{-1} , while weak absorptions due to the C-H stretching were observed in the range 2860-3121 cm^{-1} . The asymmetric stretching of the C=O groups is detected as strong peaks at 1682 and 1702 cm^{-1} , for **12** and **13** respectively, in the typical range of the amide groups. The ^1H - and ^{13}C -NMR spectra of **12** and **13**, recorded in CDCl_3 solution, showed all the expected signals for the ligands. Interestingly, a double set of resonances appears for the pyrazoles, indicating that the rings are not equivalent. The ESI-MS study was performed solubilizing **12** in MeCN and **13** in MeOH. The ESI-MS(+) spectra showed the peaks at m/z 444 and 522, attributable to the $[\text{L}^{1\text{NMDA}} + \text{H}]^+$ and $[\text{L}^{2\text{NMDA}} + \text{Na}]^+$ species, while the ESI-MS(-) spectra showed the peaks of the deprotonated compounds at m/z 442 and 498, respectively.

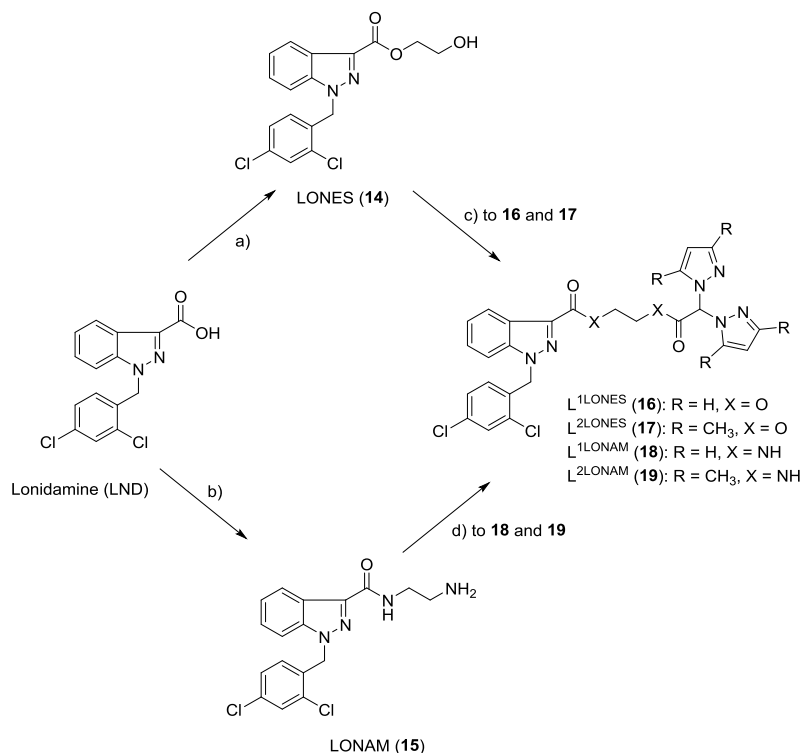


Scheme 3.7. - Synthesis of ligands **12** and **13**.

The precursors LONES (**14**) and LONAM (**15**) and the related ligands $\text{L}^{1\text{LONES}}$ (**16**), $\text{L}^{2\text{LONES}}$ (**17**), $\text{L}^{1\text{LONAM}}$ (**18**) and $\text{L}^{2\text{LONAM}}$ (**19**) were prepared according to the procedure reported in **Scheme 3.8**.

Precursors LONES (**14**) and LONAM (**15**) were synthesized using precursors ethylene glycol and ethylenediamine, respectively, and Lonidamine (LND) as starting materials. The FT-IR spectra showed all the expected bands for the precursors, in particular a broad absorption due to the O-H stretching was observed at 3480 cm^{-1} for **14**, while a broad absorption due to the N-H stretching was observed at 3282 cm^{-1} for **15**. The asymmetric stretching of the C=O groups is detected as strong peaks at 1713 and 1642 cm^{-1} , for **14** and **15** respectively. The ^1H -NMR spectra of **14** and **15**, recorded in CDCl_3 solution, showed all the expected signals for the precursors. The presence of the signals at 4.07 and 4.65 ppm for **14** (attributable to the ethylene glycol moiety) and in the range 3.01-3.58 ppm for **15** (attributable to the ethylenediamine moiety) indicates that the reactions were successful. The ESI-MS study was performed solubilizing ligands **14** and **15** in MeOH. The ESI-MS(+) spectra showed the molecular

peaks at m/z 365 and 363, attributable to the $[\text{LONES} + \text{H}]^+$ and $[\text{LONAM} + \text{H}]^+$ species, and the molecular adducts at m/z 387 and 385, attributable to the $[\text{LONES} + \text{Na}]^+$ and $[\text{LONAM} + \text{Na}]^+$ species, respectively. On the contrary, the ESI-MS(-) spectra showed the peaks of the deprotonated compounds at m/z 363 and 361, respectively.



Scheme 3.8. - Synthesis of precursors **14** and **15** and ligands **16-19**. Reagents and conditions: **a)** HOCH₂CH₂OH, H₂SO₄, 85 °C, 1 h; **b)** H₂NCH₂CH₂NH₂, CDI, THF, 18 h; **c)** **1** or **2**, DMAP, EDCI·HCl, 16 h; **d)** **1** or **2**, HOBT·xH₂O, EDCI·HCl, DMF, 16 h.

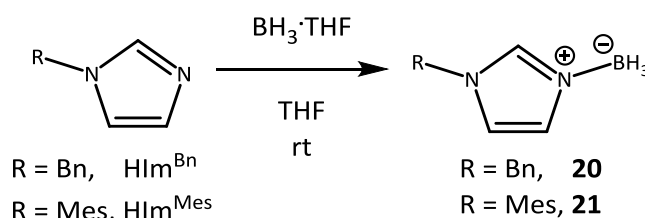
Ligands $L^{1\text{LONES}}$ (**16**) and $L^{2\text{LONES}}$ (**17**) were synthesized using precursors $L^{1\text{H}}$ (**1**) and $L^{2\text{H}}$ (**2**), respectively, and LONES (**14**) as starting materials. The FT-IR spectra showed all the expected bands for the ligands, in particular weak absorptions due to the C-H stretching were observed in the range 2928-3121 cm⁻¹. The asymmetric stretching of the C=O groups are detected in the range 1716-1763 cm⁻¹. The ¹H-NMR spectra of **16** and **17**, recorded both in DMSO-*d*₆ and in CDCl₃ solution, showed all the expected signals for the ligands: the presence of only one set of resonances for the pyrazoles indicates both the successful of the reaction and the magnetic equivalence of the rings. The ESI-MS study was performed solubilizing ligands **16** and **17** in MeOH. The ESI-MS(+) spectra showed the molecular peaks at m/z 539 and 595, attributable to the $[\text{L}^{1\text{LONES}} + \text{H}]^+$ and $[\text{L}^{2\text{LONES}} + \text{H}]^+$ species, and the main peaks of molecular adducts at m/z 561 and 617, attributable to the $[\text{L}^{1\text{LONES}} + \text{Na}]^+$ and $[\text{L}^{2\text{LONES}} + \text{Na}]^+$ species, respectively.

Ligands $L^{1\text{LONAM}}$ (**18**) and $L^{2\text{LONAM}}$ (**19**) were synthesized using precursors $L^{1\text{H}}$ (**1**) and $L^{2\text{H}}$ (**2**), respectively, and LONAM (**15**) as starting materials. The FT-IR spectra showed all the expected

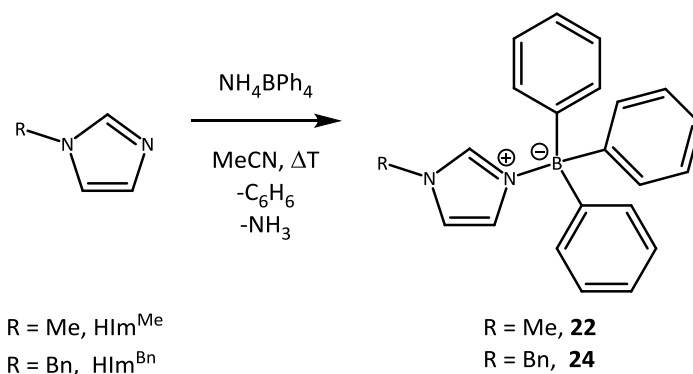
bands for the ligands, in particular broad absorptions due to the N-H stretching were observed in the range 3223-3288 cm^{-1} , while weak and medium absorptions due to the C-H stretching were observed in the range 2947-3075 cm^{-1} . The asymmetric stretching of the C=O groups are detected in the range 1641-1673 cm^{-1} . The $^1\text{H-NMR}$ spectra of **18** and **19**, recorded both in $\text{DMSO-}d_6$ and in CDCl_3 solution, showed all the expected signals for the ligands: the presence of only one set of resonances for the pyrazoles indicates both the successful of the reaction and the magnetic equivalence of the rings. The ESI-MS study was performed solubilizing ligands **18** and **19** in MeOH. The ESI-MS(+) spectra showed the molecular adducts at m/z 559 and 615, attributable to the $[\text{L}^{1\text{LONAM}} + \text{Na}]^+$ and $[\text{L}^{2\text{LONAM}} + \text{Na}]^+$ species, respectively. The ESI-MS(-) spectra showed the peaks of the deprotonated compounds at m/z 557 and 591, respectively.

3.1.4. Syntheses of imidazole-based ligands

Two different one step syntheses were performed to obtain *N*-(alkyl/aryl) imidazolium borate adducts **20-23** according to the procedure reported in **Schemes 3.9.** or **3.10.**



Scheme 3.9. - Synthesis of ligands **20** and **21**.



Scheme 3.10. - Synthesis of ligands **22** and **23**.

The colourless imidazolium-borate derivatives **20** and **21** were synthesized by the reaction of one equivalent of $\text{BH}_3\cdot\text{THF}$ and a solution of *N*-benzyl- or *N*-mesitylimidazole in nearly quantitative yields. Imidazolium trihydridoborates **20** and **21** are, respectively, white and brown solids. Adducts **22** and **23** are prepared by reaction of a MeCN solution of *N*-methyl- or *N*-

benzylimidazole and ammonium tetraphenylborate at reflux. In these conditions, it is commonly known that triphenylboranes are produced by the instability of the tetraphenylborate anion; additionally, if heated with alkylammonium salts, they can lose a phenyl ring and successively form a nitrogen-borane bond with the ammonium compound.^[112,113] In this study a similar situation happens: the by-products of reaction in **Scheme 3.10.** are volatile benzene and ammonia, obtaining the white adducts **22** and **23** in good yields. Several analytical and spectroscopic techniques confirmed the authenticity of the four precursors.

Crystals of the adducts (HIm^{Bn})BH₃ (**20**) and (HIm^{Mes})BH₃ (**21**) were obtained by slow evaporation of a CHCl₃ solution of **20** and **21**. The crystalline structures of the compounds were resolved and a representation of **20** and **21** is given in **Figure 3.4.** and **3.5.**, respectively.

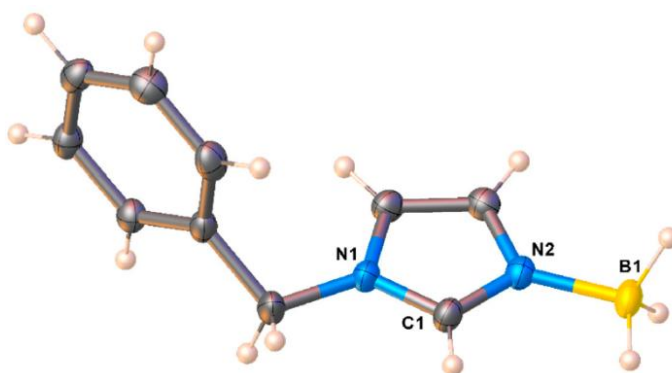


Figure 3.4. - Molecular structure of adduct **20**.

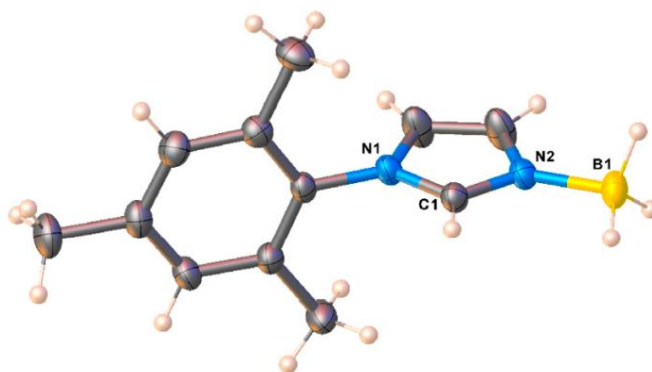


Figure 3.5. - Molecular structure of adduct **21**.

Adduct (HIm^{Bn})BH₃ (**20**), crystallizes in the orthorhombic P2₁2₁2₁ space group, it is monomeric in the solid state and C1-N1 distance is slightly higher than C1-N2 one (1.343 Å compared to 1.323 Å). Interesting selected bond distances (Å) and angles (°) are: N1-C1 1.343(2), N2-C1 1.323(2), N2-B1 1.587(2), N1-C4 1.474(2), N1-C1-N2 110.29(14), C1-N2-B1 126.58(14). Adduct (HIm^{Mes})BH₃ (**21**), crystallizes in the monoclinic P2₁/n space group with two chemically similar

but crystallographically different molecules in the asymmetric unit. Interesting selected bond distances (Å) and angles (°) are: N1-C1 1.3442(14), N2-C1 1.3207(14), N2-B1 1.5836(16), N1-C4 1.4465(14), N1-C1-N2 110.36(10), C1-N2-B1 127.91(10).

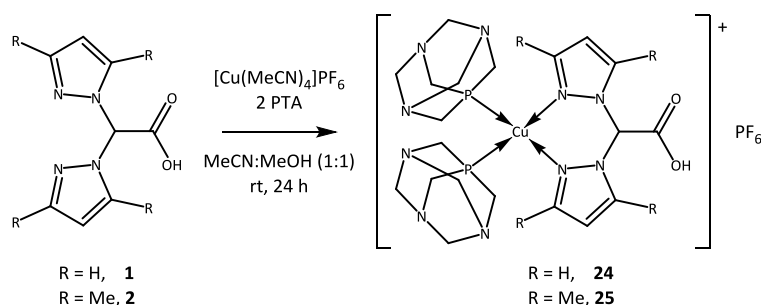
The FT-IR spectra of the four adducts show characteristic peaks. The presence of azolyl rings C-H stretching is present for compounds **20-23** in the range 3010-3177 cm^{-1} , while in compounds **20** and **21**, intense absorptions in the 2255-2374 cm^{-1} region are due to the BH_3 moieties. The ^1H - and ^{13}C -NMR spectra of the four precursors are recorded in different solvents: CDCl_3 and CD_3OD for **20** and **21** and DMSO for **22** and **23**. All derivatives show a single set of resonances for imidazolium rings; additionally, considering ^1H -NMR spectra of **20** and **21**, after two days in CD_3OD solution at room temperature, the signal at the 2-CH position does not show any sign of a reduction in intensity. This fact suggests that there is an absence of fast H-D exchange phenomenon and, therefore, lack of deuteration at this position. Regarding compounds **20** and **21**, the ^{11}B -NMR spectrum, recorded in CDCl_3 , showed a quartet at δ -19.38 (**20**) and broad doublet at δ -19.21 (**21**): these groups of signals indicate the coordination of the imidazole rings at the BH_3 moiety.^[114] In compounds **22** and **23**, the presence of the four-coordinated boron center is demonstrated by single broad resonances observed at δ -6.52 ppm for **22** in $(\text{CD}_3)_2\text{CO}$ and at δ -6.37 for **23** in CDCl_3 . These data are in accordance with literature.^[115] Considering the ESI-MS(+) spectra of **20** and **21**, peaks at m/z 195 and 223 are attributable to the molecular species $[(\text{HIm}^{\text{Bn}})\text{BH}_3 + \text{Na}]^+$ and $[(\text{HIm}^{\text{Mes}})\text{BH}_3 + \text{Na}]^+$, respectively. Additionally, these spectra display the presence of other peaks due to the fragmentation species $[\text{HIm}^{\text{R}} + \text{H}]^+$ and to the aggregates $[(\text{HIm}^{\text{R}})\text{BH}_2]^+$, being R a benzyl or mesityl group. In a similar manner, the spectra of adducts **22** and **23** show peaks at m/z 83 and 159 related to the presence of $[\text{HIm}^{\text{Me}} + \text{H}]^+$ and $[\text{HIm}^{\text{Bn}} + \text{H}]^+$ respectively, along with a fragment peak at m/z 247 ($[(\text{HIm}^{\text{Me}})\text{BPh}_2]^+$) and an aggregate peak at m/z 481 ($[(\text{Im}^{\text{Bn}})_2\text{BPh}_2]^+$) in **22** and **23** respectively.

3.2. Syntheses of the complexes

3.2.1. Syntheses of complexes bearing acid ligands

The Cu(I) complexes $[(\text{PTA})_2\text{Cu}(\text{L}^{1\text{H}})]\text{PF}_6$ (**24**) and $[(\text{PTA})_2\text{Cu}(\text{L}^{2\text{H}})]\text{PF}_6$ (**25**) were synthesized using the acceptor $[\text{Cu}(\text{MeCN})_4]\text{PF}_6$, the phosphane coligand PTA and the ligands $\text{L}^{1\text{H}}$ (**1**) and $\text{L}^{2\text{H}}$ (**2**), respectively, as starting materials, according to the procedure reported in **Scheme 3.11**. The FT-IR spectra showed all the expected bands for the complexes. The ^1H -NMR spectra of **24** and **25**, recorded both in $\text{DMSO}-d_6$ and in D_2O solution, showed all the expected signals. The

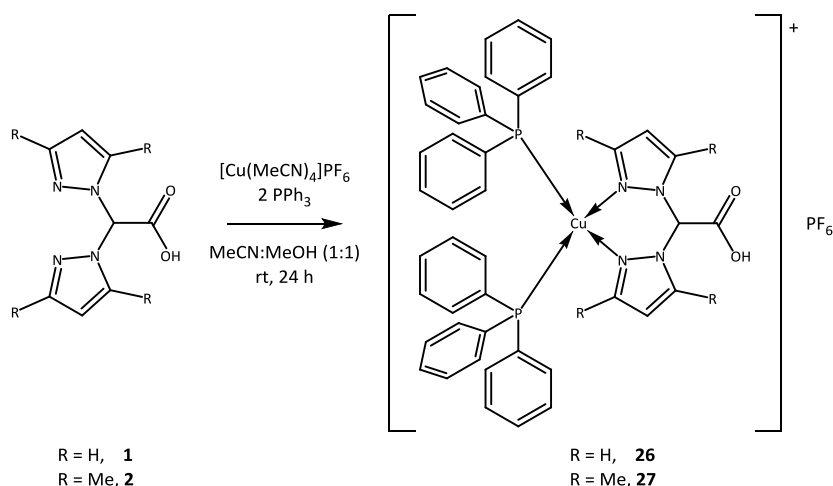
complexes showed only one set of resonances for the pyrazoles (indicating that the rings are equivalent) and a slight shift of the resonances with respect to the free ligands (due to the coordination to the metal center). The phosphanes showed a characteristic series of signals and an integration of the peaks, with respect to the ligand's resonances, which confirmed the 1:2 stoichiometric ratio between the ligand and the PTA. The ^{31}P -NMR spectra of **24** and **25**, recorded in D_2O solution, showed the characteristic heptet due to the counterion PF_6^- and singlets at -87.01 and -85.87 ppm, respectively, due to the coordinated phosphanes, shifted with respect to the signal exhibited by the free PTA (-97.07 ppm in D_2O). The ESI-MS study was performed solubilizing complexes **24** and **25** in MeCN. The ESI-MS(+) spectra showed the fragments at m/z 412 and 468, attributable respectively to the $[(\text{PTA})\text{Cu}(\text{L}^{1\text{H}})]^+$ and $[(\text{PTA})\text{Cu}(\text{L}^{2\text{H}})]^+$ species, while the ESI-MS(-) spectra of both the compounds showed the peak of the counterion $[\text{PF}_6]^-$ at m/z 145.



Scheme 3.11. - Synthesis of complexes **24** and **25**.

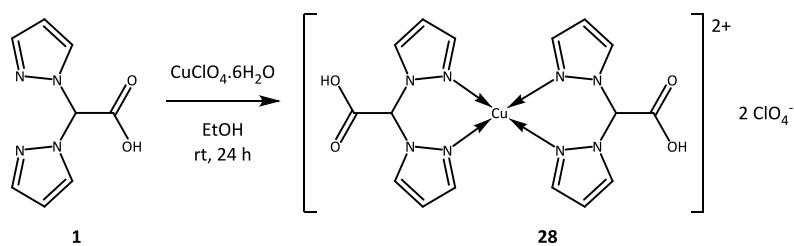
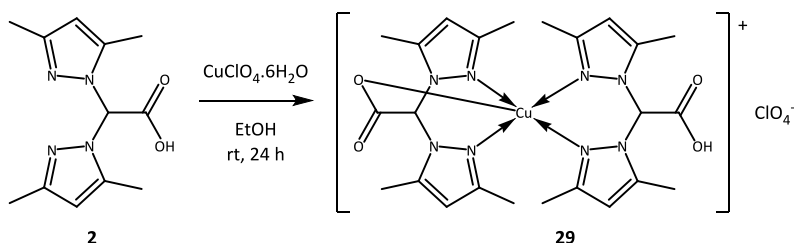
$\text{Cu}(\text{I})$ complexes $[(\text{PPh}_3)_2\text{Cu}(\text{L}^{1\text{H}})]\text{PF}_6$ (**26**) and $[(\text{PPh}_3)_2\text{Cu}(\text{L}^{2\text{H}})]\text{PF}_6$ (**27**) were synthesized using the acceptor $[\text{Cu}(\text{MeCN})_4]\text{PF}_6$, the phosphane coligand PPh_3 and the ligands $\text{L}^{1\text{H}}$ (**1**) and $\text{L}^{2\text{H}}$ (**2**), respectively, as starting materials, according to the procedure reported in **Scheme 3.12**. The FT-IR spectra showed all the expected bands for the complexes, in particular absorptions due to the asymmetric stretching of the $\text{C}=\text{O}$ groups are detected at 1752 and 1740 cm^{-1} , with no significant variations with respect to the same absorptions detectable in the spectra of the free ligands. The ^1H -NMR spectra of **26** and **27**, recorded in $\text{DMSO}-d_6$ and in CDCl_3 solution, respectively, showed all the expected signals. The complexes showed only one set of resonances for the pyrazoles (indicating that the rings are equivalent) and a slight shift of the resonances with respect to the free ligands (due to the coordination to the metal center). The phosphanes showed a characteristic series of signals in the aromatic region and an integration of the peaks, with respect to the ligand's resonances, which confirmed the 1:2 stoichiometric ratio between the ligand and the PPh_3 . The ^{31}P -NMR spectra of **26** and **27**, recorded in $\text{DMSO}-d_6$ and in CDCl_3 solution, respectively, showed the characteristic heptet due to the counterion PF_6^-

and singlets at -3.77 and -2.85 ppm, respectively, due to the coordinated phosphanes, shifted with respect to the signal exhibited by the free PPh_3 (-6.86 ppm in $\text{DMSO}-d_6$ and -5.36 in CDCl_3). The ESI-MS study was performed solubilizing complexes **26** and **27** in MeOH. The ESI-MS(+) spectra showed the fragments at m/z 517 and 573, attributable respectively to the $[(\text{PPh}_3)\text{Cu}(\text{L}^{1\text{H}})]^+$ and $[(\text{PPh}_3)\text{Cu}(\text{L}^{2\text{H}})]^+$ species, while the ESI-MS(-) spectra of both the compounds showed the peak of the counterion $[\text{PF}_6]^-$ at m/z 145.



Scheme 3.12. - Synthesis of complexes **26** and **27**.

$\text{Cu}(\text{II})$ complexes $[\text{Cu}(\text{L}^{1\text{H}})_2](\text{ClO}_4)_2$ (**28**) and $[(\text{L}^{2\text{H}})\text{Cu}(\text{L}^2)](\text{ClO}_4)$ (**29**) were synthesized using the acceptor $\text{Cu}(\text{ClO}_4)_2 \cdot 6\text{H}_2\text{O}$ and the ligands $\text{L}^{1\text{H}}$ (**1**) and $\text{L}^{2\text{H}}$ (**2**), respectively, as starting materials, according to the procedure reported in **Schemes 3.13.** and **3.14.** The FT-IR spectra showed all the expected bands for the complexes, in particular broad absorptions due to the O-H stretching were observed in the range $3459\text{-}3557\text{ cm}^{-1}$. For complex **28**, the absorption due to the asymmetric stretching of the C=O group is detected at 1736 cm^{-1} , in accordance with the presence of the uncoordinated protonated carboxylic group. Regarding complex **29**, the C=O absorptions are present at 1667 and 1705 cm^{-1} , shifted with respect to the signal observed for the free ligand **2** (1739 cm^{-1}) and in accordance with the presence of different carboxylic groups, suggesting one of them uncoordinated and protonated, while the other one coordinated to the metal center as carboxylate.^[116] Finally, strong peaks in the range $1050\text{-}1085\text{ cm}^{-1}$ confirmed the presence of the ClO_4^- groups as counterions. The ESI-MS study was performed solubilizing complexes **28** and **29** in MeCN. The ESI-MS(+) spectra showed peaks at m/z 446 and 558, attributable respectively to the $[\text{Cu}(\text{L}^1)_2 + \text{H}]^+$ and $[(\text{L}^{2\text{H}})\text{Cu}(\text{L}^2)]^+$ species, while the ESI-MS(-) spectra of both the compounds showed the peak of the counterion $[\text{ClO}_4]^-$ at m/z 99.

Scheme 3.13. - Synthesis of complex **28**.Scheme 3.14. - Synthesis of complex **29**.

Crystals of complex $[(L^{2H})Cu(L^2)](ClO_4)$ (**29**) were obtained by slow evaporation of a MeCN solution of **29**. The crystalline structure of the complex was resolved and the representation of **29** is given in **Figure 3.6.**, while the main X-ray crystallographic data are reported in **Table 3.1**. The complex comprises two bis(pyrazolyl)methane moieties functionalized with a carboxylic function. Interestingly, only one of the two ligands was found deprotonated, whereas the second ligand presented the COOH function. The carboxylic and carboxylate functions were disordered in two positions, which were refined with site occupancy factors of 0.5 each and the oxygen atom of the COO^- group of one ligand was closer to the metal center than the oxygen atom deriving from the protonated COOH. Overall, four nitrogen atoms of two ligands were located on an equatorial plane (Cu-N distances range 1.98-2.07 Å), an oxygen atom of the COO^- group occupied an apical position (Cu-O36/Cu-O36A, 2.32 and 2.36 Å, respectively), whereas the sixth position was occupied by the oxygen atom of the unprotonated carboxylic group (Cu-O13/O13A, 2.50 and 3.25 Å, respectively). This structural refinement implies that two geometries are adopted by the metal ion in the present structure. One structural image can be described as a distorted octahedron (Cu-O36 and Cu-O13 in apical position), and the second can be described as square pyramidal with Cu-O13 in apical position. The two different geometries were nonetheless in line with the electronic features of a d^9 metal ion such as Cu^{2+} . The positive charge of the complex was balanced by a severely disordered ClO_4^- anion. The complex cations formed a supramolecular chain sustained by hydrogen bonds between the carboxylate and carboxylic functions of adjacent molecules. Each supramolecular chain was surrounded by anions arranged in a columnar structural site parallel to the a axis.

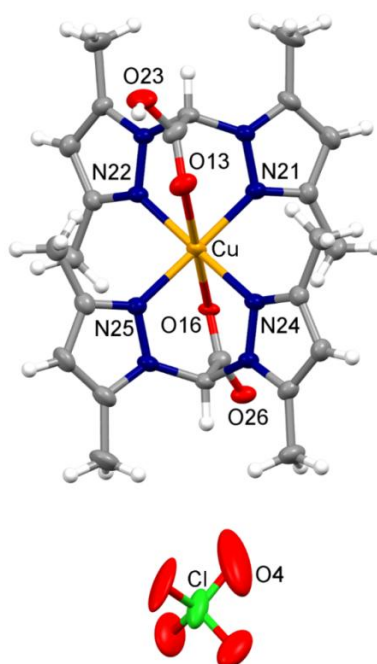
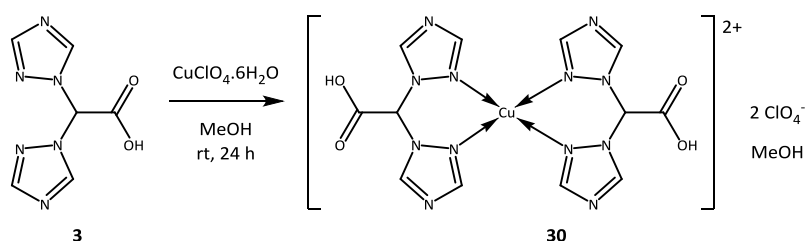


Figure 3.6. - Molecular structure of **29** with thermal ellipsoids drawn at the 30% probability level. Disordered molecular fragments were removed for clarity.

Empirical formula	C₂₄H₃₁ClCuN₈O₈
Formula weight	658.56
Temperature / K	298
Crystal system	monoclinic
Space group	P2 ₁ /a
a / Å	13.831(2)
b / Å	16.048(2)
c / Å	14.198(2)
α / °	90
β / °	114.557(2)
γ / °	90
Volume / Å ³	2866.3(7)
Z	4
ρ _{calc} g/cm ³	1.526
μ / mm ⁻¹	0.917
F(000)	1364.0
Crystal size / mm ³	0.27 × 0.18 × 0.15
Radiation	MoKα (λ = 0.71073)
2θ range for data collection / °	3.154 to 51.362
Index ranges	-16 ≤ h ≤ 16, -19 ≤ k ≤ 19, -17 ≤ l ≤ 17
Reflections collected	32067
Independent reflections	5427 [R _{int} = 0.0546, R _{sigma} = 0.0344]
Data/restraints/parameters	5427/154/528
Goodness-of-fit on F ²	1.027
Final R indexes [I ≥ 2σ (I)]	R ₁ = 0.0645, wR ₂ = 0.1669
Largest diff. peak/hole/e Å ⁻³	1.50/-0.71

Table 3.1. - Summary of X-ray crystallographic data for complex **29**.

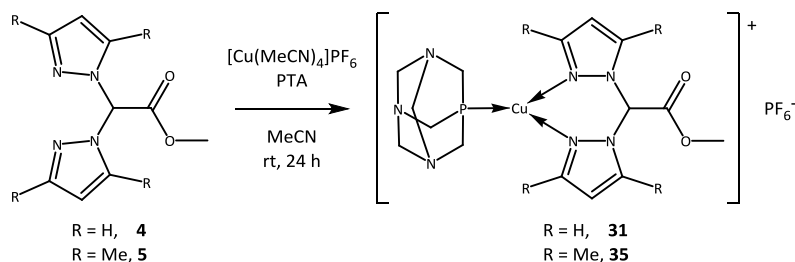
Cu(II) complex $[\text{Cu}(\text{L}^{3\text{H}})_2](\text{ClO}_4)_2 \cdot \text{MeOH}$ (**30**) was synthesized using the acceptor $\text{Cu}(\text{ClO}_4)_2 \cdot 6\text{H}_2\text{O}$ and the ligand $\text{L}^{3\text{H}}$ (**3**) as starting materials, according to the procedure reported in **Scheme 3.15**. The FT-IR spectrum showed all the expected bands for the complex, in particular a broad absorption due to the O-H stretching was observed at 3446 cm^{-1} , while the absorption due to the asymmetric stretching of the C=O group is detected at 1664 cm^{-1} , shifted with respect to the same absorption observed for the free ligand (1701 cm^{-1}) and in accordance with the presence of the uncoordinated protonated carboxylic group. Finally, strong peaks at 1125 and 1083 cm^{-1} confirmed the presence of the ClO_4^- group as counterion. The ESI-MS study was performed solubilizing complex **30** in DMSO/MeCN. The ESI-MS(+) spectrum showed the fragment at m/z 290, attributable to the $[(\text{L}^{3\text{H}})\text{Cu}(\text{MeOH})]^+$ species, while the ESI-MS(-) spectrum showed the peak of the counterion $[\text{ClO}_4]^-$ at m/z 99.



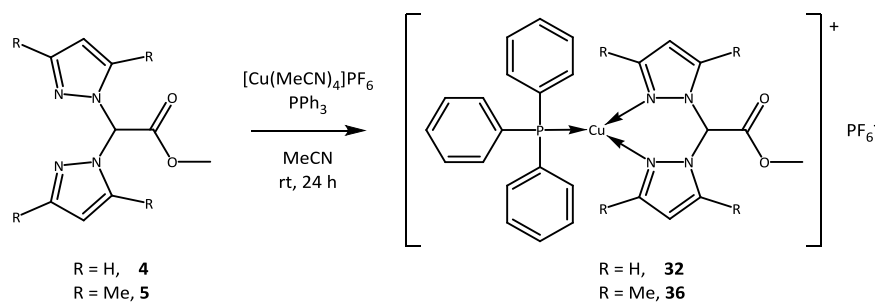
Scheme 3.15. - Synthesis of complex **30**.

3.2.2. Syntheses of complexes bearing esterified ligands

Cu(I) complexes $[(\text{PTA})\text{Cu}(\text{L}^{1\text{Me}})]\text{PF}_6$ (**31**) and $[(\text{PTA})\text{Cu}(\text{L}^{2\text{Me}})]\text{PF}_6$ (**35**) were synthesized using the acceptor $[\text{Cu}(\text{MeCN})_4]\text{PF}_6$, the phosphane coligand PTA and the ligands $\text{L}^{1\text{Me}}$ (**4**) and $\text{L}^{2\text{Me}}$ (**5**), respectively, as starting materials, according to the procedure reported in **Scheme 3.16**. Analogously, complexes $[(\text{PPh}_3)\text{Cu}(\text{L}^{1\text{Me}})]\text{PF}_6$ (**32**) and $[(\text{PPh}_3)\text{Cu}(\text{L}^{2\text{Me}})]\text{PF}_6$ (**36**) were synthesized using the same starting materials, but employing PPh_3 as phosphane, according to the procedure reported in **Scheme 3.17**.



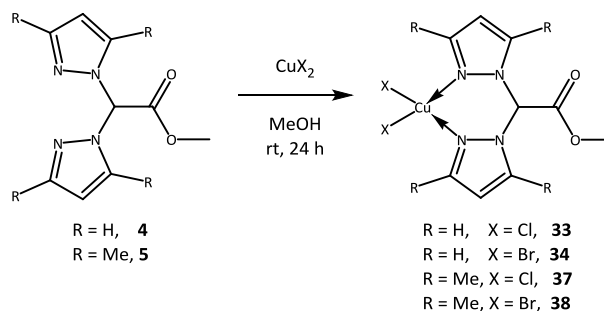
Scheme 3.16. - Synthesis of complexes **31** and **35**.



Scheme 3.17. - Synthesis of complexes **32** and **36**.

The FT-IR spectra showed all the expected bands for the scorpionate ligands and the phosphane coligands. The absorptions due to the asymmetric C=O stretching of the ester groups are in the range 1759-1768 cm^{-1} ; with no significant variations with respect to the same absorptions detectable in the spectra of the free ligands. In the lower frequency region, complexes showed a broad strong band in the range 830-836 cm^{-1} due to the vibrations of the PF_6^- anion. The $\delta(\text{PF}_6)$ bending vibrations in the spectra of all hexafluorophosphate complexes are observed as a narrow strong band at 555-558 cm^{-1} . The $^1\text{H-NMR}$ spectra of the Cu(I) complexes, recorded in CD_3CN solution, showed a single set of resonances for the pyrazoles, indicating that the rings are equivalents, with a slight shift due to the coordination to the metal center. The PTA and PPh_3 coligands showed a characteristic series of peaks at 4.09-4.58 and 7.34-7.53 ppm, respectively, with an integration of the peaks, with respect to the resonances of the ligands, which confirmed the 1:1 stoichiometric ratio between the ligand and the phosphane coligand. The $^{31}\text{P-NMR}$ spectra, recorded in CD_3CN solution at room temperature, gave singlets shifted with respect to the value of the free phosphanes PTA and PPh_3 (-102.07 and -4.85 ppm in CD_3CN , respectively). Complexes $[(\text{PTA})\text{Cu}(\text{L}^{1\text{Me}})]\text{PF}_6$ (**31**) and $[(\text{PTA})\text{Cu}(\text{L}^{2\text{Me}})]\text{PF}_6$ (**35**) gave broad singlets centered at -93.52 and -95.72 ppm, respectively, while $[(\text{PPh}_3)\text{Cu}(\text{L}^{1\text{Me}})]\text{PF}_6$ (**32**) and $[(\text{PPh}_3)\text{Cu}(\text{L}^{2\text{Me}})]\text{PF}_6$ (**36**) showed broad singlets centered at -1.48 and -2.08 ppm, respectively. In all the spectra the characteristic heptets centered between -143.51 and -144.78 ppm are due to the PF_6^- counterion. The ESI-MS study was performed solubilizing the complexes in MeCN and it confirmed the formation of the PTA and PPh_3 complexes and the presence of the hexafluorophosphate as counterion. In particular, the formation of complexes **31**, **32**, **35** and **36** was confirmed by the presence in the ESI-MS(+) spectra of the peaks attributable to the $[(\text{PTA})\text{Cu}(\text{L}^{1\text{Me}})]^+$, $[(\text{PPh}_3)\text{Cu}(\text{L}^{1\text{Me}})]^+$, $[(\text{PTA})\text{Cu}(\text{L}^{2\text{Me}})]^+$ and $[(\text{PTA})\text{Cu}(\text{L}^{2\text{Me}})]^+$ species. In the negative ion spectra $[\text{PF}_6]^-$ was observed as the main peak for all the complexes.

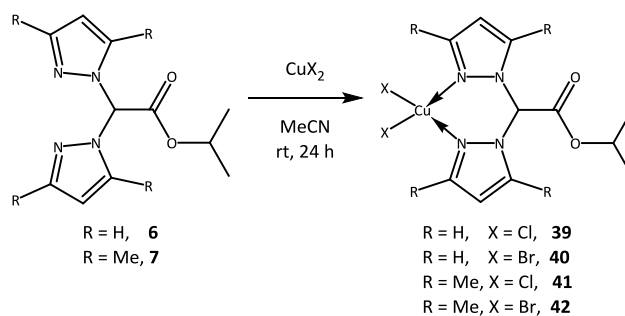
Cu(II) complexes $[\text{Cu}(\text{L}^{1\text{Me}})]\text{Cl}_2$ (**33**) and $[\text{Cu}(\text{L}^{2\text{Me}})]\text{Cl}_2$ (**37**) were synthesized using the acceptor $\text{CuCl}_2 \cdot 2\text{H}_2\text{O}$ and the ligands $\text{L}^{1\text{Me}}$ (**4**) and $\text{L}^{2\text{Me}}$ (**5**), respectively, as starting materials, according to the procedure reported in **Scheme 3.18**. These syntheses have also been performed starting from a 1:2 stoichiometric ratio between metal and ligand, obtaining the same products. Analogously, complexes $[\text{Cu}(\text{L}^{1\text{Me}})]\text{Br}_2$ (**34**) and $[\text{Cu}(\text{L}^{2\text{Me}})]\text{Br}_2$ (**38**) were synthesized using the same starting materials, but employing CuBr_2 as acceptor, according to the procedure reported in **Scheme 3.18**.



Scheme 3.18. - Synthesis of complexes **33**, **34**, **37** and **38**.

The FT-IR spectra showed all the expected bands for the scorpionate ligands. The absorptions due to the asymmetric C=O stretching of the ester groups are in the range $1748\text{--}1761\text{ cm}^{-1}$; with no significant variations with respect to the same absorptions detectable in the spectra of the free ligands (1753 and 1760 cm^{-1} for **4** and **5**, respectively) and in accordance with the presence of the uncoordinated protonated carboxylic group. The copper centre results in a tetracoordinated environment with the ligand chelating in a bidentate fashion and the other two positions occupied by the chlorides or bromides. In the lower frequency region, complexes **33** and **37** showed a very strong band in the range $278\text{--}279\text{ cm}^{-1}$ due to the Cu-Cl bond. Analogously, complexes **34** and **38** showed a very strong band in the range $229\text{--}235\text{ cm}^{-1}$ due to the Cu-Br bond. The ESI-MS study was performed solubilizing the complexes in MeOH. In the ESI-MS(+) spectrum of **33** peaks at m/z 269 and 475 were attributed to the $[\text{Cu}(\text{L}^{1\text{Me}} - \text{H})]^+$ and $[(\text{L}^{1\text{Me}})\text{Cu}(\text{L}^{1\text{Me}} - \text{H})]^+$ species, while in the spectrum of **34** peaks at m/z 269 and 350 were attributed to the $[\text{Cu}(\text{L}^{1\text{Me}} - \text{H})]^+$ and $[(\text{L}^{1\text{Me}})\text{CuBr}]^+$ species. In the ESI-MS(+) spectrum of **37** a peak was detected at m/z 420 attributable to the $[(\text{L}^{2\text{Me}})\text{CuCl}_2 + \text{Na}]^+$ adduct, while in the spectrum of **38** peaks at m/z 572 and 586 were attributed to the $[(\text{L}^{2\text{Me}})\text{Cu}(\text{L}^{2\text{Me}})]^+$ and $[(\text{L}^{2\text{Me}})\text{Cu}(\text{L}^{2\text{Me}} - \text{H})]^+$ species. The ESI-MS(-) spectra of complexes **33** and **37** showed peaks at m/z 170 attributable to the $[\text{CuCl}_3]^-$ species, while in the spectra of **34** and **38** peaks at m/z 304 were attributed to the $[\text{CuBr}_3]^-$ species, confirming the presence of the halides in all the complexes.

The Cu(II) complexes $[\text{Cu}(\text{L}^{1\text{iPr}})]\text{Cl}_2$ (**39**) and $[\text{Cu}(\text{L}^{2\text{iPr}})]\text{Cl}_2$ (**41**) were synthesized using the acceptor $\text{CuCl}_2 \cdot \text{H}_2\text{O}$ and the ligands $\text{L}^{1\text{iPr}}$ (**6**) and $\text{L}^{2\text{iPr}}$ (**7**), respectively, as starting materials, according to the procedure reported in **Scheme 3.19**. Analogously, complexes $[\text{Cu}(\text{L}^{1\text{iPr}})]\text{Br}_2$ (**40**) and $[\text{Cu}(\text{L}^{2\text{iPr}})]\text{Br}_2$ (**42**) were synthesized using the same starting materials, but employing CuBr_2 as acceptor, according to the procedure reported in **Scheme 3.19**.

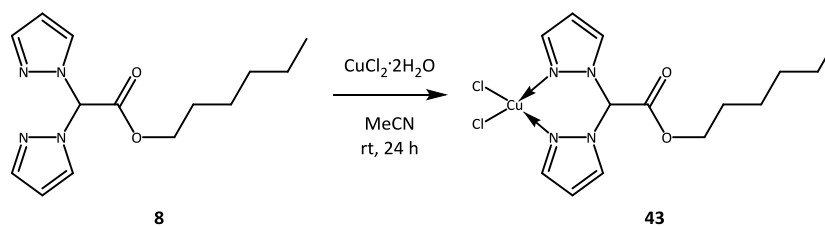


Scheme 3.19. - Synthesis of complexes **39-42**.

The FT-IR spectra showed all the expected bands for the complexes, in particular strong absorptions due to the asymmetric stretching of the C=O groups are observed in the range $1735\text{-}1748\text{ cm}^{-1}$, in the typical range of esters and with no significant variation with respect to the same absorption detectable in the spectra of the free ligands (1747 and 1748 cm^{-1} for **6** and **7**, respectively), indicating that the carbonyl is not involved in the coordination to the metal center. The ESI-MS study was performed solubilizing complexes **39-42** in MeCN. Both the ESI-MS(+) spectra of compounds **39** and **40** showed the peaks at m/z 297 and 531, attributable respectively to the $[\text{Cu}(\text{L}^{1\text{iPr}} - \text{H})]^+$ and $[(\text{L}^{1\text{iPr}})\text{Cu}(\text{L}^{1\text{iPr}} - \text{H})]^+$ species, while in both the spectra of compounds **41** and **42** is detectable the peak at m/z 353, assignable to the $[\text{Cu}(\text{L}^{2\text{iPr}} - \text{H})]^+$ species. In the ESI-MS(+) spectrum of **41** is also present the peak at m/z 643, attributable to the $[(\text{L}^{2\text{iPr}})\text{Cu}(\text{L}^{2\text{iPr}} - \text{H})]^+$ species, and in the spectrum of **42** the peak at m/z 434 is assignable to the $[(\text{L}^{2\text{iPr}})\text{CuBr}]^+$ molecular fragment.

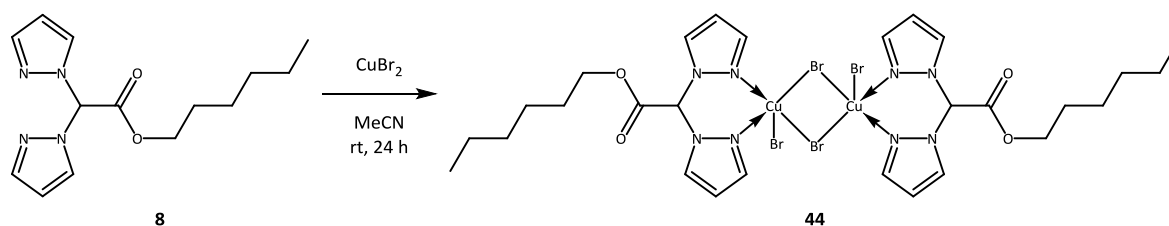
Complex $[\text{Cu}(\text{L}^{1\text{Hex}})]\text{Cl}_2$ (**43**) was prepared using ligand **8** and $\text{CuCl}_2 \cdot 2\text{H}_2\text{O}$ as starting materials, according to the procedure reported in **Scheme 3.20**. The FT-IR spectrum showed all the expected bands for the complex, in particular weak and medium absorptions due to the C-H stretching were observed in the range $2867\text{-}3142\text{ cm}^{-1}$. The asymmetric stretching of the C=O group is detected as a strong peak at 1742 cm^{-1} , without a significant variation with respect to the absorption detectable in the spectrum of the free ligand ($\nu_{\text{asym}} \text{C}=\text{O}$ 1754 cm^{-1}), indicating that in the solid state the carbonyl group is not involved in the coordination of the metal. The ESI-MS study was performed solubilizing complex **43** in MeCN: the ESI-MS(+) spectrum showed

a peak at m/z 374, attributable to the species $[(L^{1Hex})CuCl]^+$ that confirms the complex formation, while the ESI-MS(-) spectrum showed the main peak at m/z 170, assignable to the species $[CuCl_3]^-$.



Scheme 3.20. - Synthesis of complex **43**.

Complex $\{[Cu(L^{1Hex})]Br(\mu-Br)\}_2$ (**44**) was prepared using ligand **8** and $CuBr_2$ as starting materials, according to the procedure reported in **Scheme 3.21**. The FT-IR spectrum showed all the expected bands for the complex, in particular weak and medium absorptions due to the C-H stretching were observed in the range 2865 - 3146 cm^{-1} . The asymmetric stretching of the C=O group is detected as a strong peak at 1740 cm^{-1} , without a significant variation with respect to the absorption detectable in the spectrum of the free ligand ($\nu_{asym} C=O$ 1754 cm^{-1}), indicating that the carbonyl group is not involved in the coordination of the metal, in accordance with X-ray crystal structure with the ligands chelating in a κ^2 -N,N bidentate fashion. The ESI-MS study was performed solubilizing complex **44** in MeCN: the ESI-MS(+) spectrum showed peaks at m/z 339 and 615, attributable to the species $[Cu(L^{1Hex} - H)]^+$ and $[(L^{1Hex})Cu(L^{1Hex} - H)]^+$, respectively.



Scheme 3.21. - Synthesis of complex **44**.

Crystals of complex **44** were obtained by slow evaporation of a Me_2CO solution of **44**. A summary of the crystal/structure refinement data is given in **Table 3.2.**, selected bond lengths and angles were reported in **Table 3.3.**, an ORTEP-like^[117] representation of the complex is given in **Figure 3.7.** and the distorted square pyramidal polyhedra about the two Cu centres were highlighted in **Figure 3.8.** The crystal structure investigation has revealed that in the solid state the compound exists as a dimer of formula $\{[Cu(L^{1Hex})]Br(\mu-Br)\}_2$, with the Br(1) ions binding two symmetry-related units to each other. This complex is one of the few mono- or dinuclear bis(pyrazolyl)acetate copper complexes^[118,119] with uncoordinating acetate moieties

and also one of the relatively not-so-abundant copper complexes showing μ -bridging bromide ions coupled with two pentacyclic N-based ligands.^[120-125]

Empirical formula	C₁₄H₂₀N₄O₂CuBr₂
Formula weight	499.70
Temperature / K	296.9(9)
Crystal system	Monoclinic
Space group	<i>P</i> 2 ₁ / <i>c</i>
<i>a</i> / Å	13.0171(4)
<i>b</i> / Å	9.8111(2)
<i>c</i> / Å	15.8632(4)
α / °	90
β / °	110.248(3)
γ / °	90
Volume / Å ³	1900.73(9)
<i>Z</i>	4
ρ_{calc} g/cm ³	1.746
μ / mm ⁻¹	5.366
<i>F</i> (000)	988.0
Crystal size / mm ³	0.6 × 0.4 × 0.01
Radiation	Mo K α (λ = 0.71073)
Index ranges	-15 ≤ <i>h</i> ≤ 17, -13 ≤ <i>k</i> ≤ 12, -19 ≤ <i>l</i> ≤ 20
Reflections collected	22513
Independent reflections / <i>R</i> _{int}	4228 / 0.0437
Data / Restraints / Parameters	4228 / 78 / 293
Goodness-of-fit on <i>F</i> ²	1.058
Final <i>R</i> indexes [<i>I</i> ≥ 2 σ (<i>I</i>)]	<i>R</i> ₁ = 0.0351, <i>wR</i> ₂ = 0.0666
Largest diff. peak / hole / e Å ⁻³	0.50 / -0.46

Table 3.2. - Summary of crystal data and structure refinement for complex **44**.

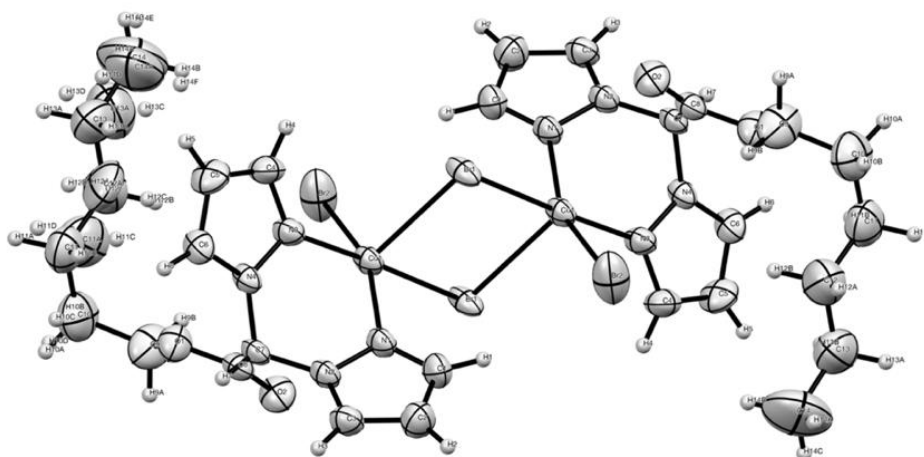


Figure 3.7.

ORTEP-like molecular structure of complex **44** with thermal ellipsoids drawn at the 30% probability level.

Br(1)-Cu(1)	2.4302(4)	Br(2)-Cu(1)	2.3687(6)
Br(1)-Cu(1) ¹	2.7600(5)	Cu(1)-N(1)	2.017(2)
Cu(1)-N(3)	2.042(3)	N(1)-N(2)	1.357(3)
N(3)-N(4)	1.369(3)	N(1)-C(3)	1.330(4)
N(2)-C(1)	1.342(4)	N(3)-C(6)	1.305(4)
N(4)-C(4)	1.338(4)	N(2)-C(7)	1.445(3)
N(4)-C(7)	1.434(4)	C(1)-C(2)	1.344(5)
C(2)-C(3)	1.384(5)	C(4)-C(5)	1.355(5)
C(5)-C(6)	1.399(5)	C(7)-C(8)	1.533(4)
O(1)-C(8)	1.198(3)	O(2)-C(8)	1.310(4)
Cu(1)-Br(1)-Cu(1) ¹	93.544(13)	Br(1)-Cu(1)-Br(1) ¹	86.456(13)
N(1)-Cu(1)-Br(1) ¹	93.87(7)	N(3)-Cu(1)-Br(1) ¹	97.29(7)
Br(2)-Cu(1)-Br(1)	93.260(18)	N(1)-Cu(1)-Br(1)	176.35(7)
N(3)-Cu(1)-Br(2)	157.34(7)	N(1)-Cu(1)-N(3)	85.69(10)
N(1)-Cu(1)-Br(2)	90.16(8)	N(3)-Cu(1)-Br(1)	90.67(7)
N(2)-N(1)-Cu(1)	122.68(17)	N(4)-N(3)-Cu(1)	121.3(2)
N(1)-N(2)-C(7)	118.8(2)	N(3)-N(4)-C(7)	119.4(2)
N(1)-C(3)-C(2)	110.6(3)	N(3)-C(6)-C(5)	111.5(3)
C(1)-N(2)-N(1)	111.2(2)	C(4)-N(4)-N(3)	110.6(3)
N(2)-C(1)-C(2)	107.3(3)	N(4)-C(4)-C(5)	107.9(3)
N(4)-C(7)-N(2)	110.1(2)	C(1)-C(2)-C(3)	106.2(3)
C(4)-C(5)-C(6)	104.8(4)	O(2)-C(8)-C(7)	108.8(2)
O(1)-C(8)-C(7)	124.6(3)	O(1)-C(8)-O(2)	126.6(3)

Table 3.3. - Bond lengths (Å) and angles (deg) of complex **44**.

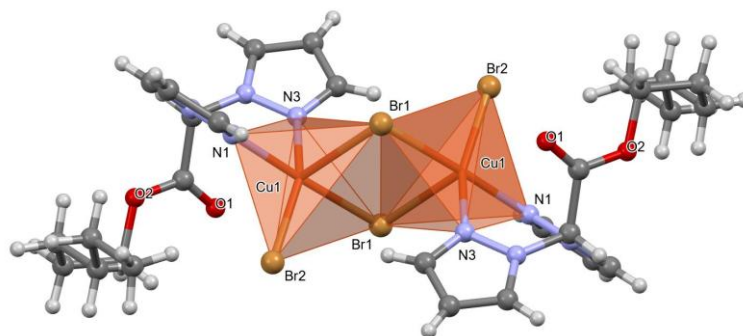
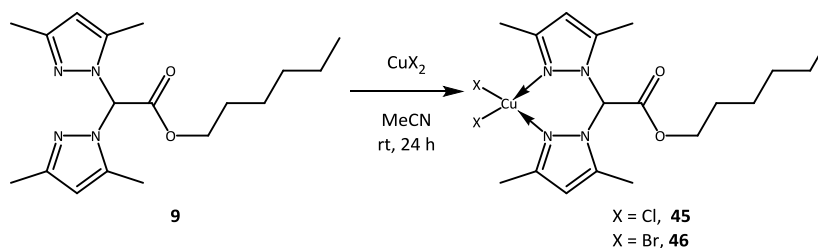


Figure 3.8. - Mercury^[126] ball-and-stick representation of the dimeric complex highlighting the square pyramidal environment of the copper atoms. Only one of the hexyloxy chain arrangement has been shown for clarity. Monomeric units on the left and on the right show, respectively, apical bromide or basal square plane towards the observer.

In the dimer, two μ -bridging Br(1) and two Cu atoms define a Cu₂Br₂ tetracycle. The Cu atom is penta-coordinated and the environment has a distorted square planar shape; the latter seems to be the preferred one in similar compounds. In the pyramid basal plane sit the N(1) and N(3) atoms of the two pyrazolyl rings, that are in *trans* position with the Br(1) and Br(2) atoms, respectively. As for metal-involving bonds, the Cu(1)-Br(2) length of the terminal bromide ion

(see **Table 3.3.**) is about 0.06 Å shorter than the Cu(1)-Br(1) distance (2.3687(6) vs 2.4302(4) Å); the Cu(1)-Br(1)^l bond length of the μ -bridging Br ion is instead appreciably longer at 2.7600(5), about 0.33 Å longer than the terminal Cu-Br bond. This value is higher than the reported average for similar compounds (2.59 Å), but fits within the reported range (2.37-3.06 Å). Similar considerations can apply to Cu-N(1) and Cu-N(3) distances, respectively, 2.017(2) and 2.042(3) Å (mean: 2.00, range: 1.97-2.09 Å). The situation closely matches that found in the two known compounds showing also a bis-pyrazolyl moiety.^[119,123] The N-N and C-N bond distances in the pyrazole residues and the C-C bonds in the hexyl chain appear in line with known data and do not deserve further comment. It is instead worth noting that the O(1) oxygen of the carboxylic moiety is roughly in *trans* position with respect to the symmetry related bridging Br(1) atom (angle O(1)-Cu(1)-Br(1)^l of 162.6°), in a virtual sixth Cu coordination position, however, the Cu(1)-O(1) distance is 3.174 Å, well above the sum of the Cu and O Van Der Waals radii (1.92 Å). The same situation has been found in a recent report.^[119]

Complexes $[\text{Cu}(\text{L}^{2\text{Hex}})]\text{Cl}_2$ (**45**) and $[\text{Cu}(\text{L}^{2\text{Hex}})]\text{Br}_2$ (**46**) were prepared using ligand **9** and $\text{CuCl}_2 \cdot 2\text{H}_2\text{O}$ or CuBr_2 , respectively, as starting materials, according to the procedure reported in **Scheme 3.22**. The FT-IR spectra showed all the expected bands for the complexes, in particular weak and medium absorptions due to the C-H stretching were observed in the range 2859-3137 cm^{-1} . The asymmetric stretching of the C=O groups are detected as strong peaks at 1761 and 1756 cm^{-1} , respectively, in the range of the ester groups, without significant variations with respect to the absorption detectable in the free ligand ($\nu_{\text{asym}} \text{C}=\text{O}$ 1755 cm^{-1}), indicating that in the solid state the carbonyl group is not involved in the coordination of the metal. The ESI-MS study was performed solubilizing complexes **45** and **46** in MeCN: the ESI-MS(+) spectra showed the peaks at m/z 430 and 476, attributable to the species $[(\text{L}^{2\text{Hex}})\text{CuCl}]^+$ and $[(\text{L}^{2\text{Hex}})\text{CuBr}]^+$, respectively, that confirm the complexes formation, while the ESI-MS(-) spectra showed the main peak at m/z 170 and 304, assignable to the $[\text{CuX}_3]^-$ species (X = Cl or Br, respectively).



Scheme 3.22. - Synthesis of complexes **45** and **46**.

Due to unsuccessful efforts in attempts to crystallize the compounds **43**, **45** and **46** to obtain crystals suitable for the SC-XRD, it has been chosen to exploit the X-ray Photoelectron

Spectroscopy (XPS) and X-ray Absorption Fine Structure (XAFS) spectroscopy (in the near edge and in the extended regions) to achieve details about the electronic states (C, N, O, Cu) and the local coordination geometry in the complexes.

The XPS data analysis results concerning C1s, N1s, O1s, Cl2p and Cu2p core levels (Binding Energy (BE), Full Width Half Maximum (FWHM) and assignments) confirmed the proposed molecular structures. The C1s signal can be always resolved by curve fitting analysis into three components corresponding, respectively, to aromatic and aliphatic C-C carbons (BE = 284.7 eV), to C-N carbons of the pyrazole-like rings and C-O of the carboxylate tail (BE = 286.6 eV) and to O-C=O carbon atoms of carboxylate (BE = 289 eV) tail. In addition, a small intensity signal attributed to C=O is individuated at about 288 eV and attributed to impurities always found on the surface of samples deposited in air. C1s spectra of the ligand **9** and the related coordination compound **45** are reported in **Figure 3.9.(a)** and **Figure 3.9.(b)**, respectively.

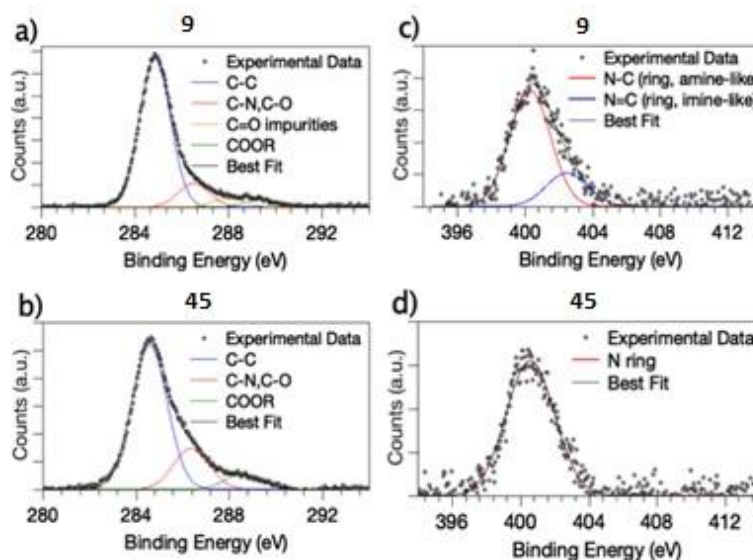


Figure 3.9. - a) XPS C1s core level spectrum of **9**; b) XPS C1s core level spectrum of **45**; c) XPS N1s core level spectrum of **9**; d) XPS N1s core level spectrum of **45**.

N1s spectrum of the ligand **9** (**Figure 3.9.(c)**) shows a couple of main signals at respectively 400.3 eV and 402.4 eV BE, indicative for the two types of nitrogen on the pyrazole rings, i.e. respectively amine-like and imine-like. As for the coordination compounds, it is expected that, when the two nitrogen atoms coordinate a metal ion, only the amine-like contribution appears, as reported in the literature for heterocycles coordinating metal ions (for example porphyrins or phthalocyanines),^[127,128] as well as for pyrazole molecules anchored to copper substrates.^[129] In excellent agreement with this prediction, in both complexes **45** (**Figure 3.9.(d)**) and **43** a single N1s component can be observed at about 400.5 eV: it is attributed to the symmetrized nitrogen atoms coordinated to Cu(II). For the two coordination compounds **45** and **43**, Cu2p

and Cl2p spectra were also collected and analyzed. Cl2p signals are noisy (as expected due to the low atomic percent of chlorine in the proposed molecular structure); a couple of spin-orbit components is observed for both complexes at about 197.5 eV, as expected for chlorine atoms in metal coordination compounds.^[130]

With the aim to gather further information about the functional groups presence and stability in the copper(II) coordination compounds, Near Edge X-ray Absorption Fine Structure (NEXAFS) spectroscopy measurements were also carried out at C and N K-edges. Spectra of **43**, **45** and **46** (that for sampling issues was difficult to measure with XPS) were collected in an experimental geometry avoiding any dichroic effect induced by molecular orientation in the ligand molecules, i.e. with the photon beam impinging at grazing angle (30°) of incidence on the sample surface. Spectra of the C K-edge and N K-edge of the samples analysed are reported in **Figure 3.10**. Peak position and assignment of the main features detected in the C and N K-edge spectra of the analysed samples are also shown in **Table 3.4**.

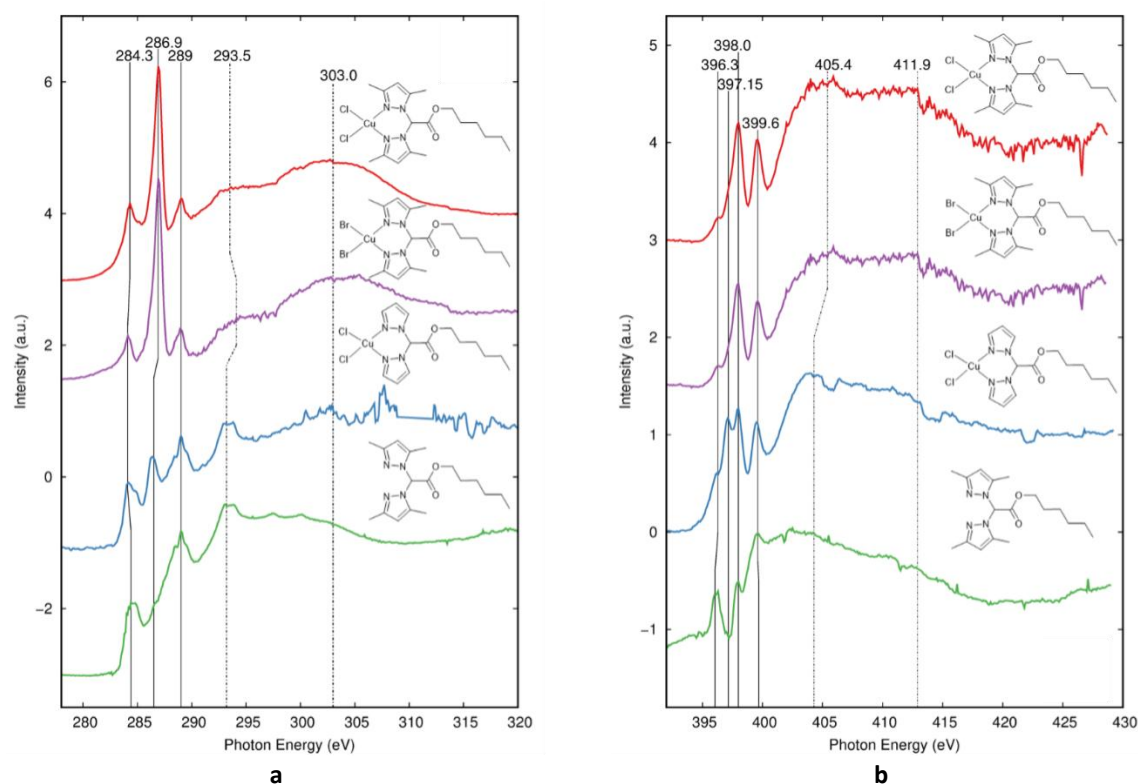


Figure 3.10. - C K-edge (a) and N K-edge (b) NEXAFS spectra of samples **9**, **43**, **45** and **46**.

The spectra of the three coordination compounds (particularly **45** and **46**) appear very similar, therefore they will be discussed together. For the C K-edge spectra the energy scale is referenced to the $\pi^*_{C=O}$ transition at 289 eV^[131] while for the N K-edge spectra to the π^*_1 transition at 398 eV. In the C K-edge spectra, the features observed agree with the expected

peaks reported in **Table 3.4.**: below the edge C1s→ π^* transitions originating respectively from C=C carbons and C=N carbons of the pyrazole rings ($\pi^*_{C=C}$ at 284.1 eV for **45** and **46** and at 284.3 eV for **43** and **9**, $\pi^*_{C=C}$ at 286.9 eV for **43** and **45** and 286.5 eV for **46** and **9**) and from the O-C=O carbon of the ester function ($\pi^*_{C=O}$ at 289 eV).^[132,133] Above the edge, two large features are related to C1s→ σ^* transitions of the alkyl side chains (σ^*_{C-C}) and of the pyrazole rings ($\sigma^*_{C=N}$).

	9	43	45	46	Assignment
C K-edge	284.3	284.3	284.1	284.1	$\pi^*_{C=C}$
	286.5	286.9	286.9	286.5	$\pi^*_{C=N}$
	289.0	289.0	289.0	289.0	$\pi^*_{C=O}$
	293.2	293.5	294.1	293.2	σ^*_{C-C}
	303.0	303.0	303.0	303.0	$\sigma^*_{C=N}$
N K-edge	398.0	398.0	398.0	398.0	π^*_1
	399.6	399.6	399.6	399.6	π^*_2
	-	405.4	405.4	404.3	$\sigma^*_{C=N}$
	-	411.9	411.9	411.9	σ^*_{C-N}

Table 3.4. - Peak position (eV) and relative assignment of the main features appearing in the C and N K-edge NEXAFS spectra of samples **9**, **43**, **45** and **46**.

The features detected in the N K-edge NEXAFS spectra are mainly related to the pyrazole rings: below the edge a shoulder at 396.3 eV is observed, then two different N1s→ π^* transitions (π^*_1 at 398 eV and π^*_2 at 399.6 eV) arising by two non-equivalent nitrogen atoms appear in the spectra, coherently with literature data reported for similar heterocyclic systems. Above the edge, the two broad bands can be ascribed to $\sigma^*_{C=N}$ and σ^*_{C-N} resonances while the first two peaks appearing in **Figure 3.10.** and not mentioned in **Table 3.4.** correspond to impurities already observed in the literature.^[134,135] The presence of all the expected signals in both C and N K-edges spectra confirms the stability of the ligands molecular structure after the coordination compounds formation.

XAS measurements were carried out at Cu K-edge on complexes **43** and **45**. The analysis was carried out in the near edge (XANES) and extended (EXAFS) regions to achieve reliable and deep understanding about the average Cu local atomic structure and coordination chemistry. The analysis of the XANES features provides information about the average oxidation state of the absorber (Cu ion) and the local ligands geometry around it.

In **Figure 3.11.** the normalized Cu K-edge XANES spectra of complexes **43** and **45** were reported and similar features can be observed. Accordingly to the literature^[136-138] the main edge energy, the weak pre-edge peak at low energy and the pre-edge shoulder confirm the Cu(II) oxidation state, in agreement with XPS data analysis results. Comparing the experimental

XANES spectra of **43** and **45** complexes with literature^[139] XANES of Cu(II) sites having different local coordination chemistry, it results a close similarity between our data and those of Cu-glycine complex, suggesting for **43** and **45** data a roughly planar geometry. Noticeably, although all the Cu-compounds present very similar features, looking at **Figure 3.11.(a)** differences are quite evident: the pre-edge shoulder of **43** and the first peak of the edge appear less pronounced compared to **45**. To understand the origin of these differences in samples **45** and **43**, the *ab initio* XANES spectra of a simple model for the Cu local environment have been calculated using the FEFF 8.2^[140] program. The model was a Cu absorber coordinated to 2 Cl and 2 N atoms in a square planar configuration. Then the Cl atom pair was rotated out of the structure evolving from the planar toward a tetragonal geometry. The behavior of the XANES spectra as a function of the angle Cl-pair (5 deg. steps) is reported in **Figure 3.11.(b)** and it reveals an interesting behavior: as the two Cl atoms progressively tilt out of the plane Cu-N₂, the main white line peak broadens and decreases shifting toward high energies. At the same time the pre-edge shoulder becomes less pronounced and weaker. This behavior suggests a square planar coordination geometry for **43** and a tilted structure for **45**. Such a different behavior is likely due to the methyl groups bounded to the pyrazole rings that, when they are present as in complex **45**, induce a steric distortion of the Cu coordination geometry allocated tilting the Cl atoms out of the square planar geometry.

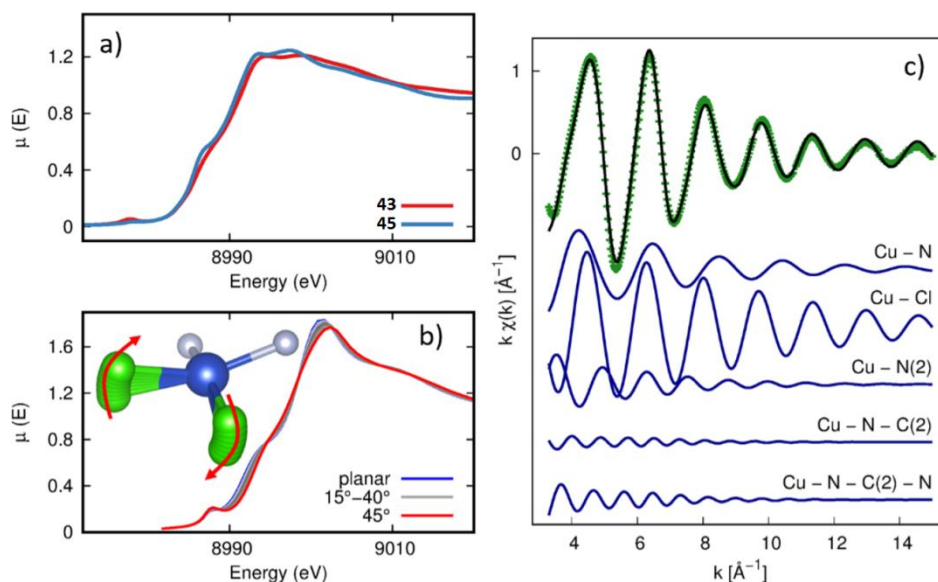


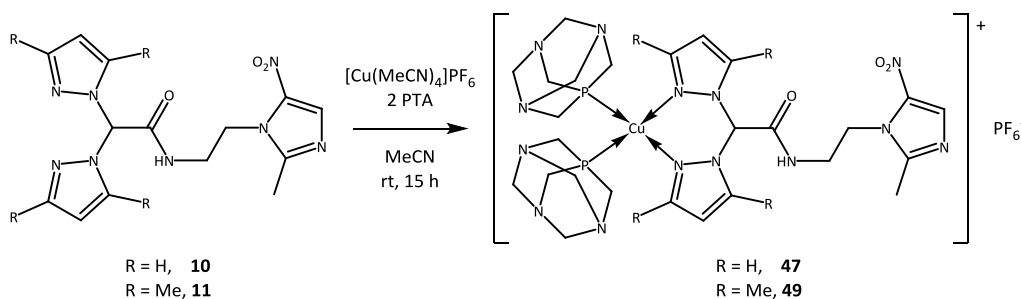
Figure 3.11. - a) Comparison of the Cu K-edge XANES spectra of complexes **43** (red) and **45** (blue); b) evolution of the XANES spectral features in CuCl₂N₂ model molecule as a function of distortions from a square planar geometry (see text); c) results of the quantitative EXAFS analysis in k space for complex **43**: k² weighed k²χ(k) experimental data (green dots) and the best fit curve (black line) are presented. The k² weighed partial contributions χ_ith are presented vertically shifted for sake of clarity.

The EXAFS analysis provides further details about the local atomic structure around Cu in complexes and can be used to validate the coordination model after the synthesis procedure in case of complex molecules. The raw k^2 spectra were fitted in the k-space (3-15 \AA^{-1} range) and the results of the fit in k-space are reported in **Figure 3.11.(c)** together with the partial contributions included in the fit. The first shell was made by the single scattering (SS) contribution of the 2 Cl and 2 N bonded to the central Cu, the second shell comes from the bond with the Cu-N(2) where N(2) is the furthest N atom in the pyrazole ring and the last two contributions are associated to the SS and multiple scattering (MS) to C(2) (furthest C atoms in the pyrazole ring) atoms through N which results relevant due to the almost aligned configuration. The quantitative investigation of the EXAFS region allowed to explore the nearest shells around Cu confirming that the Cu-complexes coordination took place accordingly to what expected from the synthesis procedure.

3.2.3. Syntheses of complexes bearing bioconjugated ligands

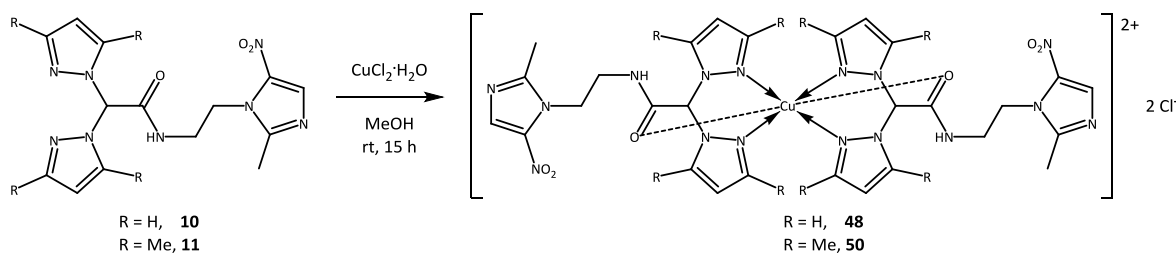
The Cu(I) complexes $[(\text{PTA})_2\text{Cu}(\text{L}^{1\text{MN}})]\text{PF}_6$ (**47**) and $[(\text{PTA})_2\text{Cu}(\text{L}^{2\text{MN}})]\text{PF}_6$ (**49**) were synthesized using the acceptor $[\text{Cu}(\text{MeCN})_4]\text{PF}_6$, the phosphane coligand PTA and the ligands $\text{L}^{1\text{MN}}$ (**10**) and $\text{L}^{2\text{MN}}$ (**11**), respectively, as starting materials, according to the procedure reported in **Scheme 3.23**. The FT-IR spectra showed all the expected bands for the presence of the scorpionate and phosphane donors: broad peaks at 3453 and 3398 cm^{-1} , respectively, attributable to the N-H stretching, broad absorptions at 1695 and 1673 cm^{-1} , respectively, due to the carbonylic asymmetric stretching, slightly shifted with respect to the same absorptions observed in the spectra of the free ligands. Symmetric vibrations of the C-nitro group in nitroimidazole are observed in the range 1363-1365 cm^{-1} , while the symmetric ones together with ring "breathing" vibrations are detectable in the 1524-1532 cm^{-1} region. The $^1\text{H-NMR}$ spectra of **47** and **49**, recorded in D_2O solution, showed that copper coordination induces a slight downfield shift of the PTA methylene protons with respect to the chemical shift observed in uncoordinated ligands and generally determines signals broadening and/or loss of multiplicity. In addition, the relative integrations of azolyl protons and phosphane methylene protons support the "1 + 1 + 2"-type coordination mode. Moreover, the presence of unique azolyl proton signals in the spectra of both complexes indicates the magnetic equivalence of the two rings. $^{31}\text{P-NMR}$ spectra of **47** and **49**, recorded both in CD_3OD and in D_2O solution showed, along with the characteristic heptet centered at about -144 ppm due to the PF_6 counteranion, a broad singlet generally downfield shifted compared to the signal exhibited by the uncoordinated PTA (-97.70

ppm in D₂O). The presence of a unique signal in the spectra of **47** and **49** indicated the magnetic equivalence of the two phosphanes, confirming the evidence arising from proton spectra. The ESI-MS(+) spectra of complexes **47** and **49** displayed peaks attributable to the protonated phosphane ([PTA + H]⁺, *m/z* 158) and scorpionate ligands [L^{1MN} + H]⁺ and [L^{2MN} + H]⁺ at *m/z* 345 and 401, respectively. More interestingly, the ESI-MS(+) data confirmed the existence of the complexes **47** and **49** under ESI conditions. In addition, the spectrum of **49** displayed two copper containing peaks at *m/z* 463 ([Cu(L^{2MN})]⁺) and 620 ([(PTA)Cu(L^{2MN})]⁺). In the ESI-MS(-) spectra of compounds **47** and **49**, the main peak attributable to the [PF₆]⁻ species is observed at *m/z* 145, along with minor peaks due to the fragments [L^{1MN} - H]⁻ and [L^{2MN} - H]⁻ at *m/z* 343 and 399, respectively.



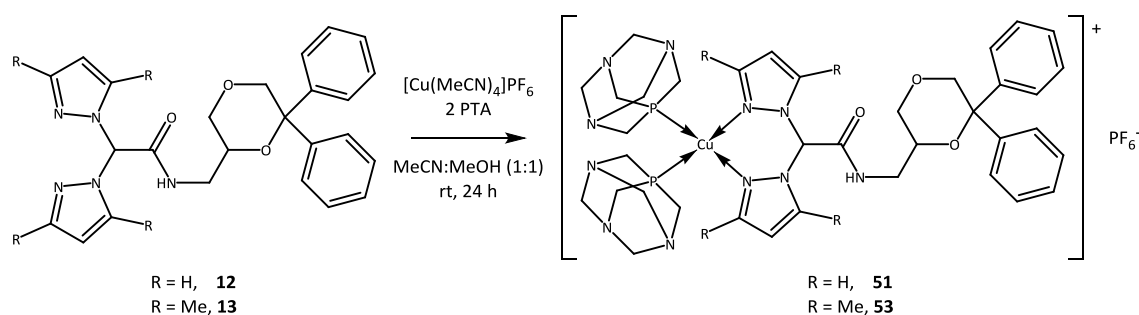
Scheme 3.23. - Synthesis of complexes **47** and **49**.

The Cu(II) complexes [Cu(L^{1MN})₂]Cl₂ (**48**) and [Cu(L^{2MN})₂]Cl₂ (**50**) were synthesized using the acceptor CuCl₂·H₂O and the ligands L^{1MN} (**10**) and L^{2MN} (**11**), respectively, as starting materials, according to the procedure reported in **Scheme 3.24**. The FT-IR spectra of **48** and **50** showed all the expected bands for the complexes, in particular absorptions at 1668 and 1665 cm⁻¹, respectively, due to the carbonylic asymmetric stretching, slightly shifted with respect to the same absorptions observed for the free ligands. The ESI-MS study was performed solubilizing complexes **48** and **50** in MeOH. The ESI-MS(+) spectra showed copper-containing fragments at *m/z* 406 and 863, attributable to the [Cu(L^{1MN} - H)]⁺ and [(L^{2MN})Cu(L^{2MN} - H)]⁺ species, respectively.



Scheme 3.24. - Synthesis of complexes **48** and **50**.

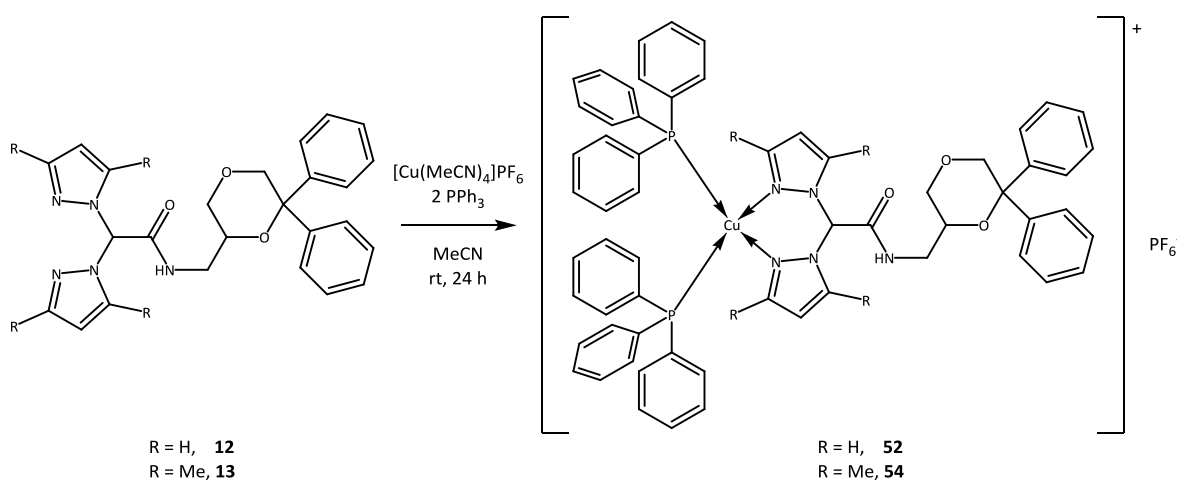
The Cu(I) complexes $[(\text{PTA})_2\text{Cu}(\text{L}^{1\text{NMDA}})]\text{PF}_6$ (**51**) and $[(\text{PTA})_2\text{Cu}(\text{L}^{2\text{NMDA}})]\text{PF}_6$ (**53**) were synthesized using the acceptor $[\text{Cu}(\text{MeCN})_4]\text{PF}_6$, the phosphane coligand PTA and the ligands $\text{L}^{1\text{NMDA}}$ (**12**) and $\text{L}^{2\text{NMDA}}$ (**13**), respectively, as starting materials, according to the procedure reported in **Scheme 3.25**. The FT-IR spectra showed all the expected bands for the complexes, in particular the absorptions due to the asymmetric stretching of the C=O groups are detected at 1696 and 1699 cm^{-1} , with no significant variations with respect to the related absorptions detectable in the spectra of the uncoordinated ligands (1682 cm^{-1} for **12** and 1702 cm^{-1} for **13**), indicating that the carbonyl is not involved in the coordination to the metal center. The $^1\text{H-NMR}$ spectra of **51** and **53**, recorded both in $\text{DMSO-}d_6$ and in CDCl_3 solution, showed all the expected signals attributable to the ligands and the coligands. The phosphanes showed a characteristic series of signals and an integration of the peaks, with respect to the resonances of the ligand, which confirmed the 1:2 stoichiometric ratio between the ligand and the PTA. The $^{31}\text{P-NMR}$ spectra of **51** and **53**, recorded in CD_3CN solution, showed the characteristic heptet due to the counterion PF_6^- and singlets at -91.63 and -89.00 ppm, respectively, due to the coordinated phosphanes, shifted with respect to the signal exhibited by the free PTA (-102.07 ppm in CD_3CN) and in accordance with the presence of two PTA coligands in the metal coordination core. The ESI-MS study was performed solubilizing complexes **51** and **53** in MeCN. The ESI-MS(+) spectra showed the peaks of the copper-containing fragments at m/z 663 and 719, attributable to the $[(\text{PTA})\text{Cu}(\text{L}^{1\text{NMDA}})]^+$ and $[(\text{PTA})\text{Cu}(\text{L}^{2\text{NMDA}})]^+$ species, respectively, diagnostic about the formation of the complexes. The ESI-MS(-) spectra of the compounds showed the peak of the counterion $[\text{PF}_6]^-$ at m/z 145 as main peak.



Scheme 3.25. - Synthesis of complexes **51** and **53**.

The Cu(I) complexes $[(\text{PPh}_3)_2\text{Cu}(\text{L}^{1\text{NMDA}})]\text{PF}_6$ (**52**) and $[(\text{PPh}_3)_2\text{Cu}(\text{L}^{2\text{NMDA}})]\text{PF}_6$ (**54**) were synthesized using the acceptor $[\text{Cu}(\text{MeCN})_4]\text{PF}_6$, the phosphane coligand PPh_3 and the ligands $\text{L}^{1\text{NMDA}}$ (**12**) and $\text{L}^{2\text{NMDA}}$ (**13**), respectively, as starting materials, according to the procedure reported in **Scheme 3.26**. The FT-IR spectra showed all the expected bands for the complexes,

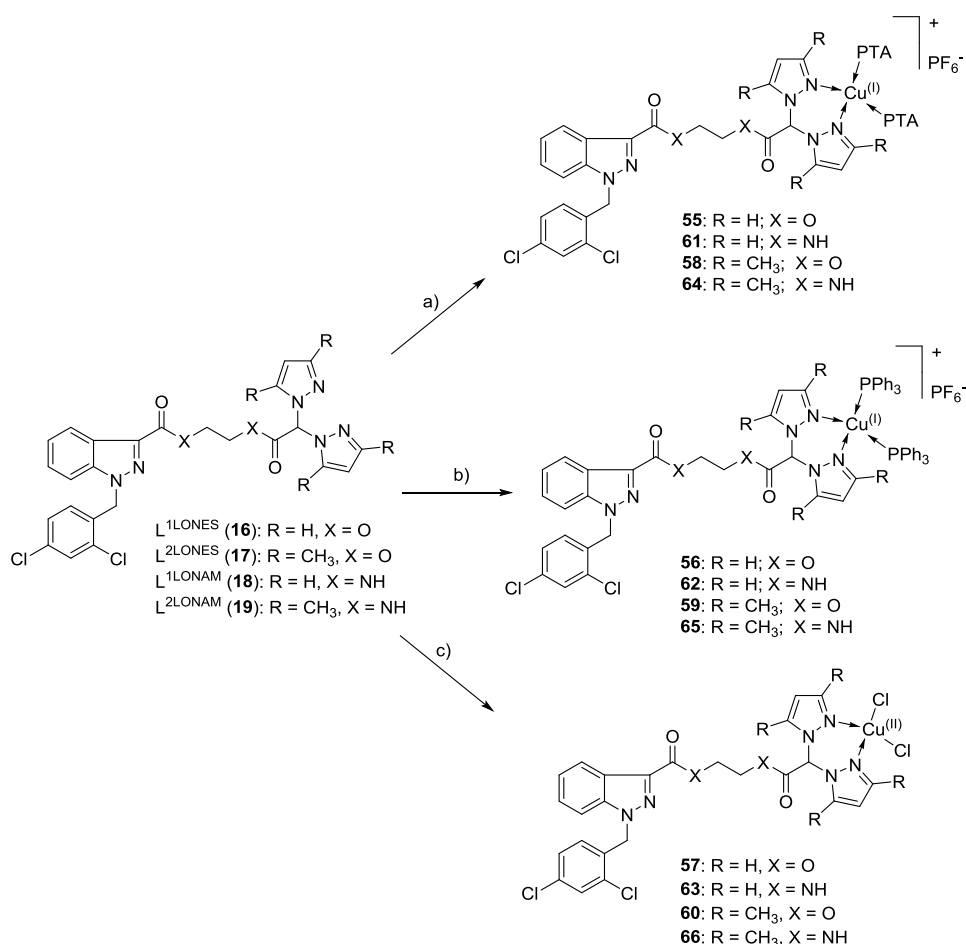
in particular the absorptions due to the asymmetric stretching of the C=O groups are detected at 1681 and 1674 cm^{-1} , slightly shifted at lower frequencies with respect to the uncoordinated ligands (1682 cm^{-1} for **12** and 1702 cm^{-1} for **13**). The $^1\text{H-NMR}$ spectra of **52** and **54**, recorded in CDCl_3 solution, showed all the expected signals attributable to the ligands and the coligands, with a slight shift of the frequencies due to the coordination to the metal center. Interestingly, in the $^1\text{H-NMR}$ spectrum of **54** a double set of resonances appears for the pyrazoles, indicating that the rings are not equivalent, while in the spectrum of **52** is present only one set of resonances. The phosphanes showed a characteristic series of signals in the aromatic region and an integration of the peaks, with respect to the resonances of the ligand, which confirmed the 1:2 stoichiometric ratio between the ligand and the PPh_3 . Finally, a significant shift to higher frequencies of the NH signal at 8.17 ppm, for compound **52**, was probably due to a secondary interaction between the hydrogen and the metal center. The $^{31}\text{P-NMR}$ spectra of **52** and **54**, recorded in CDCl_3 solution, showed the characteristic heptet due to the PF_6^- counterion and singlets at 0.25 and -3.85 ppm, respectively, due to the coordinated phosphanes, shifted with respect to the signal exhibited by the free PPh_3 (-5.36 ppm in CDCl_3) and in accordance with the presence of two PPh_3 coligands in the metal coordination core. The ESI-MS study was performed solubilizing complexes **52** and **54** in MeOH and MeCN, respectively. The ESI-MS(+) spectra showed the peaks of the copper-containing fragments at m/z 768 and 824, attributable to the $[(\text{PPh}_3)\text{Cu}(\text{L}^{1\text{NMDA}})]^+$ and $[(\text{PPh}_3)_2\text{Cu}(\text{L}^{2\text{NMDA}})]^+$ species, respectively, diagnostic about the formation of the complexes. The ESI-MS(-) spectra of the compounds showed the peak of the counterion $[\text{PF}_6]^-$ at m/z 145 as main peak.



Scheme 3.26. - Synthesis of complexes **52** and **54**.

The Cu(I) complexes $[(\text{PTA})_2\text{Cu}(\text{L}^{1\text{LONES}})]\text{PF}_6$ (**55**), $[(\text{PTA})_2\text{Cu}(\text{L}^{2\text{LONES}})]\text{PF}_6$ (**58**), $[(\text{PTA})_2\text{Cu}(\text{L}^{1\text{LONAM}})]\text{PF}_6$ (**61**) and $[(\text{PTA})_2\text{Cu}(\text{L}^{2\text{LONAM}})]\text{PF}_6$ (**64**) were synthesized using the acceptor

$[\text{Cu}(\text{MeCN})_4]\text{PF}_6$, the phosphane coligand PTA and the ligands $\text{L}^{1\text{LONES}}$ (**16**), $\text{L}^{2\text{LONES}}$ (**17**), $\text{L}^{1\text{LONAM}}$ (**18**) and $\text{L}^{2\text{LONAM}}$ (**19**), respectively, as starting materials, according to the procedure reported in **Scheme 3.27**. Analogously, the Cu(I) complexes $[(\text{PPh}_3)_2\text{Cu}(\text{L}^{1\text{LONES}})]\text{PF}_6$ (**56**), $[(\text{PPh}_3)_2\text{Cu}(\text{L}^{2\text{LONES}})]\text{PF}_6$ (**59**), $[(\text{PPh}_3)_2\text{Cu}(\text{L}^{1\text{LONAM}})]\text{PF}_6$ (**62**) and $[(\text{PPh}_3)_2\text{Cu}(\text{L}^{2\text{LONAM}})]\text{PF}_6$ (**65**) were synthesized using the same starting materials, but employing PPh_3 as phosphane, according to the procedure reported in **Scheme 3.27**.



Scheme 3.27. - Synthesis of complexes **55-66**. Reagents and conditions: **a)** PTA, $[\text{Cu}(\text{MeCN})_4]\text{PF}_6$, MeCN, overnight; **b)** PPh_3 , $[\text{Cu}(\text{MeCN})_4]\text{PF}_6$, MeCN, overnight; **c)** $\text{CuCl}_2 \cdot 2\text{H}_2\text{O}$, MeCN, 24 h.

The FT-IR spectra showed all the expected bands for the complexes. The absorptions due to the asymmetric stretching of the C=O of the ester groups for complexes **55**, **56**, **58** and **59** showed no significant variations with respect to the same absorptions of the carbonyl groups detectable in the spectra of the free ligands, while the absorptions due to the C=O of the amide groups for **61**, **62**, **64** and **65** are slightly shifted at lower frequencies with respect to those of the uncoordinated ligands. The $^1\text{H-NMR}$ spectra of the Cu(I) complexes, recorded in $\text{DMSO-}d_6$ solution, showed a single set of resonances for the pyrazoles, indicating that the rings are equivalents, with a slight shift due to the coordination to the metal center. A significant shift to

higher frequencies of the *NH* signals is detected only for compounds **64** (8.43 and 9.07 ppm) and **65** (8.38 and 9.35 ppm), probably due to a secondary interaction between the hydrogen atoms and the copper center. The PTA and PPh₃ coligands showed a characteristic series of signals at 4.04-4.73 and 7.20-7.80 ppm, respectively, with an integration, with respect to the resonances of the ligands, which confirmed the 1:2 stoichiometric ratio between the ligand and the phosphane coligands. The ³¹P-NMR spectra of the Cu(I) complexes, recorded in DMSO-*d*₆ and CD₃CN solution, showed the characteristic heptet due to the PF₆⁻ counterion and the singlet, due to the coordinated phosphanes, shifted with respect to the signal exhibited by the free phosphanes. The ESI-MS study was performed solubilizing the Cu(I) complexes in MeCN. The spectra confirmed the formation of the PTA and PPh₃ complexes and, in all the ESI-MS(-) spectra, the peak of the counterion [PF₆]⁻ at *m/z* 145 was present as main peak.

The Cu(II) complexes [Cu(L^{1LONES})]Cl₂ (**57**), [Cu(L^{2LONES})]Cl₂ (**60**), [Cu(L^{1LONAM})]Cl₂ (**63**) and [Cu(L^{2LONAM})]Cl₂ (**66**) were synthesized using the acceptor CuCl₂·2H₂O and the ligands L^{1LONES} (**16**), L^{2LONES} (**17**), L^{1LONAM} (**18**) and L^{2LONAM} (**19**), respectively, as starting materials, according to the procedure reported in **Scheme 3.27**. The FT-IR spectra showed all the expected bands for the complexes. The strong absorptions due to the asymmetric stretching of the C=O of the ester and amide groups showed no significant variations with respect to the same absorptions of the carbonyl groups detectable in the spectra of the free ligands. These data indicate that the carbonyl groups are not involved in the coordination of the metal: the copper center results in a tetracoordinated environment with the ligand chelating in a bidentate fashion and the other two positions being occupied by the chlorides. The ESI-MS study was performed solubilizing the Cu(II) complexes in MeCN. The recorded spectra confirmed the formation of the complexes and, in all the ESI-MS(-) spectra, the peak of the counterion [CuCl₃]⁻ is present at *m/z* 170.

Due to unsuccessful efforts in attempts to crystallize the compounds **55-66** to obtain crystals suitable for the SC-XRD, it has been chosen to exploit the X-ray Photoelectron Spectroscopy (XPS) and X-ray Absorption Fine Structure (XAFS) spectroscopy (in the near edge and in the extended regions) to achieve details about the electronic states (C, N, O, Cu) and the local coordination geometry in the complexes.

The electronic and molecular structures of coordination compounds **63**, **65** and **66**, in comparison with the ligand **19**, were probed by Synchrotron Radiation-induced X-ray Photoelectron Spectroscopy (SR-XPS). SR-XPS spectra were collected at C1s, N1s, O1s, Cl2p, P2p (for **65**), F1s (for **65**) and Cu2p core levels and the data analysis results (Binding Energy (BE), Full

Width Half Maximum (FWHM) and assignments) confirmed the proposed molecular structures for the complexes and the stability of the ligand **19** molecular structure upon coordination to copper. In the following, the most interesting signals are described and compared for the three analysed samples, considered representative of Cu(I) and Cu(II) coordination compounds. The C1s signal can always be resolved by curve fitting analysis into several components corresponding to the different C atoms in the proposed molecular structure. More in detail, in order of increasing BE, the contributions are assigned as follows: aromatic and aliphatic C-C carbons (BE = 284.7 eV), C-N carbons of the pyrazole-like rings (BE = 286.6 eV), C=O carbonyls of amide groups and imine-like C=N groups (BE = 288.0 eV), -COOH impurities, always found on the surface of samples deposited in air (BE = 289.3 eV) and C-Cl groups (BE = 291.5 eV). C1s spectra of ligand **19** and complexes **63** and **65** are reported in **Figure 3.12.A-C**.

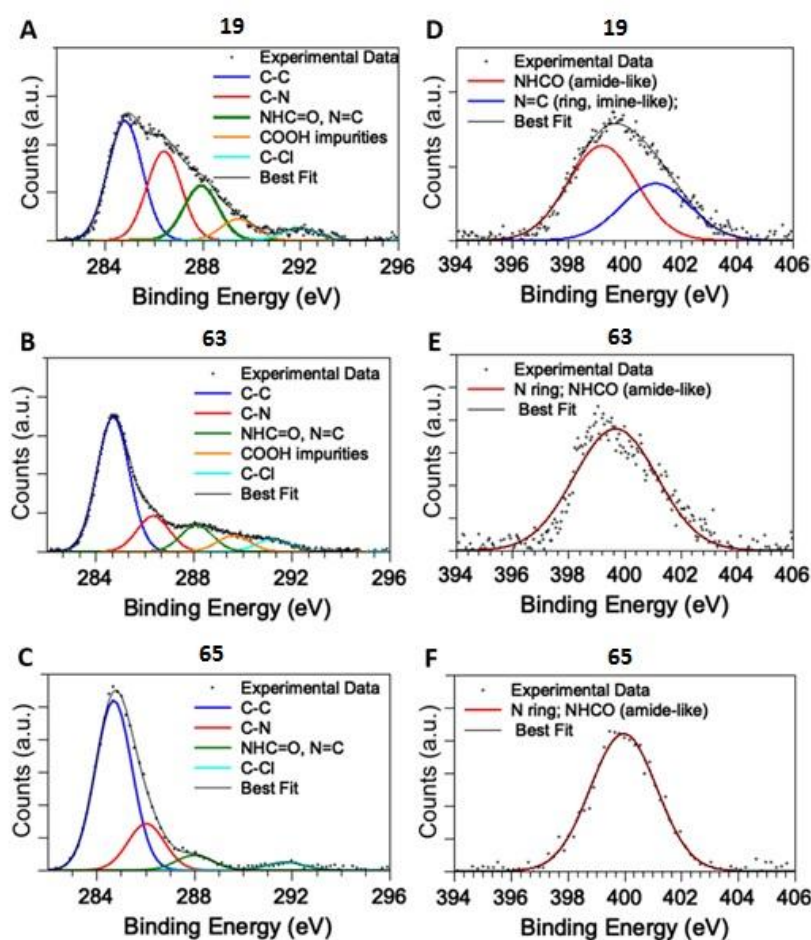


Figure 3.12. - **A)** C1s spectrum of ligand **19**; **B)** C1s spectrum of Cu(II) complex **63**; **C)** C1s spectrum of Cu(I) complex **65**; **D)** N1s spectrum of ligand **19**; **E)** N1s spectrum of Cu(II) complex **63**; **F)** N1s spectrum of Cu(I) complex **65**.

N1s spectra of the ligand **19** and complexes **63** and **65** are reported in **Figure 3.12.D** and **3.12.F**, respectively. For **19** a couple of main signals can be detected at 399.5 eV and 401.0 eV BE, indicative for the two kinds of nitrogens of the pyrazole rings, i.e. amine-like and imine-like,

respectively.^[141] Amide-like N atoms are found at a BE value very close to the amine-like and cannot be resolved due to the experimental resolution (0.6 eV). As for the coordination compounds, it is expected that only the amine-like contribution appears when the two nitrogen atoms coordinate a metal ion, as reported in the literature for heterocycles coordinating metal ions (for example porphyrins or phthalocyanines).^[127,128] In excellent agreement with this prediction, in complexes **63**, **65** (**Figure 3.12.E** and **3.12.F**, respectively) and **66** a single N1s component at about 400.0 eV, attributed to the symmetrized nitrogen atoms coordinating copper ions (and to the indistinguishable amide-like N) can be observed. Cl2p BE values observed for both ligand **19** and the three coordination compounds **63**, **65** and **66** (Cl2p_{3/2} BE = 200 eV) are compatible with chlorine atoms covalently bonded to carbon in organic molecules. In addition, in Cl2p spectra of **63** and **66** a contribution of slightly higher intensity at lower BE (198 eV BE) can be observed, as expected for chlorine atoms bonded to Cu(II) ions in the coordination compounds.^[130] Cu2p spectra collected for complexes **63** and **66** show a spin-orbit pair with the Cu2p_{3/2} component centered at 936 eV, indicative for Cu(II) ions in coordination compounds, in excellent agreement with analogous systems. On the other hand, Cu2p spectrum collected on complex **65** has the Cu2p_{3/2} spin-orbit component centered at 932.0 eV BE, as expected for Cu(I) ions in coordination compounds.

Near Edge X-ray Absorption Fine Structure (NEXAFS) spectroscopy measurements were carried out at C and N K-edges on the ligand **19** and on the coordination compounds **63** and **66**, with the aim to obtain further information about the influence of the metal coordination on the electronic structure of the ligand. Experimental spectra of the C K-edge and N K-edge of **19**, **63** and **66** samples are reported in **Figure 3.13**. They were collected at grazing incidence of the polarized photon beam with respect to the sample surface: no angular dependence was observed on the NEXAFS spectra of the investigated compounds when the incidence angle of the impinging radiation was changed from grazing to magic and normal, indicating the absence of preferential orientation of the investigated molecules on the sample surface. Peak positions and assignments of the main features detected in the C and N K-edge spectra of the analysed samples are shown in **Table 3.5**. For the C K-edge spectra, the energy scale is referenced to the $\pi_{\text{C=O}}^*$ transition of the amide function in the side chain of Ionidamine, while for the N K-edge spectra to the π_2^* transition of the pyrazole ring.^[132] The C K-edge spectra present the expected $\pi_{\text{C=C}}^*$ and $\pi_{\text{C=N}}^*$ features of the pyrazole ring and the $\pi_{\text{C=O}}^*$ feature related to the amide group at 288.4 eV. It can be noticed (**Table 3.5**.) that the first two peaks lie at lower energy in **19** and that the $\pi_{\text{C=C}}^*$ peak results attenuated in Cu-complexes **63** and **66** with respect to ligand **19**.

These effects could be related to the Cu-complexation of the pyrazole nitrogens. All the samples exhibit a $\sigma_{\text{C-H}}^*$ resonance originated by the presence of the aliphatic chains. Above the edge the two large features $\sigma_{\text{C-C}}^*$ and $\sigma_{\text{C=N}}^*$ can be observed. The N K-edge spectra show the $\text{N}1s \rightarrow \pi^*$ transitions (π_1^* and π_2^*) coming from two distinct nitrogen atoms. As shown in **Table 3.5.**, the energy of the π_1^* peak is higher for Cu complexes **63** and **66** than for the ligand **19**: this effect might be further evidence of the complexation with copper.

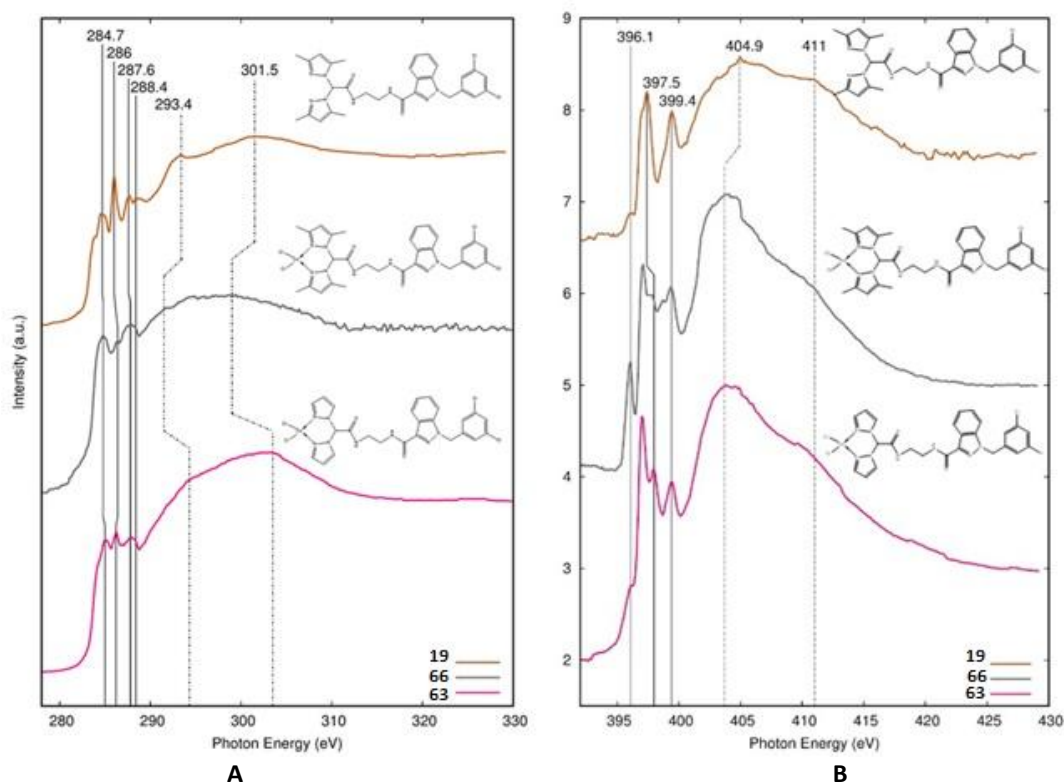


Figure 3.13. - C K-edge (A) and N K-edge (B) NEXAFS spectra of ligand **19** and Cu(II) complexes **63** and **66**.

	19	63	66	Assignment
C K-edge	284.7	285.1	284.8	$\pi_{\text{C=C}}^*$
	286.0	286.2	286.4	$\pi_{\text{C=N}}^*$
	287.6	287.8	287.8	$\sigma_{\text{C-H}}^*$
	288.4	288.4	288.4	$\pi_{\text{C=O}}^*$
	293.4	294.3	291.5	$\sigma_{\text{C-C}}^*$
	301.5	303.5	299.0	$\sigma_{\text{C=N}}^*$
N K-edge	396.1	396.1	396.1	
	397.5	397.9	397.9	π_1^*
	399.4	399.4	399.4	π_2^*
	404.9	403.7	403.7	$\sigma_{\text{C=N}}^*$
	411.0	411.0	411.0	$\sigma_{\text{C-N}}^*$

Table 3.5. - Peak position (eV) and relative assignment of the main features appearing in the C and N K-edge NEXAFS spectra of samples **19**, **63** and **66**.

X-ray absorption data collected at the Cu K-edge on complexes **63**, **65** and **66** were analysed in the near edge (XANES) and extended (EXAFS) regions with the aim of understanding the local coordination chemistry and electronic structure around Cu. The Cu K-edge normalized XANES spectra measured on **63**, **65** and **66** complexes are presented in **Figure 3.14**. together with those measured on reference compounds, for sake of comparison. The edge energy of complex **65** matches the edge energy measured on pure Cu₂O reference compound, while the edge energies of complexes **63** and **66** match the edge energy of pure CuO reference compound and this confirms the Cu(I) oxidation state in complex **65** and the Cu(II) one in complexes **63** and **66**. A roughly planar geometry could be assumed for sample **63** due to the close similarity with the XANES of glycine complex reported in literature.^[139] The XANES spectrum measured from complex **66** (**Figure 3.14**.) depicts a raising of the white line (around 8995 eV) with respect to complex **63** and an attenuation of the pre-edge shoulder, this behaviour being compatible with the Cu coordination geometry changing from square planar in complex **63** to nearly octahedral in complex **66**. The Cu XANES features measured on complex **65** are closely similar to those of Cu₂O reference compound and the pronounced pre-edge peak suggests tetrahedral-like coordination geometry in complex **65**. The squeezing of the structural oscillations in the XANES region, with respect to the Cu₂O spectrum, suggests averagely longer neighbour distances in complex **65**. The analysis of the extended region of the spectra allows to strength this hypothesis. The Cu K-edge XANES spectrum measured for complex **65** appears low energy shifted, accordingly to the Cu(I) oxidation state (**Figure 3.14**.).

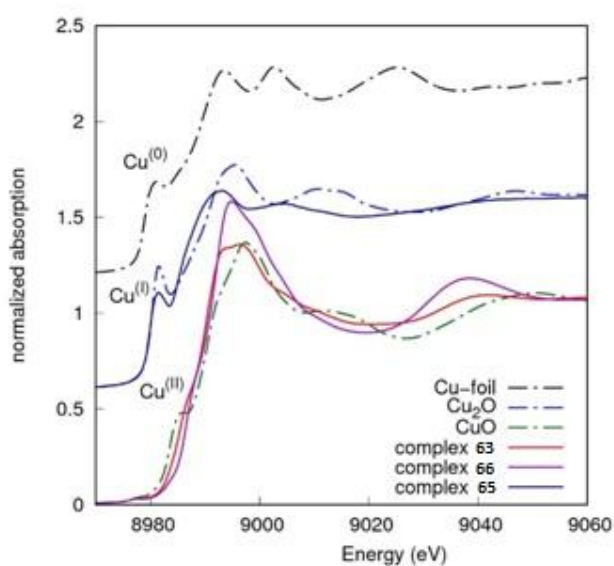


Figure 3.14. - Cu K-edge normalized XANES spectra measured on complexes and reference compounds, shifted for shake of clarity. Edge energies of the Cu(II) complexes **63** and **66** match the edge energy of CuO reference compound. The edge energy of Cu(I) complex **65** matches the edge energy of Cu₂O.

Looking at the k^2 -weighted EXAFS signal in k-space and at its Fourier Transform (FT) in the real space, remarkable differences are evident among the samples (**Figure 3.15.**). In particular, looking at the complexes **63** and **66**, the $k^2_\chi(k)$ signal presents a prominent first oscillation in sample **66**, while in sample **63** two oscillations of equal and lower intensity are visible. Moreover, from the first oscillation onwards the signals become partially out of phase. Such a different behaviour corresponds to differences in the real space for the FT spectra. Noticeably, the modulus and imaginary part of the FT depict very similar shapes (**Figure 3.15.**, dashed lines) except around 2 Å (**Figure 3.15.**, red arrow), where a lack of structural signal is found in the sample **66** data with respect to sample **63**. This behaviour may point out some antiphase structural signal coming from a different neighbour arrangement around Cu in the two complexes. Noticeably, complex **66** has two CH₃ substituents that may provide such an additional coordination shell, in agreement with the XANES features suggesting the nearly octahedral coordination. Moreover, such different coordination seems to promote greater rigidity of the structure providing larger next neighbour signals in the next neighbour region (highlighted by dashed lines in **Figure 3.15.B**). Looking at the $k^2_\chi(k)$ signal of complex **65**, it is evident that the local structure around Cu(I) is definitively more disordered than those of Cu(II) complexes with the weaker next neighbour shells. The EXAFS data analysis was carried out using the atomic coordinates of the two residues as starting point for the data refinement that was carried out fitting the k^2 weighted structural signal $k^2_\chi(k)$ in the k-space (without Fourier Filtering) in the 3-15 Å⁻¹ k-range. The appropriate single (SS) and multiple (MS) scattering paths were selected on the basis of their amplitude and statistical significance,^[142] grouping in a single contribution those paths with similar geometry and composition. To reduce the correlation among the parameters the path multiplicity numbers were constrained to the molecular structure (**Table 3.6.**). The experimental data, best fit and examples of the used paths are presented in **Figure 3.15**. The differences among the spectra of the three samples (**Figure 3.15.A**) can be understood in a more intuitive way looking at the FT moduli |FT| (**Figure 3.15.B**): the complex **63** data present a major main peak around 1.5 Å (uncorrected for the phase shift), originating from 2 N at around 2 Å and 2 Cl at around 2.2 Å. In the next neighbour region the two main |FT| features at around 2.5 Å and 3.5 Å (uncorrected for the phase shift) are ascribed, one to N(2) and C neighbours from the pyrazole rings (around 3 Å), the other to the SS and MS paths to the C(2) atoms. These MS contributions are relevant due to the almost aligned configurations Cu-N-C(2), Cu-N(2)-C(2) and Cu-C-C(2).^[143] In complex **63**, R is a hydrogen

atom, which is expected to provide a negligible EXAFS signal. On the contrary, the carbon atoms of CH₃ groups of complex **66** are expected to provide a sizable signal.

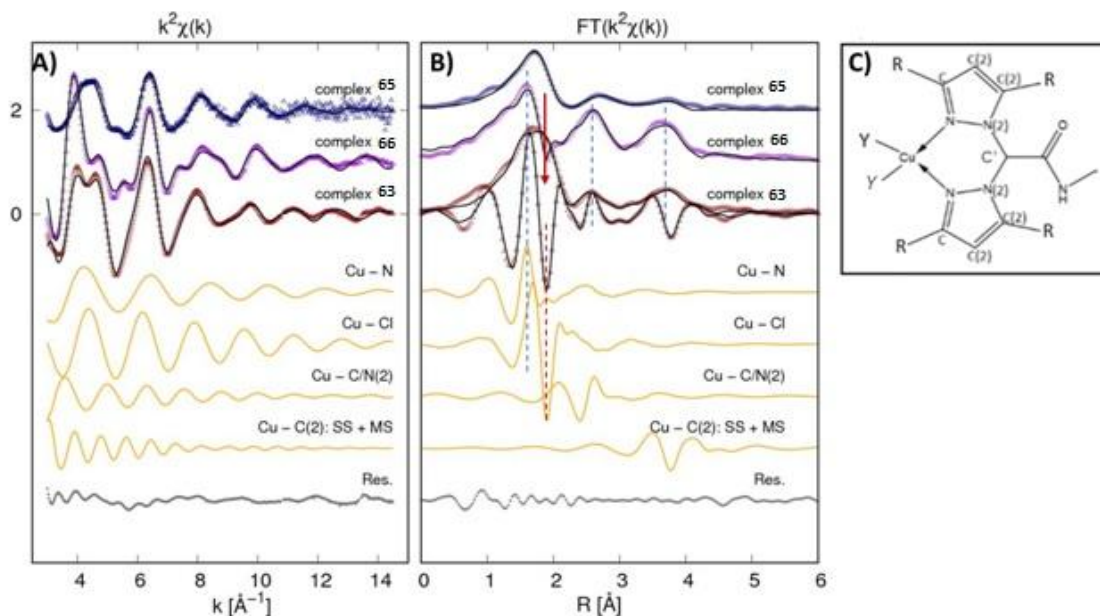


Figure 3.15. - In **A**) Cu K-edge EXAFS data analysis on complexes **63**, **65** and **66** are reported. At the top the experimental $k^2_{\text{exp}}(k)$ (dots) and best fit curves $k^2_{\text{fit}}(k)$ (black lines) are presented (vertically shifted for clarity). The middle curves (orange) represent the partial contributions used in the analysis of the Cu(II) complex **63** (vertically shifted for clarity) for sake of the example, lowest curve (grey) is the best fit residual ($k^2_{(\text{fit}-\text{th})}$). In **B**) the corresponding FT moduli are shown for experimental k^2 weighted EXAFS data (dots) and best fit (black lines). The Fourier transform imaginary (Imm-FT) part of experimental spectrum, best fit, and partial contributions are shown for complex **63** for sake of example. Dashed lines highlight in-phase Imm-FT oscillations for Cu-N and Cu-Cl contributions in the Cu(II) complexes **63** and **66**. The red arrow points out the structural signal lack in the region of Cu-Cl shell (red dashed line) likely due to some anti-phase structural signals. In **C**) the local structure around Cu is shown to highlight the neighbour shells involved in the analysis, being R = H (complex **63**) or R = CH₃ (complexes **65** and **66**), Y = Cl (Cu(II) complexes **63** and **66**) and Y = P (Cu(I) complex **65**).

The distances and Mean Square Relative Displacement (MSRD) σ^2 obtained from the refinement are reported in **Table 3.6**. for SS contributions. In complex **63** the distances demonstrate a good agreement with the expected molecular structure: the Cu-N nearest neighbour shell is found at 1.96 Å, the Cl is at 2.23 Å from Cu. The Cu-C and Cu-N(2) shells are indistinguishable in complexes **63** and **65** and a single contribution ($N = 4$) was used (the very similar backscattering amplitude and phase functions of C and N make them difficult to distinguish in the analysis). The analysis of complex **66** requires an additional contribution at around 1.89 Å. This finding definitively demonstrates the modification of Cu coordination geometry from roughly square planar (complex **63**) to roughly octahedral (complex **66**). This contribution is mandatory to achieve reliable fit; without it the Cu-Cl shell results unphysically short. It is possible that such additional link originates from the CH₃ residue. Moreover, the Cu-C/N(2) shell appears splitted in two: a shorter shell at around 2.9 Å and a long one at around 3.3 Å suggesting the tilting of pyrazole rings. In complex **65** the Cu-N distance is slightly longer,

due to the lower Cu(I) electronegativity providing a more loosely bound structure. It's possible to notice that in this case no Cu-C^R is required in the EXAFS fitting; a single contribution is used to reproduce the Cu-C and Cu-N(2) shells but an additional contribution at around 3.3 Å is required. Moreover, it's possible to assume that this last comes out from the C atoms of the phenyl rings linked to P (PPh₃). In summary, the Cu oxidation and the local structure around Cu provided by XAFS is consistent with the expected complex structure; the Cu(I) local structure appears more distorted likely due to the more loosely bound neighbour.

	N	63 Cu(II)		66 Cu(II)		65 Cu(I)	
		R (Å)	$\sigma^2 \cdot 10^2$ (Å ²)	R (Å)	$\sigma^2 \cdot 10^2$ (Å ²)	R (Å)	$\sigma^2 \cdot 10^2$ (Å ²)
Cu-N	2	1.959(5)	0.68(5)	1.967(7)	0.24(3)	2.001(3)	3.2(2)
Cu-C ^R	2	-	-	1.89(2)	1.62(2)	-	-
Cu-Cl(P)	2	2.23(1)	0.64(4)	2.21(2)	2.3(2)	2.16(1)	0.69(3)
Cu-C/N(2)	4	2.97(3)	0.86(2)	2.85(2) 3.35(3)	0.75(3) 0.45(2)	2.92(2)	1.3(2)
Cu-C ^{Ph3}	9	-	-	-	-	3.29(3)	1.4 (5)
Cu-C(2) (SS+MS)	4	4.08(3)		4.40(3)	0.8	4.05(8)	2.1

Table 3.6. - Best fit results for Cu K-edge XAFS data analysis of complexes **63**, **65** and **66**. The Cu-C^R shell originates from the carbons of R = CH₃ groups of the pyrazoles, the Cu-C^{Ph3} originates from the C atoms of phenyl rings bonded to P of PPh₃. Standard uncertainties on the last digit are reported in parenthesis.

3.3. Application of copper complexes

3.3.1. Cu(I) and Cu(II) complexes as anticancer agents

The *in vitro* antitumor activity of the copper(II) ([Cu(L^{1MN})₂]Cl₂ = **48** and [Cu(L^{2MN})₂]Cl₂ = **50**) and copper(I) complexes ([(PTA)₂Cu(L^{1MN})]PF₆ = **47** and [(PTA)₂Cu(L^{2MN})]PF₆ = **49**) and of the corresponding uncoordinated ligands (L^{1MN} = **10** and L^{2MN} = **11**) were evaluated by means of the 3-(4,5-dimethylthiazol-2-yl)-2,5-diphenyltetrazolium bromide (MTT) assay against a panel of human tumor cell lines derived from solid tumors. The cytotoxicity parameters, in terms of half maximal inhibitory concentration (IC₅₀) obtained after 72 hours of exposure, are listed in **Table 3.7**. Cell lines representative of cervical (A431), pancreatic (BxPC3), colon (HCT-15), breast (MCF-7), lung (A549) and ovarian (2008) cancers were included. For comparison purposes, cytotoxicity of cisplatin, the most widely used metal-based anticancer drug, was assessed under the same experimental conditions. The uncoordinated ligands proved to be scarcely effective in decreasing cancer cell viability (average IC₅₀ values were always over 50 μM), whereas both

copper(II) and copper(I) complexes elicited IC_{50} values in the micromolar range (1.4-15.8 μM). Both copper(II) complexes, **48** and **50**, were on average less effective than cisplatin against all tested cancer cell lines, with the exception of human HCT-15 colon cancer cells (notoriously poor sensitive to cisplatin) against which **48** and **50** were about 1.8 and 2.6 times more cytotoxic than the reference metal-drug, respectively. Copper(I) complexes **47** and **49** were much more effective showing IC_{50} values on average one-half lower than those calculated for the corresponding copper(II) complexes and similar or even appreciably lower than those obtained with cisplatin. In particular, derivative **49** was the most effective compound, showing mean IC_{50} values about 1.4-fold lower than those of both complex **47** and cisplatin. Notably, against HCT-15 colon cancer cells, complex **49** promoted a growth inhibitory effect about 2.5 times higher than that of cisplatin.

Compound	IC_{50} (μM) \pm SD					
	A431	BxPC3	HCT-15	MCF-7	A549	2008
L^{1MN} (10)	>50	>50	>50	>50	>50	>50
L^{2MN} (11)	>50	>50	>50	>50	>50	>50
$[(\text{PTA})_2\text{Cu}(L^{1MN})]\text{PF}_6$ (47)	5.4 \pm 1.2	6.4 \pm 2.1	9.3 \pm 2.1	4.1 \pm 1.0	7.4 \pm 1.3	8.5 \pm 0.4
$[\text{Cu}(L^{1MN})_2]\text{Cl}_2$ (48)	11.3 \pm 2.1	10.5 \pm 4.1	8.3 \pm 2.4	10.9 \pm 2.9	8.1 \pm 1.9	11.1 \pm 2.9
$[(\text{PTA})_2\text{Cu}(L^{2MN})]\text{PF}_6$ (49)	1.40 \pm 0.91	3.4 \pm 1.2	6.2 \pm 0.8	7.3 \pm 1.4	5.6 \pm 1.1	6.1 \pm 1.5
$[\text{Cu}(L^{2MN})_2]\text{Cl}_2$ (50)	15.7 \pm 1.7	9.5 \pm 1.6	5.8 \pm 2.3	12.7 \pm 2.9	15.6 \pm 4.1	15.8 \pm 2.9
Cisplatin	1.7 \pm 0.5	7.3 \pm 1.2	15.3 \pm 2.2	8.8 \pm 1.4	7.5 \pm 1.2	2.2 \pm 1.0

Table 3.7. - Cytotoxic activity. Cells ($3\text{-}8\cdot 10^4\text{ mL}^{-1}$) were treated for 72 h with increasing concentrations of tested compounds. Cytotoxicity was assessed by MTT test. IC_{50} values were calculated by a four parameter logistic model ($P < 0.05$). SD = standard deviation.

Given the high activity of copper(I) and Cu(II) derivatives against colon cancer cells, their *in vitro* antitumor activity was evaluated on a human colon cancer cell line pair which was selected for sensitivity/resistance to oxaliplatin (OXP), the key drug in FOLFOX (folinic acid, 5-fluorouracil and oxaliplatin) regimens in the treatment of colorectal cancers.^[144] Similarly to cisplatin, the clinical efficacy of oxaliplatin is limited by the development of cellular resistance and, currently, no other drugs in advanced clinical development for the treatment of patients with oxaliplatin-refractory colorectal cancer are available. Cytotoxicity on sensitive and resistant cells was assessed after 72 hours of drug treatment by MTT test. **Table 3.8.** shows the cytotoxicity parameters, in terms of IC_{50} and Resistance Factor (RF), the latter defined as the ratio between IC_{50} values calculated for resistant cells and those obtained with sensitive ones. All copper complexes exhibited activity levels very similar on both oxaliplatin-sensitive and -resistant cell lines, indicating a different cross-resistance profile than oxaliplatin. Actually, the

calculated RF values were 10-12 times lower than that of oxaliplatin, ruling out cross-resistance phenomena.

Compound	IC ₅₀ (μM) ± SD		
	LoVo	LoVo-OXP	RF
[(PTA) ₂ Cu(L ^{1MN})]PF ₆ (47)	4.9±1.0	4.6±0.8	0.9
[Cu(L ^{1MN}) ₂]Cl ₂ (48)	4.3±0.5	4.6±1.0	1.1
[(PTA) ₂ Cu(L ^{2MN})]PF ₆ (49)	2.1±1.1	1.9±0.9	0.9
[Cu(L ^{2MN}) ₂]Cl ₂ (50)	5.9±0.6	5.1±0.5	0.9
Oxaliplatin	1.4±0.3	15.2±2.2	10.9

Table 3.8. - Cross-resistance profiles. Cells ($3\cdot 8\cdot 10^4\cdot \text{mL}^{-1}$) were treated for 72 h with increasing concentrations of tested compounds. Cytotoxicity was assessed by MTT test. IC₅₀ values were calculated by a four parameter logistic model ($P < 0.05$). SD = standard deviation. RF = IC₅₀ (resistant subline)/IC₅₀ (wild-type subline).

The marked cell-killing effect has been observed against human HCT-15 colon carcinoma cells and, therefore, the *in vitro* antitumor activity of all copper derivatives was evaluated on 3D colon cancer cell cultures. As opposed to 2D monolayer culture, cells growing in 3D culture systems form aggregates or spheroids that are comprised of cells in various stages. The outer layers of the spheroid, being highly exposed to the medium, are mainly formed by viable and proliferating cells, whereas the core cells, receiving less oxygen, growth factors and nutrients, tend to be in a quiescent or hypoxic state.^[145] Such cellular heterogeneity is very similar to *in vivo* tumors, making 3D cell cultures more predictive than conventional 2D monolayer cultures in screening drugs potentially useful as inhibitors of tumor (including hypoxic one) proliferation. **Table 3.9.** summarizes the IC₅₀ values obtained after treatment of 3D cell spheroids of human HCT-15 colon cancer cells with the newly synthesized copper(I) and copper(II) complexes, using cisplatin and oxaliplatin as reference. In accordance with 2D chemosensitivity assays, complex **49** proved to be the most effective compound, showing an efficacy in decreasing cancer spheroid viability about 2 times higher than that of cisplatin and similar to that of oxaliplatin. Conversely, complexes **47** and **48** were as effective as cisplatin, but markedly less cytotoxic than oxaliplatin, whereas complex **50**, differently from what observed in monolayer HCT-15 cell cultures, was scarcely effective, eliciting IC₅₀ values significantly higher than those of cisplatin and oxaliplatin.

HCT-15	IC ₅₀ (μM) ± SD				Cisplatin	Oxaliplatin
	[(PTA) ₂ Cu(L ^{1MN})]PF ₆ (47)	[Cu(L ^{1MN}) ₂]Cl ₂ (48)	[(PTA) ₂ Cu(L ^{2MN})]PF ₆ (49)	[Cu(L ^{2MN}) ₂]Cl ₂ (50)		
	70.6±6.5	73.2±5.5	36.8±7.2	98.9±8.9	68.3±4.6	30.2±2.4

Table 3.9. - Cytotoxicity towards colon cancer cell spheroids. Spheroids ($2.5 \cdot 10^3$ cells/well) were treated for 72 h with increasing concentrations of tested compounds. The growth inhibitory effect was evaluated by means of APH test. IC₅₀ values were calculated from the dose-survival curves by the four parameter logistic model ($P < 0.05$). SD = standard deviation.

The LoVo cells were treated for 24 or 36 hours with equimolar concentrations (5 μM) of copper complexes. The cellular Cu levels were quantified by means of GF-AAS analysis and the results, expressed as ppb Cu per 10^6 cells, are shown in **Figure 3.16**. Although to a different extent, all derivatives were accumulated in a time-dependent manner, as shown by the time-dependent increase in cellular copper content. Among all, derivative **49** was the most internalized complex. By matching the cytotoxic activity values with the cellular uptake data, a direct and linear correlation was evidenced ($R^2 = 0.9$). Actually, the cellular copper content of LoVo cells follows the same cytotoxicity trend **49** > **47** ≈ **48** > **50**.

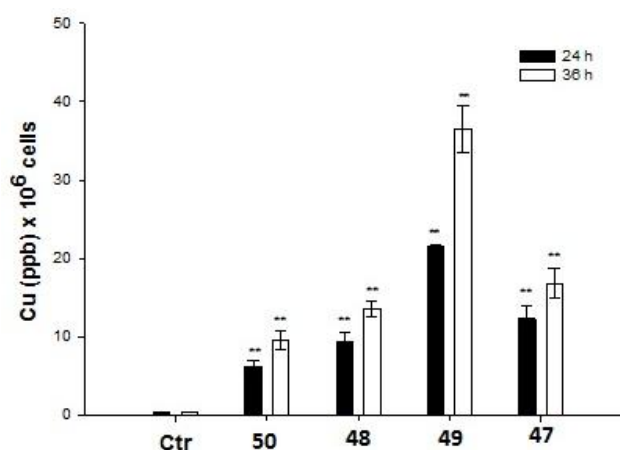


Figure 3.16. - Cellular uptake for complexes **47-50**.

To better characterize cellular morphological changes induced by the most effective complex **49**, LoVo cells exposed to IC₅₀ of **49** for 48 hours were subjected to TEM analysis (**Figure 3.17**). Morphological analysis of complex **49**-treated LoVo cells showed a massive cytoplasmic vacuolization (**Figure 3.17.b** and **3.17.c**) compared to control untreated cells (**Figure 3.17.a**). Interestingly, autophagy inhibitors, 3-methyladenine (3-MA) and monensin, did not abrogate cellular cytoplasmic vacuolization induced by **49**, and vacuoles were not positive to monodansylcadaverine staining, thus confirming the nonautophagic nature of **49**-induced vacuoles. No signs of classic apoptotic changes, such as cell shrinkage, chromatin condensation and apoptotic body formation were evidenced, thus indicating that exposure to **49** was not

associated with apoptosis induction. In addition, mitochondria appeared conserved in shape and internal structures and no swelling features (increase in size and decrease in turbidity) were detected. These evidences point to the induction of paraptosis cell death pathway, an apoptosis alternative cell death which has been previously described for several classes of metal complexes and organic molecules.^[146]

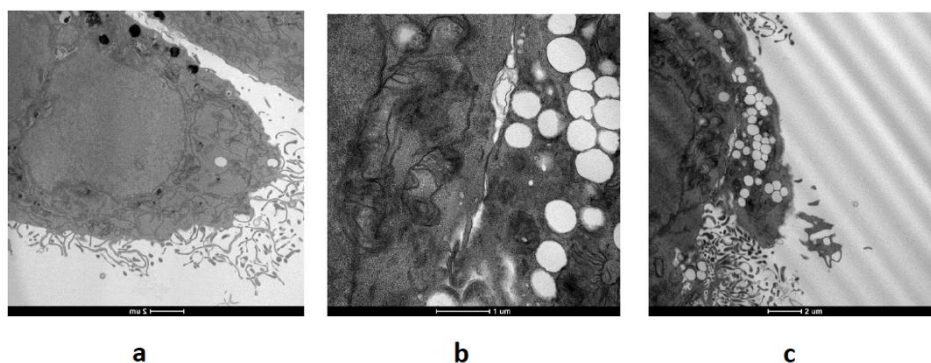


Figure 3.17. - TEM analysis on LoVo cells: (a) control untreated cells; (b) and (c) complex **49**-treated cells.

The *in vitro* antitumor activity of the copper(I) complexes **24-27** ($[(\text{PTA})_2\text{Cu}(\text{L}^{1\text{H}})]\text{PF}_6 = \mathbf{24}$, $[(\text{PTA})_2\text{Cu}(\text{L}^{2\text{H}})]\text{PF}_6 = \mathbf{25}$, $[(\text{PPh}_3)_2\text{Cu}(\text{L}^{1\text{H}})]\text{PF}_6 = \mathbf{26}$ and $[(\text{PPh}_3)_2\text{Cu}(\text{L}^{2\text{H}})]\text{PF}_6 = \mathbf{27}$) and **51-54** ($[(\text{PTA})_2\text{Cu}(\text{L}^{1\text{NMDA}})]\text{PF}_6 = \mathbf{51}$, $[(\text{PPh}_3)_2\text{Cu}(\text{L}^{1\text{NMDA}})]\text{PF}_6 = \mathbf{52}$, $[(\text{PTA})_2\text{Cu}(\text{L}^{2\text{NMDA}})]\text{PF}_6 = \mathbf{53}$ and $[(\text{PPh}_3)_2\text{Cu}(\text{L}^{2\text{NMDA}})]\text{PF}_6 = \mathbf{54}$) and of the corresponding uncoordinated ligands **1, 2, 12** and **13** ($\text{L}^{1\text{H}}$, $\text{L}^{2\text{H}}$, $\text{L}^{1\text{NMDA}}$ and $\text{L}^{2\text{NMDA}}$) were evaluated by means of the MTT assay against a panel of human tumor cell lines derived from solid tumors. The human cancer cell line panel contained examples of pancreatic (PSN-1 and BxPC3), breast (MCF-7), lung (H157), cervical (A431) and ovarian (A2780) cancers. Cisplatin was used as reference compound and was tested under the same experimental conditions. The cytotoxicity parameters, expressed in terms of IC_{50} after 72 hours of drug exposure, are reported in **Table 3.10**. Uncoordinated ligands **1, 2** and **13** proved to be scarcely effective against all tested cancer cell lines. On the contrary, NMDA-ANT^[147] and **12** showed a cytotoxic activity in the micromolar range. However, their cytotoxicity was significantly lower compared to that of the relative complexes **51-54**. Unfunctionalized complexes and those functionalized with NMDA-ANT were, on average, similarly active, suggesting that the ability of the ligand to bind NMDA receptor had a marginal role in the cytotoxicity of this class of complexes, with respect to that of copper. Such a hypothesis was supported by the observation that the complexes embedding the NMDA receptor antagonist (**51-54**) did not show particularly higher activity toward cell lines expressing NMDA receptors. Interestingly, all of them were more potent than cisplatin against all tested cancer cell lines.

Among the examined cell lines, pancreatic BxPC3 resulted to be the most sensitive one, with all derivatives, showing IC_{50} values $\leq 0.34 \mu\text{M}$. Complex **52** was the most active functionalized compound, with average IC_{50} values against all cancer cells roughly 80 times better than those elicited by cisplatin and in particular against pancreatic BxPC3 cancer cells, with values more than 300 times lower. It is also interesting to note that, on average, complexes with PPh_3 (**26**, **27**, **52** and **54**) showed activities comparable to those with PTA (**24**, **25**, **51** and **53**).

The human tumor cell lines panel also included two cell lines selected for their resistance to cisplatin (A431-Pt and A2780cis) or belonging to the MDR phenotype (A2780-ADR) (**Table 3.10**). By comparing the RF values, it was proven that all new compounds were able to overcome cisplatin resistance.

To further evaluate the anticancer potential of the copper(I) compounds, they were also screened against 3D spheroids of lung (H157) and pancreatic (BxPC3) cancer cells. The cancer spheroids were treated with copper(I) complexes or cisplatin for 72 hours and cell viability was assessed by means of the acid phosphatase (APH) assay (**Table 3.11**). Interestingly, all the compounds showed a growth-inhibitory effect significantly higher than cisplatin in both cell lines. In particular, against BxPC3 cells, the IC_{50} values of compounds proved to be from 10-fold (compound **24**) to even 84-fold (compound **53**) lower than that of cisplatin.

Compound	IC ₅₀ ± SD (μM)											
	PSN-1	BxPC3	MCF-7	H157	A431	A431-Pt	RF ^b	A2780	A2780cis	RF ^b	A2780 ADR	RF ^b
NMDA-ANT	10.4±2.6	8.3±2.7	12.1±3.2	5.3±0.7	11.2±2.3	-	-	19.8±3.3	-	-	-	-
L ^{1H} (1)	>50	21.2±3.2	>50	19.4±2.6	>50	-	-	>50	-	-	-	-
L ^{2H} (2)	>50	>50	>50	21.4±3.0	>50	-	-	45.5±7.3	-	-	-	-
L ^{1NMDA} (12)	9.6±2.3	13.1±3.5	7.4±2.2	6.6±1.4	7.6±0.9	-	-	15.5±2.6	-	-	-	-
L ^{2NMDA} (13)	>50	42.1±3.0	>50	>50	>50	-	-	>50	-	-	-	-
[(PTA) ₂ Cu(L ^{1H})]PF ₆ (24)	1.20±0.04	0.30±0.01	1.0±0.1	1.0±0.1	2.8±1.2	1.3±0.2	0.5	0.20±0.05	0.3±0.2	1.5	0.2±0.1	1.2
[(PTA) ₂ Cu(L ^{2H})]PF ₆ (25)	0.02±0.01	0.04±0.02	0.60±0.03	2.3±0.5	0.20±0.03	0.3±0.6	1.7	0.9±0.2	1.1±0.3	1.2	1.3±0.2	1.5
[(PPh ₃) ₂ Cu(L ^{1H})]PF ₆ (26)	3.1±1.9	0.30±0.05	1.0±0.1	1.3±0.3	0.6±0.1	1.1±0.4	1.7	0.5±0.3	0.7±0.1	1.6	0.5±0.1	1.2
[(PPh ₃) ₂ Cu(L ^{2H})]PF ₆ (27)	1.6±0.2	0.10±0.05	1.80±0.01	1.1±0.2	2.7±0.5	1.3±0.1	0.5	0.60±0.17	0.7±0.2	1.0	0.9±0.3	1.5
[(PTA) ₂ Cu(L ^{1NMDA})]PF ₆ (51)	1.0±0.3	0.20±0.02	0.50±0.03	0.4±0.2	3.3±0.7	5.9±1.5	1.8	0.40±0.04	0.4±0.1	1.1	0.4±0.1	1.1
[(PPh ₃) ₂ Cu(L ^{1NMDA})]PF ₆ (52)	0.40±0.04	0.02±0.01	0.8±0.1	0.4±0.1	0.20±0.01	0.10±0.01	0.7	0.10±0.01	0.10±0.01	0.5	0.20±0.02	1.7
[(PTA) ₂ Cu(L ^{2NMDA})]PF ₆ (53)	0.6±0.3	0.30±0.06	1.8±0.1	0.8±0.2	3.2±0.3	1.9±0.5	0.6	0.04±0.01	0.01±0.01	0.3	0.10±0.02	1.3
[(PPh ₃) ₂ Cu(L ^{2NMDA})]PF ₆ (54)	1.7±0.7	0.07±0.02	2.5±0.6	1.1±0.5	0.6±0.1	1.0±0.2	1.7	0.2±0.1	0.19±0.05	1.3	0.3±0.1	1.9
Cisplatin	12.1±2.9	7.3±1.2	8.8±0.2	26.7±3.2	1.4±0.3	2.9±0.6	2.0	0.45±0.10	2.6±0.2	5.8	-	-
Doxorubicin	-	-	-	-	-	-	-	0.004±0.001	-	-	0.09±0.01	21.5

Table 3.10. - *In vitro* antitumor activity of complexes (24-27 and 51-54), related precursors and ligands (1, 2, NMDA-ANT, 12 and 13), cisplatin, and doxorubicin. Cells (3-8·10³ mL⁻¹) were treated for 72 h with increasing concentrations of tested compounds. Cytotoxicity was assessed by MTT test. Half maximal inhibitory concentration (IC₅₀) values were calculated using a four-parameter logistic model (P < 0.05). SD = standard deviation. RF^b = IC₅₀ resistant/IC₅₀ parental cell lines.

Compound	IC ₅₀ ± SD (μM)	
	H157	BxPC3
[(PTA) ₂ Cu(L ^{1H})]PF ₆ (24)	11.9±2.0	10.2±2.3
[(PTA) ₂ Cu(L ^{2H})]PF ₆ (25)	10.0±0.4	5.5±0.9
[(PPh ₃) ₂ Cu(L ^{1H})]PF ₆ (26)	4.7±0.3	3.1±0.5
[(PPh ₃) ₂ Cu(L ^{2H})]PF ₆ (27)	3.3±1.0	2.4±0.2
[(PTA) ₂ Cu(L ^{1NMDA})]PF ₆ (51)	13.0±1.1	8.5±0.9
[(PPh ₃) ₂ Cu(L ^{1NMDA})]PF ₆ (52)	10.9±3.0	4.5±1.3
[(PTA) ₂ Cu(L ^{2NMDA})]PF ₆ (53)	2.9±0.5	1.2±0.2
[(PPh ₃) ₂ Cu(L ^{2NMDA})]PF ₆ (54)	2.7±0.5	6.5±1.1
Cisplatin	52.51±1.31	100.5±12.1

Table 3.11. - Activity of **24-27**, **51-54** and cisplatin in 3D cell cultures. Spheroids ($2.5 \cdot 10^3$ cells/well) were treated for 72 h with increasing concentrations of tested compounds. The growth-inhibitory effect was evaluated by means of the APH test. IC₅₀ values were calculated from the dose-survival curves using a four-parameter logistic model ($P < 0.05$). SD = standard deviation.

With the aim to correlate the cytotoxic potential of the complexes with their ability to enter in cancer cells, it has been evaluated the cellular uptake in BxPC3 cancer cells treated for 24 hours with equimolar concentrations (1 μM) of tested compounds (**Figure 3.18.**). All the compounds were able to cross cellular plasmalemma and copper accumulated in treated cancer cells without a strict dependence on the lipophilic character of the whole Cu(I) complex. This could be in relation to the involvement of a carrier-mediated transport mechanism, as evidenced for other classes of cytotoxic Cu(I) species. A partially direct and linear correlation between the cytotoxic activity and the cellular uptake of the tested compounds was found ($R^2 = 0.62$).

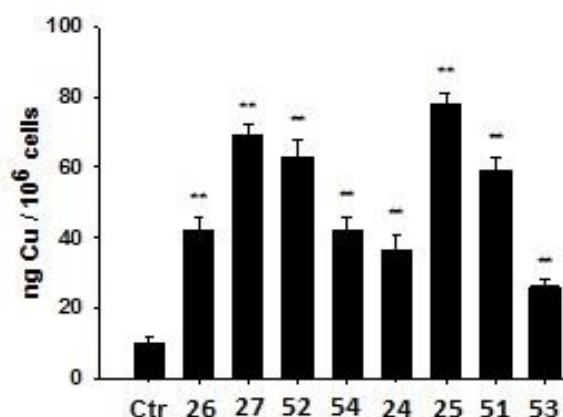


Figure 3.18. - Cellular uptake for complexes **24-27** and **51-54**. BxPC3 cells were incubated for 24 h with 1 μM of tested complexes. The amount of cellular Cu was estimated by GF-AAS. The error bars indicate the SD.

As many studies identified DNA as the main molecular target for copper compounds, the complexes and the related free ligands were evaluated about the ability to interact with isolated circulating tumor DNA (ctDNA) via ultraviolet (UV) electronic absorption titrations. Upon increasing the concentration of the compounds, a dose-dependent modification of the DNA absorption bands was detected. Interestingly, the free ligands were also slightly effective in inducing a modification of DNA spectra, thus indicating their ability to interact with DNA in cell-free conditions. In particular, a slight blueshift effect was evidenced for complexes with free or functionalized L^{2H} (**2**) ligand, indicative of a partial groove binding and partial destabilization of the DNA chain.

On the other hand, cell studies performed using alkaline single-cell gel electrophoresis (comet assay) revealed that complex **53**, the most active against 3D spheroids of BxPC3 cells, was only slightly effective in inducing cleavage of nuclear DNA in BxPC3 human pancreatic cancer cells, being significantly less effective than cisplatin even at the higher dose (**Figure 3.19**). In particular, cells treated with 1 μM of **53** displayed an increase of about 18% of well-formed comets compared to the 55% comet formation induced by the reference metallodrug.

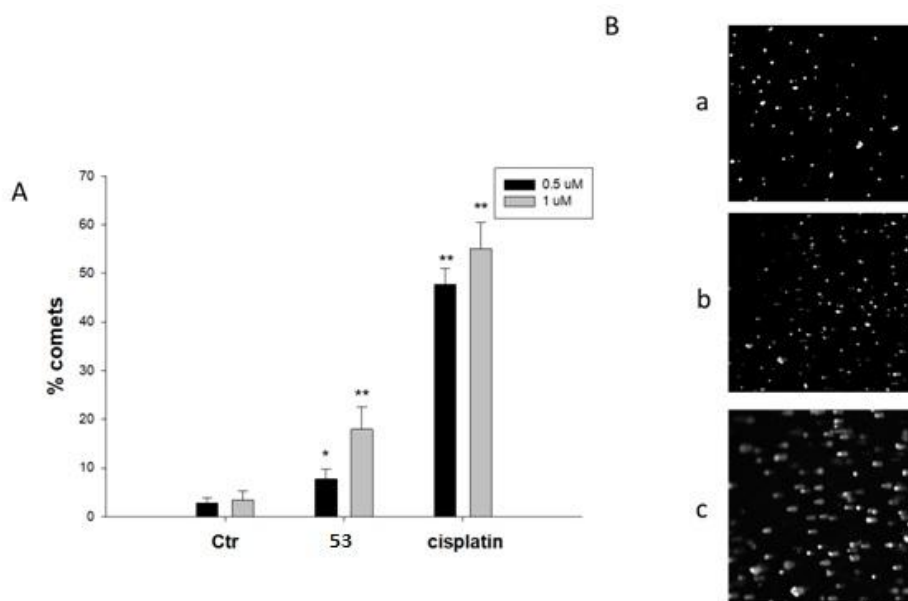


Figure 3.19. - Comet assay. BxPC3 cells were treated for 3 h with 1 μM of compound **53** or cisplatin and then processed for comet assay. **A**) Number of cells with well-formed comets measured by ImageJ software. The error bars indicate the SD. **B**) Representative images of control BxPC3 cells (**a**) or cells treated with 1 μM of **53** (**b**) and cisplatin (**c**).

Copper complexes have been regarded as redox active compounds and redox modulators. Actually, copper complexes may catalyze H₂O₂ in the form of Fenton-like inside the cell to produce ROS, altering cellular redox homeostasis and, thus, driving cells toward oxidative stress. On this basis, the ability of the complexes has been evaluated to increase the cellular

basal production of ROS in BxPC3 cancer cells. Notably, the treatment with the complexes determined a slight but not significant time-dependent increase in basal hydrogen peroxide formation (**Figure 3.20.A**), thus excluding the occurrence of significant oxidative stress. On the contrary, antimycin, a classic inhibitor of the mitochondrial respiratory chain at the level of complex III, induced a substantial increase in ROS formation in this cancer cell line. In order to characterize the cellular morphological changes induced by the copper(I) compounds, it has been observed the BxPC3 cancer cells treated for 24 hours with IC_{50} concentrations of the most representative compound **53** by using TEM. Analogously to what was observed with other Cu(I) complexes,^[30] morphological analysis revealed that **53** induced a massive swelling of the endoplasmic reticulum (ER) membrane, which is a clear sign of ER stress (**Figure 3.20.B.c**). In addition, at 48 hours of treatment, clear mitophagic signs of mitochondria damage and mitophagy induction were evident (**Figure 3.20.B.d**).

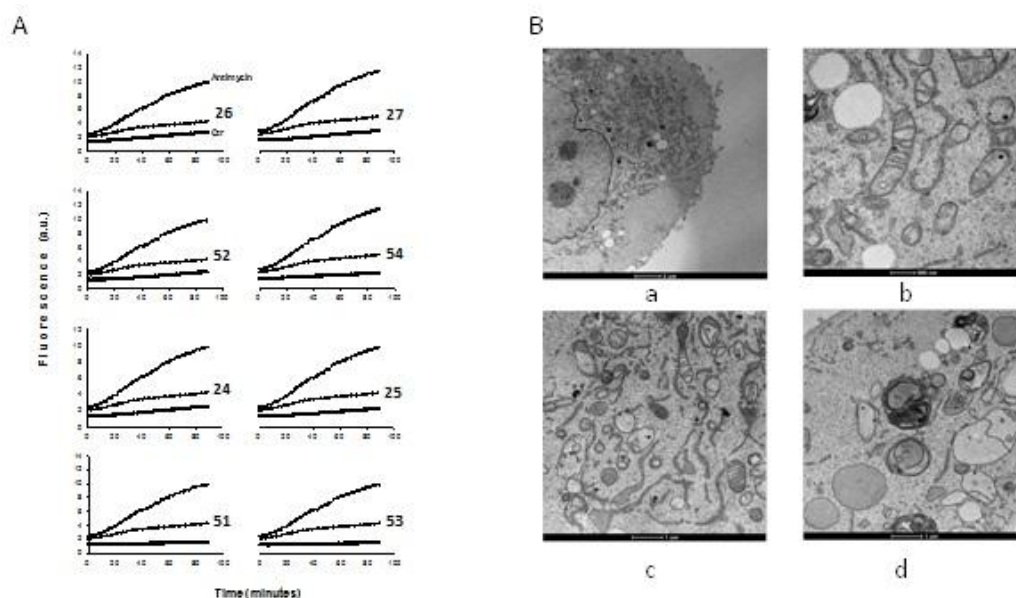


Figure 3.20. - ROS production and morphological changes. **(A)** Effect of the complexes on H_2O_2 formation in BxPC3 cells. BxPC3 cells were pre-incubated in phosphate-buffered saline (PBS) containing 10 mM glucose medium for 20 min at 37 °C in the presence of 10 μ M 5-(and-6)-chloromethyl-2',7'-dichlorodihydrofluorescein diacetate acetyl ester (CM-DCFDA) and then treated with the IC_{50} of copper(I) compounds as a function of time (minutes). **(B)** TEM analysis of BxPC3 cells after 24 h or 48 h of treatment with complex **53**: **(a)** and **(b)** controls; **(c)** 24 h after the treatment with compound **53**; **(d)** 48 h after the treatment with compound **53**.

The *in vitro* antitumor activity of the copper(I) $[(PTA)_2Cu(L^{1LONES})]PF_6 = \mathbf{55}$, $[(PPh_3)_2Cu(L^{1LONES})]PF_6 = \mathbf{56}$, $[(PTA)_2Cu(L^{2LONES})]PF_6 = \mathbf{58}$, $[(PPh_3)_2Cu(L^{2LONES})]PF_6 = \mathbf{59}$, $[(PTA)_2Cu(L^{1LONAM})]PF_6 = \mathbf{61}$, $[(PPh_3)_2Cu(L^{1LONAM})]PF_6 = \mathbf{62}$, $[(PTA)_2Cu(L^{2LONAM})]PF_6 = \mathbf{64}$ and $[(PPh_3)_2Cu(L^{2LONAM})]PF_6 = \mathbf{65}$ and copper(II) complexes $[Cu(L^{1LONES})]Cl_2 = \mathbf{57}$, $[Cu(L^{2LONES})]Cl_2 = \mathbf{60}$, $[Cu(L^{1LONAM})]Cl_2 = \mathbf{63}$ and $[Cu(L^{2LONAM})]Cl_2 = \mathbf{66}$, the corresponding uncoordinated ligands **16-19** (L^{1LONES} , L^{2LONES} , L^{1LONAM} and L^{2LONAM}) and related precursors (LND, LONES = **14** and LONAM =

15) were evaluated by means of the MTT assay for their ability to promote cell death in a panel of human cancer cell lines derived from solid tumors: ovarian (2008), colon (HCT-15), pancreatic (PSN-1), cervical (A431) and lung (H157) carcinoma cells. The cytotoxicity parameters, expressed in terms of IC₅₀ and obtained after 72 hours of drug exposure, are reported in **Table 3.12**. For comparison purposes, the cytotoxicity of cisplatin was assessed under the same experimental conditions. LND and the precursors **14** and **15** did not induce a significant reduction of cell viability (the IC₅₀ values were greater than 25 μM). Uncoordinated ligands **16-19** possess a moderate cytotoxic potency that was, however, on average, from 3 to 10 times lower compared to that of the corresponding metal complexes. Actually, all the tested copper complexes showed a promising cytotoxic potential, with IC₅₀ values in the low- or sub-micromolar range towards all the human cancer cell lines belonging to the panel and proved to be more effective than the reference chemotherapeutic drug cisplatin. These results suggest that both LND and copper might contribute to the potent antitumor activity of these complexes.

Compound	IC ₅₀ (μM) ± SD				
	2008	HCT-15	PSN-1	H157	A431
Lonidamine (LND)	24.9±3.3	>25	24.6±2.9	>25	>25
LONES (14)	>25	>25	21.3±2.4	>25	>25
LONAM (15)	18.2±0.9	>25	>25	>25	>25
L ^{1LONES} (16)	11.70±0.02	13.4±5.3	14.3±3.8	16.8±2.4	12.5±2.1
L ^{2LONES} (17)	21.3±3.5	6.2±0.5	2.7±0.3	5.2±0.7	3.2±0.2
L ^{1LONAM} (18)	7.9±2.2	4.7±1.6	3.1±0.9	5.6±1.4	3.7±1.6
L ^{2LONAM} (19)	2.9±1.1	1.9±1.0	1.5±0.5	1.3±0.6	1.4±0.5
[(PTA) ₂ Cu(L ^{1LONES})]PF ₆ (55)	2.4±0.9	2.5±0.5	1.2±0.1	1.3±0.5	0.4±0.1
[(PPh ₃) ₂ Cu(L ^{1LONES})]PF ₆ (56)	2.2±0.8	1.7±0.6	1.4±0.1	1.30±0.03	0.6±0.3
[Cu(L ^{1LONES})]Cl ₂ (57)	2.8±0.9	1.6±0.4	1.6±0.4	0.6±0.2	0.70±0.02
[(PTA) ₂ Cu(L ^{2LONES})]PF ₆ (58)	2.2±0.9	2.2±0.4	1.0±0.4	0.5±0.2	0.6±0.1
[(PPh ₃) ₂ Cu(L ^{2LONES})]PF ₆ (59)	1.4±0.1	3.4±0.1	0.6±0.1	1.2±0.2	0.7±0.1
[Cu(L ^{2LONES})]Cl ₂ (60)	1.3±0.2	4.7±0.9	0.5±0.1	1.0±0.2	1.5±0.6
[(PTA) ₂ Cu(L ^{1LONAM})]PF ₆ (61)	0.8±0.3	0.4±0.1	0.6±0.2	0.6±0.1	0.60±0.01
[(PPh ₃) ₂ Cu(L ^{1LONAM})]PF ₆ (62)	1.1±0.3	0.30±0.01	0.5±0.1	0.40±0.01	1.0±0.2
[Cu(L ^{1LONAM})]Cl ₂ (63)	1.20±0.02	0.2±0.1	0.5±0.2	0.5±0.2	1.6±0.8
[(PTA) ₂ Cu(L ^{2LONAM})]PF ₆ (64)	0.7±0.2	0.3±0.1	1.0±0.3	0.900±0.001	0.5±0.2
[(PPh ₃) ₂ Cu(L ^{2LONAM})]PF ₆ (65)	0.6±0.1	0.3±0.1	0.6±0.1	0.3±0.1	0.4±0.2
[Cu(L ^{2LONAM})]Cl ₂ (66)	0.8±0.8	0.2±0.1	1.6±0.2	0.60±0.02	1.00±0.01
Cisplatin	2.2±1.0	15.3±2.6	12.1±2.8	2.1±0.8	2.1±0.9

Table 3.12. - *In vitro* antitumor activity of complexes (**55-66**), related ligands (**16-19**), precursors (**LND**, **14**, **15**) and cisplatin. Cells (3-8·10³ mL⁻¹) were treated for 72 h with tested compounds. Cell viability was measured by MTT test. The IC₅₀ values were calculated by 4-PL logistic model (P < 0.05). SD = standard deviation.

In general, **16** and **17** derivatives were on average less effective than the corresponding **18** and **19** complexes and, among the series, no significant differences in terms of *in vitro* antitumor activities were detected for Cu(I) and Cu(II) complexes. It is important to note that complexes with ligands **16** and **17** were less stable in physiological media compared to the complexes bearing **18** and **19**. Hence, their lower cytotoxic effectiveness could be attributed, at least in part, to their instability in physiological conditions. Among all, complex **65** was the most effective derivative eliciting, on average, IC₅₀ values about 16 times lower than those detected with cisplatin. On the contrary, compound **55** was the weakest among the series, with a cytotoxic potency that was, however, more than 4 times higher than cisplatin.

Considering the very promising antiproliferative effects and keeping in mind that drug resistance represents a key determinant for the variable efficacy of the anticancer therapy, the ability of the complexes has also been evaluated to bypass acquired drug resistance. In particular, complexes were evaluated for their antiproliferative activity against some cancer cell lines selected for sensitivity/resistance to oxaliplatin or MDR cells, namely LoVo, LoVo-OXP and LoVo-MDR human colon cancer cells. The degree of resistance was evaluated by means of the RF (**Table 3.13.**). The main molecular mechanisms involved in oxaliplatin resistance appear to depend upon: (i) decreased cellular accumulation, which is thought to be related to a greater activity of the ATP7B exporter and multidrug resistance protein 1 (MRP1); (ii) more efficient repair of oxaliplatin-induced DNA-damage by Nucleotide Excision Repair (NER).^[148] LoVo-OXP cells (derived from LoVo cells grown in the presence of increasing concentration of oxaliplatin) were about 13-fold more resistant to oxaliplatin than parental cells. The compounds were tested for their potential ability to overcome platinum resistance. The RF values show that all complexes were equally effective against sensitive (LoVo) and resistant (LoVo-OXP) colon cancer cells, thus attesting their ability to overcome the oxaliplatin resistance. **Table 3.13.** also reports the data obtained by testing Cu(I) and Cu(II) complexes towards a MDR subline, human colon LoVo-MDR cancer cells, in which the resistance to doxorubicin, a drug belonging to the MDR spectrum, is associated with an overexpression of drug transporters. All compounds possessed RFs much lower than that of doxorubicin, thus confirming their ability to overcome the MDR phenomena.

Compound	IC ₅₀ (μM) ± SD				
	LoVo	LoVo-OXP	RF	LoVo-MDR	RF
[(PTA) ₂ Cu(L ^{1LONES})]PF ₆ (55)	2.4±0.3	1.8±0.5	0.8	1.6±0.7	0.7
[(PPh ₃) ₂ Cu(L ^{1LONES})]PF ₆ (56)	1.4±0.4	1.1±0.3	0.8	1.2±0.4	0.9
[Cu(L ^{1LONES})]Cl ₂ (57)	1.8±0.5	1.7±0.6	0.9	1.0±0.4	0.6
[(PTA) ₂ Cu(L ^{2LONES})]PF ₆ (58)	2.8±0.7	2.2±0.9	0.8	2.5±0.4	0.9
[(PPh ₃) ₂ Cu(L ^{2LONES})]PF ₆ (59)	2.2±0.4	1.6±0.3	0.7	1.7±0.6	0.8
[Cu(L ^{2LONES})]Cl ₂ (60)	2.8±0.7	2.1±0.6	0.8	2.0±0.5	0.7
[(PTA) ₂ Cu(L ^{1LONAM})]PF ₆ (61)	0.9±0.1	0.7±0.2	0.8	0.7±0.3	0.9
[(PPh ₃) ₂ Cu(L ^{1LONAM})]PF ₆ (62)	0.20±0.05	0.30±0.04	1.5	0.10±0.03	0.5
[Cu(L ^{1LONAM})]Cl ₂ (63)	0.6±0.1	0.7±0.1	1.0	0.8±0.2	1.3
[(PTA) ₂ Cu(L ^{2LONAM})]PF ₆ (64)	0.4±0.1	0.7±0.1	1.8	0.7±0.2	1.0
[(PPh ₃) ₂ Cu(L ^{2LONAM})]PF ₆ (65)	0.20±0.02	0.20±0.03	1.0	0.10±0.01	0.5
[Cu(L ^{2LONAM})]Cl ₂ (66)	0.8±0.1	0.9±0.3	1.1	1.1±0.3	1.4
Oxaliplatin	1.5±0.6	19.6±1.9	13.1	-	-
Doxorubicin	1.1±0.5	-	-	19.4±2.2	17.4

Table 3.13. - Cross-resistance profiles of complexes **55-66**, oxaliplatin and doxorubicin. Cells ($5 \cdot 10^3$ mL⁻¹) were treated for 72 h with tested compounds. Cell viability was measured by MTT test. IC₅₀ values were calculated by 4-PL logistic model ($P < 0.05$). SD = standard deviation. RF = IC₅₀ (resistant cells)/IC₅₀ (wild-type cells).

In an attempt to better investigate the antitumor potential of the complexes **55-66** that contain lonidamine conjugated ligands, their cytotoxic profiles were compared with those of similar unconjugated or differently conjugated (pyrazolyl)acetate complexes.^[149] No significant differences in terms of antiproliferative activity and of overcoming drug resistance were detected. The calculated IC₅₀ values, both in sensitive and resistant cancer cells, were always in the very low or submicromolar range.

The complexes **55-66** were also screened against 3D spheroids of pancreatic PSN-1 cancer cells, to further evaluate their anticancer potential. The spheroids were treated with tested complexes or cisplatin for 72 hours and the cell viability was assessed by means of the APH test (**Table 3.14.**). Notably, all complexes were much more effective than cisplatin against the three-dimensional model. Similarly to 2D studies, **16** and **17** derivatives were less effective than the corresponding **18** and **19** complexes. In addition, considering Cu(I) complexes, PTA containing complexes were generally less effective than the corresponding PPh₃ analogues. However, differently from cytotoxicity studies performed on monolayer cell cultures, in cancer spheroid models Cu(I) complexes with PPh₃ as coligand proved to be much more effective than Cu(II) derivatives. These results could be related to the more lipophilic character of PPh₃ containing Cu(I) complexes, which makes them more effective at penetrating across the entire spheroid domain, including the inner core. Complex **65** again emerged as the most promising derivative,

with an IC_{50} value roughly 12-folds better than that of cisplatin and complex **55** as the less effective derivative of the series.

Compound	IC_{50} (μ M) \pm SD PSN-1
$[(PTA)_2Cu(L^{1LONES})]PF_6$ (55)	40.4 \pm 2.0
$[(PPh_3)_2Cu(L^{1LONES})]PF_6$ (56)	8.3 \pm 1.2
$[Cu(L^{1LONES})]Cl_2$ (57)	33.0 \pm 3.0
$[(PTA)_2Cu(L^{2LONES})]PF_6$ (58)	31.9 \pm 4.0
$[(PPh_3)_2Cu(L^{2LONES})]PF_6$ (59)	22.0 \pm 2.1
$[Cu(L^{2LONES})]Cl_2$ (60)	34.0 \pm 2.1
$[(PTA)_2Cu(L^{1LONAM})]PF_6$ (61)	11.6 \pm 1.6
$[(PPh_3)_2Cu(L^{1LONAM})]PF_6$ (62)	6.8 \pm 0.4
$[Cu(L^{1LONAM})]Cl_2$ (63)	7.6 \pm 0.3
$[(PTA)_2Cu(L^{2LONAM})]PF_6$ (64)	6.6 \pm 0.5
$[(PPh_3)_2Cu(L^{2LONAM})]PF_6$ (65)	4.5 \pm 0.4
$[Cu(L^{2LONAM})]Cl_2$ (66)	13.7 \pm 3.7
Cisplatin	52.6 \pm 4.9

Table 3.14. - Cytotoxicity towards PSN-1 cancer cell spheroids of complexes **55-66** and cisplatin. Cancer cells spheroids ($2.5 \cdot 10^3$ cells/well) were treated for 72 h with tested compounds. Cell viability was evaluated by the APH test. IC_{50} values were calculated from the dose-response curves by 4-PL logistic model ($P < 0.05$). SD = standard deviation.

Being compound **65** the most promising derivative emerged from cytotoxicity studies in both 2D and 3D models, it was selected for uptake and mechanistic studies. Derivatives **64** and **66**, bearing the same ligand but different coligands or different Cu oxidation state, were included in these studies for useful comparison. The copper accumulation in cancer cells is one of the most important factors affecting copper complex cytotoxicity: in an attempt to correlate cytotoxic activity with cellular accumulation, copper content was evaluated in PSN-1 cells treated for 24 or 36 hours with 1 μ M of complexes **64-66**. The intracellular copper amount was quantified by means of GF-AAS analysis and the results, expressed as metal ppb per 10^6 cells, are showed in **Figure 3.21**. Although to a different extent, all three copper complexes accumulated into cancer cells. Notably, the intracellular Cu levels follow the trend **65** > **64** > **66** after 24 hours, thus suggesting that Cu(I) complexes are more effective in crossing cancer cell membrane with respect to the Cu(II) derivative. Interestingly, in the case of the Cu(II) complex **66**, the intracellular copper levels significantly increased with exposure time, whereas Cu(I) complexes **64** and **65** seemed to accumulate in a time-independent manner. These results may suggest that Cu(I) and Cu(II) complexes are internalized by different internalization mechanisms.

Moreover, by comparing uptake and cytotoxicity data in human pancreatic PSN-1 cancer cells, a direct correlation between cellular accumulation and cytotoxic potency can be highlighted.

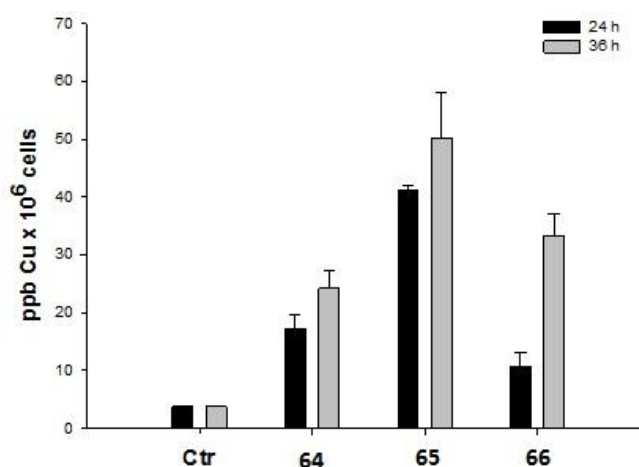


Figure 3.21. - Intracellular copper content after treatment with compounds **64-66**. PSN-1 cells were treated for 24 or 36 h with 1 μ M of copper complexes and intracellular copper amount was estimated by GF-AAS analysis. Error bars indicate the standard deviation.

Copper complexes are able to produce ROS inside the cells, altering the cellular redox homeostasis and driving the cells towards oxidative stress. In addition, it has previously been reported that LND acts as an antitumor drug by inhibiting both mitochondrial respiration and glycolysis, thus leading the cells to a more oxidized redox state.^[150] Moreover, some classes of copper complexes were found to exert an effective antiproliferative action by dysregulating mitochondrial function in cancer cells.^[151] On these bases, the ability of **64-66** to alter cellular redox homeostasis has been evaluated in terms of total cellular sulfhydryl content, ROS production and perturbation of the mitochondrial membrane potential in PSN-1 cells (**Figure 3.22.**). Interestingly, Cu(I) complexes **64** and **65** were completely ineffective in modulating total thiol content in treated PSN-1 cancer cells, whereas treatment with **66** induced a substantial time-dependent alteration of total cellular sulfhydryl content, determining an 18 and 25% reduction of thiol groups with respect to control (untreated PSN-1 cells) after 24 or 36 hours of exposure, respectively (**Figure 3.22.A**). The treatment of PSN-1 cells with complex **66** determined a substantial time-dependent increase in the cellular basal ROS production, while the treatment with **64** and **65** did not result in an increase in the basal cellular ROS production (**Figure 3.22.B**). Notably, the treatment of the cells with **66** determined a substantial increase in basal H₂O₂ formation which was even higher than that obtained with antimycin, a classical inhibitor of the mitochondrial respiratory chain at the level of complex III.

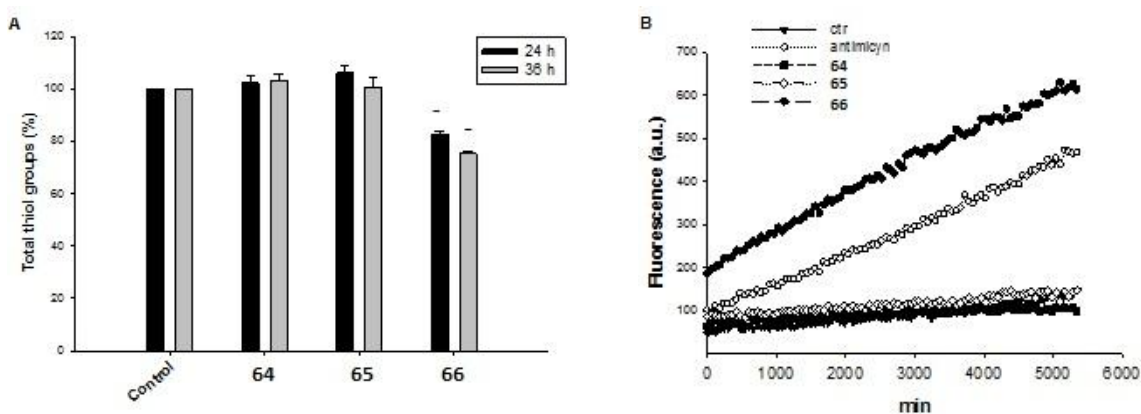


Figure 3.22. - **A)** Sulfhydryl content in treated PSN-1 cancer cells incubated for 24 or 36 h with tested compounds **64-66**. The sulfhydryl group amount was determined by the DTNB assay. Error bars indicate SD. **B)** Effect of the copper compounds on H_2O_2 formation in PSN-1 cells. PSN-1 cells were pre-incubated in PBS/10 mM glucose medium for 20 min at 37 °C in presence of 10 μ M CM-DCFDA and then treated with 10 μ M of tested compounds.

Overall, these results demonstrate that the Cu(II) complex (**66**) induced an oxidative stress in PSN-1 cells. On the contrary, Cu(I) complexes (**64** and **65**) seemed to act through a mechanism of action that does not encompass oxidative stress induction. A persistent increase in the rate of ROS production and the induction of thiol redox stress can, in turn, lead to the collapse of the mitochondrial membrane potential as well as the loss of mitochondrial shape and integrity (swelling) that can cause the induction of cell apoptosis.^[152] The effect determined by treatment with complexes **64-66** was evaluated in terms of modification of the mitochondrial pathophysiological characteristics, such as the mitochondrial membrane potential and the induction of cell death. For the mitochondrial membrane potential detection, PSN-1 cells were treated with IC_{50} concentrations of the tested complexes and the percentage of cells with altered mitochondrial membrane potential was determined. According to the results showed in **Figure 3.23.A**, as expected, complex **66** induced a 31% decrease in the dye red fluorescence, rather similar to that induced by the reference compound carbonyl cyanide-*m*-chlorophenylhydrazine (CCCP), thus attesting a significant increase in the percentage of hypopolarized cells. On the other hand, **64** and **65** induced a slight (about 12 and 19%, respectively) increase in the dye red fluorescence, thus indicating a modest increase in cancer cell population with hyperpolarized mitochondrial membrane potential. Considering these results, it is possible to state that Cu(I) complexes (**64** and **65**) possess a rather different mechanism of action compared to Cu(II) complex (**66**). It has been widely described that Cu(I) and Cu(II) complexes can induce different types of cell death. In order to analyse the mechanism involved in loss of cancer cell viability, the ability of selected complexes to induce cancer cell death by means of apoptosis, was evaluated. **Figure 3.23.B** shows the results

obtained upon monitoring cellular morphological changes in PSN-1 cells treated for 48 hours with IC₅₀ doses of **64-66** and stained with Hoechst 33258 fluorescent probe. Compared with control cells, cells treated with **66** presented brightly stained nuclei and morphological features typical of cells undergoing apoptosis, such as chromatin condensation and fragmentation, thus confirming the ability of the Cu(II) complex **66** to induce cancer cell death by means of apoptosis. On the other hand, cells treated with **64** and **65** did not show any classical sign of apoptosis induction and appeared increased in size and complexity.

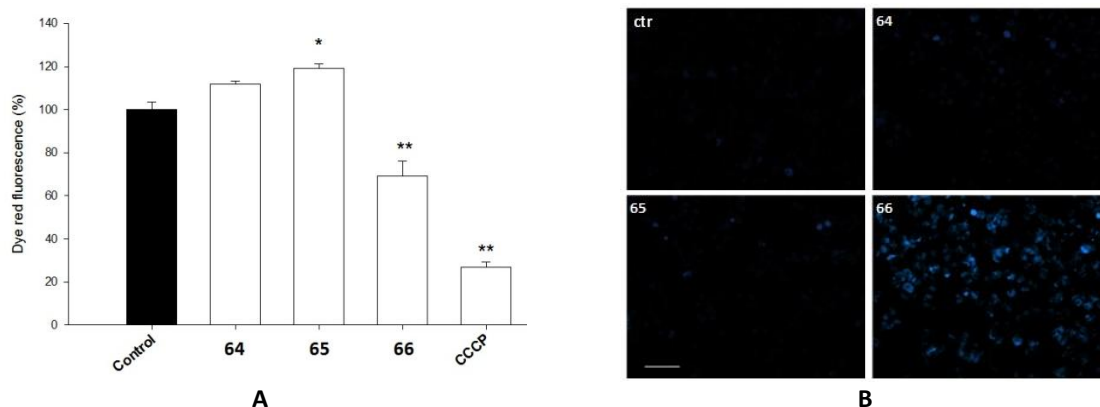


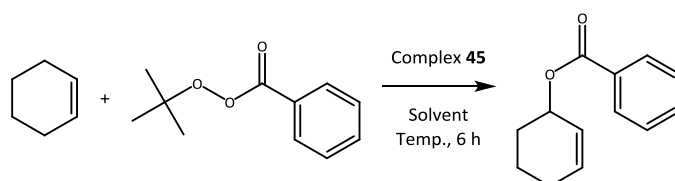
Figure 3.23. - **A)** PSN-1 cells were treated for 24 h with IC₅₀ concentrations of tested complexes or CCCP (3 μ M). The mitochondrial membrane potential was determined by Mito-ID[®] Membrane Potential Kit. Data are the means of three independent experiments. Error bars indicate SD. **B)** Hoechst staining of PSN-1 cells incubated for 48 h with IC₅₀ doses of **64-66**.

These results clearly suggest that Cu(II) complex (**66**) leads the cancer cell to death via an apoptotic pathway, whereas Cu(I) complexes (**64** and **65**) kill cancer cells by means of an apoptosis alternative cancer cell death, possibly paraptosis, that has been recognised as a strategic pathway of the cancer cells that are resistant to apoptotic mechanisms. Paraptosis is a type of programmed cell death, morphologically distinct from apoptosis and necrosis. Features of paraptosis are cytoplasmic vacuolation and lack of apoptotic morphology (cell shrinkage, apoptotic bodies, chromatin condensation and nuclear fragmentation). Like apoptosis and other types of programmed cell death, the cell is involved in causing its own death. Considering all the collected data, complex **65** can be recommended for a more detailed investigation of its biological properties, such as the assessment of its interactions with important biomolecules and the evaluation of the *in vivo* efficacy.

3.3.2. Cu(II) complexes as catalysts

Copper complexes [Cu(L^{1Hex})]Cl₂ (**43**), [Cu(L^{2Hex})]Cl₂ (**45**) and [Cu(L^{2Hex})]Br₂ (**46**) were studied as catalysts for the oxidation of alkenes *via* the Kharasch-Sosnovsky reaction, based on previous

experimental attempts using analogous copper(II) complexes bearing ligands with the methyl ester (L^{2Me}), in which the product was obtained just in traces. In particular, the hexyl derivative (L^{2Hex}) was chosen in order to increase the contact in a homogeneous mixture, avoiding the use of further solvents. Thus, in order to demonstrate the catalytic activity of complex $[Cu(L^{2Hex})]Cl_2$ (**45**), a series of preliminary tests was performed changing stoichiometry, temperature and solvents. After this screening, an interesting catalytic activity of complex **45** was actually observed, obtaining the best yield in the presence of 10 mol% of the complex, an excess of cyclohexene with respect to the perester (10:1) at 60°C (**Table 3.15.**, entry *j*).

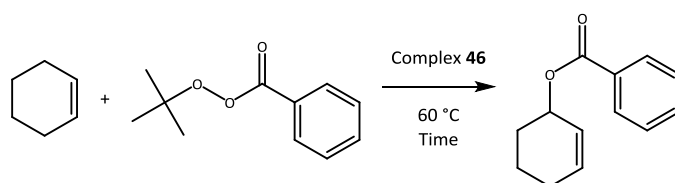


Entry	45 mol%	Alkene:Perester ratio	Solvent	Temperature (°C)	Product yield (%) ^a
<i>a</i>	20	3:1	CH ₃ CN ^b	rt	6
<i>b</i>	20	3:1	CH ₃ CN ^b	60	25
<i>c</i>	20	3:1	CHCl ₃ ^b	60	28
<i>d</i>	20	3:1	-	rt	25
<i>e</i>	20	3:1	-	60	40
<i>f</i>	20	3:1	-	80	29
<i>g</i>	20	10:1	-	60	65
<i>h</i>	20	7.5:1	-	60	59
<i>i</i>	20	5:1	-	60	54
<i>j</i>	10	10:1	-	60	68
<i>k</i>	5	10:1	-	60	40
<i>l</i>	1	10:1	-	60	31

^a Yield of pure isolated product. ^b 1M concentration.

Table 3.15. - Study on the catalytic activity of complex **45**.

Once reaction conditions were optimized for complex **45**, the attention was turned on complex $[Cu(L^{2Hex})]Br_2$ (**46**). The latter complex showed better catalytic performance and, in particular, working under the same reaction conditions, the reaction time decreased from 24 to 6 hours and the yield passed from 68 to 75%. A further significant improvement was recognized performing the reaction in a sealed vial, by which it was possible to minimize the variation of the concentration of the alkene due to the volatility of cyclohexene. Under these conditions and after some additional tests, the product was isolated in 85% of yield using only 5 mol% of complex **46** (**Table 3.16.**, entry *b*).



Entry	46 mol%	Alkene:Perester ratio	Time (h)	Product yield (%) ^a
<i>a</i>	10	10:1	3	84
<i>b</i>	5	5:1	6	85
<i>c</i>	1	5:1	24	73
<i>d</i>	-	5:1	24	-

^a Yield of pure isolated product.

Table 3.16. - Additional tests performed in a sealed vial promoted by complex **46**.

Subsequently, based on previous optimization steps (**Table 3.16.**, entry *b*), the catalytic activity of $[\text{Cu}(\text{L}^{1\text{Hex}})]\text{Cl}_2$ (**43**) was tested. However, this complex resulted less active than **46**, isolating the product in just 30% of yield. Nevertheless, satisfactory yields can be reached increasing the alkene:perester ratio to 10:1 and the amount of catalyst up to 20 mol%, obtaining 70% of yield after 24 hours at 60 °C. These results are probably due to the fact that the methyl groups slightly increase the solubility of complexes **45** and **46** in cyclohexene.

A similar study was also performed under the same conditions with simple copper(II) salts, such as CuCl_2 and CuBr_2 , obtaining very poor yields of the target compound, 15% and 18% respectively, after 24 hours at 60 °C.

Once proved the catalytic activity of these complexes and in particular identifying the complex $[\text{Cu}(\text{L}^{2\text{Hex}})]\text{Br}_2$ (**46**) as the most effective one, the optimised reaction conditions were tested on cyclopentene and cyclooctene, obtaining in both cases from good to excellent yields (**Figure 3.24.**).

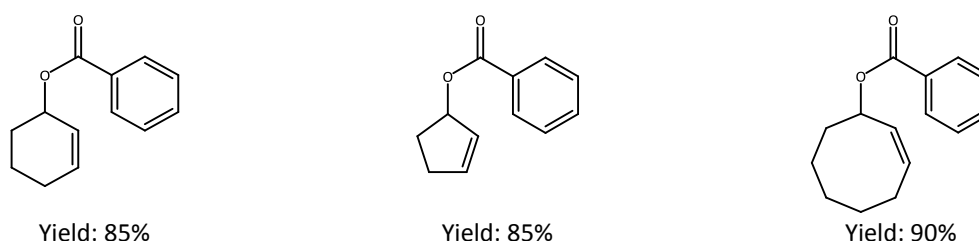
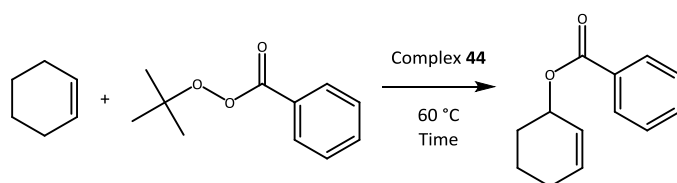


Figure 3.24. - Synthesis of oxygenate allylic compounds *via* Kharasch-Sosnovsky reaction using **46** as catalyst.

Regarding $\{[\text{Cu}(\text{L}^{1\text{Hex}})]\text{Br}(\mu\text{-Br})\}_2$ (**44**), the last of the series of the complexes bearing an esterified ligand with an hexyl chain, the crystallographic resolution has made to decide to test also this compound in the Kharasch-Sosnovsky reaction, even if complex **46** already proved to

be the most effective one among the studied complexes, given its interesting dimeric structure. Starting from the results obtained with complex **46** (Table 3.16.) a further strategy was developed, in order to reduce the amount of catalyst and increase the yield. To determine the catalytic activity of complex **44**, a series of preliminary tests were carried out. The starting point was related to the use of 5 mol% of the catalyst **44** leaving the reaction 6 hours at 60 °C, with an alkene:perester ratio of 5:1, achieving only 73% of yield (Table 3.17., entry *a*). After this first trial, several attempts were conducted and the best result was observed using 0.5 mol% of **44**, a slight excess of cyclohexene (alkene:perester ratio of 3:1) at 60 °C for 24 hours (Table 3.17., entry *h*). Using an alkene:perester ratio of 5:1, with 5 mol% of the catalyst and a 24 hours reaction time, the yield was almost quantitative (Table 3.17., entry *b*). This yield decreased a bit reducing the ratio to 3:1, due to the scarce and non-proportional amount of cyclohexene and Luperox (Table 3.17., entry *c*). A noteworthy upgrade was obtained carrying out the reaction with 1 mol% of **44**, for 24 hours at 60 °C: in this setting the yields were comparable with those obtained before (Table 3.17., entry *d* = 77% of yield and entry *e* = 74% of yield). So, based on above mentioned optimization steps, the catalytic activity of complex **44** was further developed, decreasing the amount to 0.5 mol%. Nonetheless, an almost quantitative yield can be reached increasing the alkene:perester ratio to 10:1, using 0.5 mol% of the catalyst and obtaining 95% of yield after 24 hours at 60 °C. A reduction of the ratio means a reduction of the amount of an alkene that could be, somehow, precious and not easily available and therefore a decreasing the waste of starting materials. Therefore, the use of a 3:1 ratio of cyclohexene:Luperox allowed to obtain a very good yield, up to 90% (Table 3.17., entry *h*).



Entry	44 mol%	Alkene:Perester ratio	Time (h)	Product yield (%) ^a
<i>a</i>	5	5:1	6	73
<i>b</i>	5	5:1	24	95
<i>c</i>	5	3:1	24	79
<i>d</i>	1	5:1	24	77
<i>e</i>	1	3:1	24	74
<i>f</i>	0.5	10:1	24	95
<i>g</i>	0.5	5:1	24	90
<i>h</i>	0.5	3:1	24	90
<i>i</i>	0.5	1:1	48	33

^a Yield of pure isolated product.

Table 3.17. - Study on the catalytic activity of complex **44**.

Finally, once confirmed the very virtuous catalytic performance of this complex, the optimised reaction conditions were tested on cyclopentene and cyclooctene, obtaining in both cases good yields (**Figure 3.25**).

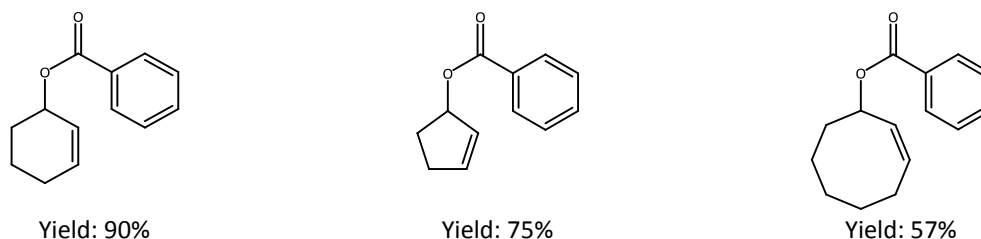
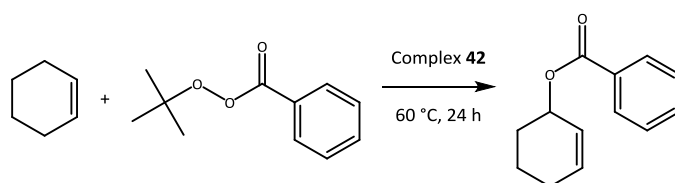


Figure 3.25. - Synthesis of oxygenate allylic compounds *via* Kharasch-Sosnovsky reaction using **44** as catalyst.

In order to assure the generality of the method for the previously optimized reaction conditions, complex $[\text{Cu}(\text{L}^{2\text{iPr}})]\text{Br}_2$ (**42**) was taken in account as further catalyst. The reaction conditions previously found for complex $\{[\text{Cu}(\text{L}^{1\text{Hex}})]\text{Br}(\mu\text{-Br})_2\}$ (**44**) were kept at the same values (**Table 3.17.**, entry *h*) for the study of the catalytic activity of compound **42**: 0.5 mol% of catalyst, cyclohexene:Luperox ratio of 3:1, carrying out the reaction at 60 °C for 24 hours in a sealed vial and obtaining the product in 76% yield (**Table 3.18.**, entry *a*). After that, a second reaction was carried out increasing the molar percentage of **42** from 0.5 to 1%, but keeping constant the other reaction conditions, obtaining a comparable yield (**Table 3.18.**, entry *b*).



Entry	42 mol%	Alkene:Perester ratio	Time (h)	Product yield (%) ^a
<i>a</i>	0.5	3:1	24	76
<i>b</i>	1	3:1	24	80

^a Yield of pure isolated product.

Table 3.18. - Study on the catalytic activity of complex **42**.

Once confirmed the catalytic activity of complex **42**, the feasibility of this reaction on cyclopentene and cyclooctene was examined, under the optimized experimental conditions, obtaining in both cases good yields (**Figure 3.26.**).

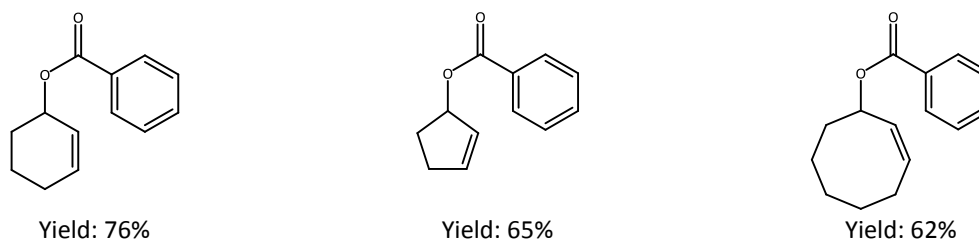


Figure 3.26. - Synthesis of oxygenate allylic compounds *via* Kharasch-Sosnovsky reaction using **42** as catalyst.

A possible explanation of the different yields reached employing compounds **42** and **44** as catalysts could be found in the different structural conformations of cycloalkenes which allow a different interaction with the complexes.

4. CONCLUSIONS

During my PhD research work in the inorganic chemistry laboratory of the University of Camerino, I designed, synthesized and characterized several new precursors and ligands, as well as the related novel Cu(I) and Cu(II) complexes. Copper was chosen for its chemical and biological properties: in particular it has different accessible oxidation states and geometries, it is an essential metal, there is a high need for copper in cancer tissues compared to that in normal cells and it has an important role as limiting factor for multiple aspects of tumor progression, including angiogenesis, growth and metastasis. Heteroscorpionate acetate ligands were chosen because they can be easily functionalized on the pyrazole rings and derivatized with alcohols or bioactive molecules on the carboxylic group. The complexes were prepared by reaction of ligands with copper in different oxidation states and with several counterions. For Cu(I) complexes hydrophilic or lipophilic phosphane coligands were also used to stabilize copper in the +1 oxidation state and to confer different solubility properties to the corresponding complexes.

All the obtained compounds were characterized by means of spectroscopic and analytic techniques, employing in addition the X-ray diffraction for the compounds obtained as single crystals of good quality (**7**, **11**, **20**, **21**, **29** and **44**). In some cases, when the attempts to obtain crystals were unsuccessful, information about the structure and the local coordination environment came out the XPS and XAS investigations (**43**, **45**, **46**, **63**, **65** and **66**).

Selected precursors (**1**, **2**, **14** and **15**), ligands (**10-13** and **16-19**) and copper complexes (**24-27** and **46-66**) were investigated for their cytotoxic potential on a panel of human cancer cell lines, derived from different solid tumors, also including cancer cells selected for their resistance to cisplatin, oxaliplatin or multidrugs. The complexes, in general, resulted to be more active than the reference compounds (cisplatin, oxaliplatin and doxorubicin) and the related ligands, both in 2D and 3D cell cultures, showing their effect in the low micromolar concentration, or even lower in some cases. In addition, studies were performed in order to elucidate the mechanism of action of the new copper complexes. The results clearly suggest that the Cu(II) complexes (**57**, **60**, **63**, **66**) trigger cancer cell death via an apoptotic pathway, while all the Cu(I) complexes kill cancer cells by means of an alternative programmed cancer cell death, probably paraptosis, that has been recognized as a possible strategic pathway in cancer cells that are resistant to apoptotic mechanisms. In addition, biological evaluations are still in progress for ligands **4-9** and the related complexes **31-46**.

Some of the new Cu(II) complexes (**42-46**) were investigated as catalysts in the Kharasch-Sosnovsky reaction, one of the most important allylic oxidation that leads to oxidized olefins leaving the double bond in its original position. After the optimization of the original reaction, very good yields of the products (using several cycloalkenes as substrates) were obtained employing the complexes with bromide as counterion (**42**, **44** and **46**). The main limitations of Kharasch-Sosnovsky reaction, such as long reaction times, use of benzene as solvent and high waste of olefins, were overcome using the new synthesized Cu(II) complexes, avoiding the use of any external reducing agents. Other promising Cu(II) complexes (**39-41**) are under evaluation as catalysts in the same reaction and in other synthetic pathways to provide a powerful platform for copper catalyzed reactions.

5. References

- [1] D. R. Lide; *Handbook of chemistry and physics*; CRC press; 81st edition; **2001**.
- [2] G. Audi, A. H. Wapstra, C. Thibault, J. Blachot, O. Bersillon; "The NUBASE evaluation of nuclear and decay properties"; *Nuclear Physics*; 729, 3, **2003**.
- [3] M. Harris; "Clarity uses a cutting-edge imaging technique to guide drug development"; *Nature Biotechnology*; 34, **2014**.
- [4] H. Okazawad, Y. Yonekura, Y. Fujibayashi, S. Nishizawa, Y. Magata, K. Ishizu, F. Tanaka, T. Tsuchida, N. Tamaki, J. Konishi; "Clinical application and quantitative evaluation of generator-produced copper-62-PTSM as a brain perfusion tracer for PET"; *Journal of Nuclear Medicine*; 35, 1910, **1994**.
- [5] N. N. Greenwood, A. Earnshhaw; *Chemistry of the elements*; Butterworth-Heinemann; 2nd edition; **1997**.
- [6] J. A. Mayoral, S. Rodríguez-Rodríguez, L. Salvatella; "Theoretical insights into enantioselective catalysis: the mechanism of the Kharasch-Sosnovsky reaction"; *Chemistry - A European Journal*; 14, 9274, **2008**.
- [7] R. G. Pearson; "Hard and soft acids and bases"; *Journal of the American Chemical Society*; 85, 3533, **1963**.
- [8] M. C. Linder; *Biochemistry of copper*; Plenum Press; **1991**.
- [9] J. A. Mc Cleverty, T. J. Meyer; "Comprehensive coordination chemistry II - From biology to nanotechnology"; *Journal of the American Chemical Society*; 126, 1922, **2003**.
- [10] H. Decker, N. Terwilliger; "COPs and robbers: putative evolution of copper oxygen-binding proteins"; *Journal of Experimental Biology*; 203, 1777, **2000**.
- [11] S. J. Adelstein, B. L. Vallee; "Copper metabolism in man"; *New England Journal of Medicine*; 265, 892, **1961**.
- [12] M. C. Linder, L. Wooten, P. Cerveza, S. Cotton, R. Shulze, N. Lomeli; "Copper transport"; *The American Journal of Clinical Nutrition*; 67, 965, **1998**.
- [13] E. Frieden, H. S. Hsieh; "Ceruloplasmin: the copper transport protein with essential oxidase activity"; *Advances in Enzymology and Related Areas of Molecular Biology*; 44, 187, **1976**.
- [14] S. S. Percival, E. D. Harris; "Copper transport from ceruloplasmin: characterization of the cellular uptake mechanism"; *American Journal of Physiology. Cell Physiology*; 258, 140, **1990**.

- [15] G. Khan, S. Merajver; "Copper chelation in cancer therapy using tetrathiomolybdate: an evolving paradigm"; *Expert Opinion on Investigational Drugs*; 18, 541, **2009**.
- [16] S. Trofimenko; "Boron-pyrazole chemistry"; *Journal of the American Chemical Society*; 88, 1842, **1966**.
- [17] S. Trofimenko; *Scorpionates: Polypyrazolylborate ligands and their coordination chemistry*; World Scientific Publishing; **1999**.
- [18] S. Trofimenko, J. R. Long, T. Nappier, S. G. Shore; "Poly(1-pyrazolyl)borates, their transition-metal complexes, and pyrazoboles"; *Inorganic Syntheses*; 12, 99, **1970**.
- [19] C. Santini, M. Pellei, G. Gioia Lobbia, G. Papini; "Synthesis and properties of poly(pyrazolyl)borate and related boron-centered scorpionate ligands. Part A: pyrazole-based systems"; *Mini-Reviews in Organic Chemistry*; 7, 84, **2010**.
- [20] C. Santini, M. Pellei; "Applications of scorpionate ligands in enzyme modeling and biological studies"; *Current bioactive compounds*; 5, 243, **2009**.
- [21] B. S. Hammers, B. S. Chohan, J. T. Hoffman, S. Einwächter, C. J. Carrano; "A family of dioxo-molybdenum(VI) complexes of N₂X heteroscorpionate ligands of relevance to molybdoenzymes"; *Inorganic Chemistry*; 43, 7800, **2004**.
- [22] S. Trofimenko; "Scorpionate: genesis, milestones, prognosis"; *Polyhedron*; 23, 197, **2004**.
- [23] S. Trofimenko; "Recent advances in poly(pyrazolyl)borate (scorpionate) chemistry"; *Chemical Reviews*; 93, 943, **1993**.
- [24] A. Otero, A. Lara-Sánchez, J. Fernández-Baeza, E. Martínez-Caballero, I. Márquez-Segovia, C. Alonso-Moreno, L. F. Sanchèz-Barba, A. M. Rodríguez, I. Lòpez-Solera; "New achiral and chiral NNE heteroscorpionate ligands. Synthesis of homoleptic lithium complexes as well as halide and alkyl scandium and yttrium complexes"; *Dalton Transaction*; 39, 930, **2010**.
- [25] N. Burzlaff, I. Hegelmann, B. Weibert; "Bis(pyrazol-1-yl)acetates as tripodal "scorpionate" ligands in transition metal carbonyl chemistry: syntheses, structures and reactivity of manganese and rhenium carbonyl complexes of the type [LM(CO)₃] (L = bpza, bdmpza)"; *Journal of Organometallic Chemistry*; 626, 16, **2001**.
- [26] A. Beck, B. Weibert, N. Burzlaff; "Monoanionic N,N,O-scorpionate ligands and their iron(II) and zinc(II) complexes: models for mononuclear active sites of non-heme iron oxidases and zinc enzymes"; *European Journal of Inorganic Chemistry*, 2001, 521, **2001**.

- [27] P. Atkins, T. Overton, J. Rourke, M. Weller, F. Armstrong; *Chimica Inorganica*; Zanichelli; 2nd edition; **2012**.
- [28] C. Marzano, V. Grandin, M. Pellei, D. Colavito, G. Papini, G. Gioia Lobbia, E. Del Giudice, M. Porchia, F. Tisato, C. Santini; "In vitro antitumor activity of the water soluble copper(I) complexes bearing the tris(hydroxymethyl) phosphine ligand"; *Journal of Medicinal Chemistry*; 51, 798, **2008**.
- [29] D. J. Daigle, T. J. Decuir, J. B. Robertson, D. J. Darensbourg; "1,3,5-triaza-7-phosphatrimethyldecane and derivatives"; *Inorganic Syntheses*; 32, 40, **1998**.
- [30] V. Gandin, M. Pellei, F. Tisato, M. Porchia, C. Santini, C. Marzano; "A novel copper complex induces paraptosis in colon cancer cells via the activation of ER stress signalling"; *Journal of Cellular and Molecular Medicine*; 16, 142, **2012**.
- [31] V. Gandin, C. Ceresa, G. Esposito, S. Indraccolo, M. Porchia, F. Tisato, C. Santini, M. Pellei, C. Marzano; "Therapeutic potential of the phosphino Cu(I) complex (HydroCuP) in the treatment of solid tumors"; *Scientific Report, Nature*; 7, 13936, **2017**.
- [32] L. Tschugajeff, M. Skanawy-Grigorjewa, A. Posnjak; "Über die hydrazin-carbylamin-komplexe des platins"; *Zeitschrift für Anorganische und Allgemeine Chemie*; 148, 37, **1925**.
- [33] A. J. Arduengo III, R. L. Harlow, M. Kline; "A stable crystalline carbene"; *Journal of the American Chemical Society*; 113, 361, **1991**.
- [34] W. A. Herrmann, M. Elison, J. Fischer, C. Köcher, G. R. J. Artus; "Metal complexes of N-heterocyclic carbenes - A new structural principle for catalysts in homogeneous catalysis"; *Angewandte Chemie International Edition*; 34, 2371, **1995**.
- [35] M. C. Perry, K. Burgess; "Chiral N-heterocyclic carbene-transition metal complexes in asymmetric catalysis"; *Tetrahedron: Asymmetry*; 14, 951, **2003**.
- [36] N. Fröhlich, U. Pidun, M. Stahl, G. Frenking; "Carbenes as pure donor ligands: theoretical study of beryllium-carbene complexes"; *Organometallics*; 16, 442, **1997**.
- [37] W. A. Herrmann; "N-heterocyclic carbenes: a new concept in organometallic catalysis"; *Angewandte Chemie International Edition*; 41, 1290, **2002**.
- [38] X. Hu, Y. Tang, P. Gantzel, K. Meyer; "Silver complexes of a novel tripodal N-heterocyclic carbene ligand: evidence for significant metal-carbene π -interaction"; *Organometallics*; 22, 612, **2003**.
- [39] N. M. Scott, R. Dorta, E. D. Stevens, A. Correa, L. Cavallo, S. P. Nolan; "Interaction of a bulky N-heterocyclic carbene ligand with Rh(I) and Ir(I). Double C-H activation and

- isolation of bare 14-electron Rh(III) and Ir(III) complexes"; *Journal of the American Chemical Society*; 127, 3516, **2005**.
- [40] A. A. D. Tulloch, A. A. Danopoulos, S. Kleinhenz, M. E. Light, M. B. Hursthouse, G. Eastham; "Structural diversity in pyridine-N-functionalized carbene copper(I) complexes"; *Organometallics*; 20, 2027, **2001**.
- [41] R. Dorta, E. D. Stevens, S. P. Nolan; "Double C-H activation in a Rh-NHC complex leading to the isolation of a 14-electron Rh(III) complex"; *Journal of the American Chemical Society*; 126, 5054, **2004**.
- [42] C. A. Tolman; "Steric effects of phosphorus ligands in organometallic chemistry and homogeneous catalysis"; *Chemical Reviews*; 77, 313, **1977**.
- [43] A. Poater, B. Cosenza, A. Correa, S. Giudice, F. Ragone, V. Scarano, L. Cavallo; "SambVca: a web application for the calculation of the buried volume of N-heterocyclic carbene ligands"; *European Journal of Inorganic Chemistry*; 2009, 1759, **2009**.
- [44] A. J. Arduengo III, J. R. Goerlich, W. J. Marshall; "A stable diaminocarbene"; *Journal of the American Chemical Society*; 117, 11027, **1995**.
- [45] D. Vagedes, G. Erker, G. Kehr, K. Bergander, O. Kataeva, R. Fröhlich, S. Grimme, C. Mück-Lichtenfeld; "Tris(pentafluorophenyl)borane adducts of substituted imidazoles: conformational features and chemical behavior upon deprotonation"; *Dalton Transactions*; 7, 1337, **2003**.
- [46] I. I. Padilla-Martínez, M. D. J. Rosalez-Hoz, R. Contreras, S. Kersch, B. Wrackmeyer; "From azole-borane adducts to azaboles - Molecular structure of an imidazabole"; *Chemische Berichte*; 127, 343, **1994**.
- [47] R. Fränkel, C. Birg, U. Kernbach, T. Habereeder, H. Noth, W. P. Fehlhammer; "A homoleptic carbene-lithium complex"; *Angewandte Chemie International Edition*; 40, 1907, **2001**.
- [48] A. Biffis, G. Gioia Lobbia, G. Papini, M. Pellei, C. Santini, E. Scattolin, C. Tubaro; "Novel scorpionate-type triscarbene ligands and their silver and gold complexes"; *Journal of Organometallic Chemistry*; 693, 3760, **2008**.
- [49] G. Papini, G. Bandoli, A. Dolmella, G. Gioia Lobbia, M. Pellei, C. Santini; "New homoleptic carbene transfer ligands and related coinage metal complexes"; *Inorganic Chemistry Communications*; 11, 1103, **2008**.

- [50] G. Papini, M. Pellei, G. Gioia Lobbia, A. Burini, C. Santini; "Sulfonate- or carboxylate-functionalized N-heterocyclic bis-carbene ligands and related water soluble silver complexes"; *Dalton Transactions*; 35, 6985, **2009**.
- [51] T. W. Hambley; "Developing new metal-based drugs therapeutics: challenges and opportunities"; *Dalton Transactions*; 21, 4929, **2007**.
- [52] C. Santini, M. Pellei, V. Gandin, M. Porchia, F. Tisato, C. Marzano; "Advances in copper complexes as anticancer agents"; *Chemical Reviews*; 114, 815, **2014**.
- [53] F. Arnesano, G. Natile; "Mechanistic insight into the cellular uptake and processing of cisplatin 30 years after approval by FDA"; *Coordination Chemistry Review*; 253, 2070, **2009**.
- [54] Y. Jung, S. J. Lippard; "Direct cellular responses to platinum-induced DNA damage"; *Chemical Reviews*; 107, 1387, **2007**.
- [55] T. Boulikas, A. Pantos, E. Bellis, P. Christofis; "Optimizing liposomal cisplatin efficacy through membrane composition manipulations"; *Cancer Therapy*; 5, 537, **2007**.
- [56] P. C. Bruijninx, P. J. Sadler; "New trends for metal complexes with anticancer activity"; *Current Opinion in Chemical Biology*; 12, 197, **2008**.
- [57] F. Tisato, C. Marzano, M. Porchia, M. Pellei, C. Santini; "Copper in diseases and treatments, and copper-based anticancer strategies"; *Medicinal Research Reviews*; 30, 708, **2010**.
- [58] C. Marzano, M. Pellei, F. Tisato, C. Santini; "Copper complexes as anticancer agents"; *Anticancer Agents in Medicinal Chemistry*; 9, 185, **2009**.
- [59] C. J. Anderson, M. J. Welch; "Radiometal-labeled agents (non-technetium) for diagnostic imaging"; *Chemical Reviews*; 99, 2219, **1999**.
- [60] E. Gaggelli, H. Kozlowski, D. Valensin, G. Valensin; "Copper homeostasis and neurodegenerative disorders (Alzheimer's, prion, and Parkinson's diseases and amyotrophic lateral sclerosis)"; *Chemical Reviews*; 106, 1995, **2006**.
- [61] S. K. Gupta, V. K. Shukla, M. P. Vaidya, S. K. Roy, S. Gupta; "Serum trace elements and Cu/Zn ratio in breast cancer patients"; *Journal of Surgical Oncology*; 46, 178, **1991**.
- [62] H. Xie, Y. J. Kang; "Role of copper in angiogenesis and its medicinal implications"; *Current Medicinal Chemistry*; 16, 1304, **2009**.
- [63] X. Peng, V. Gandhi; "ROS-activated anticancer prodrugs: a new strategy for tumor-specific damage"; *Therapeutic Delivery*; 3, 823, **2012**.

- [64] J. Yuan, D. B. Lovejoy, D. R. Richardson; "Novel di-2-pyridyl-derived iron chelators with marked and selective antitumor activity: in vitro and in vivo assessment"; *Blood*; 104, 1450, **2004**.
- [65] J. Yoshii, H. Yoshiji, S. Kuriyama, Y. Ikenaka, R. Noguchi, H. Okuda, H. Tsujinoue, T. Nakatani, H. Kishida, D. Nakae, D. E. Gomez, M. S. De Lorenzo, A. M. Tejera, H. Fukui; "The copper-chelating agent, trientine, suppresses tumor development and angiogenesis in the murine hepatocellular carcinoma cells"; *International Journal of Cancer*; 94, 768, **2001**.
- [66] H. I. Pass, G. J. Brewer, R. Dick, M. Carbone, S. Merajver; "A phase II trial of tetrathiomolybdate after surgery for malignant mesothelioma: final results"; *The Annals of Thoracic Surgery*; 86, 383, **2008**.
- [67] N. Kitajima, Y. Moro-oka; "Copper-dioxygen complexes. Inorganic and bioinorganic perspectives"; *Chemical Reviews*; 94, 737, **1994**.
- [68] K. D. Karlin, S. Itoh, S. Rokita; *Copper-oxygen chemistry*; Wiley; **2011**.
- [69] G. L. Eichhorn, Y. A. Shin; "Interaction of metal ions with polynucleotides and related compounds. XII. The relative effect of various metal ions on DNA helicity"; *Journal of the American Chemical Society*; 90, 7323, **1968**.
- [70] P. M. Takahara, C. A. Frederick, S. J. Lippard; "Crystal structure of the anticancer drug cisplatin bound to duplex DNA"; *Journal of the American Chemical Society*; 118, 12309, **1996**.
- [71] Y. Qin, L. Meng, C. Hu, W. Duan, Z. Zuo, L. Lin, X. Zhang, J. Ding; "Gambogic acid inhibits the catalytic activity of human topoisomerase II α by binding to its ATPase domain"; *Molecular Cancer Therapeutics*; 6, 2429, **2007**.
- [72] J. M. Peters, W. W. Franke, J. A. Kleinschmidt; "Distinct 19 S and 20 S subcomplexes of the 26 S proteasome and their distribution in the nucleus and the cytoplasm"; *Journal of Biological Chemistry*; 269, 7709, **1994**.
- [73] A. L. Goldberg; "Functions of the proteasome: the lysis at the end of the tunnel"; *Science*; 268, 522, **1995**.
- [74] Q. P. Dou, D. Smith, K. G. Daniel, A. Kazi; "Interruption of tumor cell cycle progression through proteasome inhibition: implications for cancer therapy"; *Progress in Cell Cycle Research*; 5, 441, **2003**.
- [75] H. C. Drexler; "Activation of the cell death program by inhibition of proteasome function"; *Proceedings of the National Academy of Sciences*; 94, 855, **1997**.

- [76] C. Santini, M. Pellei, G. Papini, B. Morresi, R. Galassi, S. Ricci, F. Tisato, M. Porchia, M. P. Rigobello, V. Gandin, C. Marzano; "In vitro antitumour activity of water soluble Cu(I), Ag(I) and Au(I) complexes supported by hydrophilic alkyl phosphine ligands"; *Journal of Inorganic Biochemistry*; 105, 232, **2011**.
- [77] M. A. Rudek, C. H. Chau, W. D. Figg, H. L. McLeod; *Handbook of anticancer pharmacokinetics and pharmacodynamics*; Humana Press; **2004**.
- [78] M. P. Hay, W. R. Wilson, J. W. Moselen, B. D. Palmer, W. A. Denny; "Hypoxia-selective antitumor agents. 8. Bis(nitroimidazolyl)alkanecarboxamides: a new class of hypoxia-selective cytotoxins and hypoxic cell radiosensitisers"; *Journal of Medicinal Chemistry*; 37, 381, **1994**.
- [79] A. Brecia, B. Cavalleri, G. E. Adams; *Nitroimidazoles, chemistry, pharmacology and clinical application*; Plenum; **1982**.
- [80] A. Nunn, K. Linder, H. W. Strauss; *European Journal of Nuclear Medicine*; 22, 265, **1995**.
- [81] E. L. Engelhardt, R. F. Schneider, S. H. Seeholzer, C. C. Stobbe, J. D. Chapman; "The synthesis and radiolabeling of 2-nitroimidazole derivatives of cyclam and their preclinical evaluation as positive markers of tumor hypoxia"; *Journal of Nuclear Medicine*; 43, 837, **2002**.
- [82] Z. Li, T. Chu, X. Liu, X. Wang; "Synthesis and in vitro and in vivo evaluation of three radioiodinated nitroimidazole analogues as tumor hypoxia markers"; *Nuclear Medicine and Biology*; 32, 225, **2005**.
- [83] P. D. Bonnitca, S. R. Bayly, M. B. M. Theobald, H. M. Betts, J. S. Lewis, J. R. Dilworth; "Nitroimidazole conjugates of bis(thiosemicarbazonato)⁶⁴Cu(II) - Potential combination agents for the PET imaging of hypoxia"; *Journal of Inorganic Biochemistry*; 104, 126, **2010**.
- [84] S. Patterson, S. Wyllie; "Nitro drugs for the treatment of trypanosomatid diseases: past, present, and future prospects"; *Trends in Parasitology*; 30, 289, **2014**.
- [85] D. I. Edwards; "Nitroimidazole drugs - Action and resistance mechanisms II. Mechanisms of resistance"; *Journal of Antimicrobial Chemotherapy*; 31, 201, **1993**.
- [86] J. A. Castro, M. M. de Mecca, L. C. Bartel; "Toxic side effects of drugs used to treat Chagas' disease (American Trypanosomiasis)"; *Human & Experimental Toxicology*; 25, 471, **2006**.
- [87] R. C. Santra, D. Ganguly, S. Jana, N. Banyal, J. Singh, A. Saha, S. Chattopadhyay, K. Mukhopadhyay, S. Das; "Synthesizing a Cu^{II} complex of tinidazole to tune the

- generation of the nitro radical anion in order to strike a balance between efficacy and toxic side effects"; *New Journal of Chemistry*; 41, 4879, **2017**.
- [88] A. Sanz-Clemente, R. A. Nicoll, K. W. Roche; "Diversity in NMDA receptor composition: many regulators, many consequences"; *Neuroscientist*; 19, 62, **2013**.
- [89] P. Paoletti, C. Bellone, Q. Zhou; "NMDA receptor subunit diversity: impact on receptor properties, synaptic plasticity and disease"; *Nature Reviews Neuroscience*; 14, 383, **2013**.
- [90] V. Gandin, M. Pellei, F. Tisato, M. Porchia, C. Santini, C. Marzano; "A novel copper complex induces paraptosis in colon cancer cells via the activation of ER stress signalling"; *Journal of Cellular and Molecular Medicine*; 16, 142, **2012**.
- [91] S. I. Deutsch, A. H. Tang, J. A. Burket, A. D. Benson; "NMDA receptors on the surface of cancer cells: target for chemotherapy?"; *Biomedicine & Pharmacotherapy*; 68, 493, **2014**.
- [92] A. Mehrotra; R. K. Koiri; *International journal of immunotherapy and cancer research*; 1, 13, **2015**.
- [93] K. Nath, L. L. Guo, B. Nancolas, D. S. Nelson, A. A. Shestov, S. C. Lee, J. Roman, R. Zhou, D. B. Leeper, A. P. Halestrap, I. A. Blair, J. D. Glickson; "Mechanism of antineoplastic activity of lonidamine"; *Biochimica et Biophysica Acta (BBA) - Reviews on Cancer*; 1866, 151, **2016**.
- [94] D. Cervantes-Madrid, Y. Romero, A. Duenas-Gonzalez; "Reviving lonidamine and 6-diazo-5-oxo-L-norleucine to be used in combination for metabolic cancer therapy"; *BioMed Research International*; 2015, 690492, **2015**.
- [95] L. L. Guo, A. A. Shestov, A. J. Worth, K. Nath, D. S. Nelson, D. B. Leeper, J. D. Glickson, I. A. Blair; "Inhibition of mitochondrial complex II by the anticancer agent lonidamine"; *Journal of Biological Chemistry*; 291, 42, **2016**.
- [96] R. N. Sadeghi, F. Karami-Tehrani, S. Salami; "Targeting prostate cancer cell metabolism: impact of hexokinase and CPT-1 enzymes"; *Tumor Biology*; 36, 2893, **2014**.
- [97] K. Nath, D. S. Nelson, D. F. Heitjan, D. B. Leeper, R. Zhou, J. D. Glickson; "Lonidamine induces intracellular tumor acidification and ATP depletion in breast, prostate and ovarian cancer xenografts and potentiates response to doxorubicin"; *Nmr in Biomedicine*; 28, 281, **2015**.
- [98] M. Crompton; "The mitochondrial permeability transition pore and its role in cell death"; *Biochemical Journal*; 341, 233, **1999**.

- [99] H. Chen, F. Chen, W. Hu, S. Gou; "Effective platinum(IV) prodrugs conjugated with lonidamine as a functional group working on the mitochondria"; *Journal of Inorganic Biochemistry*; 180, 119, **2018**.
- [100] R. G. Bergman; "C-H activation"; *Nature*, 446, 391, **2007**.
- [101] J. Wencel-Delord, T. Dröge, F. Liu, F. Glorius; "Towards mild metal-catalyzed C-H bond activation"; *Chemical Society Reviews*; 40, 4740, **2011**.
- [102] F. Ullmann, G. Wolfgang, Y. S. Yamamoto, F. T. Campbell, R. Pfefferkorn, J. Rounsaville; *Ullmann's encyclopedia of industrial chemistry*; volume A3; Wiley-VCH; **1985**.
- [103] M. S. Kharasch, G. Sosnovsky; "The reactions of t-butyl perbenzoate and olefins - A stereospecific reaction"; *Journal of American Chemical Society*; 80, 756, **1958**.
- [104] M. S. Kharasch, G. Sosnovsky, N. C. Yang; "Reactions of t-butyl peresters. I. The reaction of peresters with olefins"; *Journal of the American Chemical Society*; 81, 5819, **1959**.
- [105] D. J. Rawlinson, G. Sosnovsky; "One-step substitutive acyloxylation at carbon. Part I. Reactions involving peroxides"; *Synthesis*; 1972, 1, **1972**.
- [106] M. B. Andrus, J. C. Lashley; "Copper catalyzed allylic oxidation with peresters"; *Tetrahedron*; 58, 845, **2002**.
- [107] J. Eames, M. Watkinson; "Catalytic allylic oxidation of alkenes using an asymmetric Kharasch-Sosnovsky reaction"; *Angewandte Chemie International Edition*; 40, 3567, **2001**.
- [108] Q. Tan, M. Hayashi; "Novel N,N-bidentate ligands for enantioselective copper(I)-catalyzed allylic oxidation of cyclic olefins"; *Advanced Synthesis & Catalysis*; 350, 2639, **2008**.
- [109] D. Tetour, M. Novotná, J. Hodačová; "Enantioselective Henry reaction catalyzed by copper(II) complex of bis(*trans*-cyclohexane-1,2-diamine)-based ligand"; *Catalysts*; 11, 41, **2021**.
- [110] H. Sigel, R. B. Martin; "Coordinating properties of the amide bond. Stability and structure of metal ion complexes of peptides and related ligands"; *Chemical Reviews*; 82, 385, **1982**.
- [111] F. H. Allen; "The Cambridge structural database: a quarter of a million crystal structures and rising"; *Acta Crystallographica Section B*; B58, 380, **2002**.

- [112] M. Meisters, J. T. Vandeberg, F. P. Cassaretto, H. Posvic, C. E. Moore; "Studies in the tetraarylborates: part V. The influence of substituents on the stability of tetraarylborates"; *Analytica Chimica Acta*; 49, 481, **1970**.
- [113] P. K. Bakshi, A. Linden, B. R. Vincent, S. P. Roe, D. Adhikesavalu, T. S. Cameron, O. Knop; "Crystal chemistry of tetraradial species. Part 4. Hydrogen bonding to aromatic π systems: crystal structures of fifteen tetraphenylborates with organic ammonium cations"; *Canadian Journal of Chemistry*; 72, 1273, **1994**.
- [114] G. Bélanger-Chabot, S. M. Kaplan, P. Deokar, N. Szimhardt, R. Haiges, K. O. Christe; "Synthesis and characterization of nitro-, trinitromethyl-, and fluorodinitromethyl-substituted triazolyl- and tetrazolyl-trihydridoborate anions"; *Chemistry - A European Journal*; 23, 13087, **2017**.
- [115] S. G. Ridlen, N. Kulkarni, H. V. R. Dias; "Monoanionic, bis(pyrazolyl)methylborate $[(\text{Ph}_3\text{B})\text{CH}(\text{3,5-(CH}_3)_2\text{Pz})_2]^-$ as a supporting ligand for copper(I)-ethylene, *cis*-2-butene, and carbonyl complexes"; *Inorganic Chemistry*; 56, 7237, **2017**.
- [116] B. Kozlevčar, P. Gamez, R. de Gelder, Z. Jagličić, P. Strauch, N. Kitanovski, J. Reedijk; "Counterion and solvent effects on the primary coordination sphere of copper(II) bis(3,5-dimethylpyrazol-1-yl)acetic acid coordination compounds"; *European Journal of Inorganic Chemistry*; 2011, 3650, **2011**.
- [117] C. K. Johnson; ORTEP, report ORNL-5138, Oak Ridge national laboratory, Oak Ridge, TN; **1976**.
- [118] B. Kozlevčar, T. Pregelj, A. Pevec, N. Kitanovski, J. S. Costa, G. Van Albada, P. Gamez, J. Reedijk; "Copper complexes with the ligand methyl bis(3,5-dimethylpyrazol-1-yl)acetate (Mebdmpza), generated by in situ methanolic esterification of bis(3,5-dimethylpyrazol-1-yl)acetic acid"; *European Journal of Inorganic Chemistry*; 31, 4977, **2008**.
- [119] B. Quillian, W. E. Lynch, C. W. Padgett, A. Lorbecki, A. Petrillo, M. Tran; "Syntheses and crystal structures of copper(II) bis(pyrazolyl)acetic acid complexes"; *Journal of Chemical Crystallography*; 49, 1, **2019**.
- [120] M. A. Romero, J. M. Salas, M. Quiros, M. P. Sanchez, J. Romero, D. Martin; "Structural and magnetic studies on a bromine-bridged copper(II) dimer with 5,7-dimethyl[1,2,4]triazolo[1,5-a]pyrimidine"; *Inorganic Chemistry*; 33, 5477, **1994**.

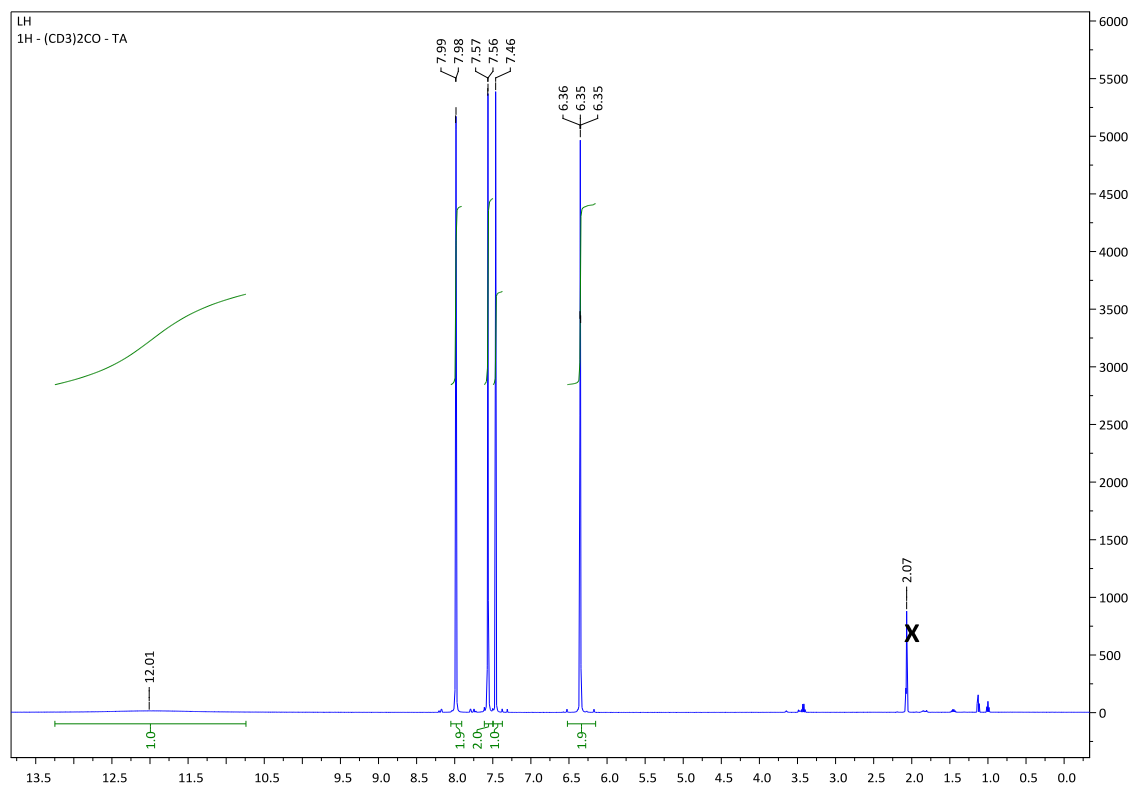
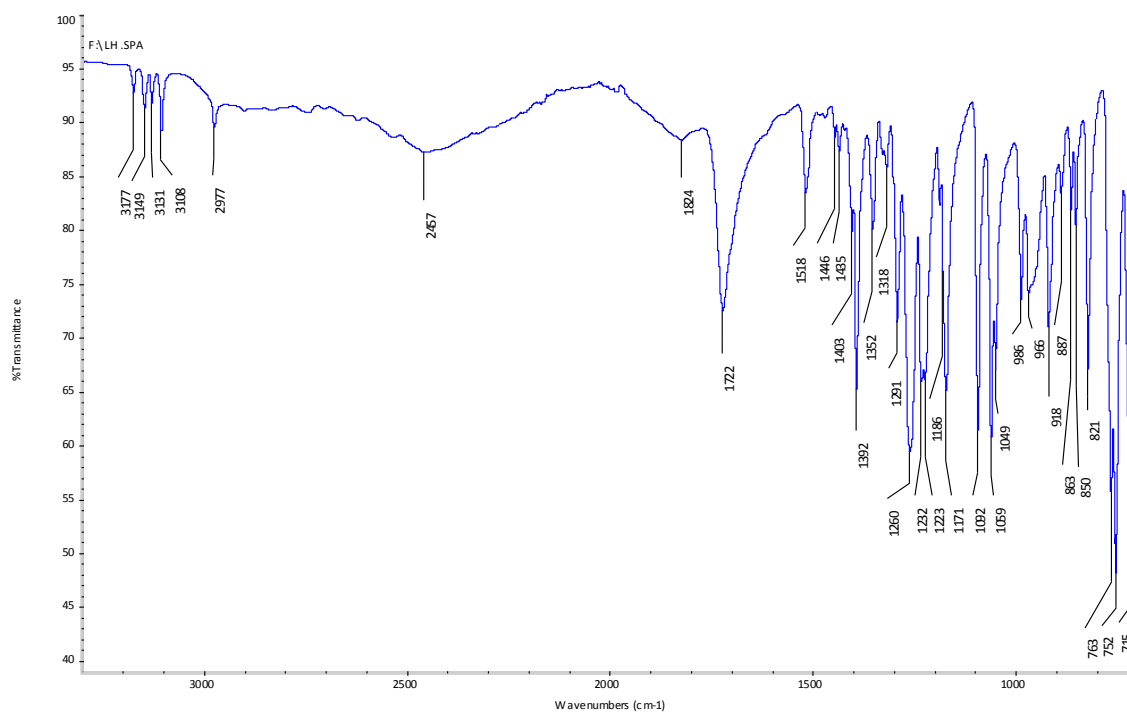
- [121] L. G. Lavrenova, V. N. Ikorskij, L. A. Sheludyakova, D. Y. Naumov, E. G. Boguslavskij; "Co(II), Ni(II) and Cu(II) complexes with 1-(4-hydroxyphenyl)-1H-1,2,4-triazole"; *Russian Journal of Coordination Chemistry*; 30, 442, **2004**.
- [122] L. Dobrzanska, D. J. Kleinhans, L. J. Barbour; "Influence of the metal-to-ligand ratio on the formation of metal organic complexes"; *New Journal of Chemistry*; 32, 813, **2008**.
- [123] A. Hoffmann, S. Herres-Pawlis; "Dissection of different donor abilities within bis(pyrazolyl)pyridinylmethane transition metal complexes"; *Zeitschrift für Anorganische und Allgemeine Chemie*; 639, 1426, **2013**.
- [124] T. N. Andreeva, A. S. Lyakhov, L. S. Ivashkevich, S. V. Voitekhovich, Y. V. Grigoriev, O. A. Ivashkevich; "1-(furan-2-ylmethyl)-1H-tetrazole and its copper(II) complexes"; *Zeitschrift für Anorganische und Allgemeine Chemie*; 641, 2312, **2015**.
- [125] I. I. Dyukova, T. A. Kuz'menko, V. Y. Komarov, T. S. Sukhikh, E. V. Vorontsova, L. G. Lavrenova; "Coordination compounds of cobalt(II), nickel(II), and copper(II) halides with 2-methyl-1,2,4-triazolo[1,5-a]benzimidazole"; *Russian Journal of Coordination Chemistry*; 44, 755, **2018**.
- [126] C. F. Macrae, I. J. Bruno, J. A. Chisholm, P. R. Edgington, P. McCabe, E. Pidcock, L. Rodriguez-Monge, R. Taylor, J. Van De Streek, P. A. Wood; "Mercury CSD 2.0 - New features for the visualization and investigation of crystal structures"; *Journal of Applied Crystallography*; 41, 466, **2008**.
- [127] C. Battocchio, I. Fratoddi, G. Iucci, M. V. Russo, A. Goldoni, P. Parent, G. Polzonetti; "Dinuclear Pt and Pd complexes with metalloporphyrin bridges: a NEXAFS study of the electronic structure and self-assembling properties"; *Materials Science and Engineering: C*; 27,1338, **2007**.
- [128] G. Polzonetti, C. Battocchio, A. Goldoni, R. Larciprete, V. Carravetta, R. Paolesse, M. V. Russo; "Interface formation between C60 and diethynyl-Zn-porphyrinato investigated by SR-induced photoelectron and near-edge X-ray absorption (NEXAFS) spectroscopies"; *Chemical Physics*; 297, 307, **2004**.
- [129] J. Y. Jhuang, S. H. Lee, S. W. Chen, Y. H. Chen, Y. J. Chen, J. L. Lin, C. H. Wang, Y. W. Yang; "Adsorption and reaction pathways of 1H-pyrazole on Cu(100) and O/Cu(100)"; *The Journal of Physical Chemistry C*; 122, 6195, **2018**.
- [130] NIST, X-ray Photoelectron Spectroscopy Database, Version 4.1, National Institute of Standards and Technology, <http://srdata.nist.gov/xps/>.

- [131] D. A. Outka, J. Stöhr, R. J. Madix, H. H. Rotermund, B. Hermsmeier, J. Solomon; "NEXAFS studies of complex alcohols and carboxylic acids on the Si(111)(7×7) surface"; *Surface Science*; 185, 53, **1987**.
- [132] A. V. Syugaev, A. N. Maratkanova, D. A. Smirnov; "Molecular orientation in electrodeposited polypyrrole films"; *Journal of Solid State Electrochemistry*; 22, 2127, **2018**.
- [133] J. Stöhr; *NEXAFS spectroscopy*; Springer Science & Business Media; **2013**.
- [134] V. Secchi, S. Franchi, D. Ciccarelli, M. Dettin, A. Zamuner, A. Serio, G. Iucci, C. Battocchio; "Biofunctionalization of TiO₂ surfaces with self-assembling layers of oligopeptides covalently grafted to chitosan"; *ACS Biomaterials Science & Engineering*; 5, 2190, **2019**.
- [135] V. Secchi, S. Franchi, M. Santi, A. Vladescu, M. Braic, T. Skála, J. Nováková, M. Dettin, A. Zamuner, G. Iucci, C. Battocchio; "Biocompatible materials based on self-assembling peptides on Ti₂₅Nb₁₀Zr alloy: molecular structure and organization investigated by synchrotron radiation induced techniques"; *Nanomaterials*; 8, 148, **2018**.
- [136] G. Aquilanti, M. Giorgetti, M. Minicucci, G. Papini, M. Pellei, M. Tegoni, A. Trasatti, C. Santini; "A study on the coordinative versatility of new N,S-donor macrocyclic ligands: XAFS, and Cu²⁺ complexation thermodynamics in solution"; *Dalton Transactions*; 40, 264, **2011**.
- [137] M. Giorgetti, L. Guadagnini, S. G. Fiddy, C. Santini, M. Pellei; "Cu K-edge EXAFS on copper(I) complexes containing dihydridobis(3-nitro-1,2,4-triazol-1-yl)borate and bis(1,2,4-triazol-1-yl)acetate ligand: evidence for the Cu-O interaction"; *Polyhedron*; 28, 3600, **2009**.
- [138] L. S. Kau, D. J. Spira-Solomon, J. E. Penner-Hahn, K. O. Hodgson, E. I. Solomon; "X-ray absorption edge determination of the oxidation state and coordination number of copper. Application to the type 3 site in *Rhus vernicifera* laccase and its reaction with oxygen"; *Journal of the American Chemical Society*; 109, 6433, **1987**.
- [139] J. Chaboy, A. Muñoz-Páez, F. Carrera, P. Merklings, E. S. Marcos; "Ab initio X-ray absorption study of copper K-edge XANES spectra in Cu(II) compounds"; *Physical Review B*; 71, 134208, **2005**.
- [140] A. L. Ankudinov, B. Ravel, J. J. Rehr, S. D. Conradson; "Real-space multiple-scattering calculation and interpretation of X-ray-absorption near-edge structure"; *Physical Review B*; 58, 7565, **1998**.

- [141] D. T. Clark, D. M. J. Lilley; "Molecular core binding energies for some five membered ring heterocycles as determined by X-ray photoelectron spectroscopy"; *Chemical Physics Letters*; 9, 234, **1971**.
- [142] C. Meneghini, F. Bardelli, S. Mobilio; "ESTRA-FitEXA: a software package for EXAFS data analysis"; *Nuclear Instruments and Methods in Physics Research Section B: Beam Interactions with Materials and Atoms*; 285, 153, **2012**.
- [143] C. Meneghini, S. Morante; "The active site structure of tetanus neurotoxin resolved by multiple scattering analysis in X-ray absorption spectroscopy"; *Biophysical Journal*; 75, 1953, **1998**.
- [144] E. Raymond, S. Faivre, S. Chaney, J. Woynarowski, E. Cvitkovic; "Cellular and molecular pharmacology of oxaliplatin"; *Molecular Cancer Therapeutics*; 1, 227, **2002**.
- [145] J. B. Kim; "Three-dimensional tissue culture models in cancer biology"; *Seminars in Cancer Biology*; 15, 365, **2005**.
- [146] A. Barilli, C. Atzeri, I. Bassanetti, F. Ingoglia, V. Dall'Asta, O. Bussolati, M. Maffini, C. Mucchino, L. Marchiò; "Oxidative stress induced by copper and iron complexes with 8-hydroxyquinoline derivatives causes paraptotic death of HeLa cancer cells"; *Molecular Pharmaceutics*; 11, 1151, **2014**.
- [147] A. Bonifazi, F. Del Bello, V. Mammoli, A. Piergentili, R. Petrelli, C. Cimarelli, M. Pellei, D. Schepmann, B. Wünsch, E. Barocelli, S. Bertoni, L. Flammini, C. Amantini, M. Nabissi, G. Santoni, G. Vistoli, W. Quaglia; "Novel potent N-methyl-D-aspartate (NMDA) receptor antagonists or σ_1 receptor ligands based on properly substituted 1,4-dioxane ring"; *Journal of Medicinal Chemistry*; 58, 8601, **2015**.
- [148] P. Noordhuis, A. C. Laan, K. van de Born, N. Losekoot, I. Kathmann, G. J. Peters; "Oxatiplatin activity in selected and unselected human ovarian and colorectal cancer cell lines"; *Biochemical Pharmacology*; 76, 53, **2008**.
- [149] M. Pellei, L. Bagnarelli, L. Luciani, F. Del Bello, G. Giorgioni, A. Piergentili, W. Quaglia, M. De Franco, V. Gandin, C. Marzano, C. Santini; "Synthesis and cytotoxic activity evaluation of new Cu(I) complexes of bis(pyrazol-1-yl) acetate ligands functionalized with an NMDA receptor antagonist"; *International Journal of Molecular Sciences*; 21, 2616, **2020**.
- [150] H. N. Xu, M. Feng, K. Nath, D. Nelson, J. Roman, H. Zhao, Z. Lin, J. Glickson, L. Z. Li; "Optical redox imaging of lonidamine treatment response of melanoma cells and xenografts"; *Molecular Imaging and Biology*; 21, 426, **2019**.
- [151] A. Zanella, V. Gandin, M. Porchia, F. Refosco, F. Tisato, F. Sorrentino, G. Scutari, M. P. Rigobello, C. Marzano; "Cytotoxicity in human cancer cells and mitochondrial dysfunction

- induced by a series of new copper(I) complexes containing tris(2-cyanoethyl)phosphines"; *Investigational New Drugs*; 29, 1213, **2011**.
- [152] J. Nordberg, E. S. J. Arnér; "Reactive oxygen species, antioxidants, and the mammalian thioredoxin system"; *Free Radical Biology and Medicine*; 31, 1287, **2001**.

SUPPORTING INFORMATION

Figure 6.1. - ¹H-NMR of ligand L^{1H} (1) in (CD₃)₂CO.Figure 6.2. - FT-IR of ligand L^{1H} (1).

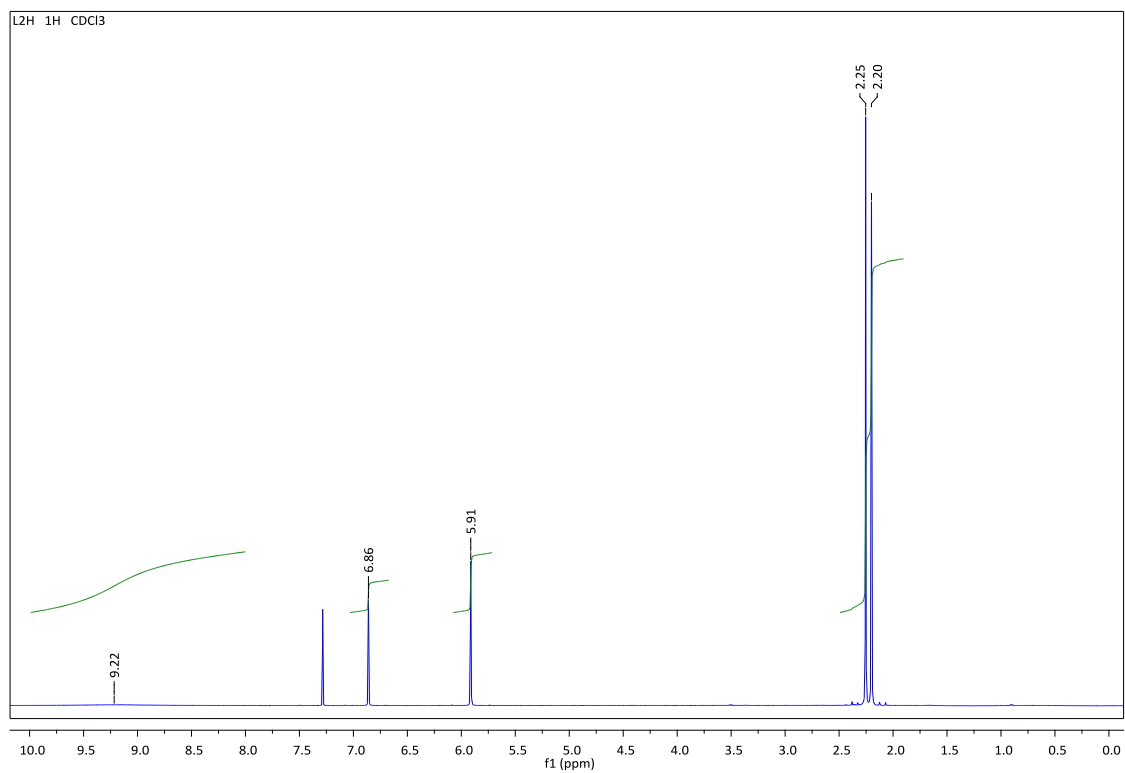


Figure 6.3. - $^1\text{H-NMR}$ of ligand $\text{L}^{2\text{H}}$ (**2**) in CDCl_3 .

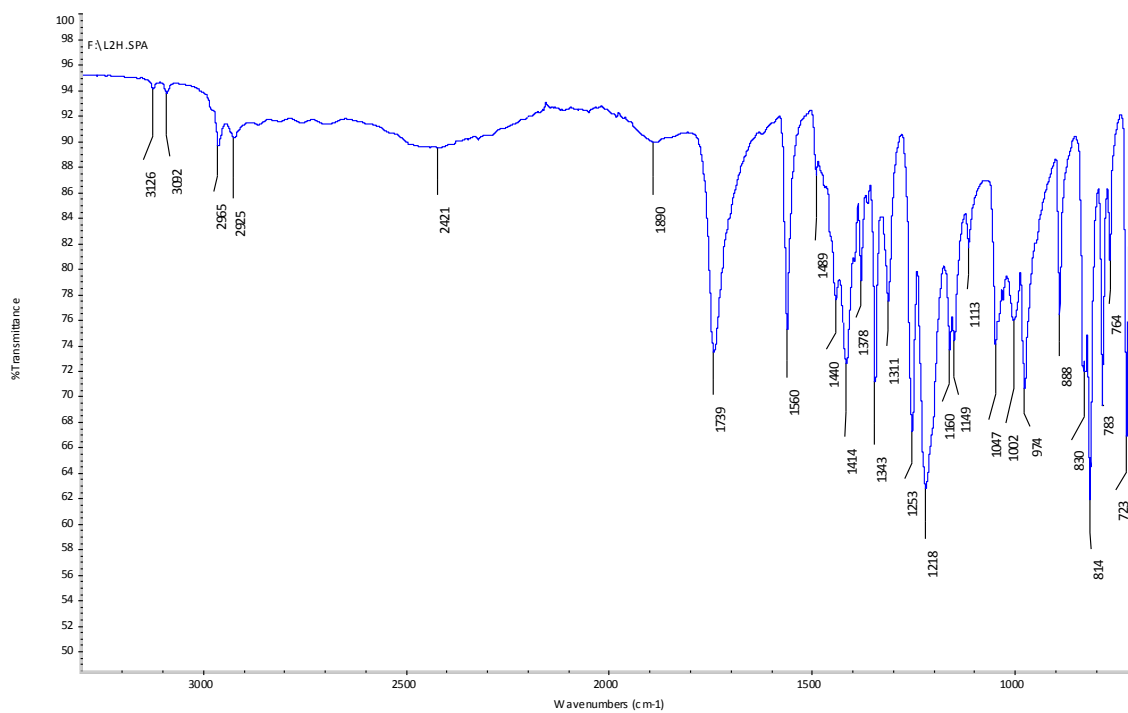


Figure 6.4. - FT-IR of ligand $\text{L}^{2\text{H}}$ (**2**).

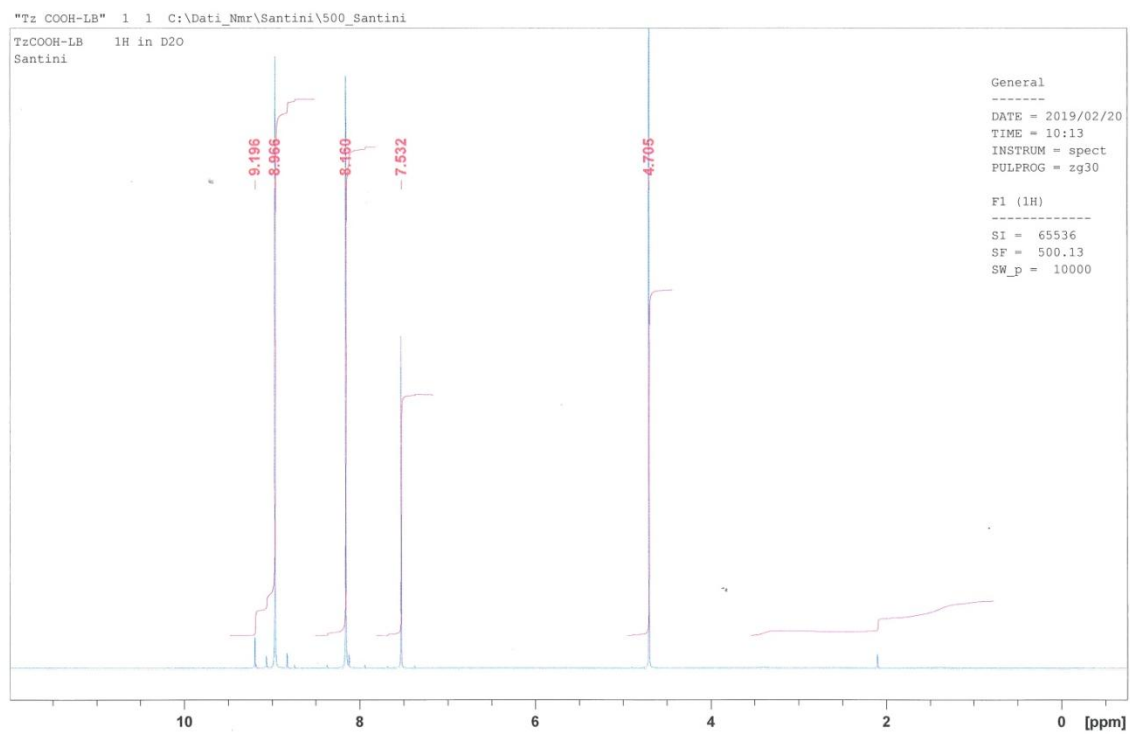


Figure 6.5. - $^1\text{H-NMR}$ of ligand $\text{L}^{3\text{H}}$ (**3**) in D_2O .

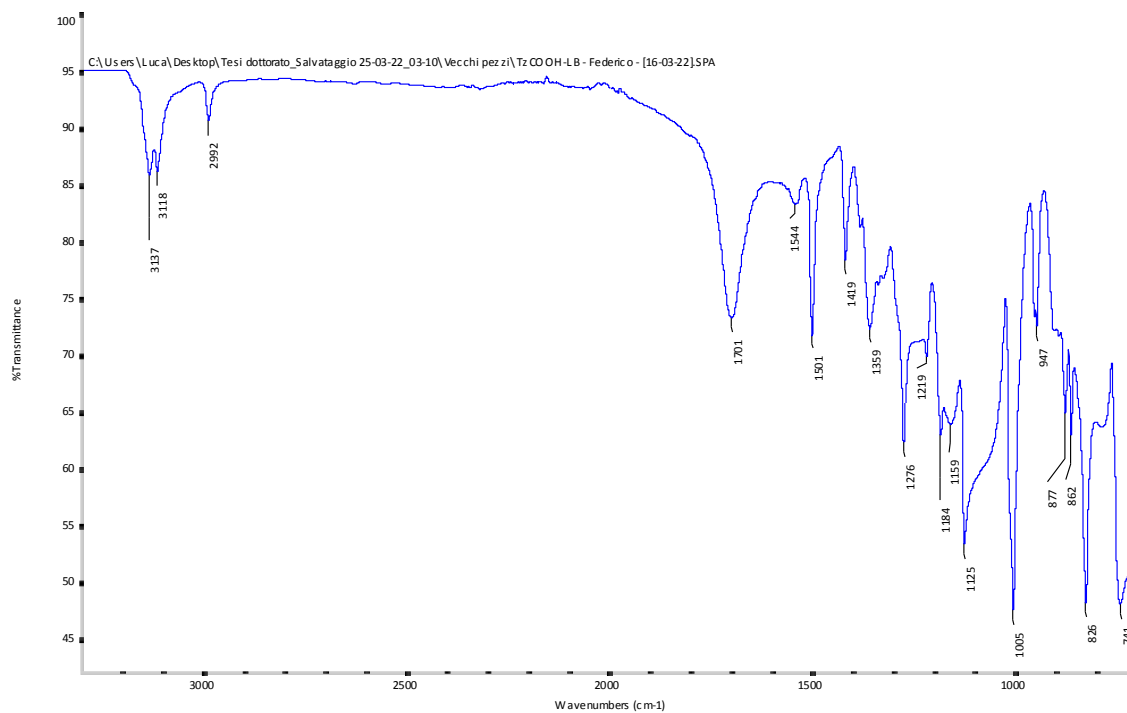


Figure 6.6. - FT-IR of ligand $\text{L}^{3\text{H}}$ (**3**).

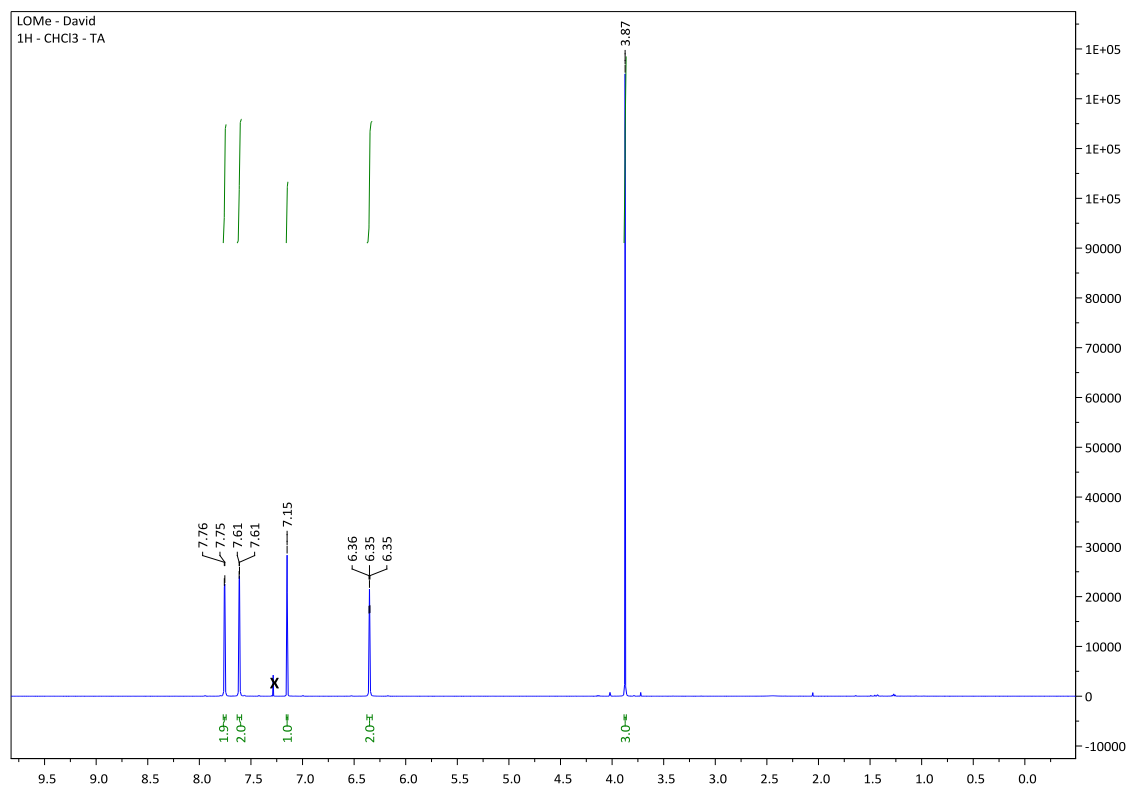


Figure 6.7. - $^1\text{H-NMR}$ of ligand $\text{L}^{1\text{Me}}$ (**4**) in CDCl_3 .

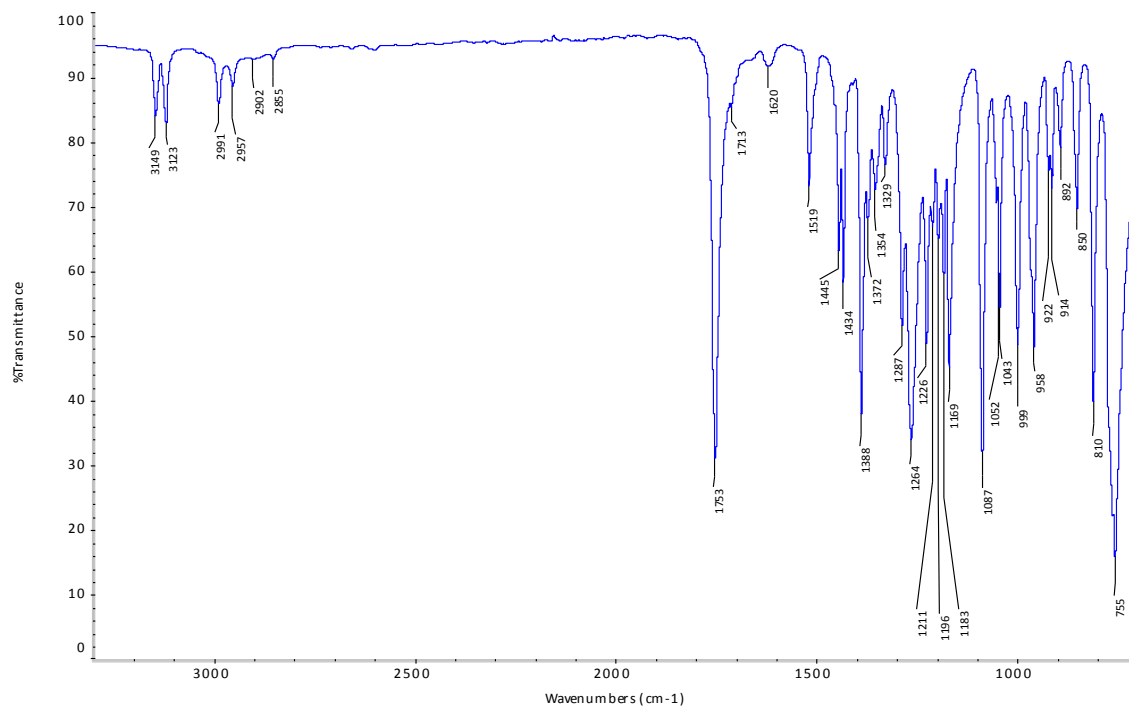
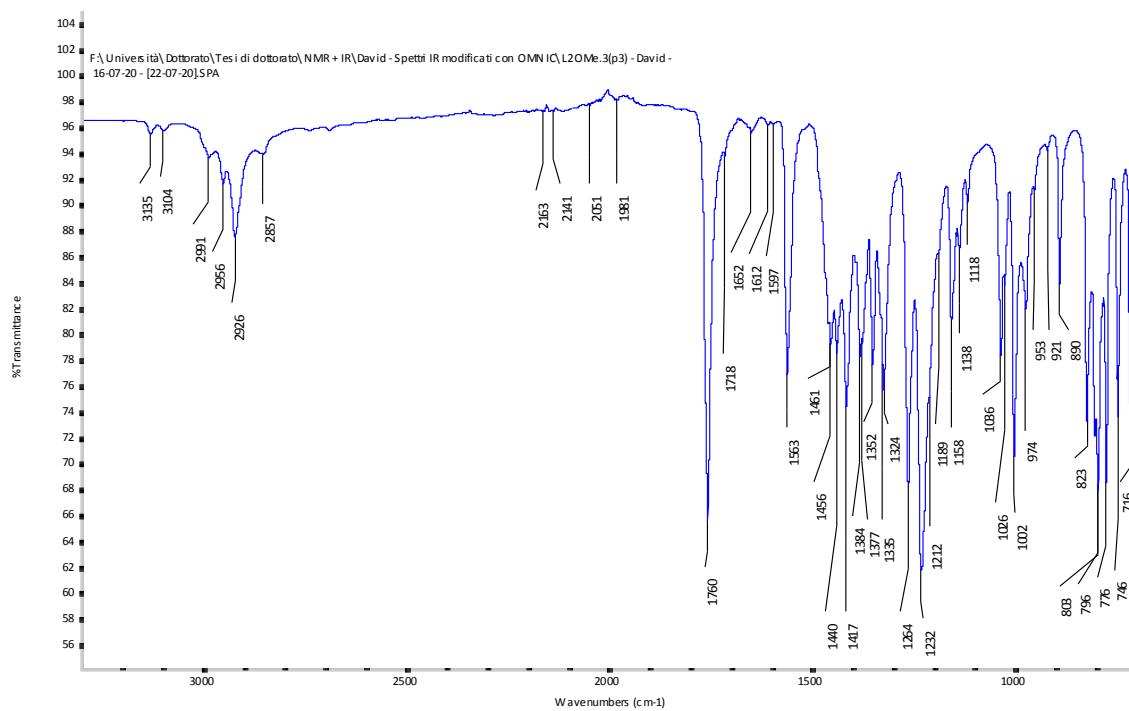
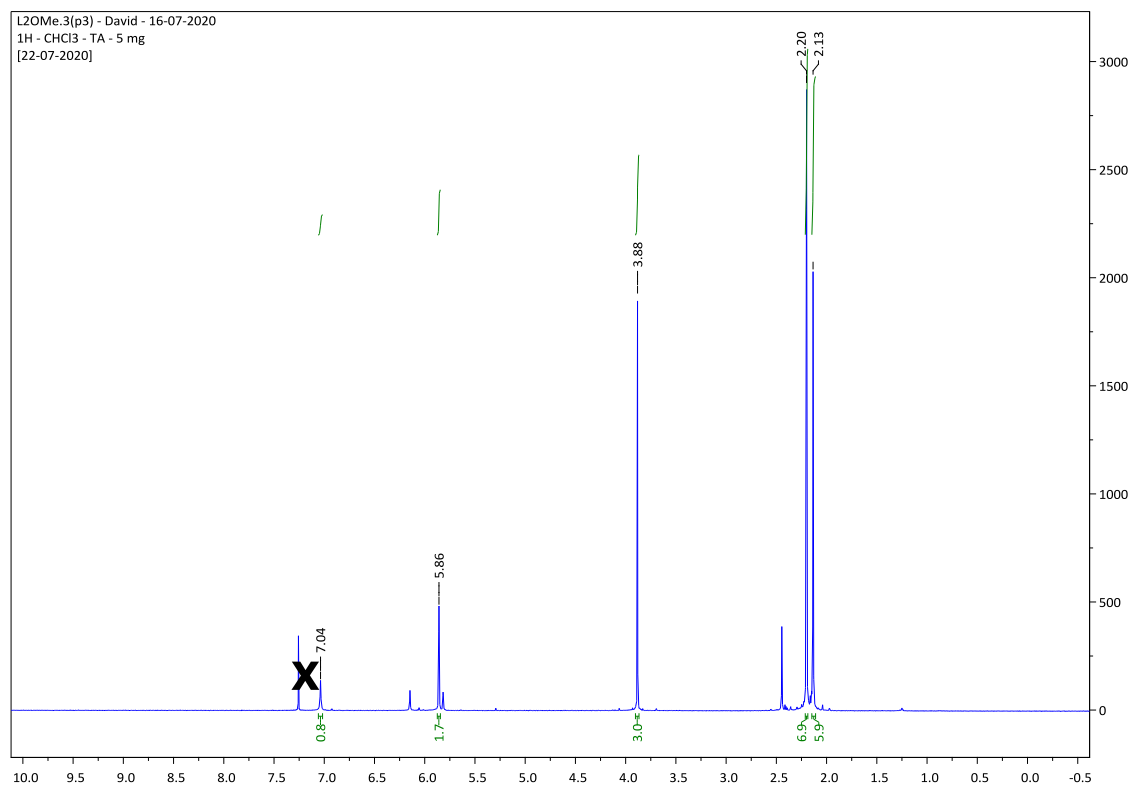


Figure 6.8. - FT-IR of ligand $\text{L}^{1\text{Me}}$ (**4**).



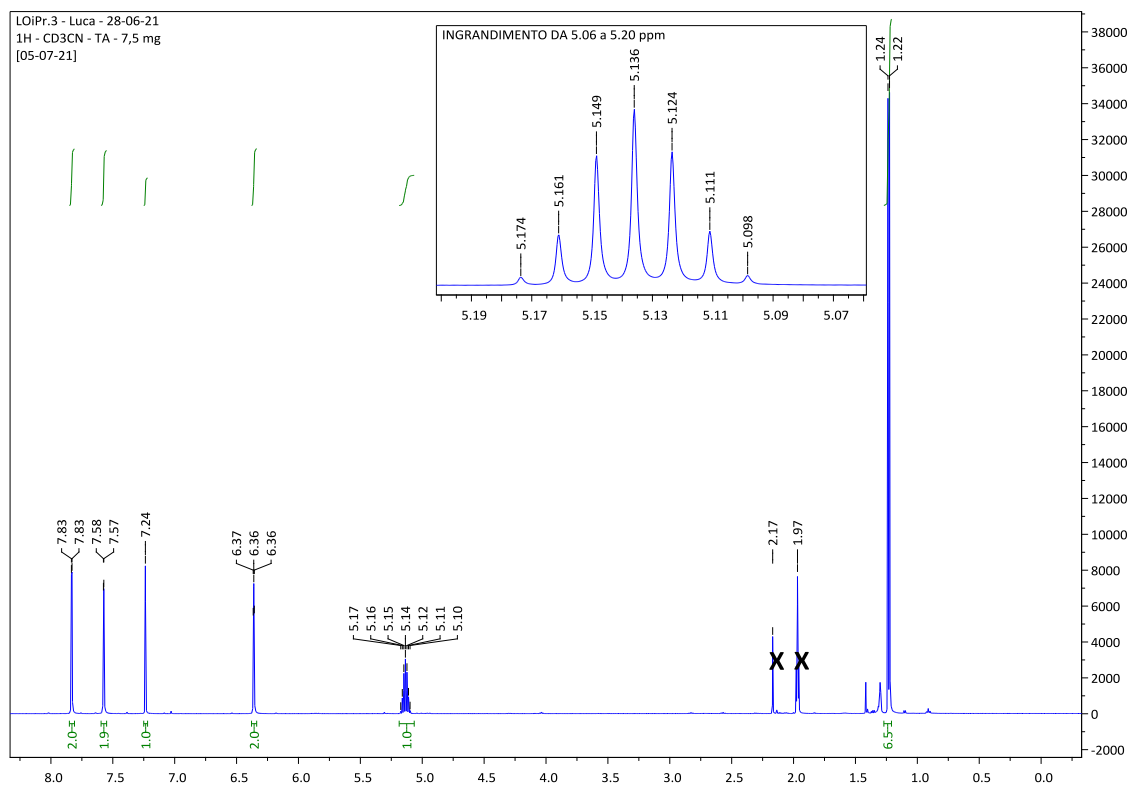


Figure 6.11. - $^1\text{H-NMR}$ of ligand $\text{L}^{1\text{iPr}}$ (**6**) in CD_3CN .

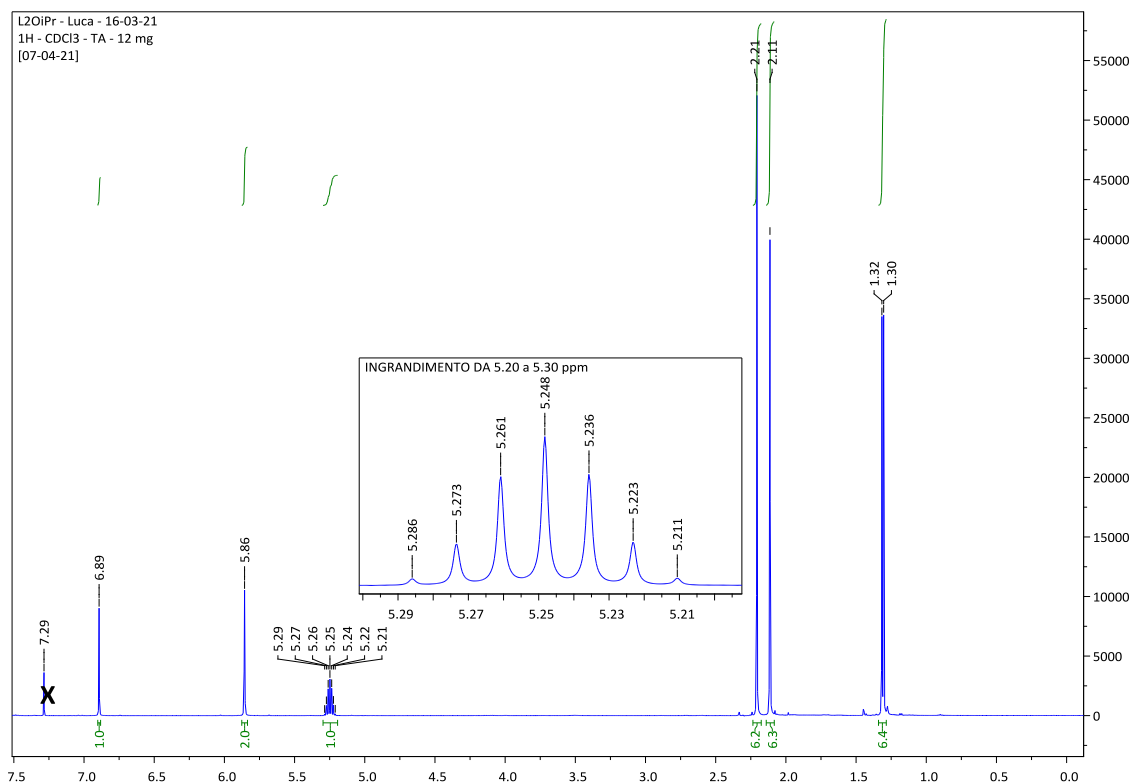


Figure 6.12. - $^1\text{H-NMR}$ of ligand $\text{L}^{2\text{iPr}}$ (**7**) in CDCl_3 .

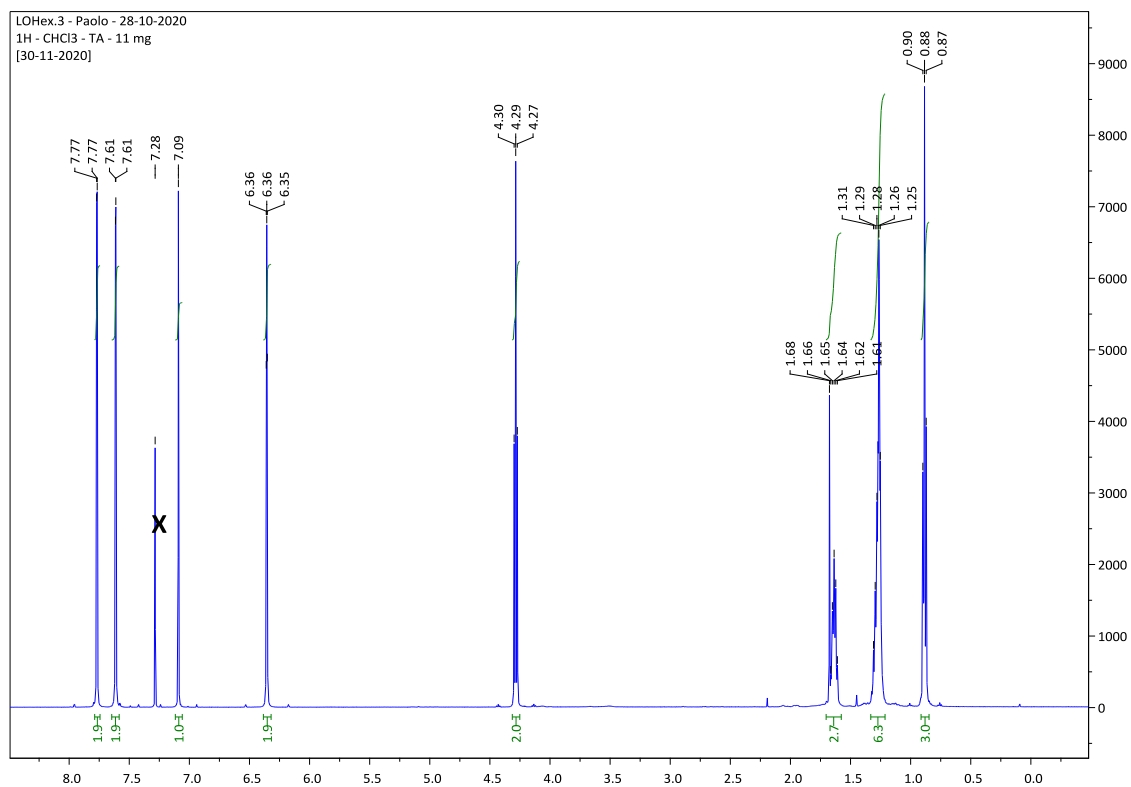


Figure 6.13. - ^1H -NMR of ligand $\text{L}^{1\text{Hex}}$ (**8**) in CDCl_3 .

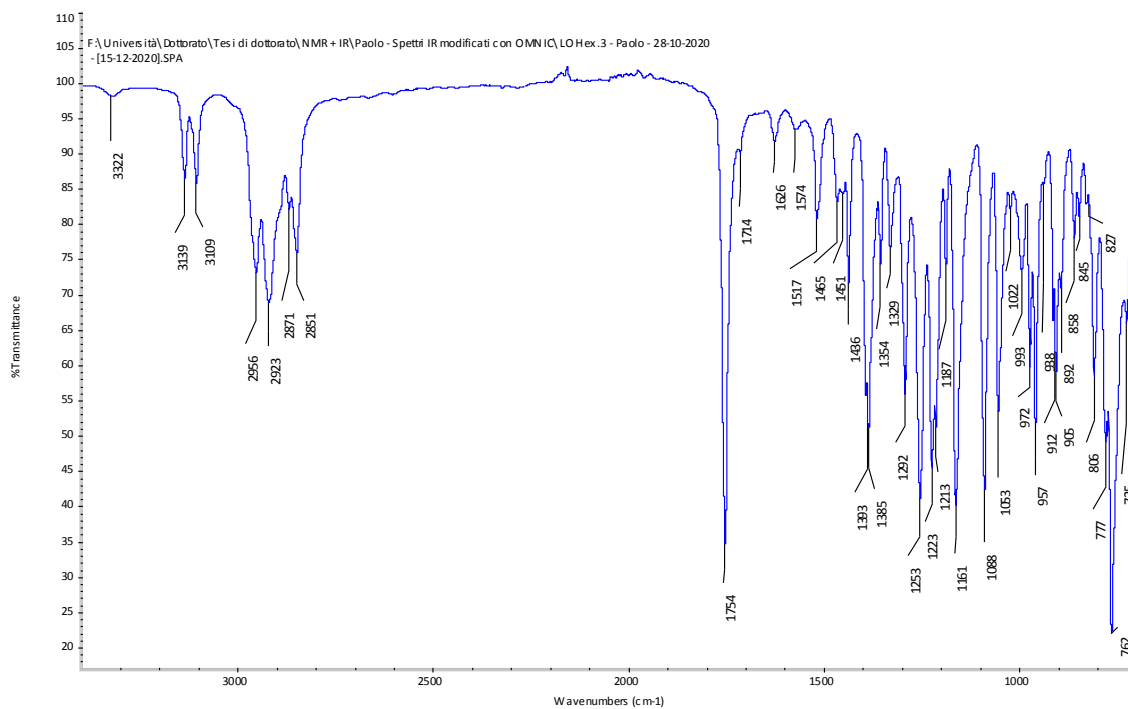
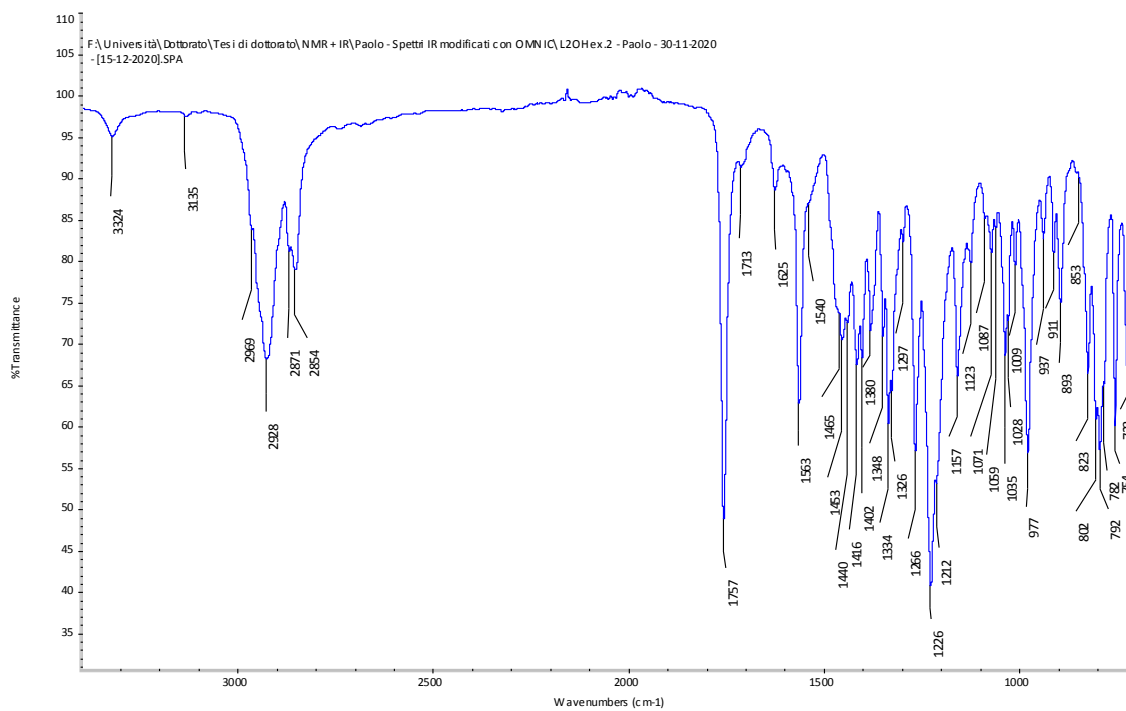
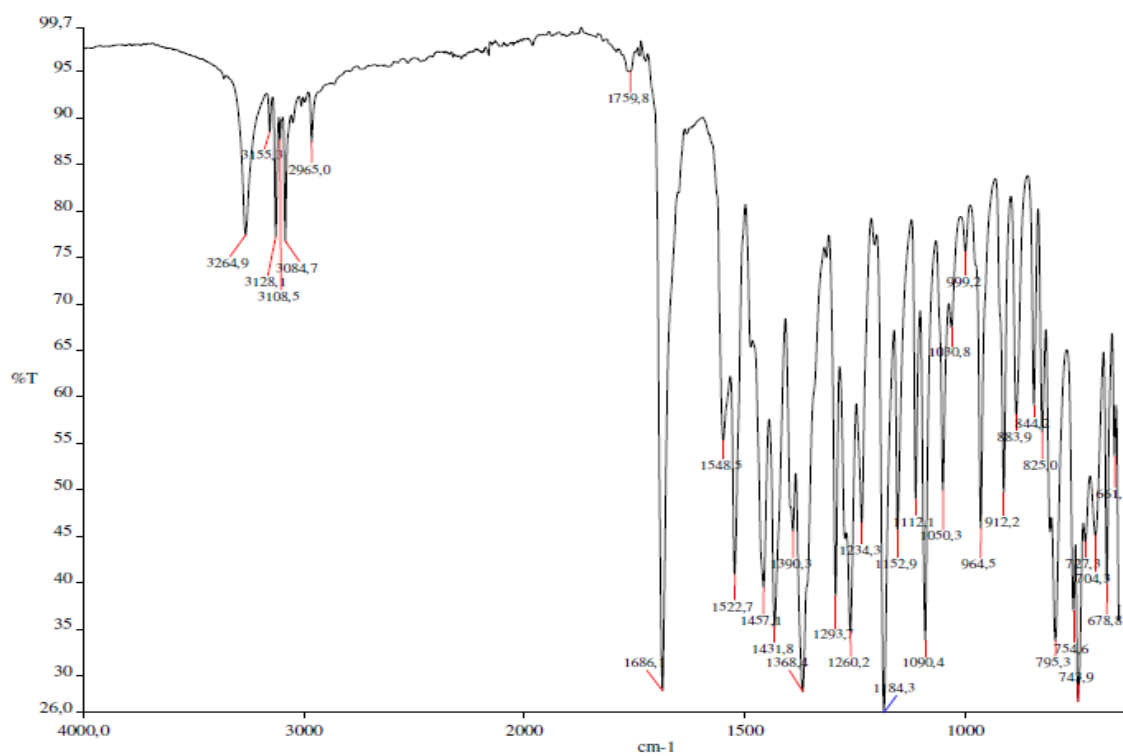


Figure 6.14. - FT-IR of ligand $\text{L}^{1\text{Hex}}$ (**8**).

Figure 6.15. - FT-IR of ligand L^{2Hex} (9).Figure 6.16. - FT-IR of ligand L^{1MN} (10).

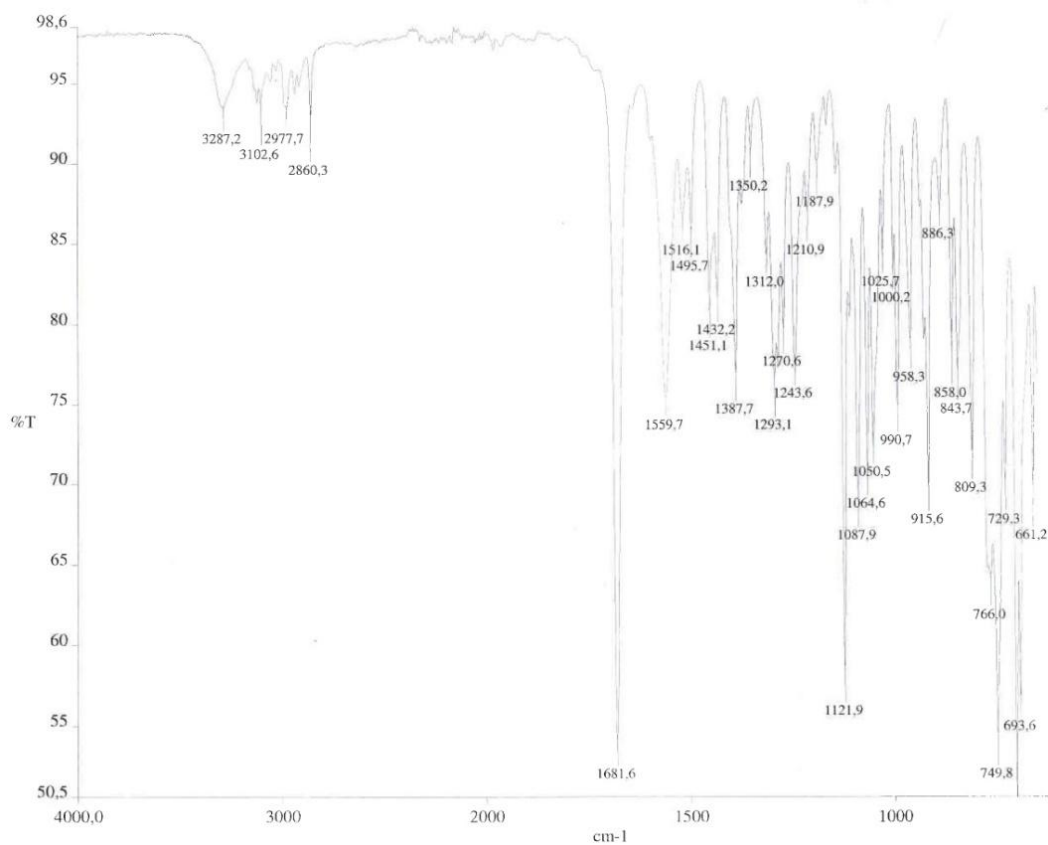


Figure 6.17. - FT-IR of ligand L^{1NMDA} (12).

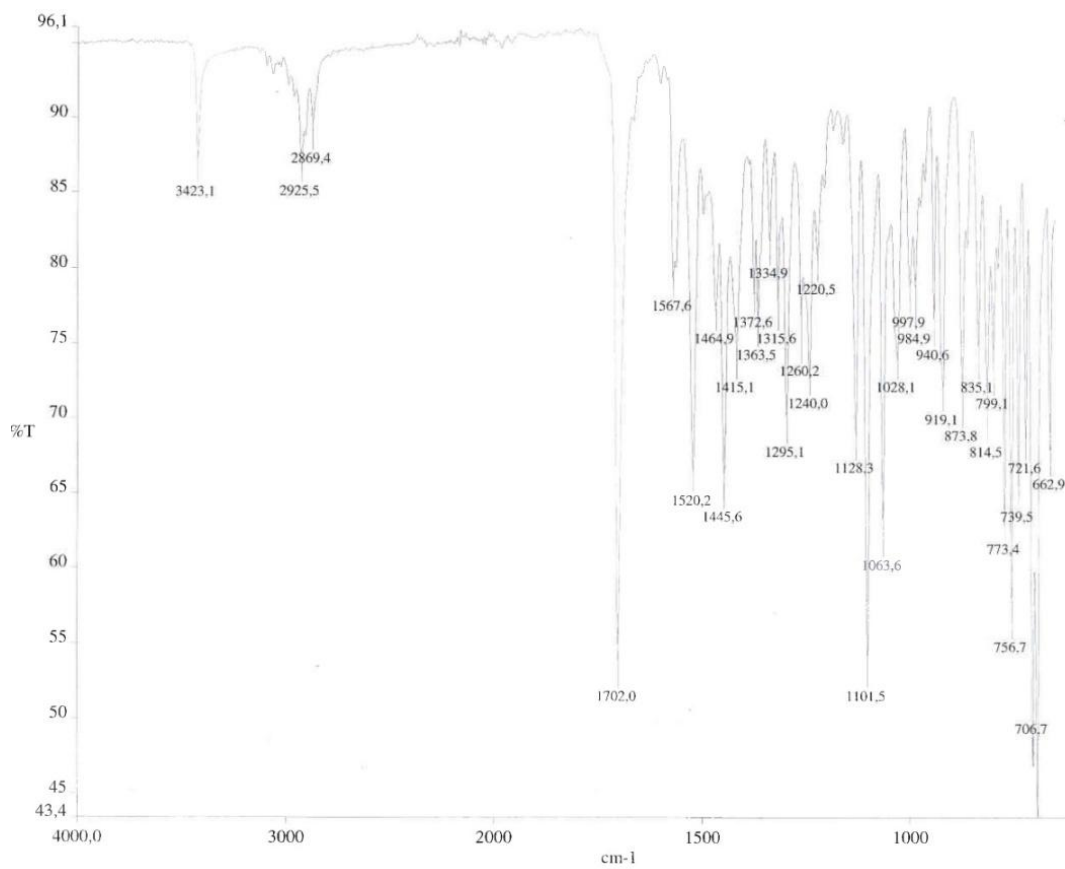


Figure 6.18. - FT-IR of ligand L^{2NMDA} (13).

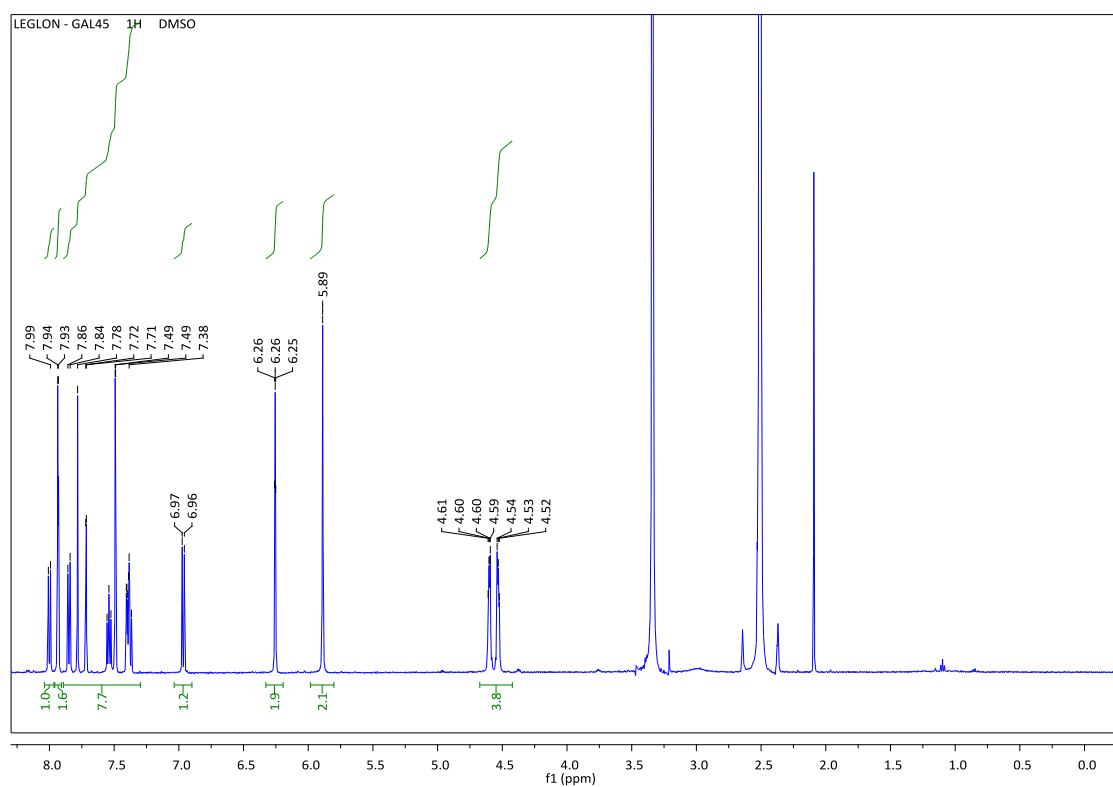


Figure 6.19. - $^1\text{H-NMR}$ of ligand $\text{L}^{1\text{LONES}}$ (**16**) in $\text{DMSO-}d_6$.

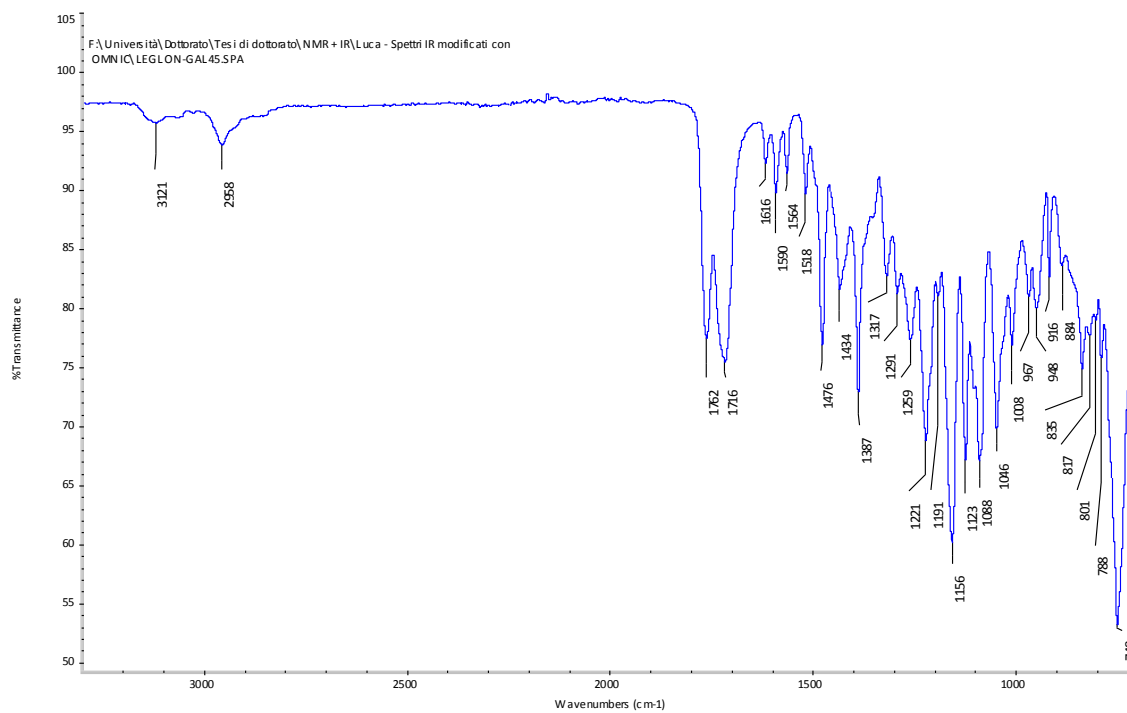


Figure 6.20. - FT-IR of ligand $\text{L}^{1\text{LONES}}$ (**16**).

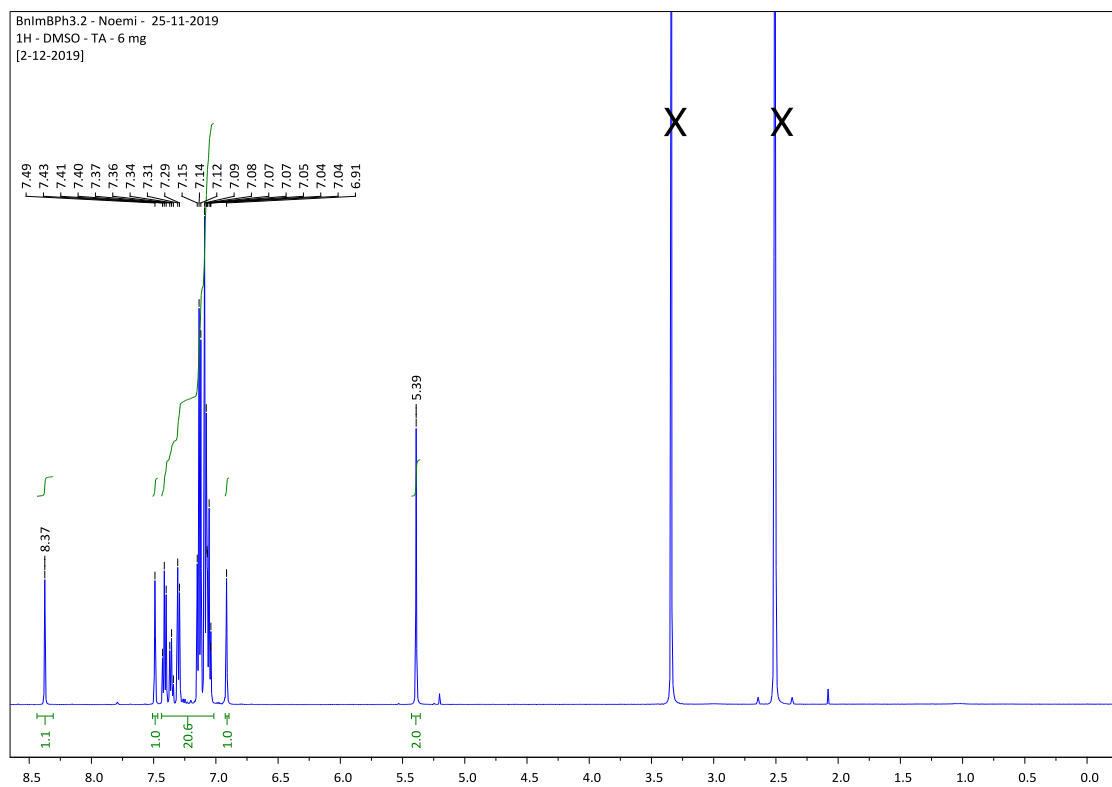


Figure 6.21. $^1\text{H-NMR}$ of ligand $(\text{Hlm}^{\text{Bn}})\text{BPh}_3$ (**23**) in $\text{DMSO-}d_6$.

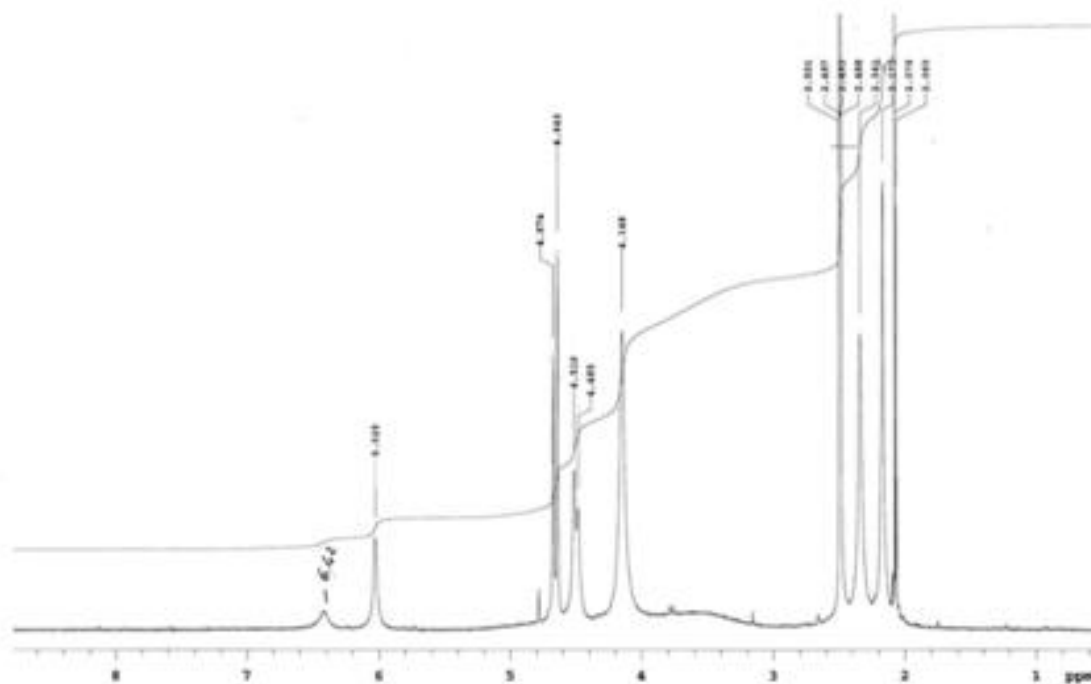


Figure 6.22. $^1\text{H-NMR}$ of complex $[(\text{PTA})_2\text{Cu}(\text{L}^{2\text{H}})]\text{PF}_6$ (**25**) in $\text{DMSO-}d_6$.

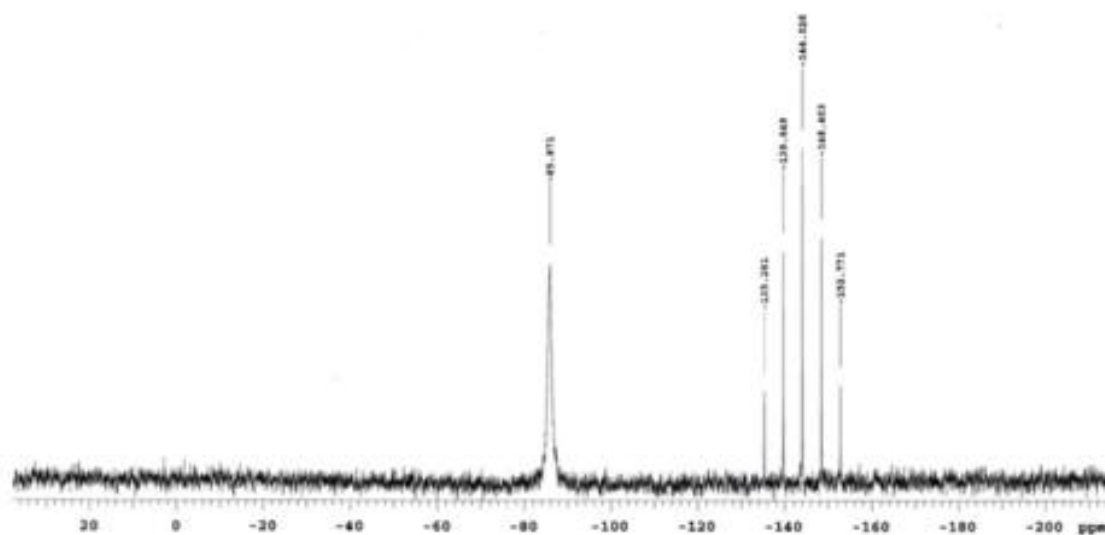


Figure 6.23. - ^{31}P -NMR of complex $[(\text{PTA})_2\text{Cu}(\text{L}^{2\text{H}})]\text{PF}_6$ (**25**) in D_2O .

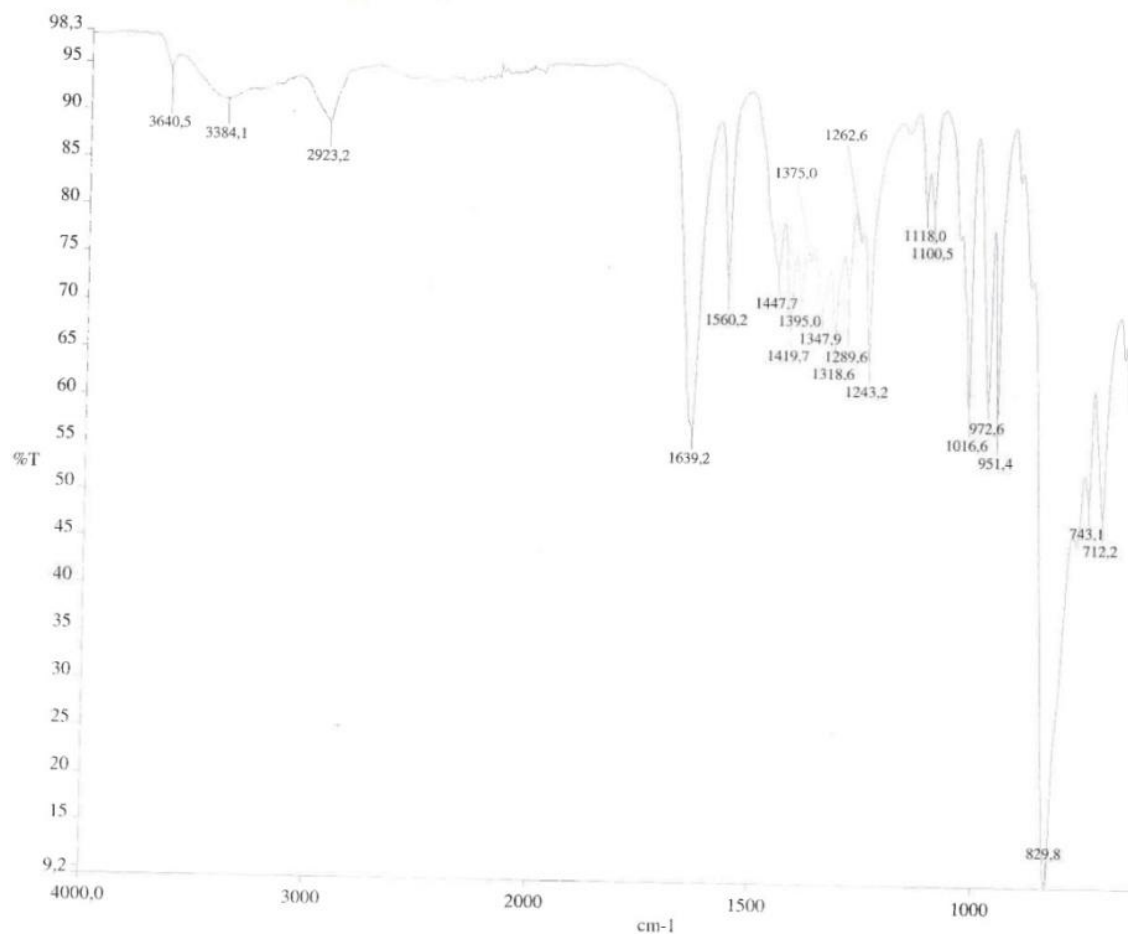


Figure 6.24. - FT-IR of complex $[(\text{PTA})_2\text{Cu}(\text{L}^{2\text{H}})]\text{PF}_6$ (**25**).

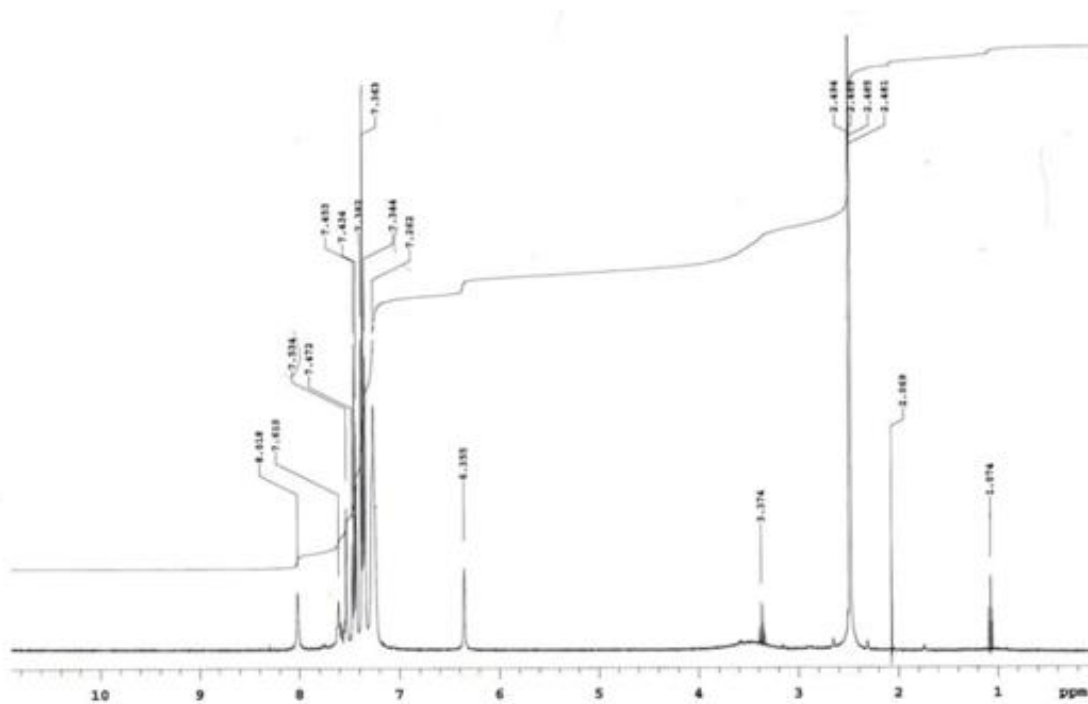


Figure 6.25. $^1\text{H-NMR}$ of complex $[(\text{PPh}_3)_2\text{Cu}(\text{L}^{\text{1H}})]\text{PF}_6$ (**26**) in $\text{DMSO-}d_6$.

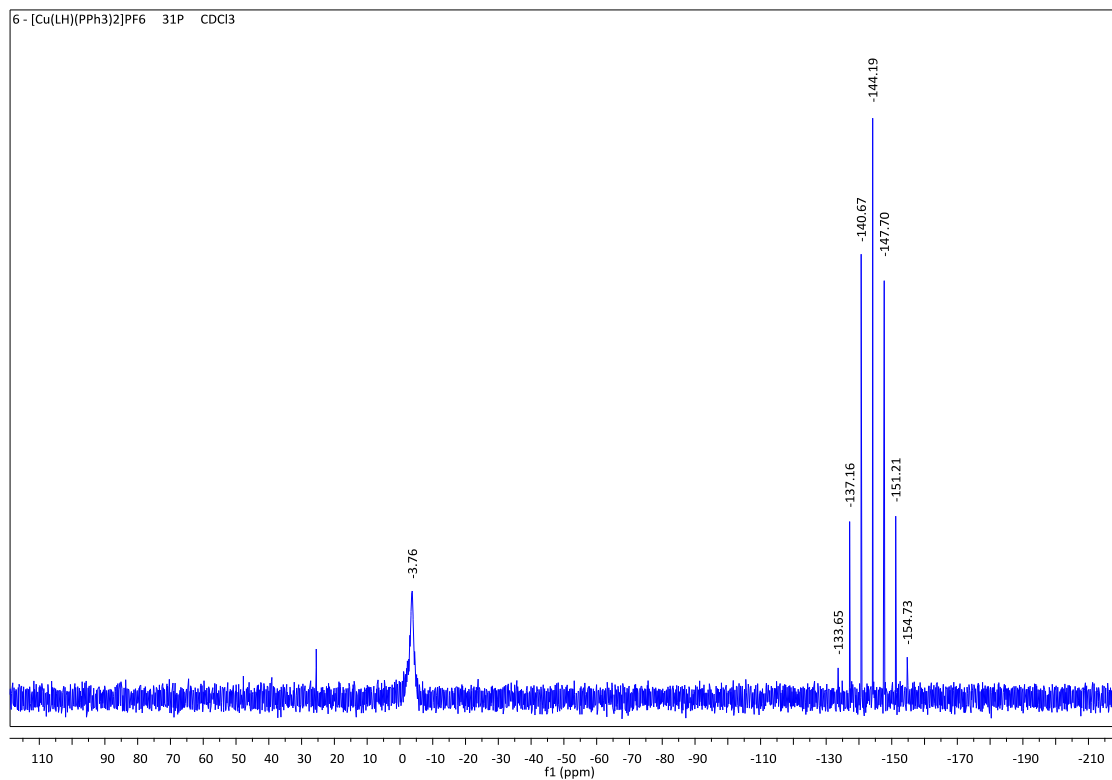


Figure 6.26. $^{31}\text{P-NMR}$ of complex $[(\text{PPh}_3)_2\text{Cu}(\text{L}^{\text{1H}})]\text{PF}_6$ (**26**) in CDCl_3 .

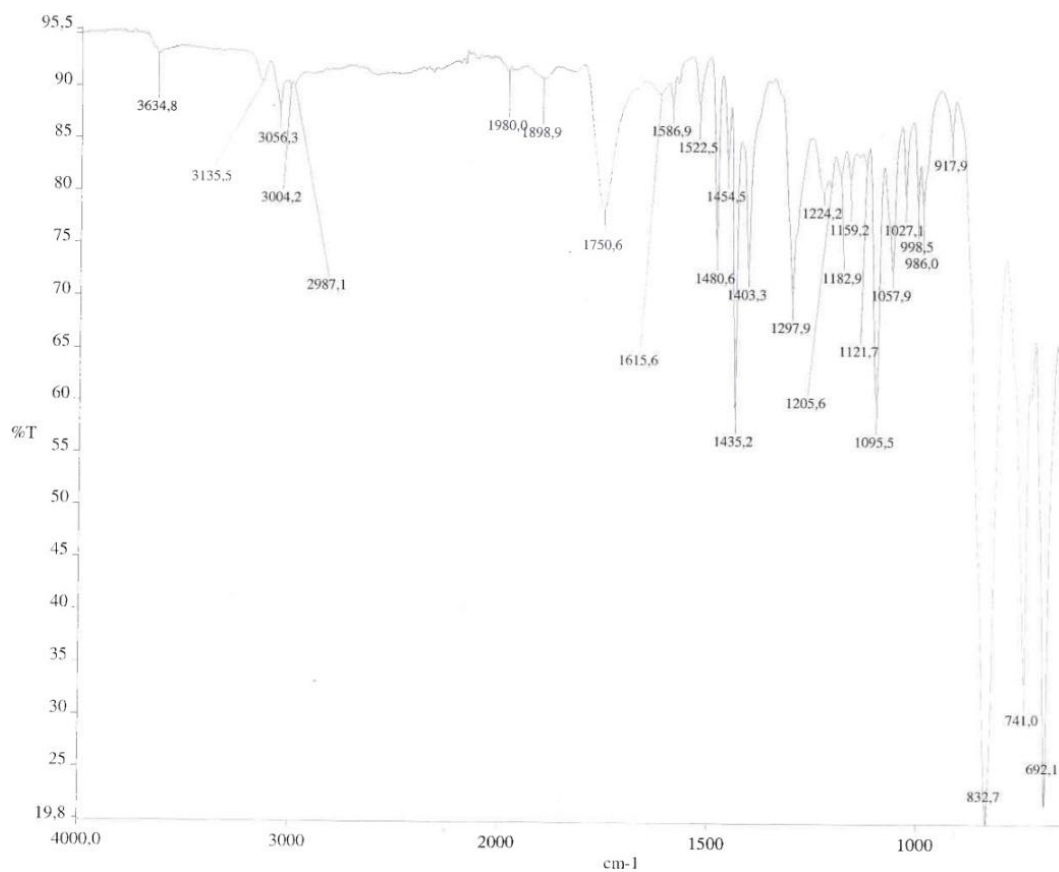


Figure 6.27. - FT-IR of complex $[(PPh_3)_2Cu(L^{1H})]PF_6$ (26).

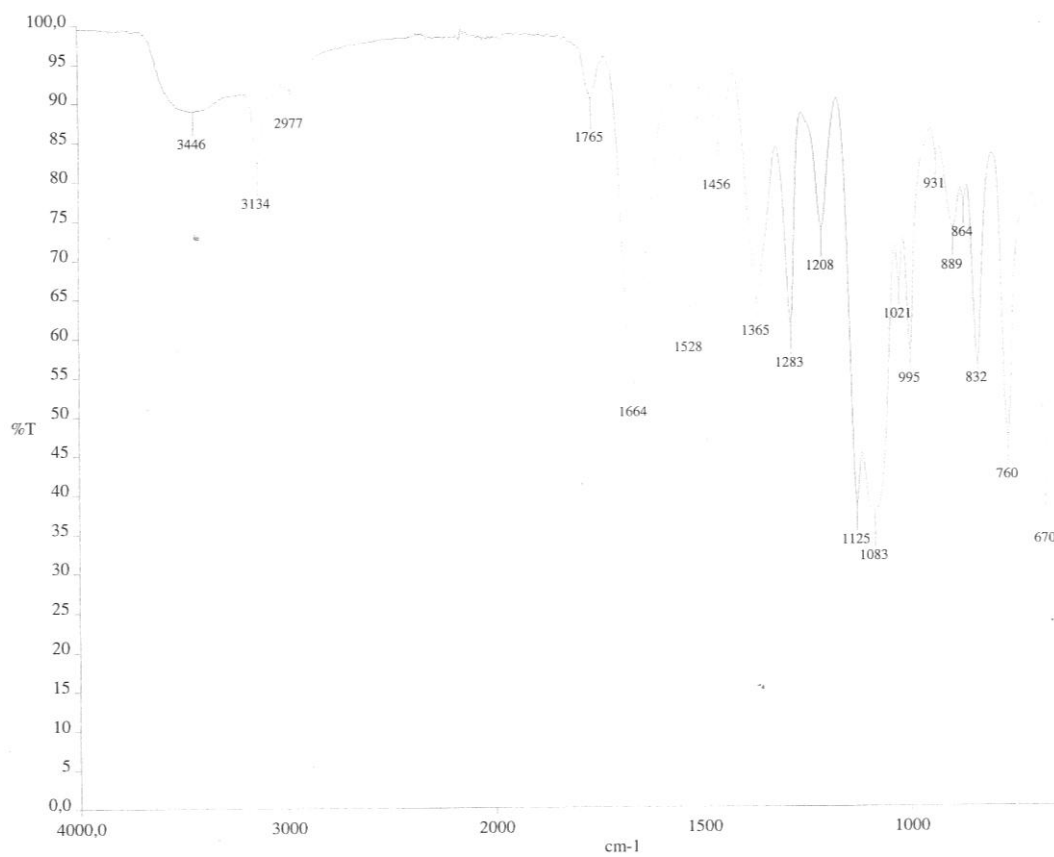


Figure 6.28. - FT-IR of complex $[Cu(L^{3H})_2](ClO_4)_2 \cdot MeOH$ (30).

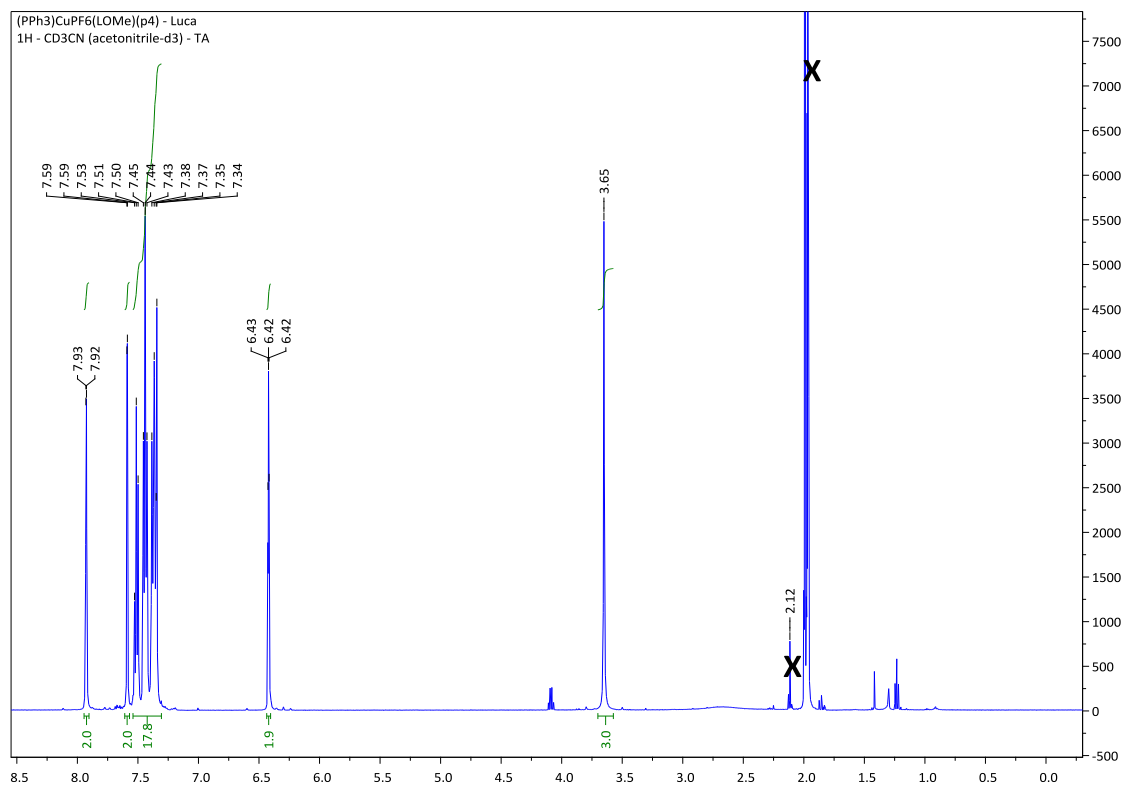


Figure 6.29. - ¹H-NMR of complex [(PPh₃)Cu(L¹Me)]PF₆ (**32**) in CD₃CN.

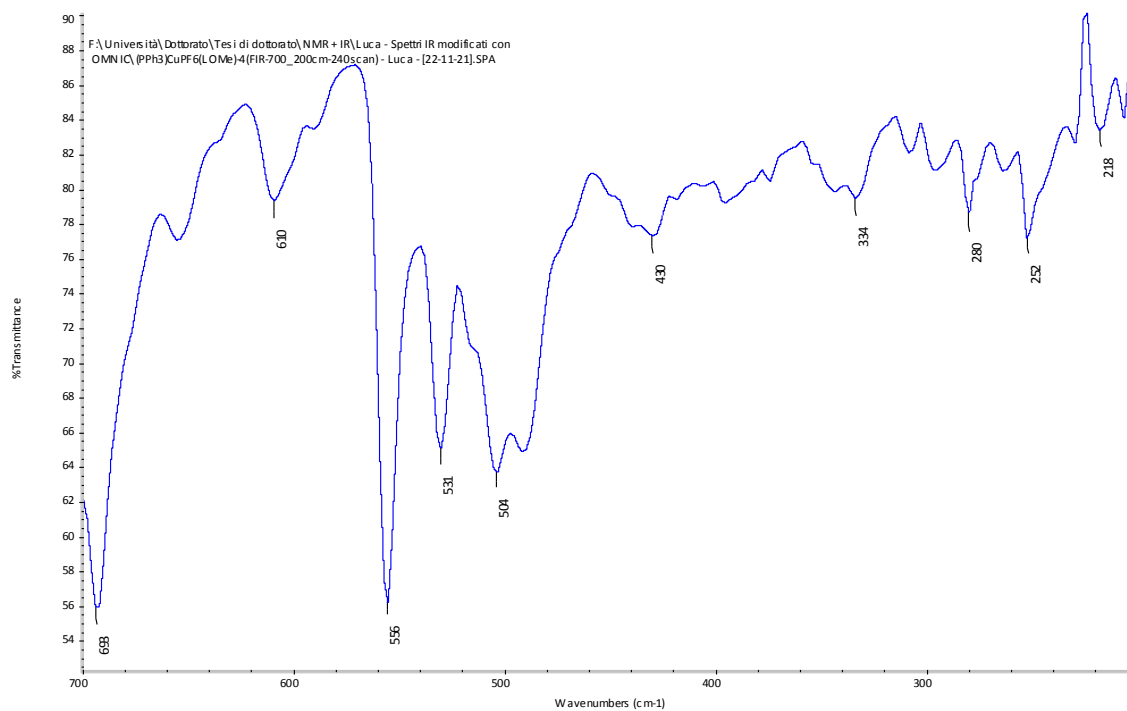


Figure 6.30. - FT-IR (FIR) of complex [(PPh₃)Cu(L¹Me)]PF₆ (**32**).

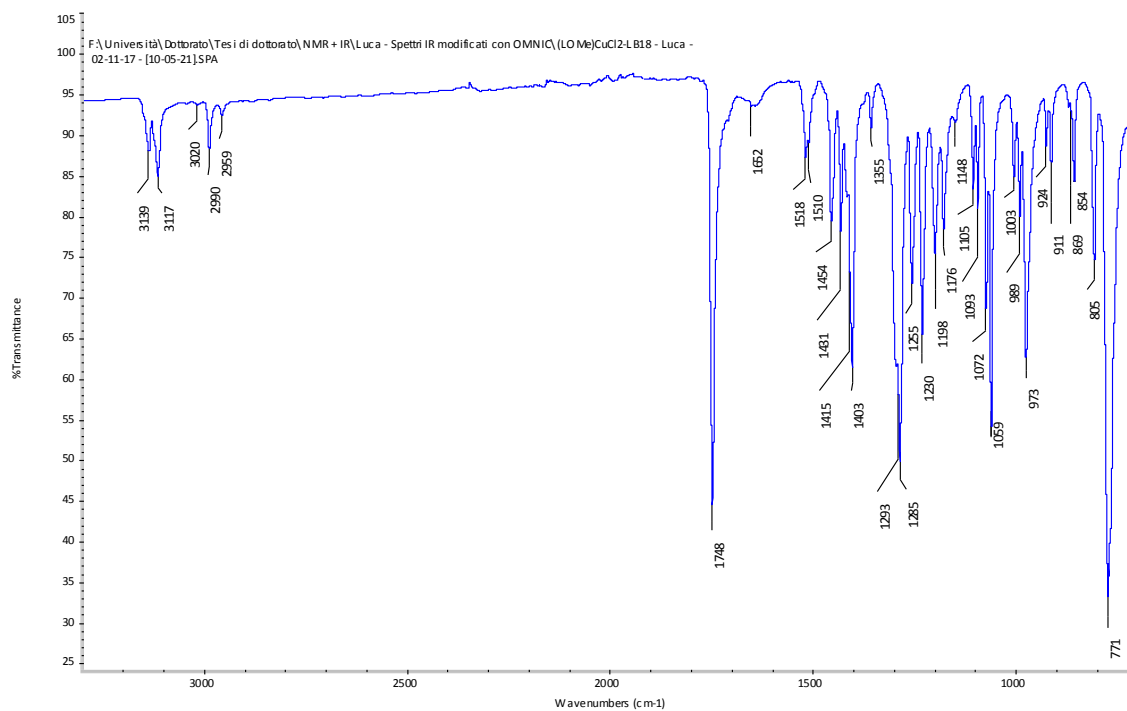


Figure 6.31. - FT-IR of complex $[\text{Cu}(\text{L}^{1\text{Me}})]\text{Cl}_2$ (**33**).

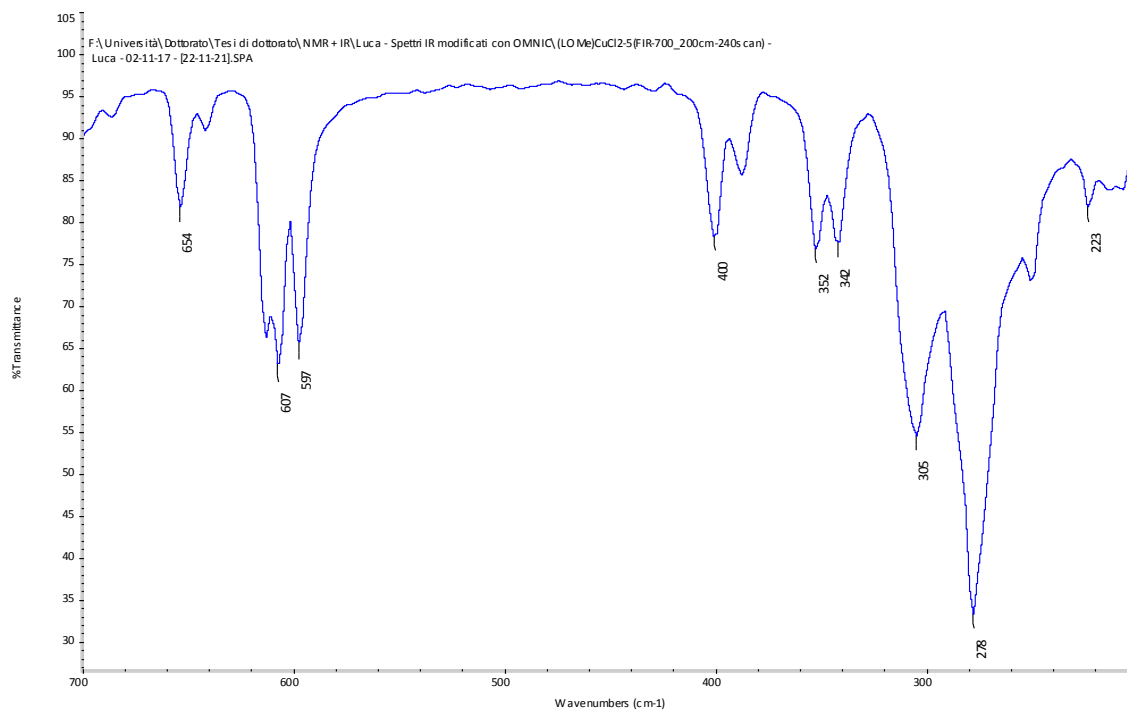


Figure 6.32. - FT-IR (FIR) of complex $[\text{Cu}(\text{L}^{1\text{Me}})]\text{Cl}_2$ (**33**).

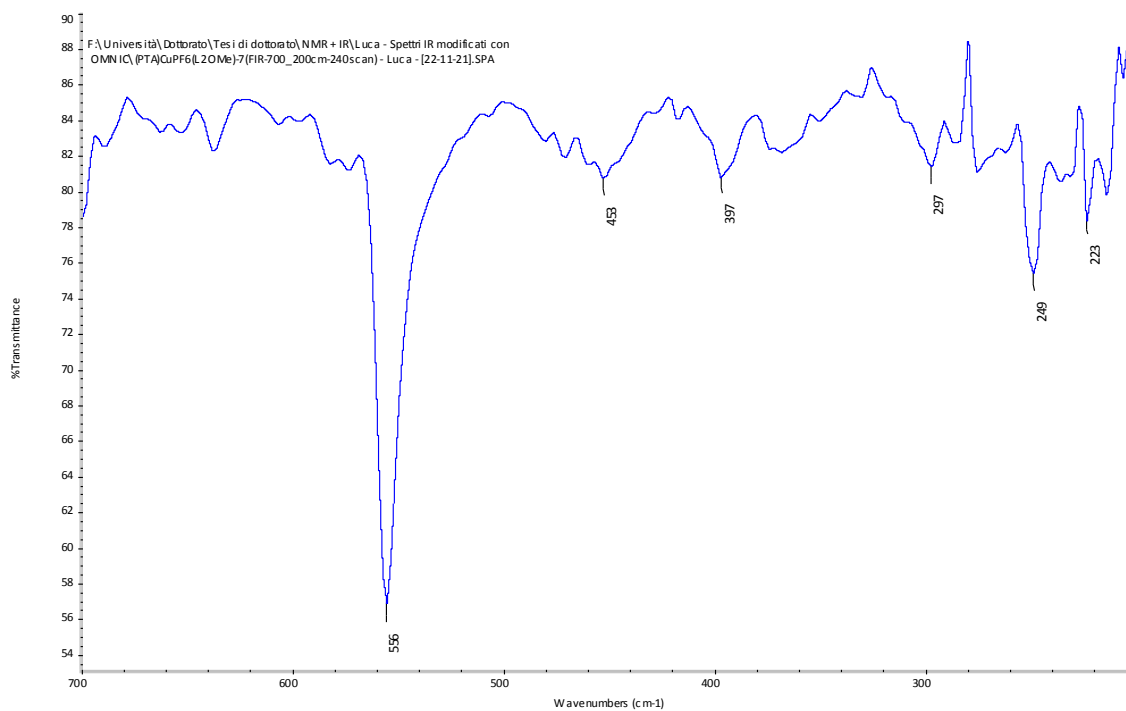


Figure 6.33. - FT-IR (FIR) of complex $[(\text{PTA})\text{Cu}(\text{L}^{2\text{Me}})]\text{PF}_6$ (35).

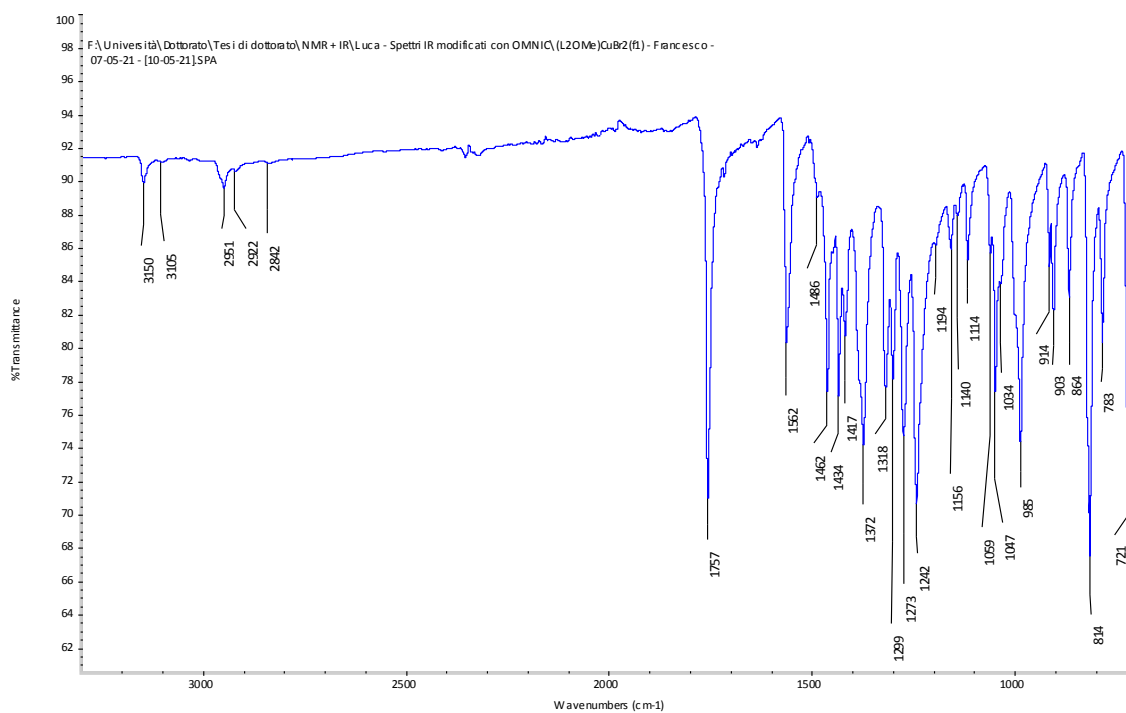


Figure 6.34. - FT-IR of complex $[\text{Cu}(\text{L}^{2\text{Me}})]\text{Br}_2$ (38).

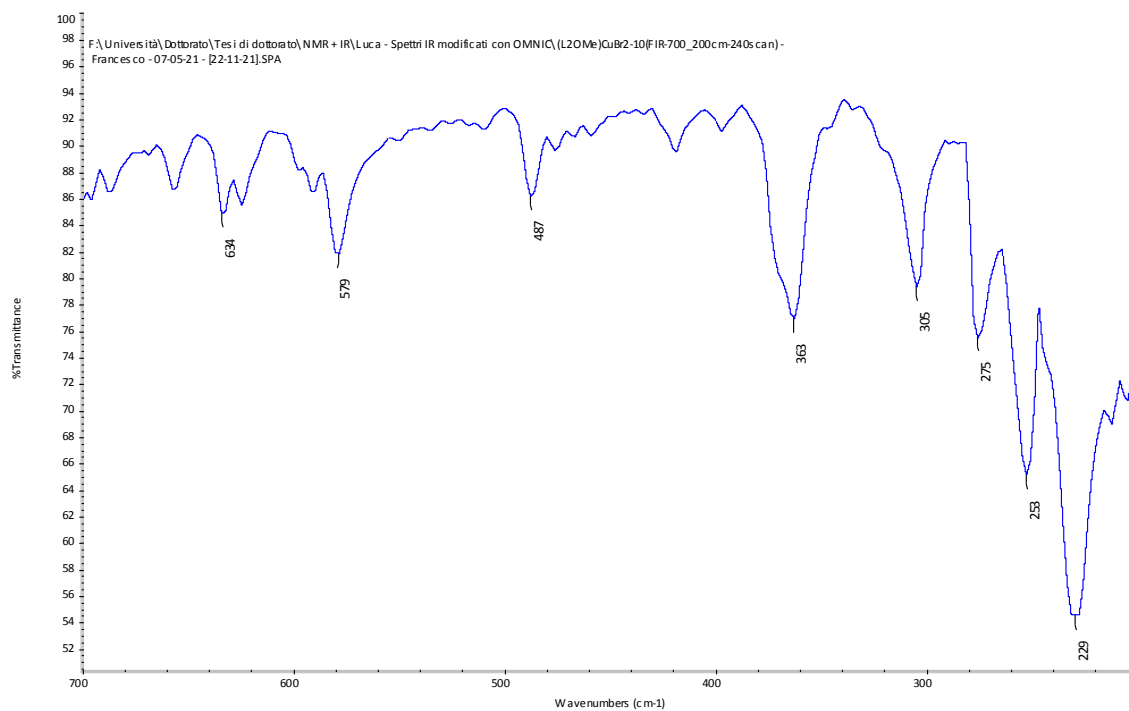


Figure 6.35. - FT-IR (FIR) of complex $[\text{Cu}(\text{L}^{2\text{Me}})]\text{Br}_2$ (38).

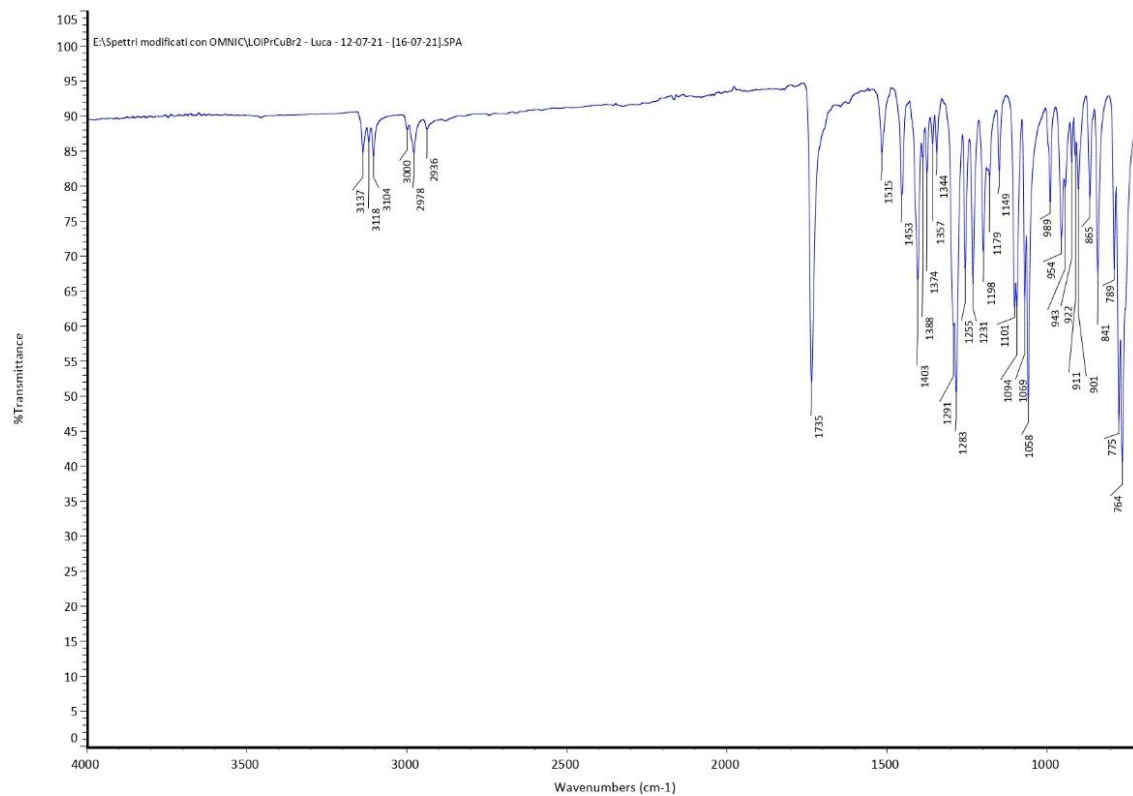


Figure 6.36. - FT-IR of complex $[\text{Cu}(\text{L}^{1\text{Pr}})]\text{Br}_2$ (40).

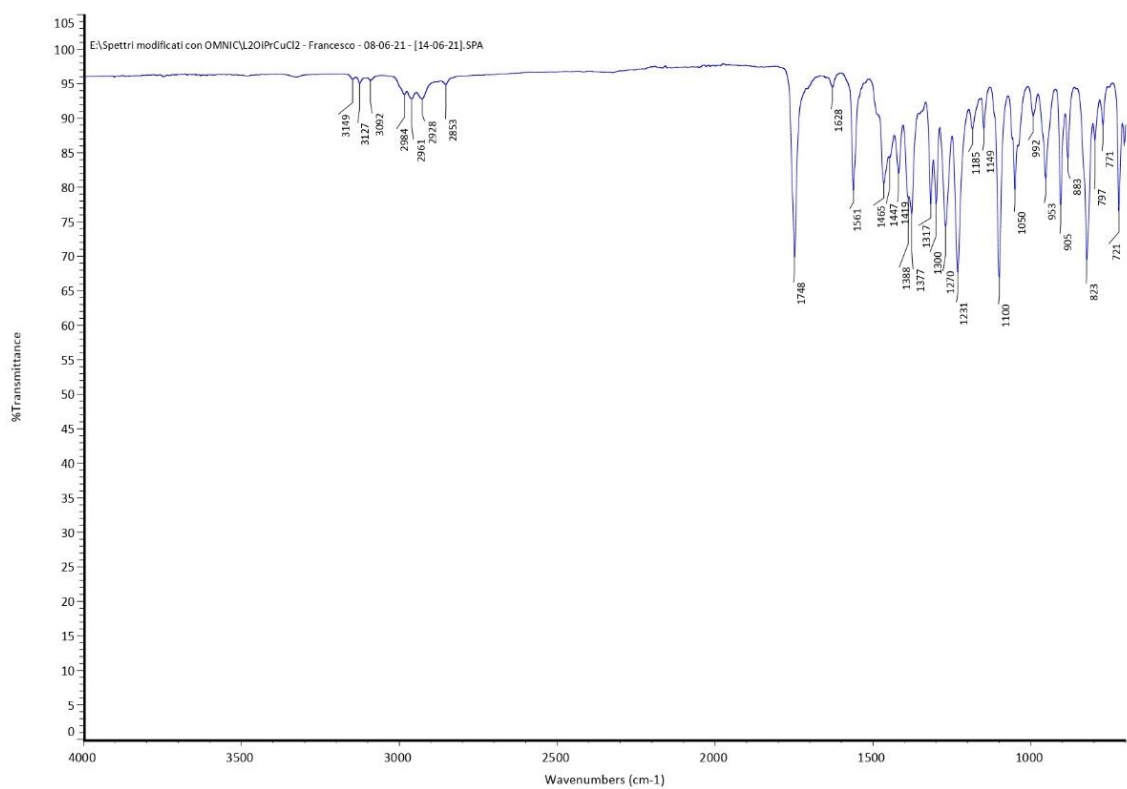


Figure 6.37. - FT-IR of complex $[\text{Cu}(\text{L}^{2\text{iPr}})]\text{Cl}_2$ (**41**).

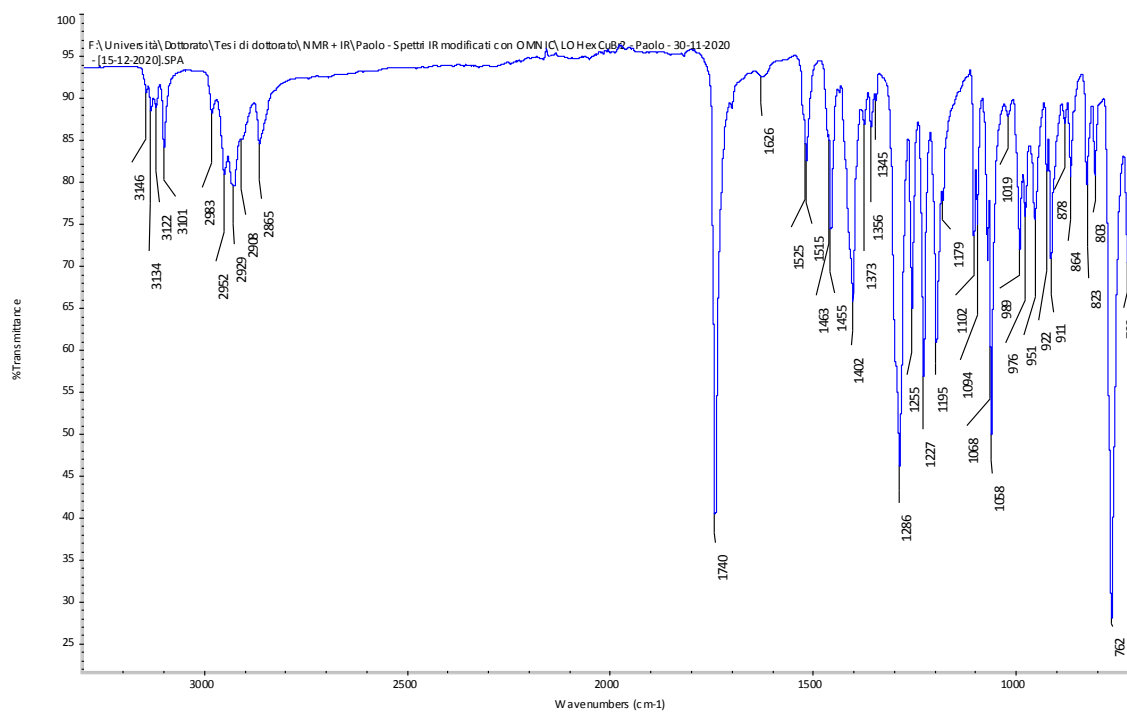


Figure 6.38. - FT-IR of complex $\{[\text{Cu}(\text{L}^{1\text{Hex}})]\text{Br}(\mu\text{-Br})\}_2$ (**44**).

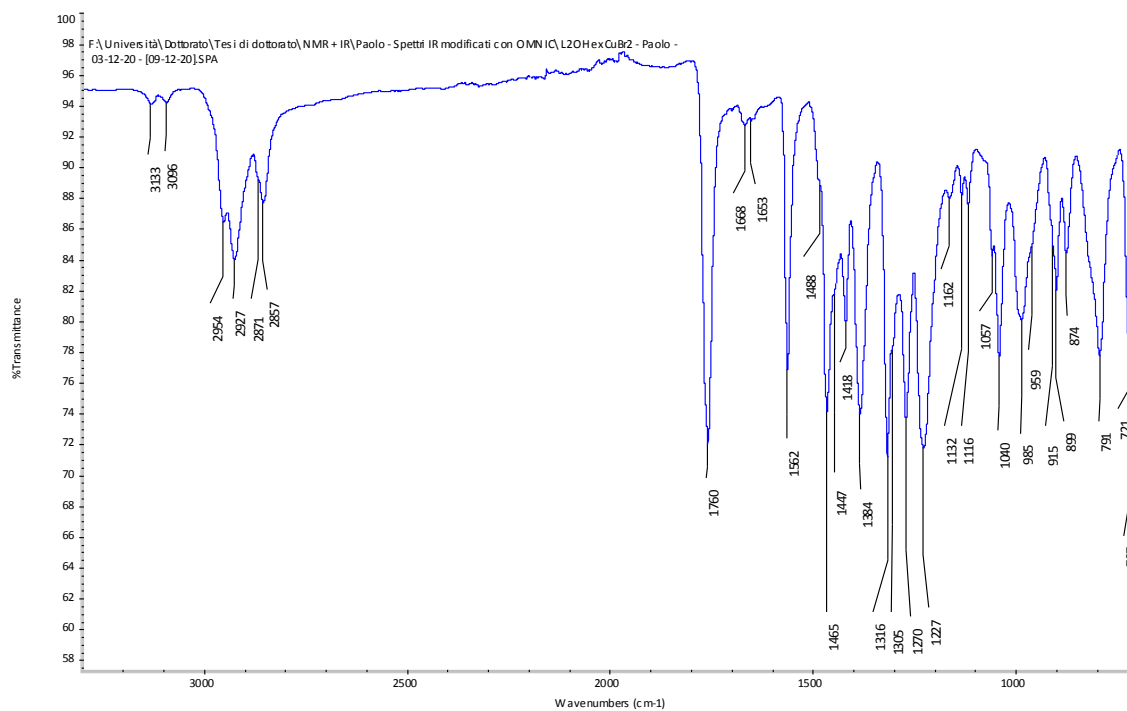


Figure 6.39. - FT-IR of complex $[\text{Cu}(\text{L}^{2\text{Hex}})]\text{Br}_2$ (46).

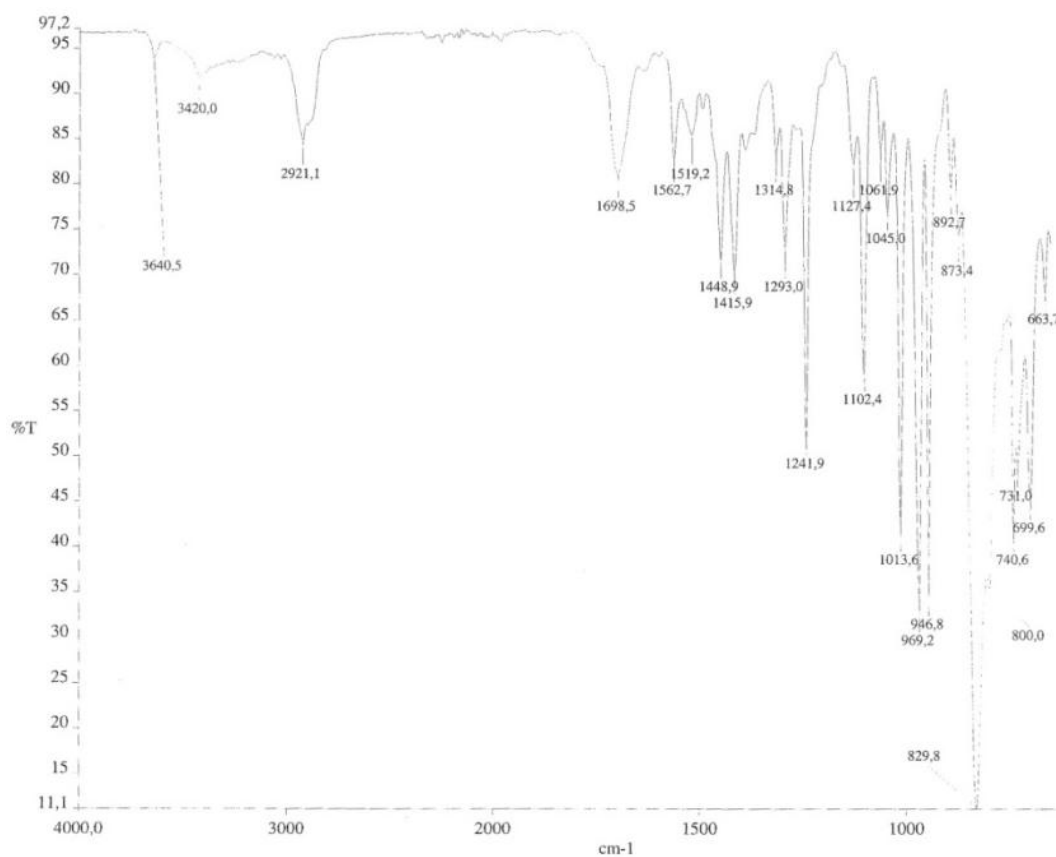


Figure 6.40. - FT-IR of complex $[(\text{PTA})_2\text{Cu}(\text{L}^{2\text{NMDA}})]\text{PF}_6$ (53).

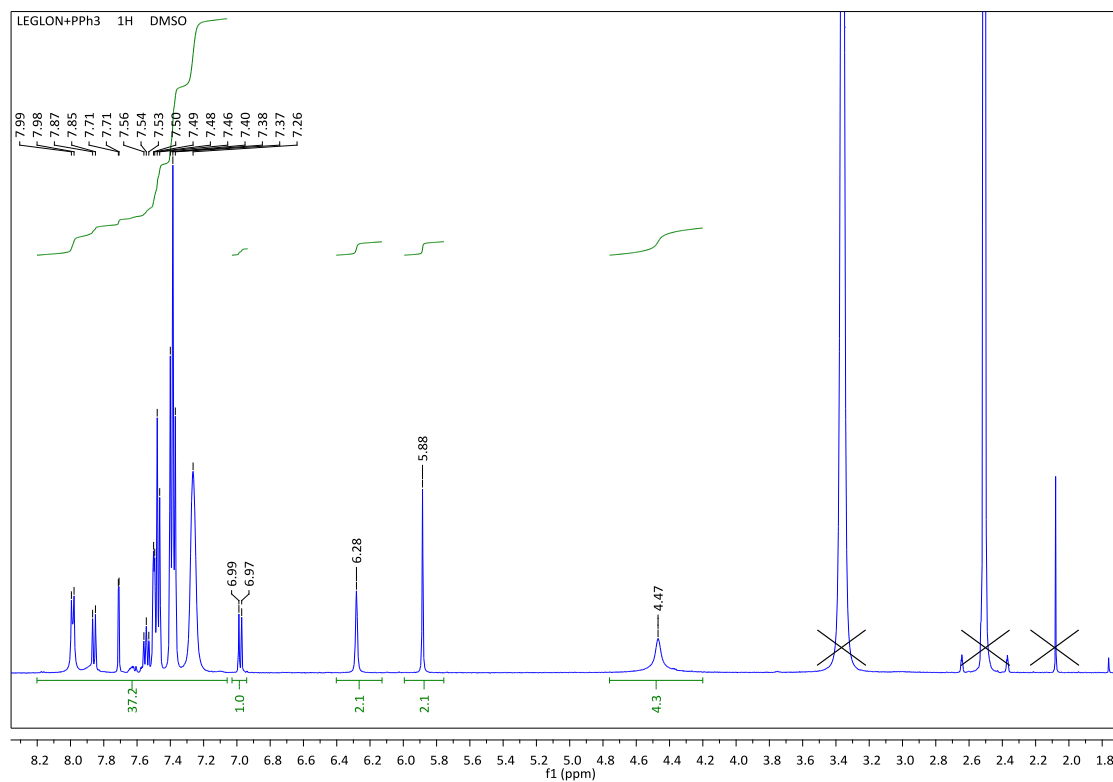


Figure 6.41. - $^1\text{H-NMR}$ of complex $[(\text{PPh}_3)_2\text{Cu}(\text{L}^{1\text{LONES}})]\text{PF}_6$ (**56**) in $\text{DMSO-}d_6$.

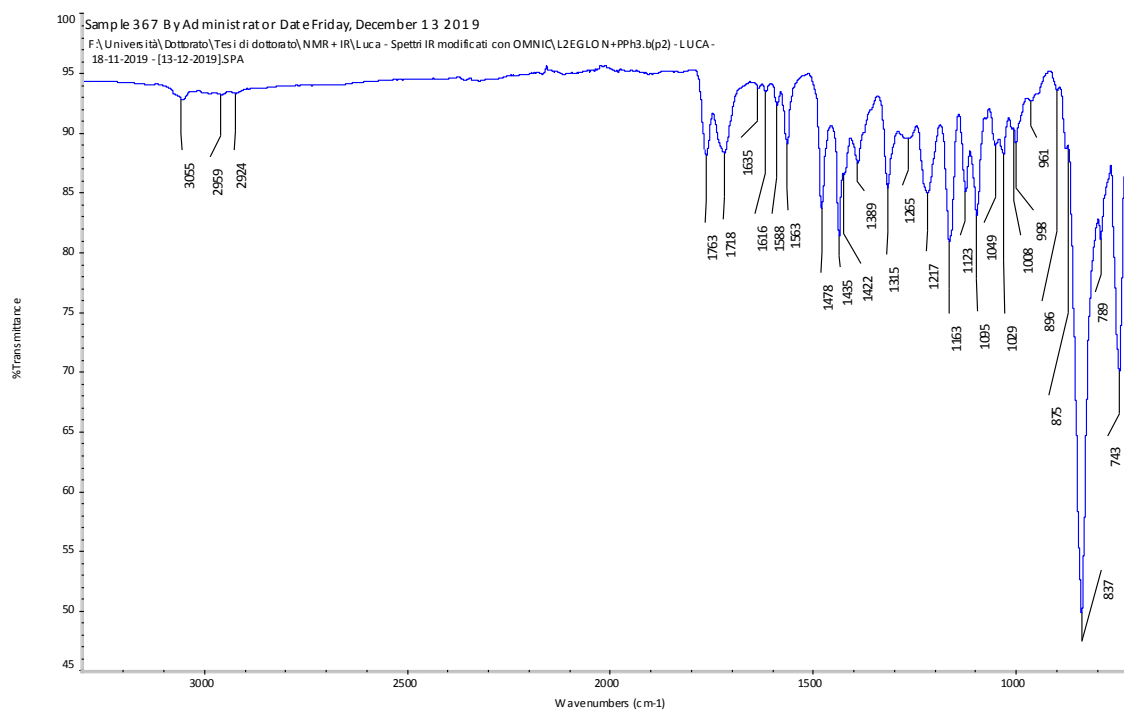


Figure 6.42. - FT-IR of complex $[(\text{PPh}_3)_2\text{Cu}(\text{L}^{2\text{LONES}})]\text{PF}_6$ (**59**).

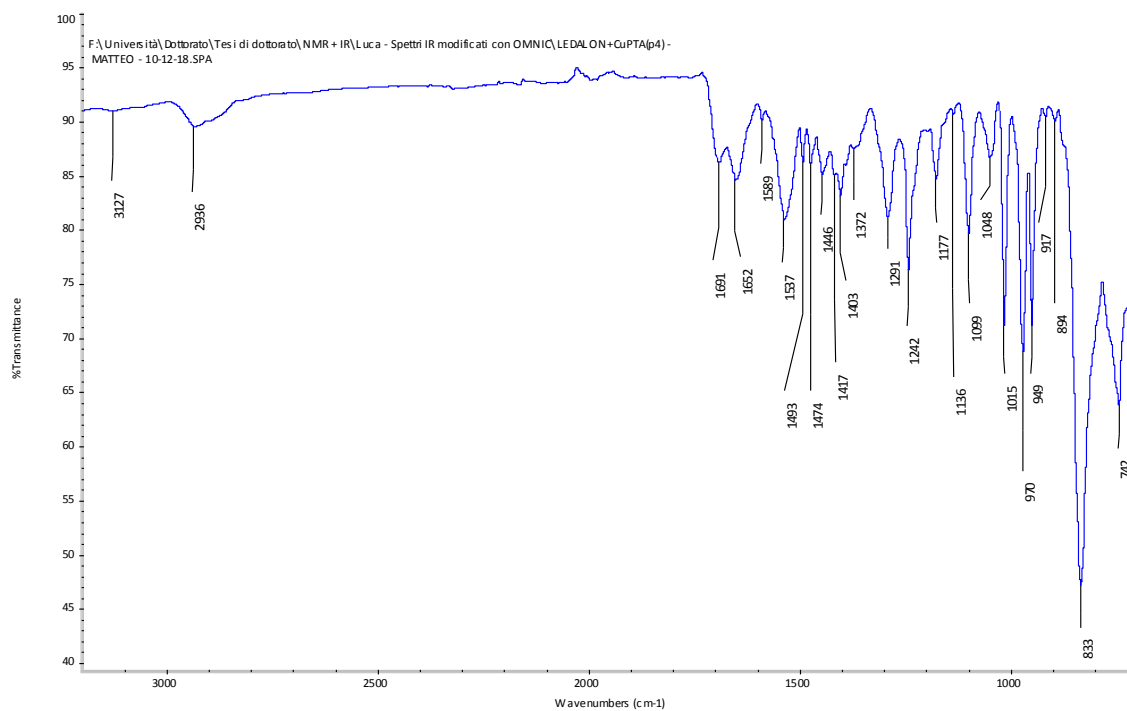


Figure 6.43. - FT-IR of complex $[(\text{PTA})_2\text{Cu}(\text{L}^{1\text{LONAM}})]\text{PF}_6$ (**61**).

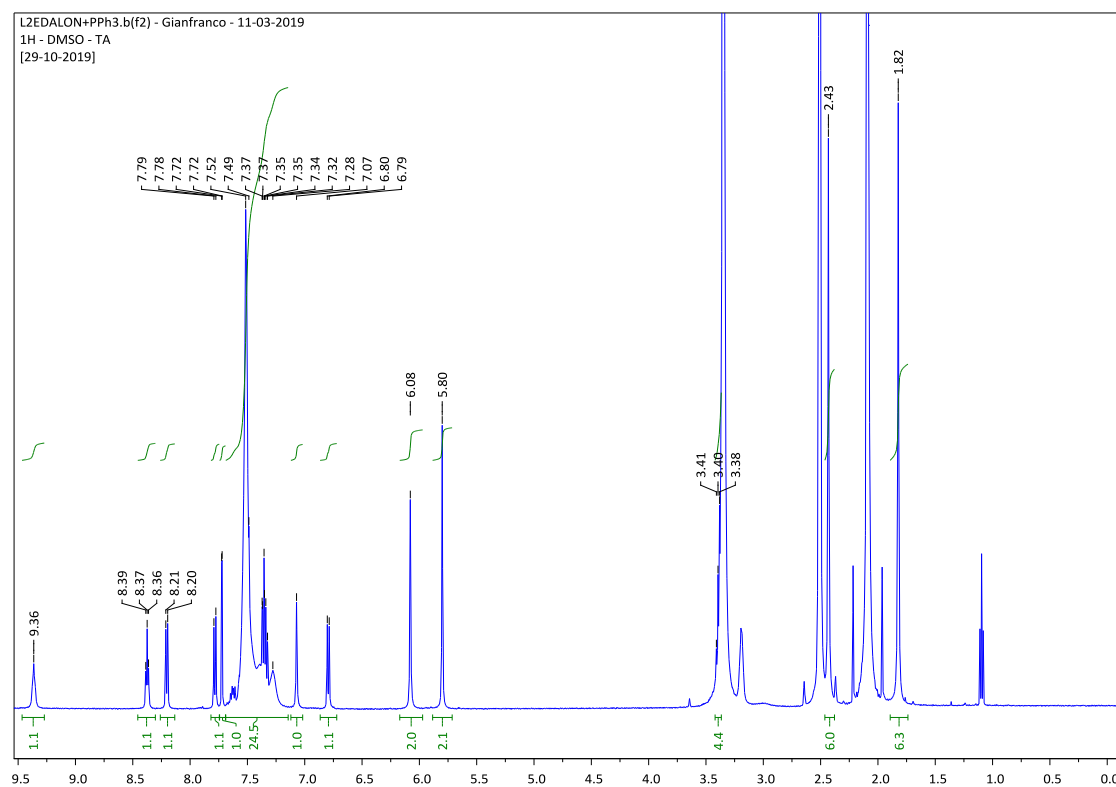


Figure 6.44. - $^1\text{H-NMR}$ of complex $[(\text{PPh}_3)_2\text{Cu}(\text{L}^{2\text{LONAM}})]\text{PF}_6$ (**65**) in $\text{DMSO-}d_6$.